STRAIN INDUCED CHANGES IN THE PERMEABILITY OF WATER SWOLLEN SEGMENTED POLYURETHANE ELASTOMERS

Thesis by

Gerald Wayne Ward

In Partial Fulfillment of the Requirements

for the Degree of

Doctor of Philosophy

California Institute of Technology

Pasadena, California

1977

(Submitted December 20, 1976)

to Wendie

ACKNOWLEDGEMENTS

I would like to take this opportunity to thank those who have contributed to the completion of this thesis:

First, I wish to thank my advisors Professors William H. Corcoran and Nicholas W. Tschoegl. They have offered encouragement and friendship as well as guidance and criticism. They have asked probing questions, offered valuable suggestions, and given me a great deal of freedom in conducting my research. For all these reasons I thank them.

I would like to thank Hollis Reamer for the many helpful discussions we have had; George Griffith, Chic Nakawatase, and Ray Reed for building and maintaining the apparatus I used in my research; and Henry Smith for assistance with the Beckman spectrophotometers.

I owe a great deal to my parents who have given me the opportunity to grow up in a loving supportive environment. Much of my success I owe to their patience, understanding, and love.

Finally, and most of all, I wish to thank my wife Wendie. She has been a great help to me all the time that I have known her. I hope she will accept this thesis as partial repayment for all that she has done for me.

ABSTRACT

The permeability of water swollen segmented polyurethane membranes has been determined for the solutes urea, glucose, sucrose, and raffinose at 26.5°C. The permeability of segmented polyurethane membranes; based on poly(oxyethylene glycol) grades 600, 1000, 1500, and 1540; was determined for the swollen unstrained films and for the swollen films at several strains. The free volume theory for diffusion through homogeneously swollen polymers was able to predict the observed changes in membrane permeability with strain for all solutes except urea. The free volume theory fails to predict the urea data accurately because the polyurethanes used absorb urea and therefore the urea can diffuse through the polymer as well as through the solvent, an eventuality not provided for in the free volume theory.

The solute reflection coefficient σ, as defined in the theory of thermodynamics of irreversible processes, was determined. The available-area-ratio and the film tortuosity were calculated from the solute reflection coefficient and the film permeability ω. Neither the available-area-ratio nor the film tortuosity correlate with changes in the film permeability.

A correlation between σ and ω was proposed. It was shown that for $0.3 \leq \sigma \leq 0.7$ the film permeability ω is inversely proportional to σ. The proposed correlation is discussed and the suggestion is made that additional experiments be conducted to determine the range of σ for which the correlation is valid.

TABLE OF CONTENTS

LIST OF FIGURES

LIST OF TABLES

INTRODUCTION

The concept of dialysis is generally attributed to Thomas Graham who, in 1861, separated a solution of gum arabic and sucrose into two solutions each containing only one of the solutes (1-3). Ferry (4) cites an earlier paper by Fick (5), published in 1855, in which Fick describes dialysis experiments. Despite these early beginnings dialysis did not receive much impetus until 1907 when Bigelow and Gemberling (6) succeeded in making uniform membranes from collodion. Within a few years other investigators had learned how to control the properties of collodion membranes.

Over the years there has been considerable effort expended to produce membranes with carefully controlled properties. A wide variety of materials have been studied with regard to their potential use as membranes. These materials include cellulose and its derivatives (7-11), metals (12,13), minerals (15-17), clays (14), rubbers (18-23), and other man-made polymers (24-25).

Several techniques have been developed for controlling the properties of artificial membranes. Among these techniques are incorporation of a poor or non-solvent into the casting solution from which the membrane is prepared (26), acid or base etching of track-etch membranes (27,28), leaching a soluble material from the membrane, swelling the membrane with a poor solvent, forming microcracks in the membrane matrix (29), mixing with or bonding to the membrane substances which change its permeability to certain solutes (30,31), and controlling the degree of crosslinking, to name several.

Once a membrane has been prepared it is sometimes desirable to change the size of the pores in the membrane. For cellulose membranes treatment with $ZnCl_2$ solutions, acetylation, and mechanical deformation have been tried (32). Track-etch membranes may be re-etched to enlarge the pores or the pore wall may be coated to reduce the pore size (33). Some types of membranes may be swollen to the desired degree in one solvent and then, by using a series of mixed solvents, the original solvent may be replaced by the solvent of interest without changing the degree of swelling.

Lyman Craig (1,32,34-37) conducted a rather extensive investigation of cellulose membranes. Craig began his studies using sausage casings made from regenerated cellulose. He and his co-workers studied the effect of stretching the membrane on the rate of transport of solutes across it. They envisioned a series of graded membranes that could be used to carry out separations in the laboratory. They also felt that such a series of membranes would have industrial applications in countercurrent dialysis or in ultrafiltration.

Craig and co-workers were limited in their attempts to study the effect of stretching on cellulose membrane permeability by the mechanical properties of cellulose. Membranes of the type they used can be stretched only 8 - 20% before breaking. Therefore they observed large changes in the rate of transport of a solute through a membrane only when the solute would just barely diffuse through the membrane in the unstretched state.

Rouse and Ultman (38) have studied the change in permeability of

reverse osmosis membranes to salt as a function of strain. They found that strains of 1.5% to 4% caused increases of up to 30% in the permeability of reverse osmosis membranes to certain salts. The strains used by Rouse and Ultman are within the elastic limit of cellulose and are typical of the strains imposed on the membrane in commercial reverse osmosis plants. Rouse and Ultman point out that since such small strains affect the performance of reverse osmosis membranes it is possible that part of the impairment of normal function of body tissues caused by edema (swelling by water influx) may be due to swelling induced changes in individual cell membrane permeabilities. Hays (39) has suggested that vasopressin may act by inducing a very small change in the structure of biological membranes and thereby cause large changes in the permeability of the membrane to small solutes.

This thesis deals with strain induced changes in the permeability of membranes. It was desirable to select a material which had a known microstructure, which was water swellable so that solutes of biological importance could be studied, and which was elastomeric so that higher strains could be attained. Segmented polyurethanes meet the requirements just listed.

In this thesis the effect of mechanical deformation on the permeability of water swollen segmented polyurethanes to urea, glucose, sucrose, and raffinose is discussed. It is shown that the change in permeability that occurs when the membrane is deformed is due to a change in the degree to which the membrane is swollen and that the

free volume theory for diffusion through highly swollen polymers adequately describes the changes in membrane permeability that occur. Also, a correlation between the solute reflection coefficient σ and the film permeability ω is proposed and the potential usefulness of the correlation is discussed.

Chapter 1

Theoretical

Because of the importance of membranes in life processes and their usefulness in the preparation and purification of chemicals, much work has gone into the development of theories to explain their behavior. Several of the theories which have been proposed to describe transport through uncharged inert membranes will be discussed here. The discussion will exclude living membranes, electrodialysis, ion exchange membranes, bilayer membranes, dynamic membranes, and, for the most part, ultra filtration through membranes. The theories covered are derived for the case of transport of non-electrolytes in aqueous solution across membranes. These theories are:

1) molecular sieve theory
2) theory of thermodynamics of irreversible processes of Onsager (1), Casimir (2), and Staverman (3,4) as formulated by Kedem and Katchalsky (5,6)
3) free volume theory

The kinetic theory of Laidler and Shuler (7-9) will not be discussed as it has been shown by Kedem and Katchalsky (5) to be incomplete.

There are only two ways by which a solute may traverse a membrane. The solute may diffuse through the solvent, or the solute may become absorbed on or dissolved in the membrane material and subsequently diffuse through the membrane matrix. In either case the driving force for transport across the membrane is a gradient of chemical potential.

1.1 *Molecular Sieve Theory*

True molecular sieve theory regards the membrane as being a solid sheet penetrated by pores of a certain size. It attempts to explain the behavior of the membrane by stating that molecules may pass through the membrane as long as they have sufficiently small cross-section.

The molecular sieve theory begins with the idealized Fick's law for one-dimensional diffusion in a solution

$$\frac{dQ}{dt} = - DA \frac{dc}{dx} \tag{1.1}$$

where dQ is the quantity of material diffusing through an area A in time dt, D is the diffusion coefficient, and $\frac{dc}{dx}$ is the concentration gradient. This treatment assumes D to be constant, independent of the concentration of the solute. To apply this equation to a porous membrane the equation is rewritten as

$$\frac{dQ}{dt} = - DA_p \frac{dc}{x_p} \tag{1.2}$$

where A_p is the effective total cross-sectional area of the pores and x_p is the mean length of the pores. Equation (1.2) is the basic equation for diffusion across a porous membrane. It is valid as long as the diffusion coefficient is constant and the ratio of pore diameter to solute diameter is greater than 30 to 1. This latter requirement was established theoretically by Lane and Riggle (10) and experimentally by Manegold (11) and Renkin (12).

Frequently (1.2) is rewritten as

$$\frac{dQ}{dt} = - kDA \frac{dc}{x_p} \tag{1.3}$$

where A and x_p are as previously defined and k is the permeability constant. Under conditions where (1.2) applies, the permeability constant, k, will have the same numerical value for all solutes. Thus k equals A_p/A and both are assumed equal to the volume fraction of the solvent (water in this study) in the membrane, ϕ_w. Generally it is ϕ_w that is determined.

To determine ϕ_w the wet and dry weight of the membrane is measured and the assumption is made that there is no volume change on mixing. If this is so, then the volume fraction of solvent in the membrane is given by

$$\phi_w = \frac{W_s - W_d}{(W_s - W_d) + W_d(\rho_w/\rho_m)} \tag{1.4}$$

where W is a weight, ρ is a density, and the subscripts s, d, w and m stand for swollen, dry, solvent (or water) and membrane, respectively. One should remember that the membrane density required is that of the material composing the membrane matrix.

Equations (1.2) and (1.3) are adequate to explain transport of small solutes through a very coarse membrane. As the solute site increases or the pore size decreases, the area ratio, A_p/A, i.e. the permeability constant, k, tend to decrease. There are several ways to explain this phenomenon. One may assume a distribution of pore sizes and conclude that the larger molecules are prevented from passing through the smaller pores due to their size. Or, as was assumed by Ferry (13,14) and by Pappenheimer et al.(15), a correction factor may be

introduced. Ferry and Pappenheimer incorporated the assumption that a molecule could enter a pore only if it did not strike the edge of the pore, Figure 1.1a. For spherical solutes and cylindrical pores, the effective pore area is represented by

$$A_p/A_o = (1 - R_s/R_p)^2 \tag{1.5}$$

where R_s is the solute radius, R_p is the pore radius, A_o is the total cross-sectional area of the pores, and A_p is the effective cross-sectional area of the pores as defined earlier. Ackers (16) arrived at the same correction factor by assuming that the solvent completely fills the pore but that the solute is excluded from a cylindrical shell near the pore wall, Figure 1.1b.

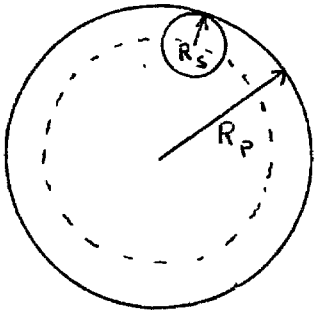

Figure 1.1a

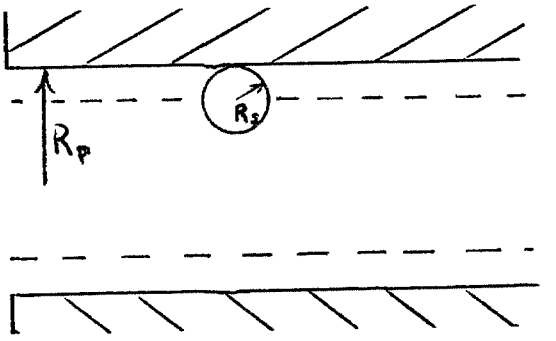

Figure 1.1b

A second correction used by Lane (17), Pappenheimer (18), and Renkin (12) was to include the frictional effect between a solute molecule, moving in a pore, and the pore wall. One form of this correction was derived by Faxen (19). He studied the problem of a spherical particle settling in a fluid filled cylinder. His equation is

$$A_p/A_o = 1 - 2.104\,\frac{R_s}{R_p} + 2.09\left(\frac{R_s}{R_p}\right)^3 - 6.95\left(\frac{R_s}{R_p}\right)^5 \tag{1.6}$$

Renkin used equation (1.7) which combines the frictional effect of

(1.6) and the exclusion effect of (1.5).

$$A_p/A_o = (1 - R_s/R_p)^2\left[1 - 2.104\,\frac{R_s}{R_p} + 2.09\left(\frac{R_s}{R_p}\right)^3 - 6.95\left(\frac{R_s}{R_p}\right)^5\right] \tag{1.7}$$

Substituting (1.7) into (1.2) yields the generalized equation for solute transport across a porous membrane.

$$\frac{dQ}{dt} = -\frac{dc}{dx}\,D\left(1 - \frac{R_s}{R_p}\right)^2\left[1 - 2.104\,\frac{R_s}{R_p} + 2.09\left(\frac{R_s}{R_p}\right)^3 - 6.95\left(\frac{R_s}{R_p}\right)^5\right] \tag{1.8}$$

The validity of equation (1.8) has been verified by Beck and Schultz (20) for microporous mica membranes formed by the track etch method (see Figure 1.2).

Equation (1.8) has been cast in many forms by various authors. Pappenheimer, for example, defines an effective diffusion coefficient for diffusion in a membrane. He absorbs (1.7) into the diffusion coefficient by defining

$$\frac{D'}{D} = \frac{(1 - R_s/R_p)^2}{1 + 2.4\,\frac{R_s}{R_p}} \tag{1.9}$$

where D' is the effective diffusion coefficient in the membrane. The denominator on the right hand side of equation (1.9) is the correction of Ladenburg (21). Ladenburg's correction is essentially the same as Faxen's except that it is not as accurate.

Kedem and Katchalsky write the equation for solute flow through

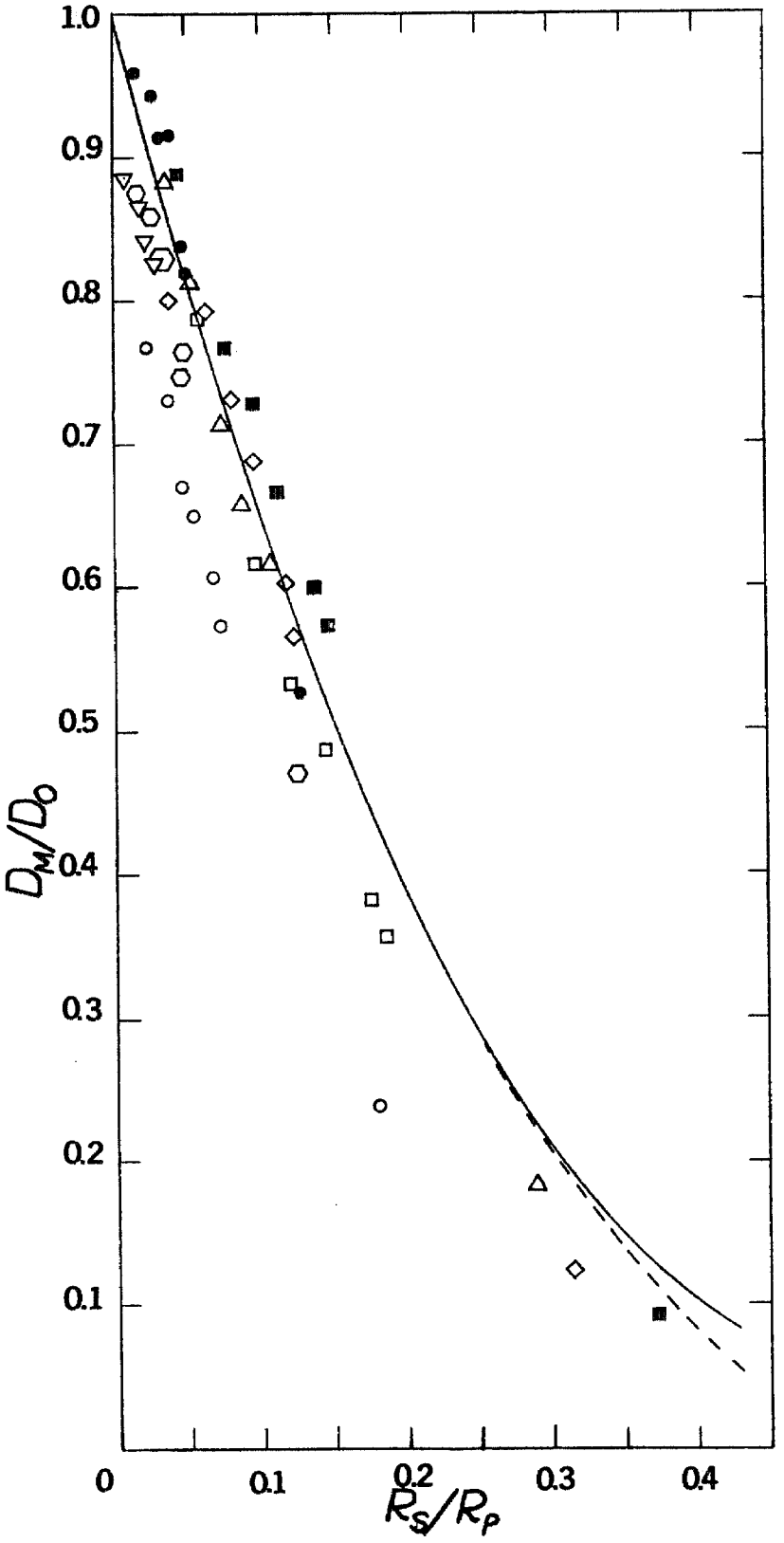

Figure 1.2. Ratio of the membrane diffusion coefficient D_m to the free diffusion coefficient D_o. Equation theoretical - (1.8).

the membrane as

$$\frac{dN_s^i}{dt} = k_s A(c_s^o - c_s^i) \tag{1.10}$$

where the subscript s denotes solute and the superscripts o and i denote the outer and inner compartment, respectively. The solute permeability constant is k_s and dN_s^i/dt is the number of moles of solute entering the inner compartment per unit time.

For the volume flow Kedem and Katchalsky write

$$\frac{dV^i}{dt} = k_w' A(\pi^i - \pi^o) \tag{1.11}$$

where π is the osmotic pressure. Equation (1.11) may be written in the same form as (1.10) by replacing π by RTc, assuming the total volume flow to be mainly the flow of the solvent, and then absorbing RT into the solvent permeability coefficient k_w'. The result is

$$\frac{dV^i}{dt} = k_w A(c_s^i - c_s^o) \tag{1.12}$$

where c is now the osmotic concentration.

By Starling's hypothesis (22) there is no difference between a hydrostatic or osmotic pressure difference as far as the volume flow is concerned. Therefore (1.12) may be generalized to

$$\frac{dV^i}{dt} = k_w' A(\Delta P - \Delta\pi) \tag{1.13}$$

where $\Delta P = P^o - P^i$ and $\Delta\pi = \pi^o - \pi^i$.

The molecular sieve theory predicts that transport across a

membrane will depend on membrane thickness, the pore size and shape, the solute size and shape, the free diffusion coefficient of the solute, and the concentration gradient. It should be remembered that the equations given here are valid only for ideal solutions and constant diffusion and permeability coefficients. The pore radius is an average pore radius and may depend on the method used to determine it. For nonspherical molecules the solute radius R_s is an approximation. The theory assumes the existence of discrete pores in the membrane and therefore is not likely to give meaningful results for swollen crosslinked elastomers and other membranes where discrete pores do not exist. Finally, in many cases this approach fails to predict correctly the volume flow across a membrane due to a concentration gradient. Kedem and Katchalsky have shown that this is because the molecular sieve theory contains only two of the three parameters required to characterize the solute-solvent-membrane system.

1.2a Thermodynamics of Irreversible Processes - Phenomenological *Coefficients*

After showing the insufficiency of conventional equations describing membrane transport, i.e., the molecular sieve theory, Kedem and Katchalsky (5) developed a theory based on the thermodynamics of irreversible processes and derived expressions relating the phenomenological permeability coefficients of their theory with the physical constants of other theories. In so doing they extended and modified the equations developed by Staverman (3,4) for osmotic pressure measurements so that they could treat biological permeability data. Their

derivation is followed below.

The entropy production per unit time for a two-component system, consisting of two solutions of the same solute and solvent separated by a membrane, is given by

$$\frac{d_i S}{dt} = \frac{1}{T}(\mu_w^o - \mu_w^i)\frac{dN_w^i}{dt} + \frac{1}{T}(\mu_s^o - \mu_s^i)\frac{dN_s^i}{dt} \tag{1.14}$$

where μ is the chemical potential, dN/dt is the number of moles entering the inner compartment, and w and s denote the solvent and solute, respectively.

It is often more convenient to rewrite (1.14) as the dissipation function per unit area

$$\phi = (T/A)\frac{d_i S}{dt} = (\mu_w^o - \mu_w^i)\dot{n}_w + (\mu_s^o - \mu_s^i)\dot{n}_s \tag{1.15}$$

where $\dot{n}_w$ and $\dot{n}_s$ are

$$\dot{n}_w = (1/A)(dN_w^i/dt) \quad \text{and} \quad \dot{n}_s = (1/A)(dN_s^i/dt) \tag{1.16}$$

It will be observed that in (1.15) the dissipation function is represented by a sum of products of fluxes and corresponding forces.

For ideal solutions the chemical potential may be replaced according to (1.17)

$$\begin{aligned} \mu_w^o - \mu_w^i &= \bar{V}_w \Delta P - RT\Delta c_s/c_w \\ \mu_s^o - \mu_s^i &= \bar{V}_s \Delta P + RT\Delta c_s/c_s \end{aligned} \tag{1.17}$$

where

$$\Delta c_s = c_s^o - c_s^i \tag{1.18a}$$

and c_s is defined by

$$\Delta c_s/c_s = \ln(c_s^o/c_s^i) \tag{1.18b}$$

In (1.17) and (1.18) P, R and T are as usually defined, $\bar{V}$ is a partial molar volume, and c represents a concentration. Introducing equations (1.17) and (1.18) into (1.15) and rearranging the dissipation function, equation (1.19) results.

$$\phi = (\dot{n}_w\bar{V}_w + \dot{n}_s\bar{V}_s)\Delta P + (\dot{n}_s/c_s - \dot{n}_w/c_w)RT\Delta c_s \tag{1.19}$$

Here ϕ is represented by new forces and fluxes which are:

$$\begin{aligned} X_V &= \Delta P \quad ; \quad X_D = RT\Delta c_s \\ J_V &= \dot{n}_w\bar{V}_w + \dot{n}_s\bar{V}_s \quad ; \quad J_D = \dot{n}_s/c_s - \dot{n}_w/c_w \end{aligned} \tag{1.20}$$

These new forces are those that are generally used in membrane permeability experiments. The hydrostatic pressure difference is ΔP and $RT\Delta c_s$ is the driving force in Fick's equation. The corresponding flows are the total volume flow and the relative velocity of the solute versus the solvent, J_v and J_D, respectively. J_D is a measure of the exchange flux.

The general theory of thermodynamics of irreversible processes postulates that the flows depend on all the forces in the system and, that as long as the forces are sufficiently small, the dependence is linear. Thus the relation between the J's and the X's is of the form

$$J_1 = L_{11}X_1 + L_{12}X_2 \quad ; \quad J_2 = L_{21}X_1 + L_{22}X_2 \tag{1.21}$$

The L's are the phenomenological coefficients. Onsager has shown that in many cases the matrix of phenomenological coefficients is symmetric, i.e., $L_{ij} = L_{ji}$. Some authors have stated that this "Onsager reciprocal relation" holds for any set of conjugated forces and fluxes. This is not true (23). Adopting the notation of Onsager (1.21) becomes

$$J_v = L_p \Delta P + L_{pD} RT \Delta c_s$$
$$J_D = L_{Dp} \Delta P + L_D RT \Delta c_s \qquad (1.22)$$

Since, by the second law of thermodynamics, entropy production must always be positive, the coefficients L_p and L_D must be positive while L_{pD} may take on any value subject to the constraint that $L_p L_D - L_{pD}^2 > 0$, assuming that Onsager's reciprocal relation holds.

Kedem and Katchalsky describe the significance of (1.22) as follows:

> The physical meaning of (1.22) may be seen in the following way: in very coarse membranes, volume flow and exchange flow are independent. Each of the flows is determined only by its conjugate force: J_v by the pressure gradient ΔP and J_D by the concentration gradient Δc_s. However in many less permeable membranes, the flows are interdependent and the gradient in solute concentration produces a flow, even though $\Delta P = 0$; this is known as osmotic flow. Similarly, a pressure difference causes not only a total volume flow but also a relative velocity in the solute-solvent flow — this is known as ultrafiltration. These interdependences are incorporated in the coefficient L_{pD}.

It is instructive to consider some special cases of (1.22). The volume flow at zero concentration difference measures the mechanical permeability of the membrane for a given solution. L_p is defined as the filtration coefficient and it is sufficient to completely characterize the system if the membrane is ideally semipermeable, because in

that case $\dot{n}_s = 0$.

When $\dot{n}_s = 0$, $J_v = \dot{n}_w \bar{V}_w$ and $J_D = -\dot{n}_w / c_w$. For dilute solutions $c_w = 1/\bar{V}_w$ and therefore in an ideally semipermeable membrane

$$J_D = -J_v \tag{1.23}$$

From (1.22) it is obvious that (1.23) may be written as

$$(L_p + L_{pD})\Delta P + (L_D + L_{pD})RT\Delta c_s = 0 \tag{1.24}$$

Since the only restriction on (1.24) is that $\dot{n}_s \neq 0$, it must hold for all pressures. This can only be true if

$$L_p = -L_{pD} = L_D \tag{1.25}$$

Thus, as previously stated, the ideally semipermeable membrane is characterized by L_p alone.

For a completely non-selective membrane, a hydrostatic pressure difference does not produce an exchange flow. Thus, for a non-selective membrane

$$J_D = 0 = L_{pD}\Delta P \rightarrow L_{pD} = 0 \tag{1.26}$$

For the case of a non-selective membrane, no volume flow is caused by a concentration gradient and again

$$J_v = 0 = L_{pD}RT\Delta c_s \rightarrow L_{pD} = 0 \tag{1.27}$$

In intermediate cases L_{pD} is negative and lies between 0 and $-L_p$. Only when the membrane is more permeable to the solute than to the solvent is L_{pD} positive.

Normally, the volume flow, J_v, is measured but J_D is not; $\dot{n}_s$ is measured and is given by (1.28).

$$\dot{n}_s = (J_v + J_D)c_s \quad \text{(dilute sol'n)} \tag{1.28}$$

If the volume is held constant when the solute flow is measured, the pressure across the membrane will be given by

$$\Delta P = (-L_{pD}/L_p)RT\Delta c_s \tag{1.29}$$

Introducing (1.22) and (1.29) into (1.28) gives

$$\dot{n}_s = \frac{L_pL_D - L_{pD}^2}{L_p} c_s RT\Delta c_s \tag{1.30}$$

There is still the problem of having the phenomenological coefficients in these equations. The filtration coefficient, L_p, is easily determined for almost all membranes, but L_{pD} and L_D still remain somewhat obscure. For this reason it is useful to define another set of coefficients in terms of L_p, L_{pD}, and L_D.

Staverman introduced the reflection coefficient, σ, which is defined in terms of L_p and L_{pD} by

$$L_{pD} = -\sigma L_p \tag{1.31}$$

Kedem and Katchalsky further defined the mobility of the solute, ω, as

$$\omega = \frac{L_pL_D - L_{pD}^2}{L_p} c_s = (L_D - L_p\sigma^2)c_s \tag{1.32}$$

From (1.29) it is apparent that ωRT is the proportionality constant between the solute flow at constant volume and Δc_s. Thus, ωRT is merely the permeability constant for the solute measured at constant

volume.

One may now rewrite the two most useful equations in terms of σ, ω, and L_p. Thus the equations for the total volume flow and the solute flow become

$$J_v = L_p(\Delta P - \sigma RT\Delta c_s)$$

$$\dot{n}_s = c_s L_p(1 - \sigma)\Delta P + [\omega - c_s L_p(1 - \sigma)\sigma]RT\Delta c_s \qquad (1.33)$$

or

$$\dot{n}_s = \omega RT\Delta c_s + (1 - \sigma)c_s J_v$$

The equation for J_v corresponds to (1.13) of the molecular sieve theory. These equations are identical only if $\sigma = 1$, i.e., if the membrane is impermeable to the solute. Therefore the simultaneous use of equations (1.3) or (1.10) and (1.12) or (1.13) of the molecular sieve theory is self contradictory. Comparison of equations (1.3) and (1.10) of the molecular sieve theory with (1.33) shows that they are identical only when $J_v = 0$. Therefore, for zero volume flow one has equality of the solute permeability coefficient, k_s, and ωRT.

The constants L_p, σ, and ω must now be determined in the following way. The filtration coefficient, L_p, is k'_w in (1.13) of the molecular sieve theory. For the case where there is no volume flow, $(J_v = 0)$, the coefficient of solute flow, k_s, of (1.10) equals ωRT. This leaves only the reflection coefficient, σ, to be determined. This coefficient may also be determined if the volume flow vanishes. The equation for the reflection coefficient is

$$\Delta P = \sigma RT\Delta c_s \qquad (J_v = 0) \qquad (1.34)$$

Another way of determining σ is suggested by equation (1.22) which may be rewritten as

$$J_v = L_p \Delta P - \sigma L_p RT \Delta c_s \tag{1.35}$$

The filtration coefficient, L_p, (also called the hydraulic permeability) may be determined from equation (1.35) when there is no solute concentration gradient, $\Delta c_s = 0$. The solute reflection coefficient σ may be determined from (1.35) when $\Delta P = 0$. Therefore σ is given by

$$\sigma = - \left(\frac{J_v}{L_p RT \Delta c_s} \right)_{\Delta P = 0} \tag{1.36}$$

1.2b Thermodynamics of Irreversible Processes - Frictional Coefficients

An alternative to the formal thermodynamic representation of section 1.2a is a physical interpretation of the permeability coefficients. The phenomenological coefficients of the irreversible thermodynamic approach are rewritten as frictional coefficients which present a clearer picture of what is happening in the membrane. Again the derivation of Kedem and Katchalsky (6) is followed.

Equation (1.21), where the flows are represented as a sum of products between the phenomenological coefficients and the forces, is rewritten as (1.37), where the forces are represented as a sum of products between the frictional coefficients, R_{ij}, and the flows, J_i.

$$\begin{aligned} X_1 &= R_{11} J_1 + R_{12} J_2 \\ X_2 &= R_{21} J_1 + R_{22} J_2 \end{aligned} \tag{1.37}$$

Assuming the R_{ij}'s obey Onsager's reciprocal relation and considering as before a two component solution, the flows at each point in the membrane are given by

$$\begin{aligned} J_s &= c_s v_s = dn_s/dt \\ J_w &= c_w v_w = dn_w/dt \end{aligned} \tag{1.38}$$

where the v represents a velocity, c a concentration, and the subscripts s and w stand for solute and solvent.

The forces are represented by the gradients of chemical potential as in previous theories. Thus (1.37) which is valid for each point in the membrane, becomes

$$\begin{aligned} -(d\mu_w/dx) &= R_{ww}J_w + R_{ws}J_s \\ -(d\mu_s/dx) &= R_{sw}J_w + R_{ss}J_s \end{aligned} \tag{1.39}$$

where $d\mu/dx$ is a gradient of chemical potential.

To translate the R_{ij}'s into frictional coefficients, it is assumed that the thermodynamic forces, X_i, are counterbalanced by mechanical forces, F_{ij}. Thus

$$\begin{aligned} X_s &= -F_{sw} - F_{sm} \\ X_w &= -F_{ws} - F_{wm} \end{aligned} \tag{1.40}$$

where F_{sw} and F_{sm} represent the mechanical friction between the solute, and the solvent or membrane, respectively. Similarly, F_{ws} and F_{wm} are the forces arising from mechanical friction of the solvent with the solute or membrane, respectively.

The F_{ij}'s can be represented in the following manner

$$F_{ij} = -f_{ij}(v_i - v_j) \tag{1.41}$$

The f_{ij}'s are the frictional coefficients per mole of component i and $(v_i - v_j)$ is the relative velocity of the ith component with respect to the jth component. Adopting this notation (1.40) becomes

$$\begin{aligned} X_s &= -(d\mu_s/dx) = f_{sw}(v_s - v_w) + f_{sm}v_s \\ X_w &= -(d\mu_w/dx) = f_{ws}(v_w - v_s) + f_{wm}v_w \end{aligned} \tag{1.42}$$

where the membrane has been taken as the frame of reference, i.e., $v_m = 0$. Substituting for the velocities according to (1.38) leads to

$$\begin{aligned} -(d\mu_s/dx) &= \frac{f_{sw} + f_{sm}}{c_s} J_s - \frac{f_{sw}}{c_w} J_w \\ -(d\mu_w/dx) &= -\frac{f_{ws}}{c_s} J_s + \frac{f_{ws} + f_{wm}}{c_w} J_w \end{aligned} \tag{1.43}$$

Equations (1.37) and (1.43) when compared yield (1.44)

$$\begin{aligned} R_{ss} &= \frac{f_{sw} + f_{sm}}{c_s} \quad ; \quad R_{sw} = -\frac{f_{sw}}{c_w} \\ R_{ww} &= \frac{f_{ws} + f_{wm}}{c_w} \quad ; \quad R_{ws} = -\frac{f_{ws}}{c_s} \end{aligned} \tag{1.44}$$

In order for Onsager's relation to be met (1.45) must hold.

$$f_{sw}/c_w = f_{ws}/c_s \tag{1.45}$$

Kedem and Katchalsky note that **Spiegler** (24) was able to derive (1.45) from purely mechanical considerations.

The coefficient f_{sw} is of the same nature as a friction coefficient for free diffusion f^o_{sw} given by Einstein as

$$f^{o}_{sw} = RT/D^{o} \tag{1.46}$$

where D^{o} is the free diffusion coefficient. To a first approximation f_{sw} would be independent of concentration, but f_{ws} would depend strongly on the solute concentration. Fortunately, f_{ws} can be replaced by using (1.45). Accordingly, (1.37) now becomes

$$\begin{aligned} -(d\mu_s/dx) &= \frac{f_{sw} + f_{sm}}{cs} J_s - \frac{f_{sw}}{c_w} J_w \\ -(d\mu_w/dx) &= \frac{\frac{c_s}{c_w} f_{sw} + f_{wm}}{c_w} J_w - \frac{f_{sw}}{c_w} J_s \end{aligned} \tag{1.47}$$

There is some question as to whether the Onsager reciprocal relation is valid for both the phenomenological coefficients, L_{ij} and the frictional coefficients, R_{ij}. Albright and Mills (25) suggest that the more fundamental formulation, and the more useful one, presents Onsager's linear laws in terms of the coefficients R_{ij}. In this derivation it has been assumed that the Onsager reciprocal relations hold for both the L_{ij} and the R_{ij}. It has been stated that "if the J_k and X_k are chosen from the entropy production $T\phi = \Sigma J_k X_k$, and if the linear laws $J_i = \Sigma L_{ij} X_j$ are valid, then $L_{ij} = L_{ji}$" (23,26).

Equations (1.47) are valid only at a point in the membrane. To arrive at the equations for flow across a membrane (1.47) must be integrated. The procedure is similar to that used by Laidler and Shuler in deriving their kinetic theory. To carry out this integration the osmotic pressure, π, the distribution coefficient, K_c, and the volume fraction of solvent in the membrane, ϕ_w, are introduced.

The distribution coefficient, K_c, is defined as

$$K_c = C_s^x / c_s^x \tag{1.48}$$

where C_s^x is the concentration of solute in a solution which would have the same solute chemical potential as the solute has at point x in the membrane. Because K_c is concentration dependent, an average value of K_c will be defined. This is done by introducing K and relating it to K_c by

$$K = \frac{-\int_{\pi_s^I}^{\pi_s^{II}} K_c \, d\pi_s}{\Delta\pi_s} \tag{1.49}$$

where superscripts I and II refer to the solutions separated by the membrane and $\Delta\pi_s = \pi_s^I - \pi_s^{II}$.

Kedem and Katchalsky have shown that the integrated form of (1.47) is

$$K\Delta\pi_s = -J_w f_{sw} \bar{V}_w \overline{K_c c_s} \Delta x/\phi_w + J_s(f_{sw} + f_{sm})\Delta x \tag{1.50}$$

$$\phi_w(\Delta P - \Delta\pi_s) = J_w(f_{wm} + f_{sw}\bar{V}_w \overline{K_c c_s}/\phi_w)\Delta x - J_s f_{sw}\Delta x \tag{1.51}$$

where $\overline{K_c c_s} = \int_o^{\Delta x} K_c c_s \, dx/\Delta x$ is the mean value of the solute concentration, Δx is the membrane thickness, and $\Delta\pi_s$ is the osmotic pressure difference across the membrane. In carrying out the integration to obtain (1.50) and (1.51), it has been necessary to assume that the flows are independent of x and that the friction coefficients are constant.

The purpose at the outset was to define the phenomenological coefficients ω, σ, and L_p in terms of frictional coefficients. This can be done by examining (1.50) and (1.51).

The permeability coefficient at zero volume flow, ω, is derived

from (1.50) by considering the case of zero solvent flow and then showing that the error between ω for zero water flow and ω for zero volume flow is negligible. Thus ω is given by

$$\omega = \frac{K}{\Delta x(f_{sw} + f_{sm})} \tag{1.52}$$

Insight into the meaning of (1.52) can be gained by comparing it to the molecular sieve theory. Substituting (1.52) into (1.50) under the constraint of zero solvent flow leads to

$$J_s = \frac{K\Delta\pi_s}{(f_{sw} + f_{sm})\Delta x} = \omega\Delta\pi_s \tag{1.53}$$

The molecular sieve theory gives

$$J_s = \phi_w D\Delta c_s/\Delta x \tag{1.54}$$

where D is the free diffusion coefficient which is equal to RT/f^o_{sw}. Mackay and Meares define the effective friction coefficient f^o_{sw}/ν where ν is the tortuosity factor which corrects for the fact that the pores may not go straight through the membrane. Substituting for D and $\Delta x/\nu$ for Δx gives

$$J_s = \frac{\nu\phi_w RT\Delta c_s}{f^o_{sw}\,\Delta x} \tag{1.55}$$

Even if $f_{sw} = f^o_{sw}/\nu$ there are still two fundamental differences between ω and $\nu\phi_w/\Delta x f^o_{sw}$. First, the permeability coefficient is inversely proportional to the sum of the solute-membrane frictional coefficients. While f_{sw} varies little in magnitude, f_{sm} ranges from zero or near zero for very coarse membranes, to infinity for ideally semipermeable membranes. Thus, ω will vary from values predicted

by the molecular sieve theory to zero.

The other important difference is in the inclusion of the distribution factor K. In some cases when $f_{sm} >> f_{sw}$, ω may still be large due to high values of K. Such a case would be more likely where transport across the membrane occurs by solute solution in the membrane rather than by diffusion through solvent filled pores.

Pappenheimer and Renkin define an available pore area for diffusion through membranes. They arrive at

$$J_s = DA_s \Delta c_s / \Delta x \tag{1.56}$$

which, by comparing (1.55), (1.56) and $\omega = \left(\frac{J_s}{s}\right)_{J_v=0}$ leads to

$$A_s = \frac{\omega RT \Delta x}{D} = \frac{Kf^o_{sw}}{f_{sw} + f_{sm}} \quad . \tag{1.57}$$

Assuming that in most membranes heavy water diffuses in the same manner as normal water, Kedem and Katchalsky were able to show that the ratio A_s/A_w is given by

$$A_s/A_w = \frac{Kf^o_{sw}}{v\phi_w(f_{sw} + f_{sm})} = \frac{Kf_{sw}}{\phi_w(f_{sw} + f_{sm})} \tag{1.58}$$

where A_w is the area available for the diffusion of the solvent (water in this case) through the membrane and A_s is the area available for diffusion of the solute through the membrane. Pappenheimer and Renkin also derived an expression for A_s/A_w (same as A_p/A_o discussed under the molecular sieve theory). These expressions relate the solute permeability coefficient to the area available for the solute to diffuse through the membrane.

An expression for the reflection coefficient can be obtained

from the equation for volume flow

$$J_v = L_p(\Delta P - \sigma\Delta\pi_s) \tag{1.59}$$

At zero volume flow the reflection coefficient, σ, becomes

$$\sigma = \left(\frac{\Delta P}{\Delta\pi_s}\right)_{J_v=0} \tag{1.60}$$

Again substituting zero solvent flow for zero volume flow and evaluating $\Delta\pi_s$ and ΔP from (1.50) and (1.51) yields

$$\sigma' = 1 - \frac{Kf_{sw}}{\phi_w(f_{sw} + f_{sm})} \tag{1.61}$$

where the prime on σ is a reminder that this equation is valid for zero solvent flow not zero volume flow. The relation between σ and σ' may be derived by expanding $(\Delta P - \Delta\pi_i)$ as a function of J_v at constant $\Delta\pi_s$ in the neighborhood of $J_v = 0$. This yields

$$\sigma = \sigma' - \frac{\omega\bar{V}_s}{L_p} \tag{1.62}$$

or

$$\sigma = 1 - \frac{\omega\bar{V}_s}{L_p} - \frac{Kf_{sw}}{\phi_w(f_{sw} + f_{sm})} \tag{1.63}$$

If f_{sw} differs from f^o_{sw} by only the tortuosity effect, then equation (1.63) may be written as

$$\sigma = 1 - \frac{\omega\bar{V}_s}{L_p} - \frac{\omega RT}{D\nu\phi_w/\Delta x} \tag{1.64}$$

or, using the concept of available areas, the reflection coefficient becomes

$$\sigma = 1 - \frac{\omega\bar{V}_s}{L_p} - \frac{A_s}{A_w} \tag{1.65}$$

1.2c Limits on σ

There are several special cases of equation (1.65). First, if the membrane is ideally semipermeable, then $\omega = 0$, and therefore $\sigma = 1$. Second, if the solvent and solute traverse the membrane by different paths, then $f_{sw} = 0$, i.e., there is no frictional interaction between the solute and solvent, and so

$$\sigma = 1 - \frac{\omega \bar{V}_s}{L_p} \tag{1.66}$$

Equation (1.66) may serve as a criterion for independent solute and solvent flows. When the solute and solvent do interact in traversing the membrane, σ will be smaller than the value predicted by (1.66). For a given ω and L_p σ must lie in the range

$$0 \leq \sigma \leq 1 - \frac{\omega \bar{V}_s}{L_p} \tag{1.67}$$

Below is a final comment on the number of coefficients required to describe membrane permeability. For free diffusion solute and solvent migrate relative to each other and therefore only one coefficient is needed to account for the resistance to diffusive flow. For the case where the flow is through a membrane, two more coefficients are needed, one for the interaction of the solvent with the membrane and one for the interaction of the solute with the membrane. In certain cases only one or two of these parameters may be important, but in general all three are needed. The molecular sieve theory and the kinetic theory of Laidler and Shuler (7-9) are incomplete because they involve only two of the three coefficients required.

1.3 Free Volume Theory of Diffusion

A free volume approach has been useful in treating data for the diffusion of penetrants through polymers (27-35). For a homogeneously swollen membrane no discrete pores exist. Because of the plasticizing effect of the solvent on the polymer, the macromolecules comprising the membrane have a substantial degree of mobility so that the size and shape of the "pores" change continuously. For crosslinked polymers the geometry of the polymer network sets an upper bound on the size of such pores and, hence, an upper bound on the size of the molecule that may pass through the membrane. Transport through the swollen polymer is dependent on the probability that a penetrant molecule has sufficient room to move, i.e., that it finds a hole adjacent to its location large enough to accommodate its effective diffusing volume. The diffusion process may be viewed as a series of activated jumps from one equilibrium position to the next. The size of the hole required is dependent upon the size of the penetrant and the distance that it jumps.

The parameters to be determined are the magnitude of the energy barrier the penetrant must overcome in going from the equilibrium to the activated state, the probability of forming a hole large enough to accommodate the penetrant, and the probability of finding in the swollen polymer space for such a hole.

The diffusion coefficient may be generally written as (36)

$$D = \nu \exp\left\{-F/kT\right\} = \nu \exp\left\{S/k\right\} \exp\left\{-E/kT\right\} \tag{1.68}$$

where ν is the translational oscillation frequency of the diffusing penetrant. It is related to the diffusional jump distance d and Boltzman's and Plank's constants by $\nu \simeq d^2(kT/h)$. The quantities F, S, and E are the free energy, entropy, and energy of activation for diffusion, respectively.

Statistical thermodynamics suggests that the entropy term in (1.68) can be related to the conformational probability W, for formation of a hole large enough to pass the penetrant. Cohen and Turnbull (37) and DiBenedetto and Paul (38) state that this probability W is given by

$$\exp\left\{S/k\right\} = W = \exp\left\{-V^*/V_f^o\right\} \tag{1.69}$$

where V* is a characteristic volume for the diffusion of the penetrant and V_f^o is the total free volume per unit volume of membrane. Substituting (1.69) into (1.68) yields

$$D = \nu \exp\left\{-E/kT\right\} \exp\left\{-V^*/V_f^o\right\} \tag{1.70}$$

Consider now the case of diffusion of the penetrant in the solvent. The diffusion coefficient may be written as

$$D_o = \nu \exp\left\{-E_o/kT\right\}\exp(-V^*/V_{f,1}^o) \tag{1.71}$$

where the activation energy E_o now refers to the diffusion of the penetrant in the solvent and $V_{f,1}^o$ is the free volume per unit volume for the pure solvent.

Dividing equation (1.70) by (1.71) yields an expression for the ratio of the diffusion coefficient of the penetrant in the swollen

membrane to the free diffusion coefficient of the penetrant in the swelling solvent

$$D/D_o = \frac{\nu \exp\left\{-E/kT\right\} \exp\left\{-V^*/V_f^o\right\}}{\nu \exp\left\{-E_o/kT\right\} \exp\left\{-V^*/V_{f,1}^o\right\}} \tag{1.72}$$

Yasuda et al. (31-35) simplify (1.72) by assuming that $\nu \exp\left\{-E/kT\right\}$ is a constant for highly swollen polymers in which the penetrant cannot diffuse through the polymer in the absence of the solvent.

The free volume in the swollen membrane is given by

$$V_f^o = HV_{f,1}^o + (1 - H)V_{f,p}^o \tag{1.73}$$

where H is the volume fraction of solvent in the swollen membrane and $V_{f,p}^o$ is the free volume of the unswollen polymer. Yasuda et al. also assume that, for penetrants which are not soluble in the membrane, the effective free volume is essentially the free volume associated with the swelling solvent, i.e., $HV_{f,1}^o$. Using these two assumptions equation (1.72) becomes

$$D/D_o = \exp\left\{-\frac{V^*}{V_{f,1}^o}\left(\frac{1}{H} - 1\right)\right\} \tag{1.74}$$

or

$$\ln(D/D_o) = K\left(\frac{1}{H} - 1\right) \tag{1.75}$$

where K is a constant. Equation (1.75) predicts that a plot of the diffusion coefficient of a penetrant in a homogeneously swollen polymer membrane versus $\frac{1}{H}$ should yield a straight line which extrapolates to D_o, the free diffusion coefficient of the penetrant in the solvent, at H = 1.

Several comments on the free volume theory are needed here. First, in the limit of an infinitely swollen membrane, (H = 1), both of Yasuda's assumptions certainly must hold. As the membrane becomes less highly swollen, these assumptions would be expected to hold down to some critical H. There is ample evidence that Yasuda's assumptions are valid in the range $1 \geq H \geq 0.5$. Spriggs and Gainer (39) measured the activation energy for diffusion of urea, glucose and sucrose through a hydrated (H = 0.52) Cuprophane membrane. Their data suggest that the assumption of a constant activation energy is incorrect. However, it must be remembered that Cuprophane is a rigid membrane **in which the polymer and the solvent (water) form separate phases.** The free volume theory assumes that there is no such phase separation. Also, Cuprophane has **pores of fixed size which do not change with time.**

Second, the free volume theory makes no attempt to deal with the elastic forces acting on a swollen polymer matrix. It may be viewed as a purely viscous theory.

Third, the free volume theory as expressed by equation (1.75) may **not be applied to data like those of Paul et al. (40), i.e. when the penetrant is substantially soluble in the unswollen polymer.**

Finally, there is, hidden within this approach, an implicit assumption as pointed out by Vrentas and Duda (41). The form of the free volume theory described above is, strictly speaking, valid only when the molecular weight of the solvent (solute) is equal to the molecular weight of a jumping unit of the polymer chain, which is approximately equal to the molecular weight of the monomer. This restriction is

most important in the limit of zero solvent concentration. It is unclear at this time how this restriction should be applied to diffusion through highly swollen elastomers, but the effect is likely to be small.

CHAPTER 2

EXPERIMENTAL

In this chapter the experimental procedures followed are outlined in detail. The preparation of the polymers is described, followed by an explanation of the casting techniques employed in the making of thick and thin films. A description of the different test cells and their use is provided. Other tests such as swelling and partition coefficient measurements are discussed next. Finally, the analytical methods are described.

2.1 Preparation of the polymers

Polymers were prepared by modifying the procedure of Chen, Eaton, Chang, and Tobolsky (1). The reasons for the modifications are described the in text.

The general reaction scheme was as follows. A poly(oxyethylene glycol) was reacted with a large excess of diisocyanate in the presence of a suitable catalyst. The resulting diisocyanate-capped poly(oxyethylene glycol) was purified and assayed to determine its isocyanate (NCO) content. A portion of the diisocyanate-capped poly-(oxyethylene glycol) was reacted overnight with a diamine present in a molar ratio of 1 to 2. Additional diisocyanate-capped poly(oxyethylene glycol) was added to bring the molar ratio to 1 to 1. The last step results in chain extension to high molecular weight.

2.1a Materials

All solvents used were analytical grade and were dried thoroughly over molecular sieves (Linde Type 5A), followed by fractional distillation in the apparatus shown in Figure 2.1. Poly(oxyethylene glycol)s were demoisturized for at least 36 hours at 60-70°C under a reduced pressure (5 to 15 mm Hg) dry nitrogen purge. This apparatus is shown in Figure 2.2. Poly(oxyethylene glycol)s 600, 1000, and 1500 were purchased from Polysciences, Inc. Poly(oxyethylene glycol) 1540 was purchased from Polysciences, Inc. and Union Carbide Corporation. Ethylene diamine was purified by fractional distillation before use. Hylene W (4,4' - dicyclohexylmethane diisocyanate) was supplied by E. I. du Pont de Nemours and Company and was used without further purification. Cincinnati Milacron Chemicals, Inc. supplied the catalyst T8 (dibutyltin bis 2-ethylhexonate) which was used without further purification.

2.1b Modifications to the procedure of Chen et al.

Two modifications were made in the diisocyanate-capping step in an effort to avoid the chain extension reported by Chen et al. (1). Instead of using a 1 to 4 molar ratio of poly(oxyethylene glycol) to Hylene W, molar ratios as high as 1 to 6.5 were used. In addition, instead of batchwise addition of the poly(oxyethylene glycol), the glycol was dissolved in methylene chloride and added dropwise over a period of approximately one hour to the reactor. These steps resulted

in less chain extension during the diisocyanate-capping reaction. Chen et al. reported products having an average of 1.5 - 1.8 polyether segments per molecule after the capping reaction. The procedure described here produces 1.02 - 1.10 polyether segments per molecule as shown in Table 2.1. Poly(oxyethylene glycol) 1500 films are discussed in section 2.1d.

TABLE 2.1

Component Polyether	Capping Reaction OH/NCO Ratio	% NCO Content Theor.	Exper.	Average # PEO Segments/Molecule
600	1 : 4.0	7.47	7.35	1.02
1000	1 : 4.2	5.51	5.25	1.05
1500	1 : 1.8	8.19	4.10	2.4
1540	1 : 6.5	4.07	3.96	1.03

2.1c Diisocyanate-capping of the poly(oxyethylene glycol)

The reactor used in the diisocyanate-capping reaction is shown in Figure 2.3. Typically, 200-300 grams of Hylene W, 1.0 gram of T8, and 500-700 ml of methylene chloride were placed in the three-neck flask, along with a Teflon encased magnetic stirrer bar. A dry nitrogen purge was started, and the magnetic stirrer turned on. After thirty minutes approximately 200 grams of a poly(oxyethylene glycol) dissolved in 300 ml of methylene chloride were placed in a separatory funnel with pressure equalizing tube and added dropwise to the reactor over a period of about one hour. The reaction mixture was allowed to stand overnight with stirring.

The following morning excess Hylene W and catalyst T8 were removed by extraction with petroleum ether. Petroleum ether (about 1 liter) was added to the stoppered flask and the contents swirled vigorously. The flask was allowed to stand until the emulsion broke; and then the top phase containing the petroleum ether, excess diisocyanate, and catalyst was decanted. A small amount (approximately 50 ml) of methylene chloride was added to the reaction flask to give a clear solution. The petroleum ether extraction and methylene chloride addition were repeated a minimum of three times. A total of 4-6 liters of petroleum ether was used to remove the excess catalyst and diisocyanate.

After purification, the diisocyanate-capped poly(oxyethylene glycol) was dried on a rotary vacuum evaporator. The material was dried at room temperature for 12-24 hours, followed by several hours at 45-55°C to drive off the last traces of Hylene W and solvent.

The purified diisocyanate-capped poly(oxyethylene glycol) was assayed for NCO content by the method reported by David and Staley (2). Typical assay results are shown in Table 2.1 under "NCO content, experimental." The purified diisocyanate-capped poly(oxyethylene glycol) was stored in a sealed aluminum foil covered flask in a desiccator until used.

2.1d Double-capping and chain extension

Once the NCO content of the diisocyanate-capped poly(oxyethylene glycol) is known it is possible to use a diamine to either double-cap

the diisocyanate-capped glycol or to chain extend it. To double-cap, a molar ratio of 1 to 2 of diisocyanate-capped glycol to ethylene diamine is used. If chain extension were desired the molar ratio would be 1 to 1.

Poly(oxyethylene glycol)s 600 and 1000 were double-capped and then chain extended. Poly(oxyethylene glycol) 1540 was chain extended without going through double-capping as a separate step. Poly(oxyethylene glycol) 1500 will be discussed later.

An example of a polymer produced by double-capping followed by chain extension, is the one that was made from poly(oxyethylene glycol) 1000. In a three-neck flask were placed a magnetic stirrer bar, 200 ml of dimethylformamide (DMF), and 6.93 grams of ethylene diamine. The magnetic stirrer and a dry nitrogen flow were started. From a dropping funnel 91.15 grams of diisocyanate-capped poly(oxyethylene glycol) 1000, dissolved in 400 ml of DMF, was added. The molar ratio of diamine to diisocyanate-capped polyether was approximately 2 to 1. After twenty hours, 93.50 grams of diisocyanate-capped polyether dissolved in 400 ml of DMF was added to the reaction flask. A molar ratio of 1 to 1 results, chain extension takes place immediately, and a high molecular weight polymer was produced.

An example of a polymer made without double-capping as a separate step is the one made from poly(oxyethylene glycol) 1540. In this case 4.4 grams ethylene diamine, 500 ml DMF, and a magnetic stirrer bar were placed in the reactor flask. A dry nitrogen purge and the magnetic stirrer were started. From a dropping funnel, 154.42 grams diisocyanate-capped poly(oxyethylene glycol) 1540, dissolved in 1000 ml

DMF, were added. The molar ratio of diamine to diisocyanate-capped polyether is 1 to 1 and chain extension to high molecular weight occurs immediately.

Poly(oxyethylene glycol) 1500 is a special case. This material was purchased from Polysciences, Inc. Polysciences, Inc. described this glycol in their 1973-74 catalogue as having a molecular weight range of 1300-1600, with a number average molecular weight of 1540. They failed to realize that the above is a description of the 1540 grade. The poly(oxyethylene glycol) 1500 is actually a blend of two grades, the 1540 and 300 (see Table 2.2).

Table 2.2

Polyethylene Glycol Grade	Formula Molecular Weight/Range	Hydroxyl Number	Freezing Range, °C
300	285-315	---	-15 to -8
600	500-600	170	20 to 25
1000	950-1050	99	37 to 40
1500*	500-600	210	38 to 41
1540	1300-1600	78	43 to 46

*A blend of equal parts Polyethylene Glycols 300 and 1540

The author was not aware of Polysciences' error and attempted the diisocyanate-capping reaction. After two puzzling failures a material having an NCO content of 4.1% was produced. Since the theoretical NCO content is 4.07%, the material was assumed to have been properly capped and it was chain extended to a polymer without difficulty.

As experiments on the poly(oxyethylene glycol) 1500 based

polymer progressed, it became obvious that something was wrong. The polyether was tested for hydroxyl content by the method reported by David and Staley (4). A hydroxyl number of 210 was measured. This was widely different from the 75-80 expected for a pure poly(oxyethylene glycol) 1540. Intrinsic viscosity measurements confirmed that the polyether was suspect. Current catalogues were consulted and the nature of the error discovered.

The polymer made from the poly(oxyethylene glycol) 1500 was studied even though it did not have the desired structure. Because of the presence of the low molecular weight grade 300 material, the hydroxyl number is approximately three times that of pure poly(oxyethylene glycol) 1540. As a result the hydroxyl to isocyanate ratio in the diisocyanate-capping ratio was only 1 to 1.8. Thus some chain extension occurs during the diisocyanate-capping step. The resulting material has 2.4 polyether segments per molecule.

2.2 Casting techniques

Two methods of casting films were employed, one for thick films and one for thin films. In all cases a solution of the polymer to be cast was made using DMF as the solvent. Various solution concentrations were tried but generally a 3% solution proved suitable. Solutions were filtered through a coarse glass fritted disk or through a medium glass fritted disk, whenever solution viscosity allowed.

2.2a Thin films

For thin film castings a glass plate approximately 14 by 17 inches was used. A bead of GE Silicone Rubber RTV 118 was placed about an inch in from the edge. The silicone rubber was allowed to cure thoroughly before the plate was used. To aid the release of the cast film, the plate was lightly sprayed with Miller-Stephensen MS-122 fluorocarbon release agent.

For casting a film the plate was placed on a fairly level surface and warmed to 35-40^{o}C by two heat lamps suspended two feet above the plate. After the plate had had a chance to warm for several hours, 100-200 ml of the filtered polymer solution was poured onto the leveled glass plate at its center.

The solution coated plate was covered with a dust cover and the solvent was evaporated over a period of 12-24 hours. During this time all personnel were excluded from the room in which the casting took place.

The dry film was cut with a razor blade into pieces about 4 by 6 inches. Each film section was gently removed from the glass plate and carefully inspected for any sign of defects or dust particles. About 1 film in 3 passed inspection.

2.2b Thick film castings

Thick films were considerably easier to cast. Such castings were made by dissolving 12 - 20 grams of the

desired polymer in 500-700 ml DMF and pouring the filtered solution onto a clean mercury surface in a 75 by 150 mm glass crystallizing dish. The crystallizing dish was placed in a warm vacuum oven (45-55^{o}C). A vacuum between 20 and 28 inches of Hg was maintained by an aspirator or vacuum pump. A continuous air purge carried away DMF vapors. Thick film castings took 3 to 7 days to complete and only once did a casting fail to form properly.

When the casting was free of solvent it was cut from the crystallizing dish with a razor blade and sent to the instrument shop to be cut into strips 0.200 inch wide. The individual samples, cut from a casting, were quite uniform in thickness. Samples were cut in such a way as to minimize thickness variations in any one sample. Samples were 0.020-0.040 inch thick, 0.200 inch wide, and up to 6 inches long.

2.3 Diffusion test apparatus

Two test cells were used for determining the properties of thin films of the various polymers. The modified National Bureau of Standards test cell will be discussed first along with its ancillary equipment. The other specialized cell was used to make measurements of the film hydraulic permeability and the solute reflection coefficient, and will be discussed later in this section.

2.3a Modified NBS test cell and ancillary equipment

In 1966 the National Institute of Health Artificial Kidney - Chronic Uremia program devoted a number of contracts to the development of membranes for artificial hemodialysis. As a result of this work and out of a desire to have standardized testing procedures, the National Bureau of Standards was asked to design a test system which would be widely available to all investigators by virtue of its simplicity and relatively low cost. The National Bureau of Standards designed such a cell and system and published a report describing it in 1968 (5).

The NBS cell has a test area 2 inches by 4 inches. Two identical half-cells are milled from 4 by 6 inch blocks of one inch thick Lucite. Each half-cell has an entrance and exit port, sealing lip, and flow channel. The NBS design incorporates a polypropylene mesh in the flow channel to promote turbulence and help distribute the flowing solutions uniformly across the cell.

The test cell used in this study is described below and is shown in Figure 2.4. It is constructed of Lucite with the exception of the mesh in the flow channel which is polypropylene, the "soft" seals which are 1/8 inch Tygon tubing, and the pressure taps which are 1/16 inch O.D. stainless steel tubing. It incorporates 4 modifications to the NBS design, the first of which is the inclusion of four pressure taps, one in each fluid entrance and exit port. Secondly, the thumb screws that held the NBS cell together were eliminated and mounting

plates added to each half-cell. The purposes of the mounting plates were to position the cell properly in the water bath and to align the sealing weight with the top half of the test cell.

The third modification was the addition of two external "soft" seals of Tygon tubing. Tygon tubing (0.125 O.D. - 0.0625 I.D.) was contained within a channel 0.125 inch wide by 0.120 inch deep, milled in each half-cell. The channel in the bottom half-cell was offset 1/4 inch from the channel in the top half-cell, which was 1/4 inch from the half-cell sealing lips. When the cell was assembled each Tygon tube pressed on the membrane and pushed it against the smooth test cell surface, which provided an effective seal. Because the tubing was soft it could deform easily and did not affect the spacing of the test cell halves, which was controlled by the relatively rigid half-cell sealing lips.

The presence of the two soft seals was necessitated by two factors. First, the weight which was used to clamp the half-cells together had to be light enough (less than 60 pounds) to be positioned by the experimenter. Second, the cell was contained in a water bath. If the cell was surrounded by air, surface tension at the air-water interface would prevent air from being drawn past the sealing lips. Water, however, can flow freely through even the smallest imperfection in the test cell seal.

The final modification in the NBS cell was the replacement of the straight entry ports with ports that are directed up or down at a 45^{o} angle to the plane of the half-cell. This modification allows the

membrane stretcher clamps to be positioned closer to the test cell and allows the use of a smaller section of film.

The relationship of the test cell to the rest of the equipment in the water bath is shown in Figure 2.5. Note the temperature conditioning coils in the back for the circulating test cell fluid. An elevation plan of the entire test system is shown in Figure 2.6. Details of the membrane stretcher and the clamps are shown in Figure 2.7. The membrane stretcher is large enough to stretch a 5 by 7 inch film 100% biaxially.

The water bath is made of Plexiglass and all seams were sealed with GE Silicone Rubber RTV 118. The membrane stretcher is constructed of 1/4 inch aluminum plate. All nuts, bolts, washers, and the crossarm drive screws are made of brass. All hexagonal material is stainless steel, as are the leveling screws at each corner. Clamps are made of 1/4 inch square aluminum bar stock with brass fittings and nylon rollers. The sample grips are padded with 1/16 inch thick natural rubber bonded to the aluminum with contact cement.

The water bath was maintained at a constant temperature by a home-made temperature controller, a circuit diagram of which is shown in Figure 2.8. Water bath circulation is provided by a centrifugal pump at a rate of 5 gallons per minute. Test cell circulation is provided by a Cole-Parmer tubing pump.

Temperature stability of the water bath was excellent, with the bath temperature steady to better than $\pm$ 0.01^{o}C. Temperature of the recirculating test cell fluid approaches that of the water bath several minutes after the start of a diffusion test. A typical time-temperature

plot is shown in Figure 2.9. After the first several minutes the recirculating test fluid temperature remains steady within ± 0.1°C. Control of test fluid temperature would have been better except for the wide daily swing in lab temperature, 22.5 ± 2.5°C.

The pressure drop through each half-cell was made nearly identical by raising or lowering the upper reservoirs and adjusting the height of the mouth of the test cell drain line in the lower reservoir. Pressure drop through each half-cell was 22.4 ± 0.2 cm of H_2O. Maximum pressure difference across the membrane at either the entrance or exit ports was always less than 0.2 cm of H_2O. The flow through each half-cell is about 600 ml per minute.

The test cell system was tested for leaks each time that it was assembled with a new membrane and each time it was opened to permit stretching of the membrane. A typical 24 hour leak test resulted in the recovery of 898.5 grams of water from each half-cell circulating loop. Each side of the test system was initially charged with 900 grams of water and the 1.5 gram difference represented evaporation from the reservoirs over a 24 hour period.

When the test cell circulating system was operating, the 900 gram charge was split up in the following manner. The lower reservoir of each half-cell held 375 grams initially. As samples were withdrawn from the system this charge dropped to about 320 grams. The upper reservoirs always held 280 grams each. The test cell halves and circulating lines held the remaining 245 grams. These figures, along with characteristic times, are shown in Figure 2.10. While the mixing within the system was not perfect, it was certainly thorough enough so that it

did not affect the results of the diffusion experiments.

Air bubbles in the test cell circulating system were not a problem. The only point in the circulating system where air bubbles were observed was the top half-cell entrance port near the pressure tap. These bubbles were removed with a syringe inserted into the pressure tap line. By drawing the syringe plunger back rapidly, the bubbles could be drawn into the pressure tap line.

2.3b The hydraulic permeability and solute reflection coefficient cell

The hydraulic permeability cell, see Figure 2.11, was made of Plexiglass with stainless steel tubing used for the ports. The contents were stirred by Teflon-coated magnetic spin bars driven at 600-800 rpm by external bar magnets. The membrane was supported on one side by a stainless steel screen covered with coarse filter paper. The other half-cell held a square grid of 0.010 inch diameter white polyester thread on 1/8 inch centers. The exposed membrane area was assumed to be the area enclosed by the innermost o-ring, 25.65 cm^2. The cell was sealed by placing a 30-40 Kg weight on the top half-cell. The pressure difference across the membrane was measured by a mercury manometer and the volume flux determined by measuring the displacement of the meniscus in a calibrated capillary tube.

For solute reflection coefficient measurements the stainless steel screen support was replaced by a square grid of polyester threads on 1/8 inch centers. This grid, and the matching grid in the other half-cell, was supported by a Lucite ring. Each ring had a ring of coarse

filter paper bonded to it on the side facing the membrane. When the cell was sealed these filter paper pads pressed tightly against the membrane. The exposed membrane area was taken to be the area enclosed by the filter paper rings, 20.27 cm^2.

The uncertainty in the exposed membrane area in the hydraulic permeability and solute reflection coefficient measurements is unavoidable. Measured values for Lp and σ are probably within 5% of their true values. Fortunately, the absolute values of Lp and σ are not as important as the ratio of these values for a stretched membrane versus an unstretched membrane. Since the area is the same in both stretched and unstretched membrane experiments, the ratio is correct even though the individual experimental values may not be.

To determine the volume flux induced by a concentration difference across the membrane, the following procedure was followed. Both half-cells were flushed with deaerated deionized water which was warmed to approximately the temperature of the water bath. This served to remove any air bubbles that might have entered the half-cells as well as to flush out any traces of solute from a previous experiment. The top half-cell was connected to a calibrated capillary tube which was mounted at the same level as the membrane. The bottom half-cell effluent line was placed in a beaker of water and the water level adjusted to be 2-3 mm higher than the level of the membrane. The 2-3 mm H_2O pressure gradient across the membrane caused the membrane to rest against the top half-cell thread support grid.

After about fifteen minutes the line connecting the top half-cell and the capillary was sealed, the bottom half-cell effluent line

placed in an empty beaker, and 100-120 cc of solution of known concentration injected into the bottom half-cell through the inlet line. Injection of the solution takes about 50-70 seconds. The injected volume is five to six times the volume of the bottom half-cell. The temperature of the injected solution is approximately that of the water bath. When the solution injection was completed, the inlet line was sealed, the effluent line placed in the beaker containing water, and the line connecting the top half-cell and capillary tube opened. Volume flux was determined by measuring the displacement of the meniscus in a calibrated capillary tube.

2.4 Other test procedures

In this section several very simple experiments are described.

2.4a Swelling measurements

The equilibrium swelling weight of a polymer sample in water was determined, using samples cut from thick film castings. The dry dimensions and weight of the sample were noted and the samples placed in test tubes containing deionized water. The test tubes were suspended in a constant temperature bath at 26.4°C. After 24 hours the samples were removed from the deionized water, using tweezers, and rapidly blotted dry.

The blotting procedure chosen was the following. The wet sample was placed on a double thickness of Kimwipe on a table top. The

Kimwipe was folded to cover the sample and was pressed gently against the sample, using the fingertips. This removed most of the excess water from the surface of the sample. The sample was then moved with dry tweezers to a dry spot on the Kimwipe and the blotting repeated. The excess water having been removed, the sample was transferred to a weighing bottle and weighed on a Mettler analytical balance to the nearest tenth of a milligram. This procedure gave very good results, provided that the samples were blotted with the Kimwipe quickly. With practice it was possible to transfer a sample from the constant temperature bath to a weighing bottle in ten seconds. After weighing, the sample was returned to deionized water and additional determinations of the swollen sample weight were made over the next couple of days.

A constant temperature bath was required for the swelling measurements because the equilibrium swelling ratio is temperature dependent. A drop in temperature from 25.75^{o}C to approximately 7^{o}C caused an increase of 28% in the amount of water a sample imbibed.

2.4b Partition coefficient measurements

The partition coefficient is the ratio of the amount of solute contained by the swollen polymer compared to the amount of solute contained by an equal volume of the solution with which the sample was equilibrated. To determine the partition coefficient, a swollen polymer sample was placed into a tube containing a solution of a solute at the desired concentration. The tube was suspended in a constant

temperature bath and the solution changed daily until the sample had equilibrated with the solution. This required 1 to 3 days, depending on the nature of the solute and the sample thickness. After equilibration the sample was removed from the solution, rinsed rapidly with deionized water, and transferred to a tube containing deionized water at room temperature.

After an equivalent length of time permitting desorption of the solute from the polymer, the polymer was removed and the fluid in the tube assayed to determine the concentration of solute. From the absorption and desorption solution concentrations, the weight of the solution in the sample, and the weight of deionized water placed in the desorption tube, it was possible to calculate the partition coefficient.

2.4c Strain induced changes in swelling and partition coefficient

The stretching frame shown in Figure 2.12a was used to hold the sample during tests to determine the effect of strain on the swelling ratio and the partition coefficient. The swollen sample was blotted dry and bonded to phosphor bronze tabs as shown in Figure 2.12b. Either Zip-Grip 10 (a beta-cyanoacrylate) or Krazy Glue (an alpha-cyanoacrylate) was used for bonding the sample to the tabs. Krazy Glue was preferred because it gave a more durable bond and its applicator was easier to manipulate.

Obtaining a good bond between the swollen polymer and the phosphor bronze tabs was not easy. The following six steps consistently

ensured a strong bond.

1. The sample surface needed to be dry. If the surface of a swollen sample was blotted dry and the sample was allowed to rest on a dry towel for 5-10 minutes, its surface became sufficiently dry to bond it successfully.

2. A minimum amount of glue was used.

3. The phosphor bronze tabs were cleaned by placing them in a beaker of deionized water containing several drops of concentrated sulfuric acid. After several minutes, the tabs were rinsed with deionized water, then rinsed with acetone, and allowed to dry on a paper towel.

4. The tabs were bent so as to hold the sample in slight compression. If this was not done the adhesive bond failed in tension at relatively low strains.

5. Only 2-3 mm of sample were extended between the tab prongs.

6. The bonded samples were placed between wet paper towels for 15-30 minutes with only the tabs and 1-2 mm of unbonded sample left uncovered. This allowed the bond to cure while keeping the polymer swollen.

The following method was used to measure the effect of strain on the equilibrium swelling of the polymer. The dry and swollen weights of the samples were first determined. The samples were then bonded to tabs, as described above, and mounted unstretched on a stretcher frame; they were then placed with their mounts in deionized water in the constant temperature bath. The samples and frame were removed and weighed twice daily until a good estimate of their combined weights

was obtained. Several measurements were needed because it was difficult to reproducibly blot dry the sample surface and the frame.

To weigh the sample and the frame, they were placed in a dry test tube, closed with a double thickness of aluminum foil, and weighed to the nearest tenth of a milligram on a Mettler analytical balance. The glass test tube and aluminum foil were then weighed separately and the difference was recorded. After a reliable estimate of the weight of the frame and unstretched polymer was obtained, the length of the polymer sample between the tabs was determined with a traveling microscope. The sample was then stretched by shortening the copper wire and the new tab-to-tab length determined. The stretched sample was returned to deionized water in the constant temperature bath and the weight of the sample and frame determined as before.

To measure the effect of strain on the partition coefficient, the dry and swollen weights of an unmounted sample were determined. The sample was mounted unstretched and placed in a solution of known concentration in the constant temperature bath. After equilibrating with the solution, the sample and frame were rinsed with deionized water and transferred to a tube containing a known amount of deionized water. After an equivalent length of time for desorption, the sample and frame were removed and the water in the tube was assayed for solute.

The sample length was measured with the traveling microscope and the sample stretched and remeasured. The stretched sample and frame were returned to a solution of known concentration in the constant temperature bath and the equilibration and desorption steps repeated.

The above approach for determining the effect of strain on the solute partition coefficient was unsuccessful. Experiments did not give reproducible results. For this reason a second approach was tried. Instead of straining the sample to induce it to swell, the temperature was lowered and the partition coefficient was measured as described in section 2.4b.

2.4d Tensile properties

Stress-relaxation and stress-strain curves for the polymers employed in this study were determined using either a table model or floor model Instron Universal Testing Machine. Sample grips were padded with 1/16 inch thick natural rubber when thin specimens were tested.

2.5 Analytical methods

Analytical procedures may be divided into two classes. One set of procedures was used to determine the concentration of a solute in a solution. A second set of procedures was used to characterize the materials used in making the polymers.

2.5a Solute concentration determinations

To determine the concentration of solutes, a Beckman Model DU Spectrophotometer was used in the early stages of the work. In later

work this was replaced by a Brice-Phoenix Differential Refractometer (9). The spectrophotometer has higher sensitivity than the differential refractometer but is more time consuming to use.

When using the spectrophotometer, sugar concentrations were determined by the method of Scott et al. (7), and urea was determined by the method of Brown (6). Brown's method involved adding a color reagent (p-dimethylaminobenzaldehyde) to the urea solution and measuring the absorbance of the resulting solution at 440 nm. Sugar concentrations were determined by addition of 95% sulfuric acid, reaction of the sugar with the acid at 70°C for thirty minutes, followed by measuring the absorbance of the reaction mixture at 323 nm at room temperature.

The spectrophotometric method is not without its problems. The absorbance of the urea-color indicator complex changes 0.6% per degree Celsius in the range 20-40°C (8). Because the laboratory temperature sometimes varied 5°C over a period of several hours, this temperature sensitivity sometimes created problems. Temperature did not affect the absorbance of reacted sugar solutions, but the method has limited accuracy for low concentrations (±2.5% for concentrations in the range below 20 ppm). By making multiple measurements of the concentration of every sample, it was possible to obtain an accuracy of ± 1% for both urea and the sugars.

The differential refractometer has a limiting sensitivity of 3×10^{-6} unit of refractive index difference. Since 1% aqueous solution of most low molecular weight solutes have a refractive index relative to pure water of 1.5×10^{-3}, one can measure a 0.1% (1000 ppm)

solution with an accuracy of about 2%. For this work concentration differences were kept above 4000 ppm when the differential refractometer was used.

2.5b Isocyanate methods

The only analytical procedure used regularly in the polymer preparation phase of this work was the assay of the diisocyanate-capped poly(oxyethylene glycol) for isocyanate content. This assay was made according to the method reported by David and Staley (2).

Several other procedures were used when needed. Acid Number, a measure of the acidity of a poly(oxyethylene glycol), was determined by another method reported by David and Staley (10). Hydroxyl Number, a measure of the OH content of a glycol, was measured by still another method reported by David and Staley (4). Normality of basic solutions was determined by titration against standardized HCl solutions. Standardized HCl solutions were produced by diluting concentrated hydrochloric acid to approximately 1 N and then determining the actual normality accurately by the method of Swift (11).

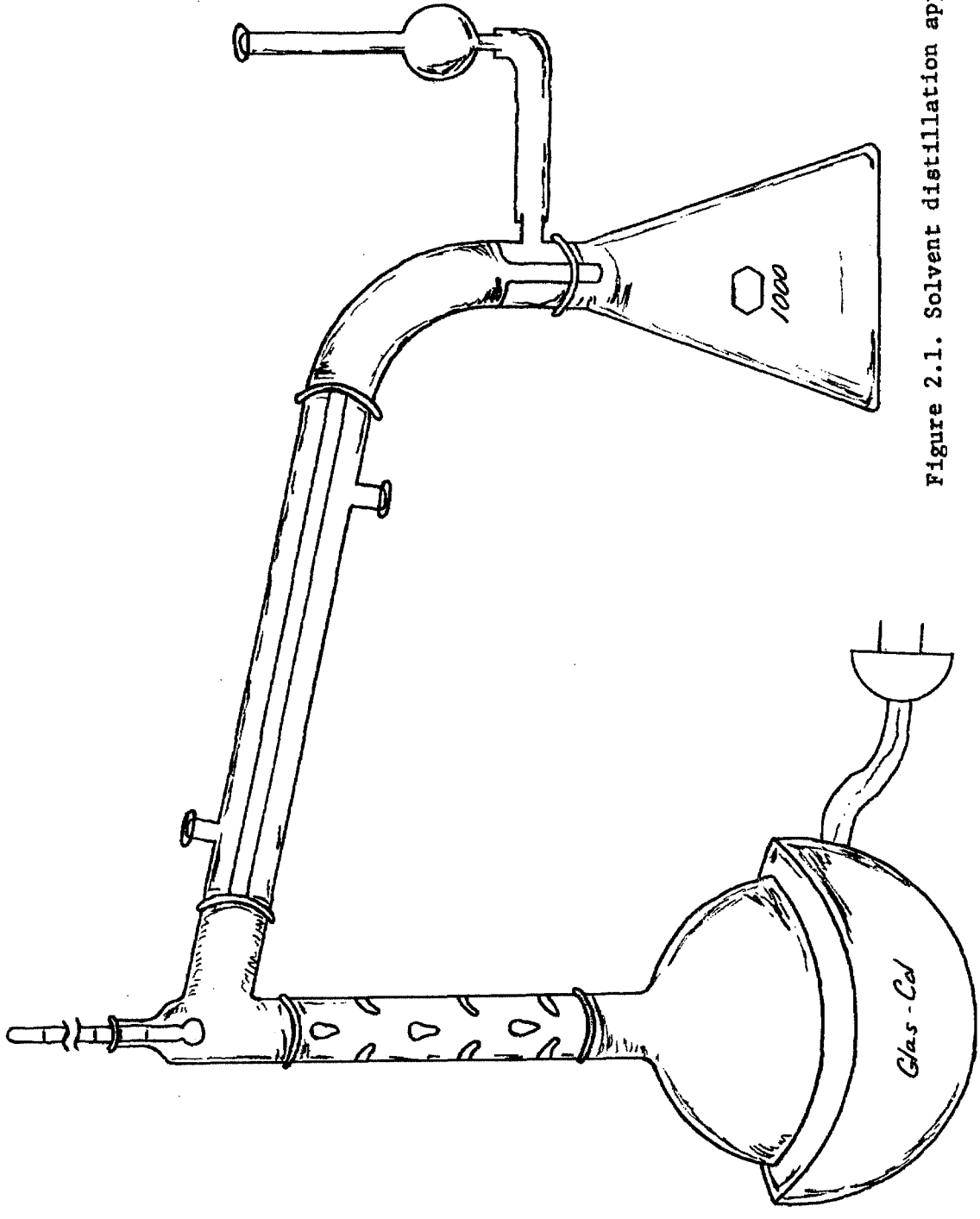

Figure 2.1. Solvent distillation apparatus.

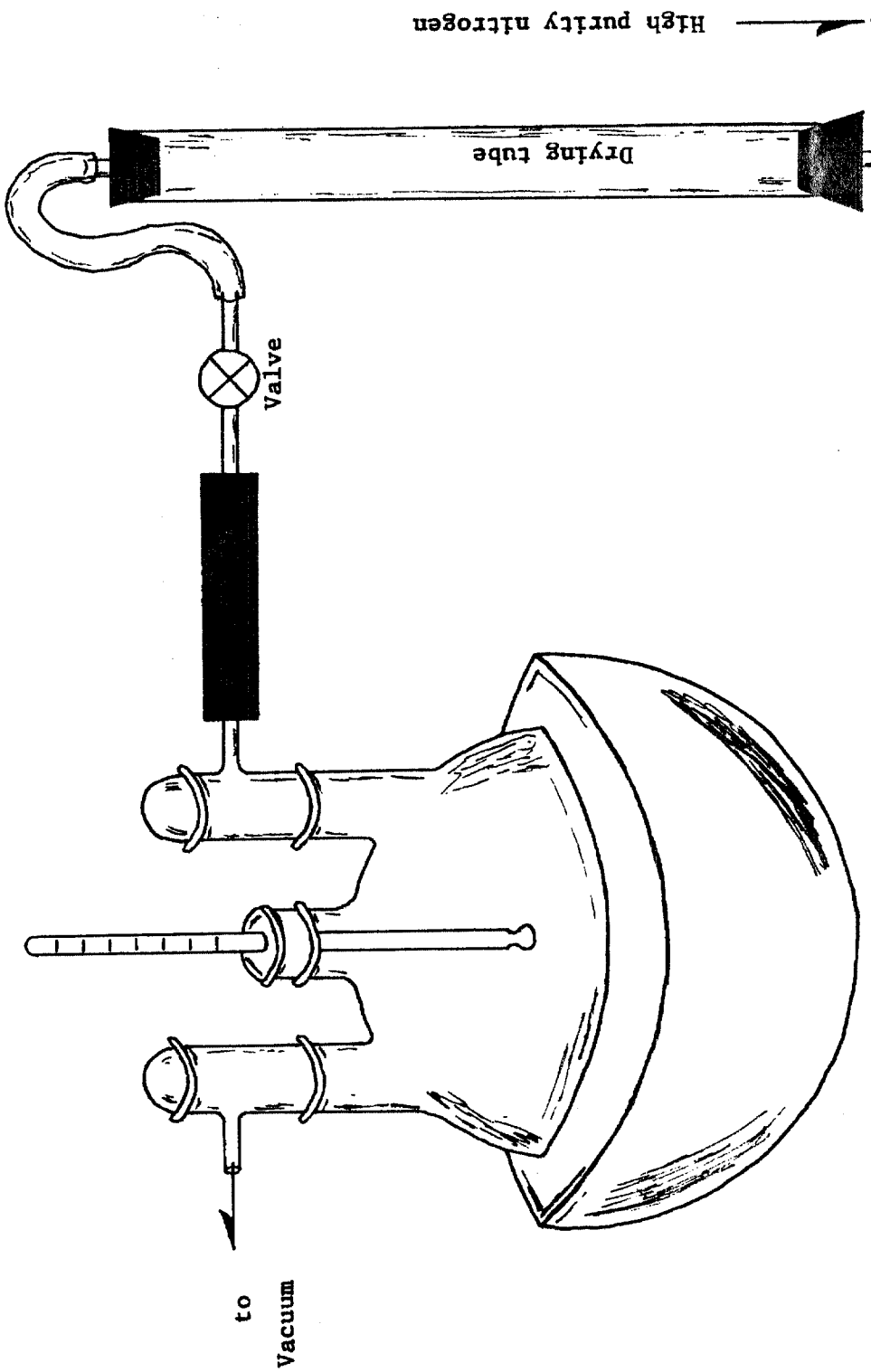

Figure 2.2. Glycol drying apparatus.

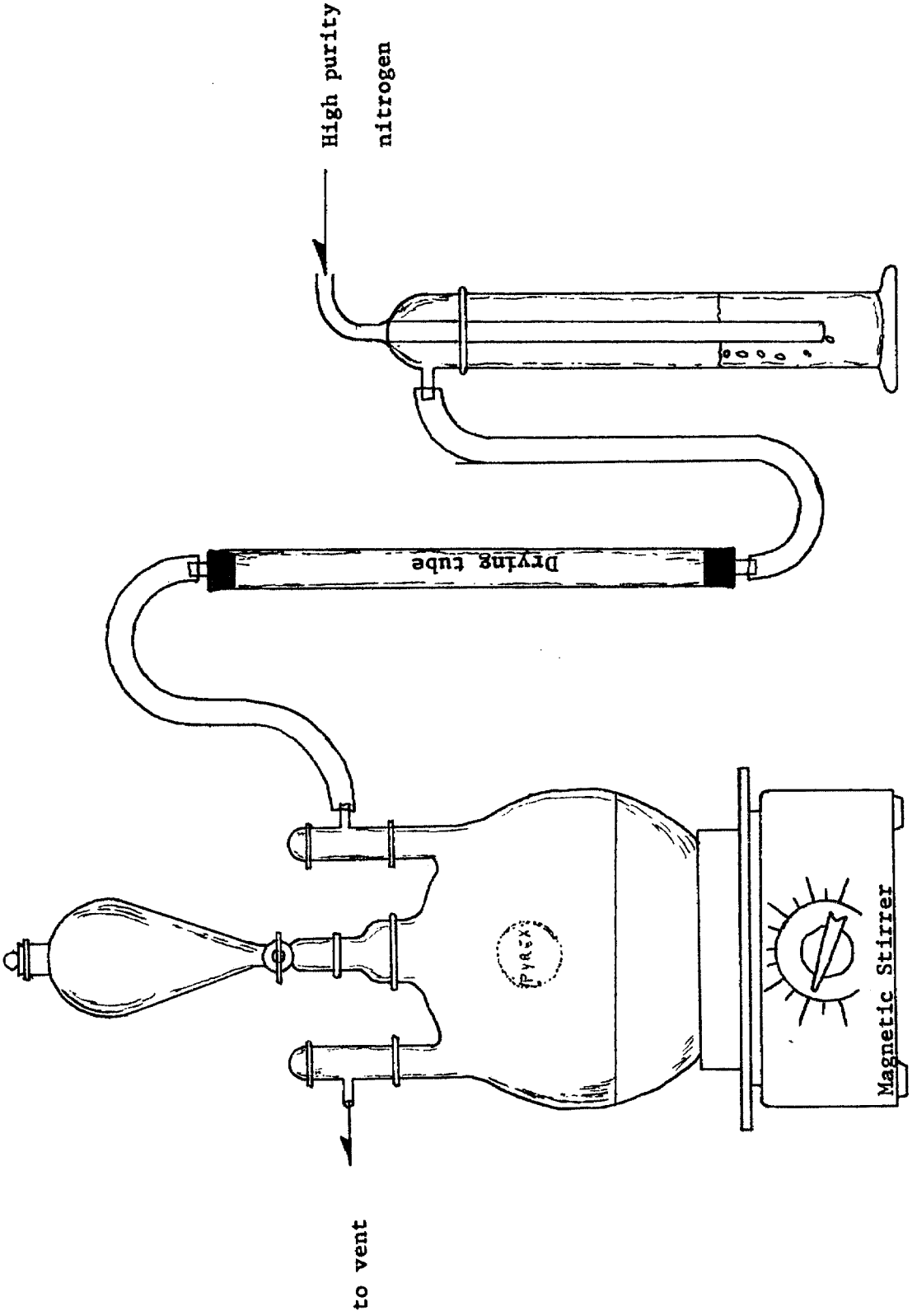

Figure 2.3. Reactor.

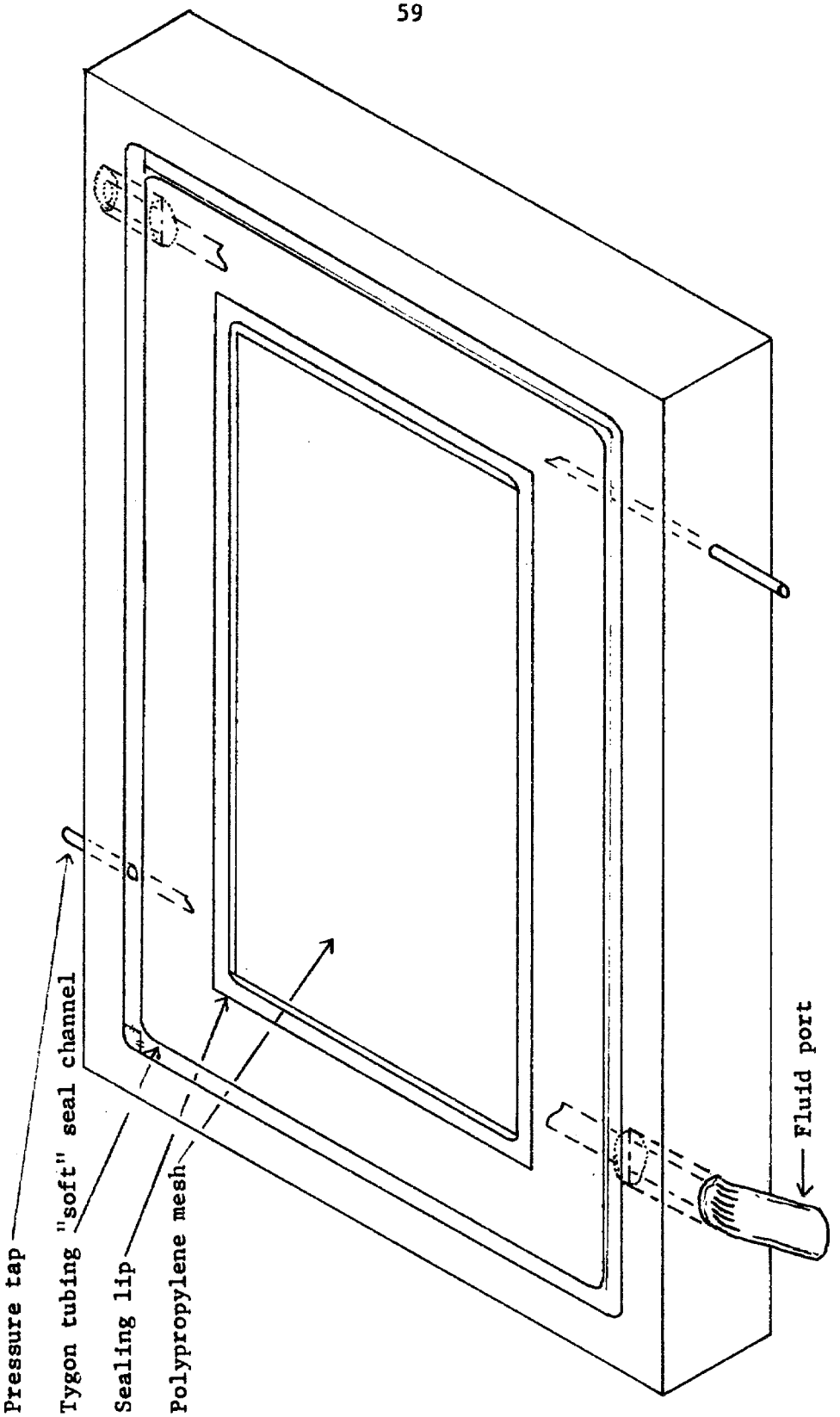

Figure 2.4. Modified NBS test cell.

Figure 2.5. Top view of the water bath.

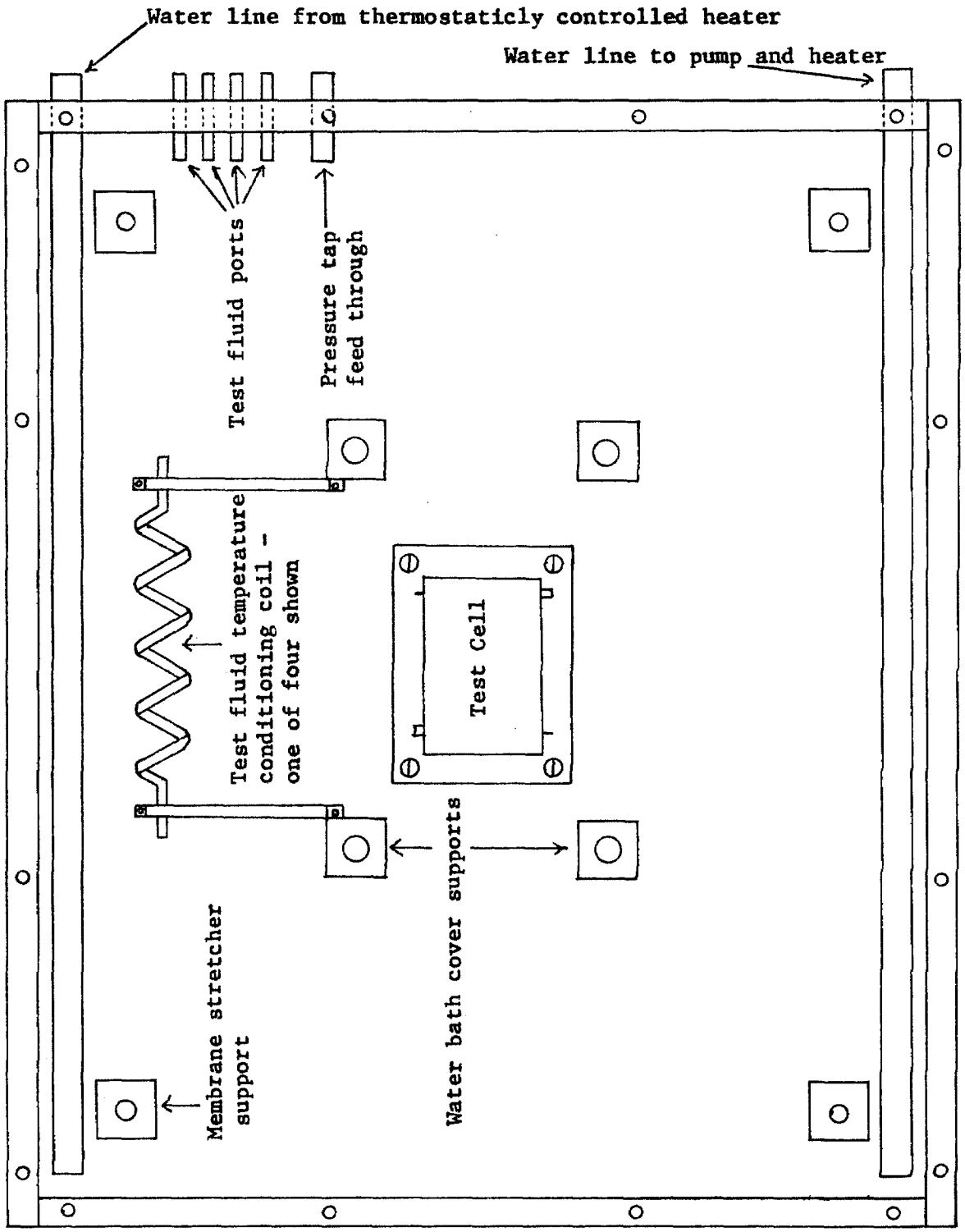

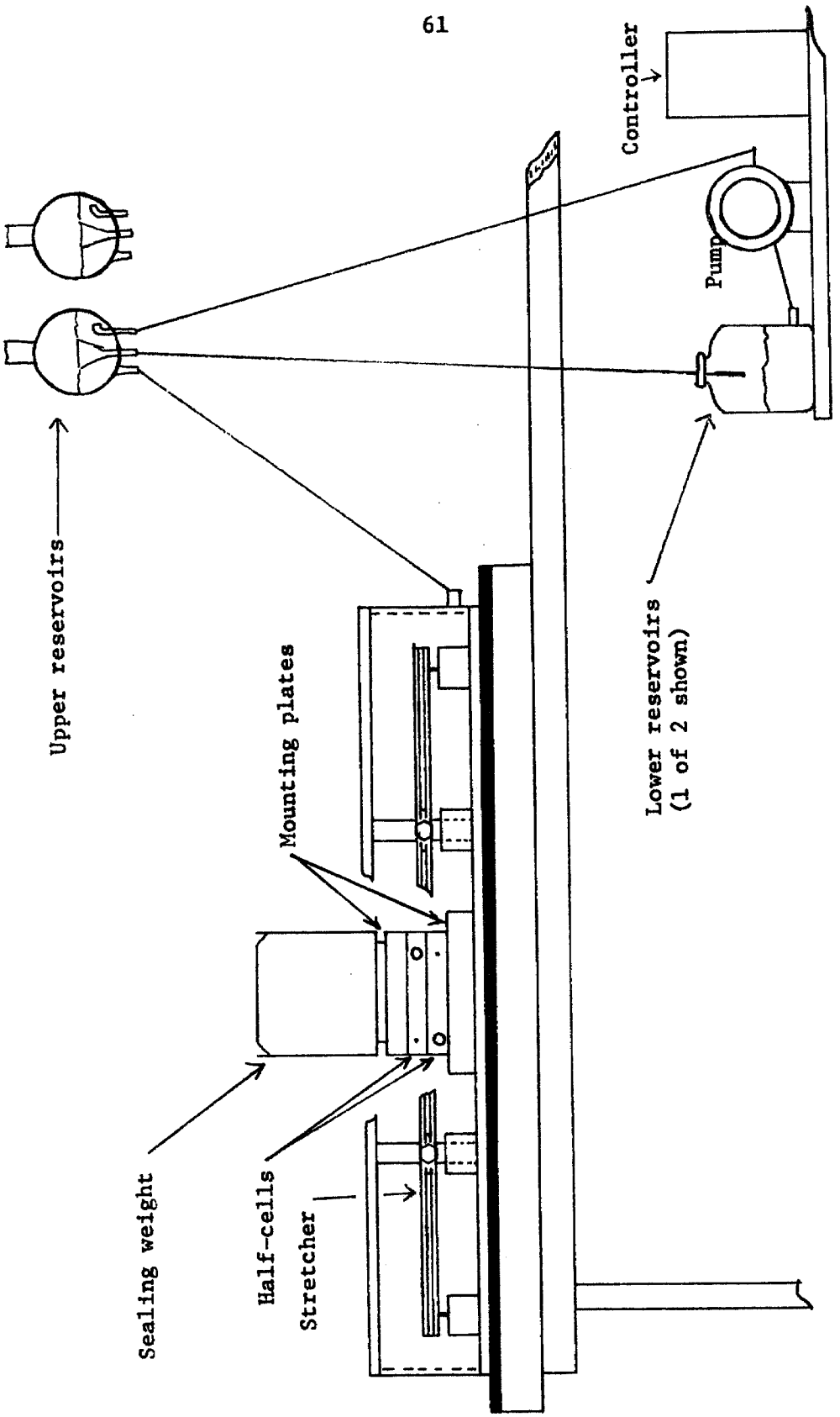

Figure 2.6. Elevation view of test system.

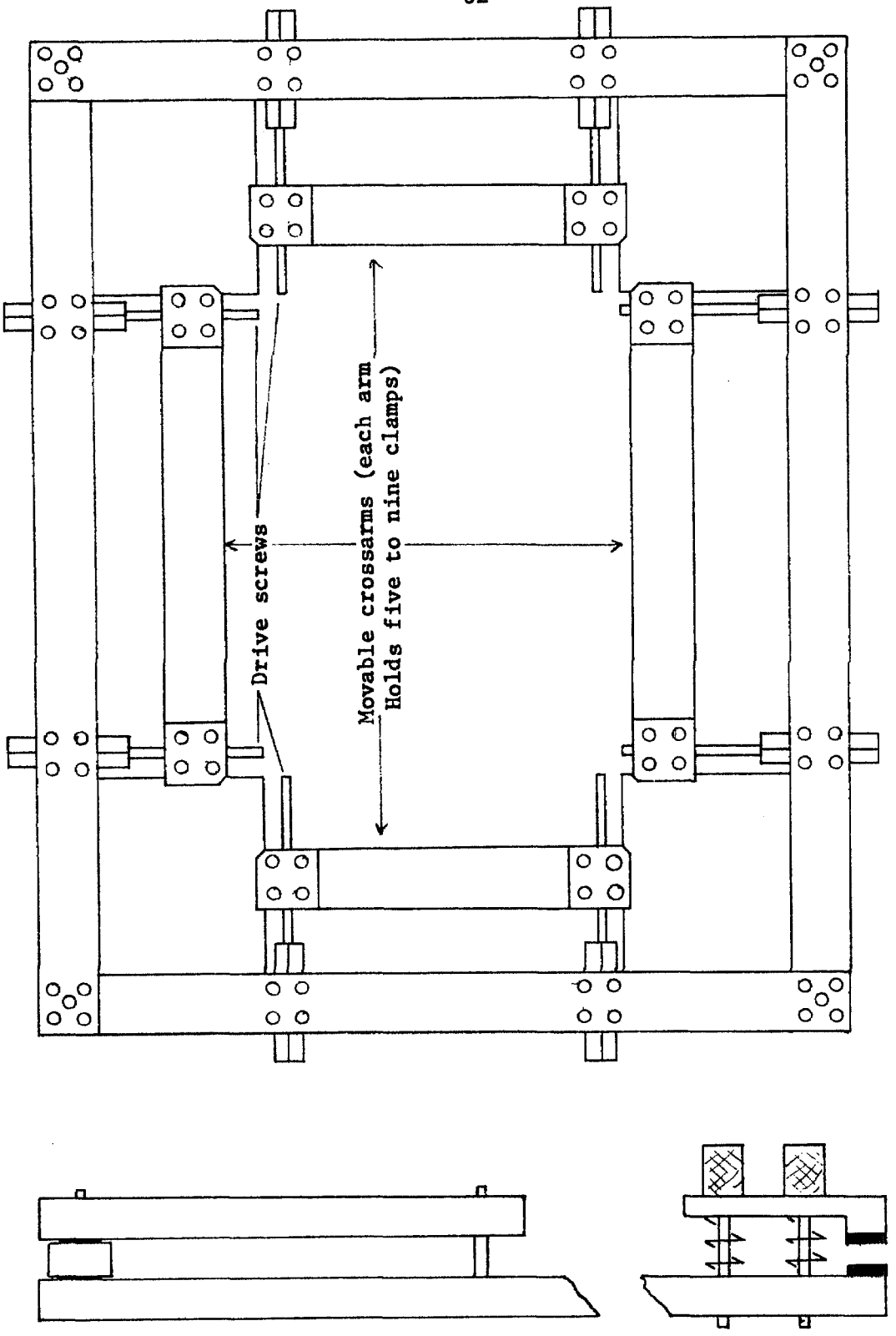

Figure 2.7. Membrane stretcher and clamp.

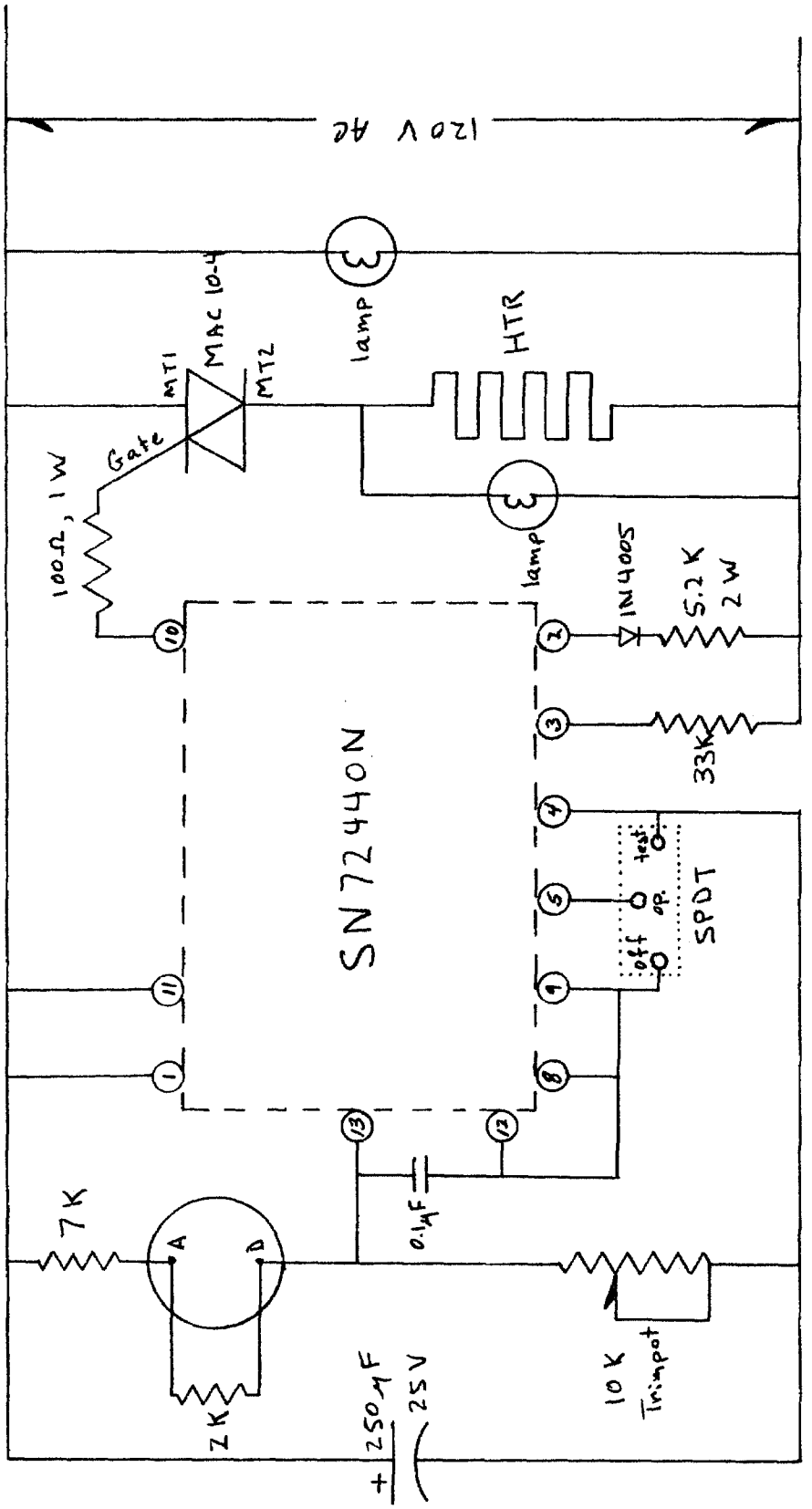

Figure 2.8. Temperature controller circuit diagram.

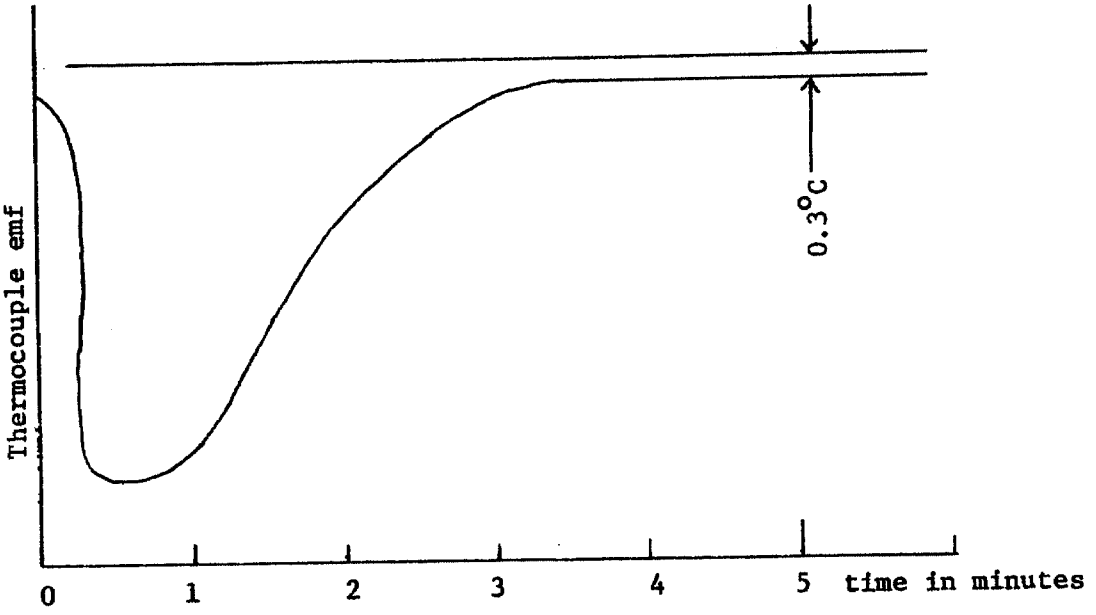

Figure 2.9. Test cell effluent temperature versus time.

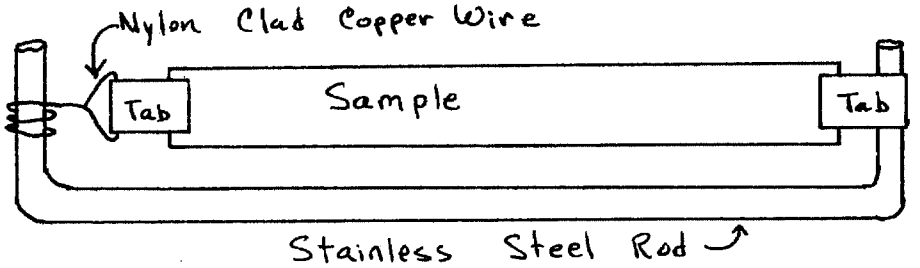

Figure 2.12a. Strain-swelling stretching frame.

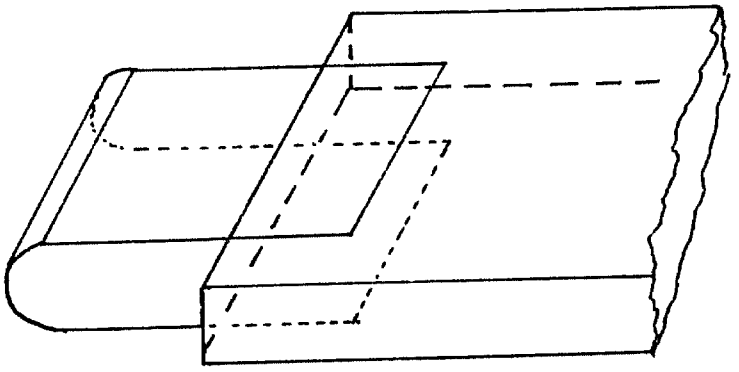

Figure 2.12b. Tab bonding detail.

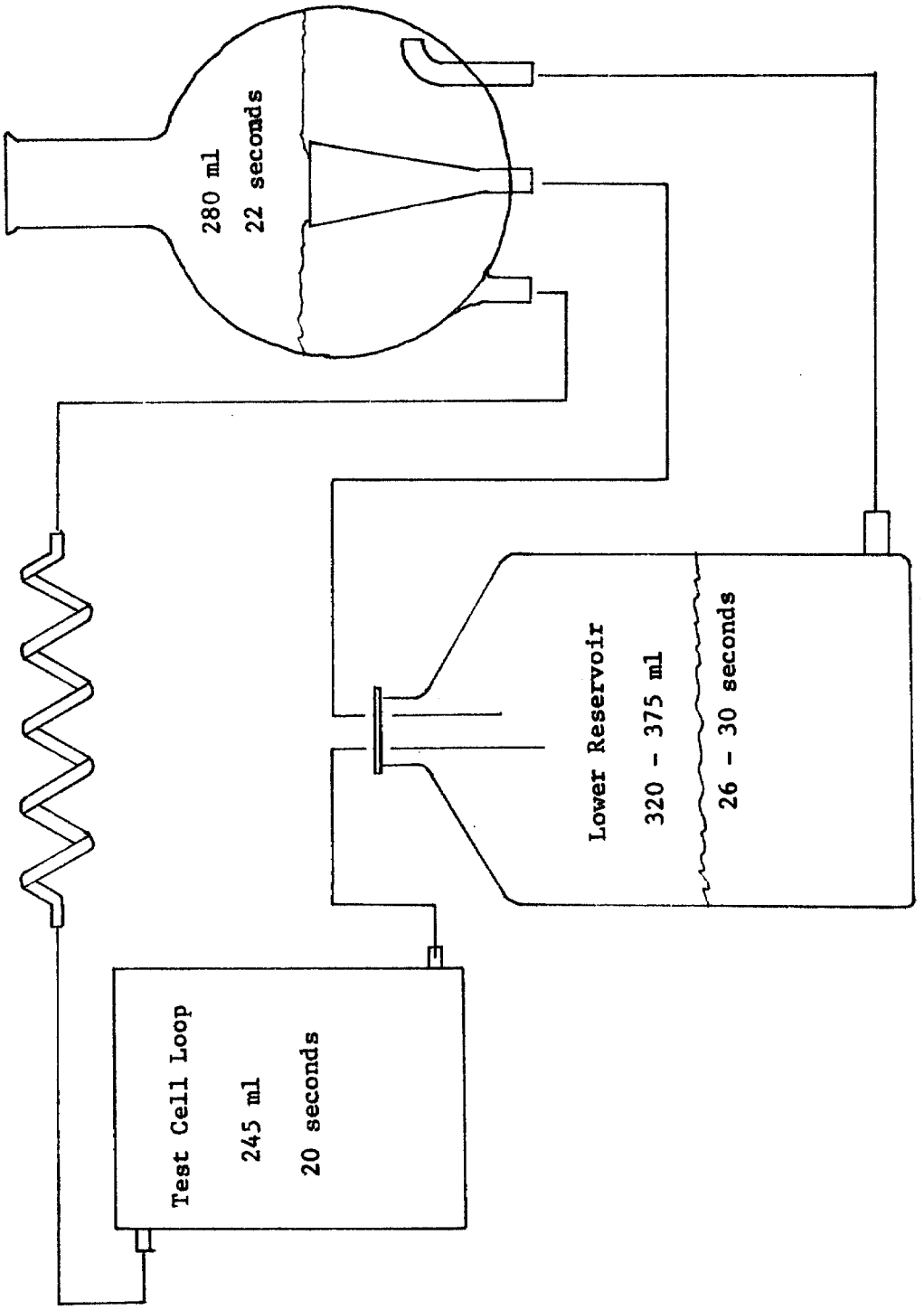

Figure 2.10. Reservoir volumes and characteristic mixing times.

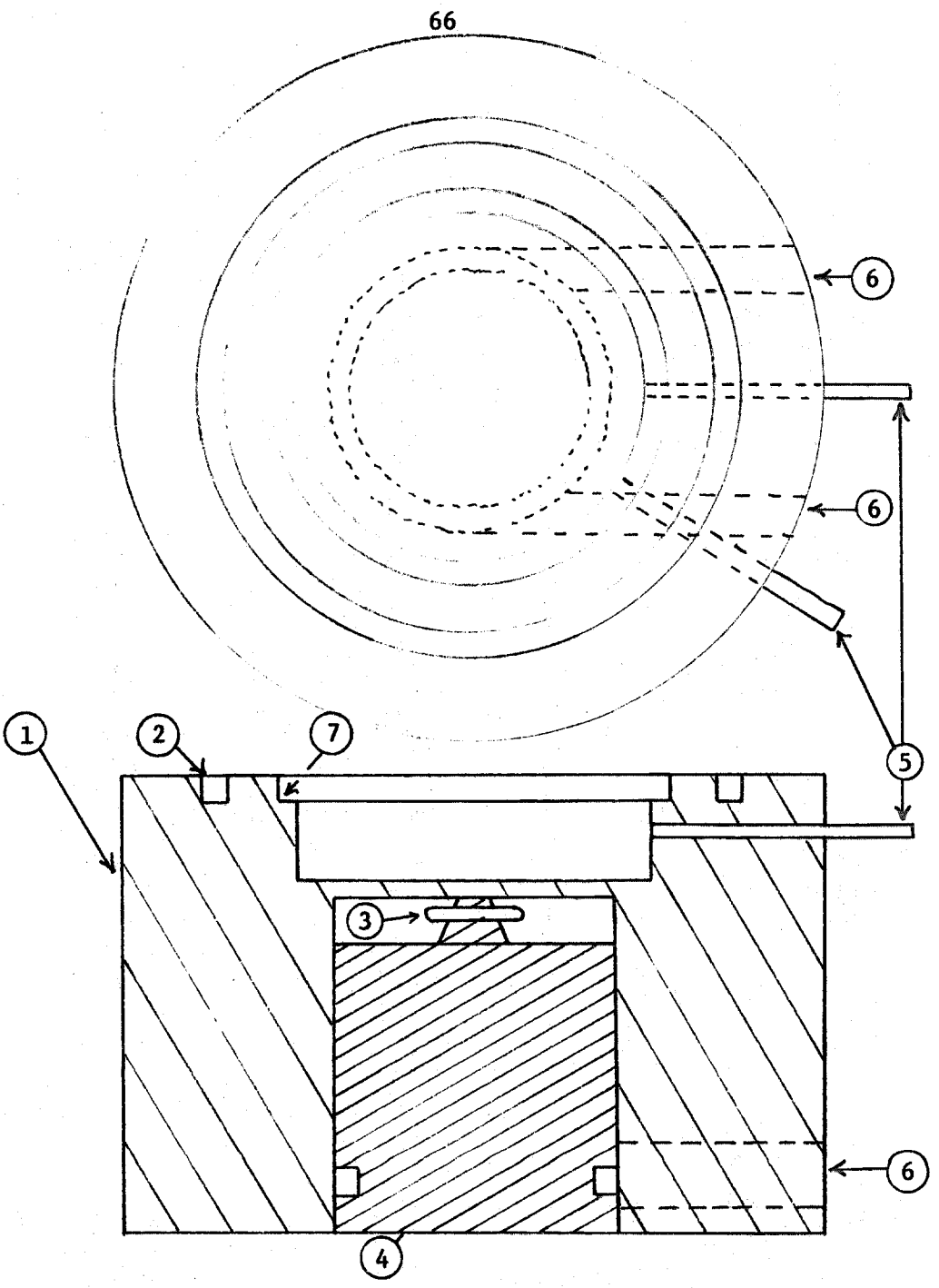

Figure 2.11. Hydraulic Permeability cell.

1. Lucite cell body
2. o-ring groove
3. magnet
4. Teflon bearing
5. fluid port
6. hole for drive belt
7. lip to support Lucite ring or pressure plate

CHAPTER 3

RESULTS

In this chapter results from the experiments conducted during this study are presented. Discussion of the data is limited to describing the probable experimental error. Some theory is included when needed to clarify the methods of handling the data.

3.1 Permeability Experiment

The analysis of data from this experiment is straightforward. It was assumed that the boundary layer resistance to diffusion was constant for each solute, that diffusion processes within the membrane were rapid enough for a psuedosteady-state Fick's law to hold, and finally that there was equilibrium at the interfaces and a constant partition coefficient. If these assumptions hold, then the solute transfer rate J at any instant is given by

$$J = \omega' RTA(c_2^L - c_1^L) \qquad (3.1)$$

where ω' is the overall permeability of the membrane and the two boundary layers, R is the gas constant, T the absolute temperature, A the exposed membrane area, and c_1^L and c_2^L the instantaneous solute concentrations in the external liquid phases. This result combined with a solute mass balance and subsequent integration yields the

working equation

$$\ln \frac{(c_2^L - c_1^L)_t}{(c_2^L - c_1^L)_0} = -\omega' RTA(1/V_1 - 1/V_2)t \qquad (3.2)$$

This equation is valid only when the test cell volumes V_1 and V_2 do not change with time.

3.1a Delay Time

When a permeability experiment is begun, the membrane initially contains no solute and some time elapses before the solute concentration gradient in the membrane reaches a psuedosteady-state. It is necessary to know how much time elapses after an experiment is begun before equation (3.2) is valid. This can be determined by solving the equation

$$\frac{\partial c}{\partial t} = D\frac{\partial^2 c}{\partial x^2} \qquad (3.3)$$

with the boundary conditions

$$\begin{aligned} c &= c_1 = 0, \quad \text{at } x = 0 \\ c &= c_2, \quad \text{at } x = \lambda \\ c &= f(x) = 0, \text{ at } t = 0 \end{aligned} \qquad (3.4)$$

This is a standard problem (1) and only the solution is given here as equation (3.5)

$$c(x,t) = c_2\frac{x}{\lambda} + \frac{2}{\pi}\sum_{1}^{\infty}\frac{c_2\cos n\pi}{n}\sin\frac{n\pi x}{\lambda}\, e^{-Dn^2 t\,\pi^2/\lambda^2} \qquad (3.5)$$

where $c(x,t)$ is the concentration at position x and time t.

The equilibrium concentration gradient is given by the first term of equation (3.5) and the deviation from the equilibrium concentration

is given by the summation. Table 3.1 presents the time that must elapse after the start of an experiment before the concentration gradient is within 1% of its psuedosteady-state value. Since the delay times are less than or approximately equal to the time at which the first data point is taken the transient conditions at the beginning of an experiment may be ignored.

3.1b Boundary Layer Resistance

The parameter of interest is the membrane permeability ω, not the experimentally determined overall permeability ω'. If the boundary layer permeability is denoted by ω_0 the following equation relating these three parameters must hold.

$$\frac{1}{\omega'} = \frac{1}{\omega} + \frac{2}{\omega_0} \tag{3.6}$$

One could further state that the boundary layer permeability is given by

$$\omega_0 = D^0/RT\delta \tag{3.7}$$

where D^0 is the diffusion coefficient of the solute in the solvent and δ is the thickness of the unstirred boundary layer. The major drawback to this approach is that the boundary layer thickness is unknown.

Another approach is to plot the reciprocal overall permeability as a function of membrane thickness and extrapolate to zero thickness. The intercept is the total boundary layer resistance R_0 or twice the reciprocal boundary layer permeability. Such a plot for poly(oxyethylene glycol) 1000 films with urea as the solute is shown in Figure 3.1.

In principle this procedure could be followed for each solute. Actually this is not possible because for the higher molecular weight solutes, the film resistance becomes so large in relation to the boundary layer resistance that the boundary layer resistance can not be accurately determined. Equation (3.7) offers a way around this problem. Assuming that the boundary layer thickness does not change with a change in solute, the ratio of the boundary layer permeabilities for urea and glucose is given by

$$\frac{\omega_0^U}{\omega_0^G} = \frac{D_U^0/RT}{D_G^0/RT} \tag{3.8}$$

The ratio of the boundary layer resistances is given by equation (3.9).

$$\frac{R_0^G}{R_0^U} = \frac{D_U^0}{D_G^0} \tag{3.9}$$

The boundary layer resistance for urea is known from Figure 3.1, and D_U^0 and D_G^0 are the urea and glucose diffusion coefficients in the solvent, respectively.

Beck and Schultz (2) show data which suggest this approach overestimates the boundary layer resistance for higher molecular weight solutes. Table 3.2 gives the boundary layer resistances used in this work, the solute diffusion coefficients in the solvent (3), and estimates of the boundary layer resistances based on the data of Beck and Schultz.

3.1c Time Shifting of the Data

During each experiment samples were withdrawn from the test cell reservoirs and assayed to determine the solute concentration. Since the samples were not returned to the system, the volume of recirculating fluid was decreased each time a pair of samples were taken. The effect of sample removal was to decrease the volume of fluid in each test cell loop and, therefore, to increase the rate of decay of the concentration difference with time over what it would have been had the sample not been taken. This can be seen clearly in equation (3.2) which is restated below.

$$\ln(\Delta c(t)/\Delta c(0)) = -\omega' RTA(1/V_1 + 1/V_2)t \qquad (3.2)$$

To account for the volume change, a simple time shift was incorporated in the computer program which was developed to determine the slope S which gave the best least squares fit of the data for equation

$$\log_{10}[\Delta c(t)/\Delta c(0)] = -St + \text{constant} \qquad (3.10)$$

The program and a sample of its output appear in Appendix II, values of S are given in Table 3.3, and typical plots of the data and equation 3.10 are shown as Figures 3.2, 3.3, 3.4, and 3.5.

3.1d Film Resistance to Diffusion

If the time t in equation 3.10 above is given in seconds, then the slope S has units of sec^{-1}. Equation (3.2) may be rewritten to give an equation for the overall resistance to diffusion in sec/cm. If the overall resistance to diffusion is denoted by R', we may write

$$\log_{10}[\Delta c(t)/\Delta c(0)] = -St = -(A/R')(1/V_1 + 1/V_2)t \qquad (3.11)$$

or, solving for R' and inserting the membrane area of 51.61 cm^2 and 900 cm^3 for both V_1 and V_2, we obtain equation (3.12).

$$R' = 0.1147/S \qquad (3.12)$$

Once the slope S which best fits the data is determined, the overall resistance to diffusion is calculated by equation (3.12). The membrane resistance to diffusion is then determined by using equation (3.13) where R_0 is the boundary layer resistance reported in Table 3.2.

$$R_{film} = R' - R_0 \qquad (3.13)$$

Values of R_{film} are reported in Table 3.3.

3.1e Film Permeability

Several different ways of reporting film permeability data have appeared in the literature (2),(4),(5). Returning to equation (3.2) it is apparent that the overall permeability ω' must have units moles/dyne-sec if the gas constant R = 8.3143 x 10^7 dyne-cm/mole-^oK is used. The units of ω, the membrane permeability, would be the same. Equation (3.14) may be used to calculate ω from R_{film}.

$$\omega = 2.303/RTR_{film} \qquad (3.14)$$

There is a problem in presenting ω in these units in that changes in the film thickness change ω. Therefore ω in Table 3.3 is normalized by the swollen film thickness y as shown in equation (3.15)

$$\omega = 2.303y/RTR_{film} \qquad (3.15)$$

and is reported in units of mole-cm/dyne-sec.

3.1f Diffusion Coefficient of the Solute in the Film

The diffusion coefficient of the solute in the swollen membrane is reported in units of cm^2/sec in the column labeled D in Table 3.3. As with the normalized permeability ω, D is most easily calculated from the known value of R_{film} by using equation

$$D = 2.303y/KR_{film} \qquad (3.16)$$

where K is the partition coefficient.

3.1g Film Thickness

The following outlines the procedure used to determine the film thicknesses reported in Table 3.4. Each film is approximately 10 by 15 cm when cut from a large film casting. Of this area, approximately the center 4 by 8 cm were exposed to the test solutions when the swollen film was clamped between the test cell halves.

Several determinations of the film thickness were made in the test area using a "Randall & Stickery" thickness gauge. The gauge has divisions every 0.001 inch, and it was possible to read it to the nearest 0.0001 inch. Figure 3.6 is a typical thickness chart showing

the dry film thickness in mils and the area enclosed by the test cell sealing lips.

The error estimates given in Table 3.4 for the dry film thickness were determined as follows. For fairly uniform films where the film thickness was measured directly, the error is ± 0.0001 inch. For uniform films that were placed between sheets of paper and the thickness determined by subtracting the papers' thickness from the total thickness, the error is ± 0.0002 inch. When the film thickness varied widely, the uncertainty in the film thickness was estimated by making several measurements over a few small areas and estimating the uncertainty from the variations observed.

Since thin sections of the film contribute more to the overall film permeability than thicker sections, the weighted average film thickness was used. The weighted average film thickness may be calculated from the measured dry film thickness y_d by equation

$$W.A.F.T. = n/[\sum_{1}^{n}(1/y_d)] \tag{3.17}$$

where n is the number of determinations of the film thickness.

The swollen film thickness is needed to calculate ω and D. The swollen film thickness y is calculated from the weighted average dry film thickness and the volume fraction of polymer v_2 at swelling equilibrium by assuming isotropic swelling and using equation

$$y = W.A.F.T./(v_2)^{1/3} \tag{3.18}$$

3.1h Estimates of Error

Errors involved in the film thickness measurement are discussed in the previous section and will not be mentioned here. The error in the film resistance to diffusion, R_{film}, is taken as the standard error in the slope, S, determined by equation (3.10) plus the uncertainty in the boundary layer resistance given in Table 3.2. The estimated error in ω and D is arrived at by adding to the estimated error in R_{film} the estimated error in the swollen film thickness. The estimated error in ω and D should be used only when comparing data obtained from experiments on different films. For comparing data obtained with the same film at different strains, the appropriate error is the error in R_{film}.

3.2 Swelling Experiments

The weight of dry and water swollen polymer samples has been determined. To be useful, this data must be converted from a weight to a volume basis. To do this, it is assumed that volume changes on mixing are negligible, i.e. that the volume of the swollen polymer-solvent system is equal to the unmixed volumes of the polymer and solvent.

3.2a Free Swelling

In Table 3.5 data for free swelling of the polymers used in this

study are presented. Polymer density was estimated by measuring the dimensions of several dry samples, weighing them, and reporting the average density. Polymer swelling data on both a weight and a volume basis are listed. Because of the structure of the polymer, it is likely that only the poly(oxyethylene glycol) portion of the polymer is swollen by water (6-9). Therefore the weight fraction poly(oxyethylene glycol) is given for each polymer along with volume swelling data calculated on the basis of the amount of poly(oxyethylene glycol) present. The density of pure poly(oxyethylene glycol)s is essentially the same as the density of the polymers formed from them (10).

3.2b Dependence of the Swelling Equilibrium on Strain

When a swollen polymer in equilibrium with the swelling solvent is subjected to a tensile stress, the amount of solvent imbibed by a given weight (volume) of polymer generally increases. If the swelling is assumed to be homogeneous, it is possible to derive equations which relate the equilibrium volume fraction of the polymer to the imposed tensile stresses and the principal extension ratios. Flory and Rehner (11) and Gee (12) considered the problem for cases of simple tension, and Treloar (13) dealt with the general case of a pure homogeneous strain. As several excellent descriptions of the problem are given elsewhere (14-16) only the appropriate equations are stated below.

For the case of simple extension we have the equation

$$\ln(1-v_2) + v_2 + \chi v_2^2 + \rho V_1/M_c\lambda_1 = 0 \qquad (3.19)$$

which may be solved for v_2 if χ and M_c are known. Here λ_1 is the principal extension ratio in the 1 direction, referred to the unswollen dimensions of the polymer sample. For a uniform two-dimensional extension ($\lambda_1 = \lambda_2$), the corresponding equation is

$$\ln(1 - v_2) + v_2 + \chi v_2^2 + \rho V_1 / M_c v_2 \lambda_1^4 = 0 \qquad (3.20)$$

while for the general case with $\lambda_2 = a\lambda_1$ where a is a constant, the equation becomes

$$\ln(1-v_2) + v_2 + \chi v_2^2 + \rho V_1 / M_c v_2 a^2 \lambda_1^4 = 0 \qquad (3.21)$$

In the above equations V_1 is the molar volume of the solvent, M_c the molecular weight between crosslinks, and χ the Flory-Huggins parameter.

Normally the Flory-Huggins parameter χ would be determined for a given polymer-solvent system by vapor pressure or osmotic pressure measurements on the swollen polymer or polymer solution. The molecular weight between crosslinks M_c would be determined from either swelling data or from the elastic modulus. This is not the approach followed here. Both χ and M_c were regarded as adjustable parameters and the strain-swelling data fit with equation (3.19). The least squares fitting program used and a sample of its output are shown in Appendix II. The values of χ and M_c and what they reveal about the polymers will be discussed in Chapter IV.

Data from the strain-swelling experiments are shown in Figures 3.7 - 3.10. Equation (3.19) is also plotted on these graphs for the

values of χ and M_c given in the column headed "Basis: Total Polymer" in Table 3.6. Also shown in Table 3.6 are values for M_f the formula molecular weight range of the poly(oxyethylene glycol)s (10).

That the value of M_c differs from that of M_f is not surprising as the polymer has been treated above as an homogeneous material which it is not. The first correction to the M_c obtained by fitting the data with equation (3.19) is made by assuming that only the poly(oxyethylene glycol) portion of the molecule is swollen by water. As these polymers are not chemically crosslinked but rather physically crosslinked through the "hard" phase (6-9), the fact that the polymers retain their strength after prolonged immersion in water indicates that the "hard" phase is not swollen appreciably by water. Since the "hard" phase behaves essentially as if it were an inert filler, the value of M_c needs to be adjusted upward to reflect the fact that only a portion of the polymer is swelling. The necessary corrections are made in v_2 and λ_1, the data computer fit, and the results listed in the column headed "Basis:Poly(oxyethylene glycol)" in Table 3.6. The adjusted data and a curve corresponding to equation (3.19) are shown in Figures 3.11 - 3.14.

A second correction to M_c is required to account for the inhomogeneous stress field that results when the poly(oxyethylene glycol) swells but the "hard" phase does not. Sternstein (17,18) has treated the problem of inhomogeneous swelling of an elastomer for the case of a single rigid spherical inclusion. The results of his work are not directly applicable to the polymers used in this study for three reasons. First, the "hard" phase domains are not isolated from one another,

second they are not infinitely rigid, and third they are probably lamella instead of spheres. Nonetheless Sternstein's approach can aid us in estimating the magnitude of the effect of the inhomogeneous stress field on swelling.

Figure 8 from Sternstein's paper (17) is reproduced here as Figure 3.15. Figure 3.15 shows that the effect of the inhomogeneous stress field is to reduce the volume swelling at the interface between the elastomer and a rigid inclusion below the free swelling value for the pure elastomer. Figure 3.16 (Sternstein's Figure 5) shows how the actual swelling differs from free swelling as a function of distance from the inclusion.

Using the molecular weight of the poly(oxyethylene glycol) as M_c we can calculate $\rho V_1/M_c$ and determine the interfacial swelling disparity for $\chi = 0.32$ and $\chi = 0.44$ from Figure 3.15. We can then estimate the interfacial swelling disparity at $\chi = 0.56$, use Figure 3.16 and the volume fraction of "hard" phase in the swollen polymer, and arrive at an estimate for the overall swelling disparity caused by the presence of the "hard" phase. These figures are reported in Table 3.7. The swelling disparity is used to correct v_2 and, through the fitting program, M_c and the result reported in Table 3.6.

The above "guesstimation" procedure is certainly not precise. It was included here to show that the effect of the inhomogeneous strain field on M_c is small. There still remains a difference between M_c and M_f in Table 3.6. This will be discussed in Chapter IV.

3.2c Predicted Swell Ratios

Equation (3.21) may be used to predict changes in the equilibrium swelling ratio when the film is stretched in the permeability experiment. The appropriate data are reported in Table 3.8. The volume swelling data, together with the weighted average dry film thickness from Table 3.4, allow the swollen film thickness to be calculated using equation (3.18). Swollen film thicknesses are reported in Table 3.4.

3.3 Partition Coefficient

The partition coefficient experiment is described in Chapter II. If the dry and swollen polymer weights are known, and the concentration of the solutions with which the polymer sample is equilibrated are determined, then the partition coefficient K^* may be calculated by

$$K^* = [(w_s - w_d) + w_e]c_e/c_a(w_s - w_d) \qquad (3.22)$$

where w_s and w_d are the swollen and dry weights of the polymer, w_e the weight of the elution fluid, and c_a and c_e the solution concentrations in the solute absorption and elution steps. The partition coefficient for the swollen polymer is then $K = K^*(1 - v_2) = K^*\phi_w$.

Data are presented in Table 3.9 for two temperatures. The swollen weight of the polymer does not change when the sample is equilibrated with glucose, sucrose, or raffinose solutions. When equilibrated with urea solutions the weight of the swollen polymer sample increases slightly.

3.4 The Hydraulic Permeability L_p and the Solute Reflection Coefficient σ

The hydraulic permeability L_p and the solute reflection coefficient σ are reported in Table 3.10. In order to determine the solute reflection coefficient it is necessary to know how the solute concentration difference across the membrane varies with time. Ginzburg and Katchalsky (5) give the equation

$$k = RTA[L_p(1 - \sigma)\sigma c^0/V_2 - \omega(V_1+V_2)/V_1V_2] \qquad (3.23)$$

where k is the time rate of change of the concentration difference, V_1 and V_2 the half cell volumes, c^0 they do not specify, and σ and L_p are as defined above. They refer the reader to a publication in press where the equation is developed but neglect to mention the journal to which the paper was submitted. A search of Chemical Abstracts and Biology Abstracts failed to produce the missing reference.

An equation similar to that of Ginzburg and Katchalsky is developed here. The theory of irreversible thermodynamics yields the following general equation for the solute flux

$$\dot{n}_s = c_s AL_p(1 - \sigma)\Delta p + [\omega - c_s L_p(1- \sigma)\sigma]RTA\Delta c_s \qquad (3.24)$$

where c_s is defined by

$$c_s = \Delta c_s/\ln(c_s^1/c_s^2) \qquad (3.25)$$

and $\Delta c_s = c_s^1 - c_s^2$. In these experiments the pressure difference was zero, the solution was placed on side one, and the solvent was placed on side two (see Figure 3.17).

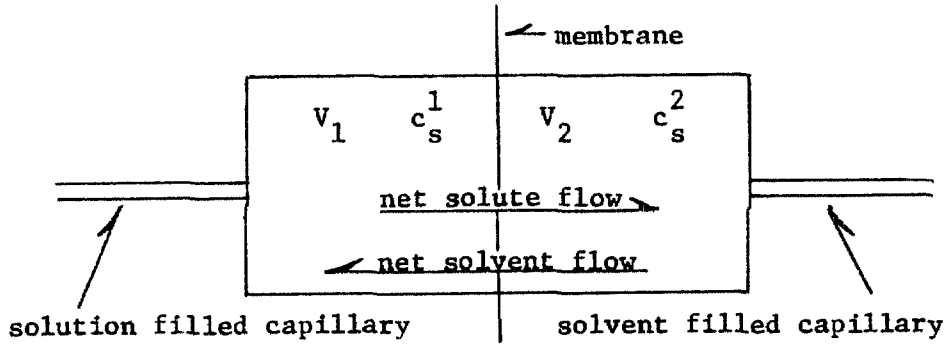

Figure 3.17 - Schematic of the σ Cell

If a psuedosteady-state equilibrium is assumed, the number of moles of solute in the membrane will not change with time and a mole balance for the solute for each half-cell may be written as shown in equations

$$N_s^1(t + \Delta t) = N_s^1(t) - \dot{n}_s \Delta t - \Delta V \bar{c}_s^1$$
$$N_s^2(t + \Delta t) = N_s^2(t) + \dot{n}_s \Delta t \qquad (3.26)$$

$N_s^1(t)$ is the number of moles of solute in half-cell 1 at time t, ΔV is the volume flux through the membrane in the time interval Δt, $\bar{c}_s^1$ is the average concentration of solute in half-cell 1 during the time interval, and $\dot{n}_s$ is the solute flux. Dividing equations (3.26) by the appropriate half-cell volume, letting $\Delta t \rightarrow 0$, and expressing the result in differential form yields

$$\frac{dc_s^1}{dt} = -\frac{RTA\Delta c_s}{V_1}[(\omega - (1-\sigma)\sigma L_p c_s) - \sigma L_p c_s^1]$$

$$\frac{dc_s^2}{dt} = \frac{RTA\Delta c_s}{V_2}[\omega - (1-\sigma)\sigma L_p c_s] \tag{3.27}$$

The difference of the two equations above yields an expression for the time rate of change of the concentration difference.

$$-\frac{d(c_s^1 - c_s^2)}{dt} = \frac{(V_1+V_2)RTA\Delta c_s}{V_1V_2}[\omega-(1-\sigma)\sigma L_p c_s] + \frac{RTA\Delta c_s}{V_1}\sigma L_p c_s^1 \tag{3.28}$$

It should be remembered that Δc_s, c_s and c_s^1 are all functions of time since they are functions of c_s^1 and c_s^2, both of which change with time. Equation (3.28) and equation (3.23) are very similar except for the presence of the extra term on the right-hand-side of equation (3.28). This term represents the dilution of the solution present on side one by the solvent flux through the membrane. In many cases this term is an order of magnitude or more greater than the first term, which gives the effect of solute diffusion through the membrane in lowering the overall concentration difference.

A computer program was written to predict the concentration difference across the membrane and the volume flux as functions of time. The program and a sample of its output are shown in Appendix II. Figures 3.18, 3.19, and 3.20 show a typical set of volume flux measurements and the computer fit.

A brief comment on the use of this computer program is needed here. The program requires an initial guess for σ in order to carry

out the calculations. Since σ is calculated from equation

$$\sigma = \frac{1.2656(\Delta V \text{ osmotic})}{(\Delta V \text{ hydraulic})\ \Delta \pi_s} \tag{3.29}$$

an estimate for σ can be made by assuming that the initial concentration difference, and therefore the initial $\Delta \pi_s$, acts throughout the experiment. By doing this one overstates $\Delta \pi_s$ and therefore underestimates σ. From the computer output a better estimate of the concentration difference across the membrane is obtained and a new value for σ may be calculated. Because of the small change in the overall concentration difference during the experiment, one run of the computer program and one recalculation of σ were all that were needed.

Theory predicts that σ should be independent of film thickness and L_p should be inversely proportional to film thickness. That this is true is shown in Figures 3.21 and 3.22.

TABLE 3.1

Time Required for Establishment of the Pseudosteady-state Concentration Profile in the Membrane

Polymer Designation	Solute	Diffusion * Coefficient $D \times 10^6$ cm^2/sec	Time in seconds** to reach 99% of the pseudosteady-state concentration profile for a film thickness of - 2.54×10^{-3}cm	5.08×10^{-3}cm	7.64×10^{-3}cm	10.16×10^{-3}cm
PEO - 600	Urea	0.3			100	170
	Glucose	0.1		130	290	510
	Sucrose	.05	70	260	580	1020
PEO - 1000	Urea	1.0				60
	Glucose	0.5				110
	Sucrose	0.3			100	170
	Raffinose	.15		90	200	340

* Approximate diffusion coefficient of the solute in the swollen membrane

** If less than 60 seconds are required no value is given

TABLE 3.1

Time Required for Establishment of the Pseudosteady-state Concentration Profile in the Membrane

Polymer Designation	Solute	Diffusion * Coefficient $D \times 10^6$ cm^2/sec	Time in seconds** to reach 99% of the pseudosteady-state concentration profile for a film thickness of - 2.54×10^{-3} cm	5.08×10^{-3} cm	7.62×10^{-3} cm	10.16×10^{-3} cm
PEO - 1500	Urea	1.0				60
	Glucose	0.5				110
	Sucrose	0.3			100	170
	Raffinose	.15		90	200	340
PEO - 1540	Urea	3.0				
	Glucose	1.5				
	Sucrose	1.0				60
	Raffinose	0.5				110

* Approximate diffusion coefficient of the solute in the swollen membrane

** If less than 60 seconds are required no value is given

TABLE 3.2

Boundary Layer Resistance to Diffusion

Solute	Diffusion * Coefficient in water at 25°C $D \times 10^6$ cm^2/sec	Boundary Layer Resistance from Equation 3.9 or Figure 3.1 R_0 sec/cm	Boundary Layer Resistance from the data of Beck & Schultz ** R_0 sec/cm
Urea	13.8	440 ± 400	440
Glucose	6.73	900 ± 800	680
Sucrose	5.21	1200 ± 1000	800
Raffinose	4.34	1400 ± 1200	900

*From Longsworth, reference (3)

**reference (2)

TABLE 3.3

Permeability and Solute Diffusion Data for Water Swollen Segmented Polyurethane Films

Polymer and/or Date Film Formed	Stretch Ratio Referred to Swollen Dimensions λ_w	λ_1	Solute	Slope $S \times 10^6$ sec^{-1}	Overall Resistance to Diffusion $R' \times 10^{-3}$ sec/cm	Film Resistance to Diffusion $R \times 10^{-3}$ sec/cm	Swollen Film Thickness cm x 10^3	Thickness Normalized Film Permeability $\omega \times 10^{18}$ mol-cm/dyne-sec	Solute Diffusivity in the Swollen Film $D \times 10^7$ cm^2/sec
PEO-600									
12-29-74	1.0	1.0	Urea	6.615±0.49	17.34±1.28	16.90±1.68	3.23±.5	17.67±4.42	8.72±2.2
			Glucose	0.592±.039	193.8±12.8	192.9±13.6		1.548±.341	3.30±.73
			Sucrose	0.182±.012	630.2±39.7	629.0±40.7		0.475±.105	1.34±.29
	1.259	0.998	Urea	9.776±0.26	11.73±0.32	11.29±0.66	2.80±.5	22.93±5.39	10.0±2.3
			Glucose	0.892±.023	128.6±3.34	127.7±4.14		2.027±.426	3.83±.80
			Sucrose	0.289±.009	396.9±12.7	395.7±13.7		0.654±.137	1.65±.34
	1.247	1.242	Urea	13.63±.068	8.415±.042	7.975±.442	2.23±.4	25.85±6.07	10.3±2.4
			Glucose	1.426±.036	80.43±2.01	79.53±2.81		2.592±.557	4.48±.94
			Sucrose	0.534±.022	214.8±9.02	213.6±10.0		0.965±.217	2.23±.50
	1.250	1.485	Urea	17.29±0.83	6.634±.318	6.196±.718	1.91±.3	28.50±6.70	10.3±2.4
			Glucose	1.987±.066	57.73±1.91	56.83±2.71		3.107±.637	4.84±1.0
			Sucrose	0.794±.029	144.5±5.20	143.3±6.20		1.232±.246	2.56±.51

TABLE 3.3 continued

Permeability and Solute Diffusion Data for Water Swollen Segmented Polyurethane Films

Polymer and/or Date Film Formed	Stretch Ratio Referred to Swollen Dimensions λ_w	λ_1	Solute	Slope $S \times 10^6$ sec^{-1}	Overall Resistance to Diffusion $R' \times 10^{-3}$ sec/cm	Film Resistance to Diffusion $R \times 10^{-3}$ sec/cm	Swollen Film Thickness cm x 10^3	Thickness Normalized Film Permeability $\omega \times 10^{18}$ mol-cm/dyne-sec	Solute Diffusivity in the Swollen Film $D \times 10^7$ cm^2/sec
PEO-600									
7-10-75	1.0	1.0	*Urea*	3.360 ± 0.04	34.14 ± 0.41	33.70 ± 0.81	6.49 ± 1.0	17.80 ± 3.20	8.79 ± 1.6
			Glucose	$0.257 \pm .018$	446.3 ± 31.2	445.4 ± 32.0		$1.347 \pm .303$	$2.88 \pm .64$
			Sucrose	$.0875 \pm .007$	$1311. \pm 101.$	$1310. \pm 102.$		$0.458 \pm .105$	$1.19 \pm .29$
PEO-1000									
8-30-74	1.0	1.0	Urea	$13.52 \pm o.31$	$8.484 \pm .195$	$8.044 \pm .595$	$5.17 \pm .6$	59.41 ± 11.3	20.1 ± 4.0
			Glucose	$2.237 \pm .076$	51.27 ± 1.74	50.37 ± 2.54		9.488 ± 1.57	8.85 ± 1.5
			Sucrose	$1.188 \pm .019$	96.55 ± 1.55	95.39 ± 2.55		$5.010 \pm .716$	$5.47 \pm .77$
			Raffinose	$.4008 \pm .006$	286.2 ± 4.29	284.8 ± 5.49		$1.678 \pm .227$	$2.86 \pm .38$
	1.246	0.996	Urea	$19.04 \pm .017$	$6.024 \pm .054$	$5.584 \pm .454$	$4.49 \pm .5$	74.33 ± 14.1	23.9 ± 4.5
			Glucose	$2.990 \pm .072$	$38.36 \pm .921$	37.46 ± 1.72		11.08 ± 1.74	9.82 ± 1.5
			Sucrose	$1.710 \pm .043$	67.08 ± 1.68	65.92 ± 2.68		$6.296 \pm .944$	$6.56 \pm .99$
			Raffinose	$.6705 \pm .006$	171.1 ± 1.56	169.7 ± 2.76		$2.446 \pm .311$	$3.98 \pm .50$
	1.239	1.249	Urea	23.76 ± 0.40	$4.827 \pm .082$	$4.387 \pm .482$	$3.93 \pm .4$	82.81 ± 17.4	25.5 ± 5.3
			Glucose	$4.334 \pm .160$	26.47 ± 0.98	25.57 ± 1.78		14.21 ± 2.42	12.1 ± 2.1

TABLE 3.3 continued

Permeability and Solute Diffusion Data for Water Swollen Segmented Polyurethane Films

Polymer and/or Date Film Formed	Stretch Ratio Referred to Swollen Dimensions λ_w	λ_1	Solute	Slope S x 10^6 sec^{-1}	Overall Resistance to Diffusion R'x 10^{-3} sec/cm	Film Resistance to Diffusion R x 10^{-3} sec/cm	Swollen Film Thickness cm x 10^3	Thickness Normalized Film Permeability ω x 10^{18} mol-cm/dyne-sec	Solute Diffusivity in the Swollen Film D x 10^7 Cm^2/sec
PEO-1000	1.239	1.249	Sucrose	2.277±.105	50.37±2.32	49.21±3.32	3.93±.4	7.382±1.233	7.36±1.2
8-30-74			Raffinose	.9596±.027	119.5±3.35	118.1±4.55		3.076±.431	4.79±.67
8-4-76	1.0	1.0	Urea	7.880±.047	14.56±.087	14.12±.487	12.41±.4	81.24±5.52	27.5±1.9
			Glucose	1.244±.032	92.20±2.40	91.30±3.20		12.56±.854	11.7±.79
			Sucrose	0.606±.012	189.3±3.79	188.1±4.79		6.099±.360	6.68±.40
			Raffinose	0.266±.010	431.2±15.5	429.8±16.7		2.669±.184	4.58±.32
	1.244	1.0	Glucose	1.843±.041	62.24±1.37	61.34±2.17	10.25±.3	15.45±.962	13.7±.84
			Raffinose	0.434±.016	264.3±9.52	262.9±10.7		3.604±.270	5.88±.45
6-20-75	1.0	1.0	Urea	17.19±.138	6.673±.053	6.233±.453	5.32±.6	78.90±14.2	26.7±4.7
			Glucose	2.998±.024	38.26±.306	37.36±1.11		13.16±1.842	12.3±1.7
			Sucrose	1.391±.011	82.46±.660	81.30±1.66		6.049±.786	6.64±.87
			Raffinose	0.623±.003	184.1±.921	182.7±2.12		2.692±.328	4.61±.51

TABLE 3.3 continued

Permeability and Solute Diffusion Data for Water Swollen Segmented Polyurethane Films

Polymer and/or Date Film Formed	Stretch Ratio Referred to Swollen Dimensions λ_w	λ_1	Solute	Slope $S \times 10^6$ sec^{-1}	Overall Resistance to Diffusion $R' \times 10^{-3}$ sec/cm	Film Resistance to Diffusion $R \times 10^{-3}$ sec/cm	Swollen Film Thickness cm x 10^3	Thickness Normalized Film Permeability $\omega \times 10^{18}$ mol-cm/dyne-sec	Solute Diffusivity in the Swollen Film $D \times 10^7$ cm^2/sec
PEO-1000									
6-23-76	1.0	1.0	Urea	$9.681^{\pm}.039$	$11.85^{\pm}.047$	$11.41^{\pm}.447$	$10.36^{\pm}1.$	$83.93^{\pm}11.75$	$28.3^{\pm}3.9$
thick			Urea	$10.15^{\pm}.041$	$11.30^{\pm}.045$	$10.86^{\pm}.445$		$88.18^{\pm}12.35$	$29.8^{\pm}4.1$
			Urea	$10.27^{\pm}.062$	$11.17^{\pm}.067$	$10.73^{\pm}.467$		$89.25^{\pm}12.50$	$30.2^{\pm}4.1$
			Glucose	$1.548^{\pm}.023$	$74.10^{\pm}1.11$	$73.20^{\pm}1.91$		$13.08^{\pm}1.635$	$12.2^{\pm}1.5$
			Glucose	$1.676^{\pm}.010$	$68.44^{\pm}.411$	$67.54^{\pm}1.21$		$14.18^{\pm}1.702$	$13.2^{\pm}1.6$
7-14-76	1.0	1.0	Urea	$14.84^{\pm}.163$	$7.730^{\pm}.085$	$7.290^{\pm}.485$	$7.22^{\pm}.3$	$91.55^{\pm}10.07$	$31.0^{\pm}3.4$
			Glucose	$2.508^{\pm}.018$	$45.73^{\pm}.320$	$44.83^{\pm}1.12$		$14.89^{\pm}.968$	$13.9^{\pm}.94$
			Sucrose	$1.196^{\pm}.012$	$95.90^{\pm}.959$	$94.70^{\pm}1.96$		$7.048^{\pm}.423$	$7.72^{\pm}.45$
			Raffinose	$0.590^{\pm}.009$	$194.4^{\pm}3.11$	$193.0^{\pm}4.31$		$3.458^{\pm}.207$	$5.92^{\pm}.36$
PEO-1500									
5-24-75	1.0	1.0	Urea	$10.74^{\pm}.118$	$10.68^{\pm}.117$	$10.24^{\pm}.517$	$5.54^{\pm}.5$	$50.01^{\pm}7.00$	$19.2^{\pm}2.6$
			Glucose	$1.926^{\pm}.058$	$59.55^{\pm}1.79$	$58.65^{\pm}2.59$		$8.732^{\pm}1.17$	$10.1^{\pm}1.4$
			Sucrose	$0.911^{\pm}.018$	$125.8^{\pm}2.52$	$124.7^{\pm}3.52$		$4.107^{\pm}.485$	$5.25^{\pm}.62$
			Raffinose	$0.397^{\pm}.015$	$288.9^{\pm}11.0$	$287.5^{\pm}12.2$		$1.781^{\pm}.235$	$3.37^{\pm}.44$

TABLE 3.3 continued

Permeability and Solute Diffusion Data for Water Swollen Segmented Polyurethane Films

Polymer and/or Date Film Formed	Stretch Ratio Referred to Swollen Dimensions λ_w	λ_1	Solute	Slope $S \times 10^6$ sec^{-1}	Overall Resistance to Diffusion $R' \times 10^{-3}$ sec/cm	Film Resistance to Diffusion $R \times 10^{-3}$ sec/cm	Swollen Film Thickness cm x 10^3	Thickness Normalized Film Permeability $\omega \times 10^{18}$ mol-cm/dyne-sec	Solute Diffusivity in the Swollen Film $D \times 10^7$ cm^2/sec
PEO-1500									
5-24-75	1.0	1.151	Urea	$13.01^{+}.169$	$8.816^{+}.115$	$8.376^{+}.515$	$5.02^{+}.5$	$55.40^{+}.892$	$20.1^{+}3.2$
			Glucose	$2.469^{+}.025$	$46.46^{+}.465$	$45.56^{+}1.27$		$10.19^{+}1.30$	$11.1^{+}1.4$
			Sucrose	$1.281^{+}.017$	$89.54^{+}1.16$	$88.38^{+}2.16$		$5.251^{+}.651$	$6.31^{+}.79$
			Raffinose	$0.620^{+}.022$	$185.0^{+}6/66$	$183.6^{+}7.86$		$2.527^{+}.361$	$4.51^{+}.64$
	1.141	1.152	Urea	$16.08^{+}.482$	$7.133^{+}.214$	$6.693^{+}.614$	$4.48^{+}.4$	$61.87^{+}10.9$	$21.4^{+}3.8$
			Glucose	$3.491^{+}.045$	$32.86^{+}.427$	$31.96^{+}1.23$		$12.96^{+}1.65$	$13.5^{+}1.7$
			Sucrose	$2.000^{+}.016$	$57.35^{+}.459$	$56.19^{+}1.46$		$7.370^{+}.855$	$8.46^{+}.97$
			Raffinose	$1.086^{+}.007$	$105.6^{+}.634$	$104.2^{+}1.83$		$3.974^{+}.990$	$6.76^{+}.73$
4-27-75	1.0	1.0	Urea	$14.47^{+}.072$	$7.927^{+}.040$	$7.487^{+}.440$	$5.31^{+}.6$	$65.56^{+}11.2$	$25.1^{+}4.2$
			Glucose	$3.176^{+}.032$	$36.10^{+}.361$	$35.20^{+}1.16$		$13.94^{+}2.04$	$16.1^{+}2.1$
			Sucrose	$2.001^{+}.162$	$57.32^{+}4.64$	$56.16^{+}5.64$		$8.740^{+}1.84$	$11.2^{+}2.4$
			Raffinose	$0.821^{+}.027$	$139.7^{+}4.61$	$138.3^{+}5.81$		$3.549^{+}.550$	$6.73^{+}1.0$

TABLE 3.3 continued

Permeability and Solute Diffusion Data for Water Swollen Segmented Polyurethane Films

Polymer and/or Date Film Formed	Stretch Ratio Referred to Swollen Dimensions λ_w	λ_1	Solute	Slope $S \times 10^6$ sec^{-1}	Overall Resistance to Diffusion $R' \times 10^{-3}$ sec/cm	Film Resistance to Diffusion $R \times 10^{-3}$ sec/cm	Swollen Film Thickness cm x 10^3	Thickness Normalized Film Permeability $\omega \times 10^{18}$ mol-cm/dyne-sec	Solute Diffusivity in the Swollen Film $D \times 10^7$ cm^2/sec
PEO-1500									
5-16-75	1.0	1.0	Urea	13.19±.145	8.696±.087	8.256±.487	5.23±.6	58.56±10.2	22.5±4.0
			Glucose	2.348±.101	48.85±2.10	47.95±2.90		10.08±1.76	11.7±2.0
			Sucrose	1.247±.025	91.98±1.84	90.82±2.84		5.323±.777	6.79±.99
			Raffinose	0.569±.011	201.6±4.03	200.2±5.23		2.415±.341	4.59±.64
7-28-75	1.0	1.0	Urea	7.975±.064	14.38±.115	13.94±.515	7.14±.6	47.35±5.78	18.2±2.2
			Glucose	1.322±.036	86.76±2.34	85.86±3.14	thickness,	7.687±.930	8.89±1.1
			Sucrose	0.595±.019	192.8±6.17	191.6±7.17	ω , and D probably	3.445±.420	4.41±.53
			Raffinose	0.280±.018	409.6±26.2	408.2±27.4	10-15% low	1.617±.246	3.07±.46
PEO-1540	used 1.29 as the partition coefficient for urea for PEO-1540 films when calculating D								
12-20-75	1.0	1.0	Urea	25.01±.200	4.586±.037	4.146±.437	7.17±.3	159.9±23.2	44.3±6.5
			Glucose	6.170±.025	18.59±.074	17.69±.874		37.19±3.42	20.5±1.9
			Sucrose	3.482±.028	32.94±.264	31.79±1.26		20.85±1.69	12.8±1.1
			Raffinose	1.809±.038	63.41±1.33	62.01±2.53		10.69±0.88	8.77±.72

TABLE 3.3 continued

Permeability and Solute Diffusion Data for Water Swollen Segmented Polyurethane Films

Polymer and/or Date Film Formed	Stretch Ratio Referred to Swollen Dimensions λ_w	λ_1	Solute	Slope $S \times 10^6$ sec^{-1}	Overall Resistance to Diffusion $R' \times 10^{-3}$	Film Resistance to Diffusion $R \times 10^{-3}$	Swollen Film Thickness cm x 10^3	Thickness Normalized Film Permeability $\omega \times 10^{18}$ mol-cm/dyne-sec	Solute Diffusivity in the Swollen Film $D \times 10^7$ cm^2/sec
PEO-1540									
12-20-75	1.211	1.002	Urea	$29.74 \pm .357$	$3.857 \pm .046$	$3.417 \pm .446$	$5.96 \pm .3$	161.2 ± 13.2	44.1 ± 7.9
			Glucose	$7.737 \pm .116$	$14.82 \pm .222$	13.92 ± 1.02		39.58 ± 4.87	21.4 ± 2.5
			Sucrose	$4.566 \pm .023$	$25.12 \pm .126$	23.95 ± 1.13		23.00 ± 2.23	14.0 ± 1.4
			Raffinose	$2.552 \pm .031$	$44.95 \pm .539$	43.55 ± 1.74		12.65 ± 1.14	$10.3 \pm .92$
	1.209	1.188	Urea	$35.70 \pm .107$	$3.213 \pm .010$	$2.773 \pm .410$	$5.01 \pm .2$	167.0 ± 31.4	45.2 ± 8.6
			Glucose	$9.559 \pm .057$	$12.00 \pm .072$	$11.10 \pm .872$		41.72 ± 4.92	22.2 ± 2.7
			Sucrose	$5.718 \pm .046$	$20.06 \pm .161$	18.90 ± 1.16		24.50 ± 2.48	14.8 ± 1.5
			Raffinose	$3.279 \pm .023$	$34.98 \pm .245$	33.58 ± 1.45		13.79 ± 1.15	$11.1 \pm .93$

used 1.29 as the partition coefficient for urea for PEO-1540 films when calculating D

TABLE 3.4

Film Thickness Data

Polymer Designation	Date Film Formed	Stretch Ratio λ_w	Stretch Ratio λ_1	Average Dry Film Thickness cm x 10^3	Weighted Average Dry Film Thickness cm x 10^3	Swell Ratio	Swollen Film Thickness cm x 10^3
PEO-600	12-29-74	1.0	1.0	$3.00 \pm .4$	$2.81 \pm .4$	1.522	$3.23 \pm .5$
		1.259	0.998	$\frac{3.180}{1.256} = 2.53 \pm .4$	$\frac{2.990}{1.256} = 2.38 \pm .4$	1.633	$\frac{3.521}{1.256} = 2.80 \pm .5$
		1.247	1.242	$\frac{3.015}{1.549} = 1.95 \pm .3$	$\frac{2.880}{1.549} = 1.86 \pm .3$	1.735	$\frac{3.461}{1.549} = 2.23 \pm .4$
		1.250	1.485	$\frac{3.028}{1.856} = 1.63 \pm .25$	$\frac{2.901}{1.856} = 1.56 \pm .25$	1.826	$\frac{3.546}{1.856} = 1.91 \pm .3$
	7-10-75	1.0	1.0	$6.02 \pm .8$	$5.64 \pm .8$	1.522	6.49 ± 1.0
	6-27-76	1.0	1.0	$6.66 \pm .3$	$6.45 \pm .3$	1.522	$7.42 \pm .4$
		1.230	1.00	$\frac{6.604}{1.230} = 5.37 \pm .3$	$\frac{6.426}{1.230} = 5.23 \pm .3$	1.621	$\frac{7.549}{1.230} = 6.14 \pm .4$
		1.225	1.169	$\frac{6.629}{1.432} = 4.63 \pm .2$	$\frac{6.477}{1.432} = 4.52 \pm .2$	1.695	$\frac{7.723}{1.432} = 5.39 \pm .3$

*Referred to swollen dimensions **From Table 3.8 or Equation 3.21 ***Based on weighted average film thickness

TABLE 3.4 continued

Film Thickness Data

Polymer Designation	Date Film Formed	Stretch Ratio* λ_w	Stretch Ratio* λ_1	Average Dry Film Thickness cm x 10^3	Weighted Average Dry Film Thickness cm x 10^3	Swell** Ratio	Swollen*** Film Thickness cm x 10^3
PEO-1000	8-30-74	1.0	1.0	$4.57 \pm .5$	$4.02 \pm .5$	2.124	$5.17 \pm .6$
		1.246	0.996	$\frac{4.910}{1.240} = 3.96 \pm .4$	$\frac{4.255}{1.240} = 3.43 \pm .4$	2.239	$\frac{5.567}{1.240} = 4.49 \pm .5$
		1.239	1.249	$\frac{5.156}{1.547} = 3.33 \pm .3$	$\frac{4.564}{1.547} = 2.95 \pm .3$	2.371	$\frac{6.086}{1.547} = 3.93 \pm .4$
	6-20-75	1.0	1.0	$4.27 \pm .5$	$4.14 \pm .5$	2.124	$5.32 \pm .6$
	6-23-76	1.0	1.0	$8.43 \pm .8$	$8.07 \pm .8$	2.124	10.36 ± 1.0
	7-14-76	1.0	1.0	$5.76 \pm .2$	$5.61 \pm .2$	2.124	$7.22 \pm .3$
	8- 4-76	1.0	1.0	$9.77 \pm .3$	$9.66 \pm .3$	2.124	$12.41 \pm .4$
		1.244	1.0	$\frac{9.863}{1.244} = 7.93 \pm .3$	$\frac{9.749}{1.244} = 7.84 \pm .3$	2.241	$\frac{12.76}{1.244} = 10.25 \pm .4$
	4-16-76	1.0	1.0	$6.68 \pm .3$	$6.60 \pm .3$	2.124	$8.49 \pm .4$

*Referred to swollen dimensions **From Table 3.8 or Equation 3.21 ***Based on weighted average

TABLE 3.4 continued

Film Thickness Data

Polymer Designation	Date Film Formed	Stretch Ratio* λ_w	Stretch Ratio* λ_1	Average Dry Film Thickness cm x 10^3	Weighted Average Dry Film Thickness cm x 10^3	Swell** Ratio	Swollen*** Film Thickness cm x 10^3
PEO-1000	4-16-76	1.0	1.0	$9.91 \pm .7$	$9.74 \pm .7$	2.124	$12.52 \pm .9$
	5-17-76	1.0	1.0	$5.69 \pm .4$	$5.60 \pm .4$	2.124	$7.20 \pm .5$
	5-26-76	1.0	1.0	$8.18 \pm .3$	$7.90 \pm .3$	2.124	$10.15 \pm .4$
		1.235	1.0	$\frac{8.180}{1.235} = 6.62 \pm .3$	$\frac{7.960}{1.235} = 6.45 \pm .3$	2.237	$\frac{10.41}{1.235} = 8.43 \pm .4$
		1.235	1.225	$\frac{8.180}{1.513} = 5.41 \pm .3$	$\frac{7.980}{1.513} = 5.27 \pm .3$	2.359	$\frac{10.62}{1.513} = 7.02 \pm .4$
PEO-1500							
	4-27-75	1.0	1.0	$4.57 \pm .5$	$4.34 \pm .5$	1.828	$5.31 \pm .6$
	5-16-75	1.0	1.0	$4.57 \pm .5$	$4.28 \pm .5$	1.828	$5.23 \pm .6$
	7-28-75	1.0	1.0	$5.94 \pm .5$ (this film is probably 10-15% thicker than indicated)	$5.84 \pm .5$	1.828	$7.14 \pm .6$

*Referred to swollen Dimensions

**From Table 3.8 or equation 3.21

**Based on weighted average film thickness

TABLE 3.4 continued

Film Thickness Data

Polymer Designation	Date Film Formed	Stretch Ratio* λ_w	Stretch Ratio* λ_1	Average Dry Film Thickness cm x 10^3	Weighted Average Dry Film Thickness cm x 10^3	Swell** Ratio	Swollen*** Film Thickness cm x 10^3
PEO-1500							
	5-24-75	1.0	1.0	$5.18 \pm .4$	$4.53 \pm .4$	1.828	$5.54 \pm .5$
		1.0	1.151	$\frac{5.320}{1.151} = 4.62 \pm .4$	$\frac{4.646}{1.151} = 4.04 \pm .4$	1.925	$\frac{5.780}{1.151} = 5.02 \pm .5$
		1.141	1.151	$\frac{5.309}{1.314} = 4.04 \pm .3$	$\frac{4.648}{1.314} = 3.54 \pm .3$	2.025	$\frac{5.880}{1.314} = 4.48 \pm .4$
	10-18-76	1.0	1.0	$7.65 \pm .4$	$7.46 \pm .4$	1.828	$9.12 \pm .5$
		1.157	1.0	$\frac{7.510}{1.157} = 6.49 \pm .4$	$\frac{7.400}{1.157} = 6.40 \pm .4$	1.933	$\frac{9.220}{1.157} = 7.97 \pm .5$
		1.157	1.143	$\frac{7.470}{1.322} = 5.65 \pm .4$	$\frac{7.350}{1.322} = 5.56 \pm .4$	2.033	$\frac{9.310}{1.322} = 7.04 \pm .5$
PEO-1540							
	12-20-75	1.0	1.0	$4.86 \pm .2$	$4.82 \pm .2$	3.30	$7.17 \pm .3$
		1.211	1.002	$\frac{4.839}{1.214} = 3.99 \pm .2$	$\frac{4.811}{1.214} = 3.96 \pm .2$	3.40	$\frac{7.234}{1.214} = 5.96 \pm .3$
		1.209	1.188	$\frac{4.775}{1.437} = 3.32 \pm .2$	$\frac{4.750}{1.437} = 3.31 \pm .2$	3.49	$\frac{7.205}{1.437} = 5.01 \pm .3$

TABLE 3.4 continued

Film Thickness Data

Polymer Designation	Date Film Formed	Stretch* λ_w	Stretch* λ_1	Average Dry Film Thickness cm x 10^3	Weighted Average Dry Film Thickness cm x 10^3	Swell** Ratio	Swollen*** Film Thickness cm x 10^3
PEO-1540							
	9-30-76	1.0	1.0	$9.92 \pm .3$	$9.90 \pm .3$	3.30	$14.74 \pm .5$
		1.235	1.0	$\frac{9.950}{1.235} = 8.06 \pm .3$	$\frac{9.930}{1.235} = 8.04 \pm .3$	3.41	$\frac{14.95}{1.235} = 12.1 \pm .5$
		1.249	1.228	$\frac{9.980}{1.534} = 6.51 \pm .3$	$\frac{9.970}{1.534} = 6.50 \pm .3$	3.51	$\frac{15.15}{1.534} = 9.88 \pm .5$

*Referred to swollen dimensions

**From Table 3.8 or equation 3.21

***Based on weighted average film thickness

TABLE 3.5

Equilibrium Swelling of Poly(oxyethylene glycol) Based Segmented Polyurethanes in Water at 26.4°C

Polymer Designation	Poly(oxyethylene glycol)	Polymer Density g/cm^3	Glycol* Specific Gravity 20/20°C	Weight % Glycol in Polymer	Free Swelling		
					Total Polymer Weight Basis	Total Polymer Volume Basis $1/v_2$	Poly(oxyethylene glycol) Volume Basis $1/v_2$
PEO-600	600	$1.12\pm.02$	1.1279	51.0	$1.466\pm.005$	$1.522\pm.01$	$2.023\pm.01$
PEO-1000	1000	$1.13\pm.02$	1.101	63.8	$2.004\pm.005$	$2.124\pm.01$	$2.762\pm.01$
PEO-1500	1500	$1.12\pm.02$	1.151	55.5	$1.739\pm.005$	$1.828\pm.01$	$2.491\pm.01$
PEO-1540	1540	$1.11\pm.01$	1.091	72.8	$3.051\pm.01$	$3.297\pm.01$	$4.155\pm.01$

*From reference (10)

TABLE 3.6

Estimated Values for χ and M_c from Strain-swelling Data

Polymer Designation	Poly(oxyethylene glycol) formula molecular weight range	Basis: Total Polymer		Basis: Poly(oxyethylene glycol)		Basis: Poly(oxyethylene glycol)	
		χ	M_c	χ	M_c	χ	M_c
PEO-600	570-630	$0.6812 \pm .03$	148 ± 18	$0.5060 \pm .02$	251 ± 26	0.5232	332 ± 33
PEO-1000	950-1050	$0.6456 \pm .01$	662 ± 48	$0.5830 \pm .01$	1300 ± 107	$0.580 \pm .01$	1567 ± 127
PEO-1500	500-600	$0.5787 \pm .02$	232 ± 15	$0.406 \pm .02$	447 ± 42	$0.497 \pm .02$	561 ± 51
PEO-1540	1300-1600	$0.6106 \pm .005$	7075 ± 822	$0.582 \pm .005$	13400 ± 1600	----------	

TABLE 3.7

Swelling Disparity Caused by the Inhomogeneous Strain Field as Estimated from Sternstein's Figures

Polymer Designation	$\frac{\rho V_1}{M_f}$	Interfacial Swelling Disparity from Figure 3.15 for χ=0.32	for χ=0.44	estimated for χ=0.56	Swollen Polymer Volume % "Hard" Phase	Estimated Overall Swelling Disparity % of Observed Swell
PEO-600	0.0336	1.181	1.125	1.08	32.2	$\lesssim$4%
PEO-1000	0.0202	1.258	1.178	1.11	17.0	$\lesssim$5%
PEO-1500	0.0402	1.160	1.112	1.07	24.3	$\lesssim$4%
PEO-1540	0.0131	1.35	1.235	1.14	8.4	$\lesssim$5%

TABLE 3.8

Swelling Ratios Predicted by Equation 3.21 for Strains Employed in Permeability Experiments

Polymer Designation	Measured Strain Referred to Swollen Dimensions		Strain Referred to Unswollen Dimensions Basis: Total Polymer		Predicted Polymer Volume Fraction v_2			Predicted Swelling Ratio
	λ_w	λ_1	λ_w	λ_1	Basis: Total Polymer	Basis: Glycol Only	Basis: Glycol & Sternstein	$1/v_2$
PEO-600	1.0	1.0	1.150	1.150	0.6567	0.6566	0.6549	$1.523 \pm .01$
	1.259	0.998	1.448	1.148	0.6123	0.6136	0.6118	$1.632 \pm .01$
	1.247	1.242	1.434	1.429	0.5765	0.5750	0.5737	$1.739 \pm .01$
	1.250	1.485	1.438	1.708	0.5475	0.5423	0.5410	$1.835 \pm .02$
PEO-1000	1.0	1.0	1.285	1.285	0.4708	0.4707	0.4700	$2.125 \pm .01$
	1.246	0.996	1.602	1.280	0.4460	0.4423	0.4415	$2.252 \pm .02$
	1.239	1.249	1.592	1.605	0.4217	0.4172	0.4170	$2.385 \pm .02$
PEO-1500	1.0	1.0	1.223	1.223	0.5470	0.5466	0.5453	$1.830 \pm .02$
	1.0	1.151	1.223	1.407	0.5183	0.5204	0.5190	$1.925 \pm .01$
	1.141	1.152	1.395	1.409	0.4931	0.4950	0.4948	$2.025 \pm .01$
PEO-1540	1.0	1.0	1.488	1.488	0.3033	0.3048		$3.30 \pm .03$
	1.211	1.002	1.802	1.491	0.2933	0.2938		$3.40 \pm .03$
	1.209	1.188	1.799	1.768	0.2865	0.2865		$3.49 \pm .05$

TABLE 3.9

Solute Partition Coefficient

Polymer Designation	Solute	Partition Coefficients at 26.4°C			Partition Coefficient at 3.5°C (1)	
		Swelling Ratio $1/v_2$	Partition Coefficients K^*	$K = K^*\phi_w$	Swelling Ratio $1/v_2$	Partition Coefficient K^*
PEO-600	Urea	$1.525 \pm .005$	$1.47 \pm .01$	0.505	-----	1.47 (2)
	Glucose	$1.522 \pm .005$	$0.34 \pm .02$	0.117	$1.672 \pm .005$	$0.34 \pm .01$
	Sucrose	"	$0.255 \pm .01$	0.088	"	$0.255 \pm .01$
	Raffinose (3)	"	$0.11 \pm .01$	0.038	"	$0.11 \pm .01$
PEO-1000	Urea	$2.139 \pm .01$	$1.39 \pm .03$	0.752	-----	$1.50 \pm .04$
	Glucose	$2.124 \pm .005$	$0.505 \pm .01$	0.267	$2.40 \pm .005$	$0.51 \pm .01$
	Sucrose	"	$0.43 \pm .01$	0.228	"	$0.424 \pm .01$
	Raffinose	"	$0.275 \pm .01$	0.146	"	$0.275 \pm .01$
PEO-1500	Urea	-----	$1.47 \pm .01$ (4)	0.649		
	Glucose	$1.84 \pm .01$	$0.475 \pm .01$	0.215		
	Sucrose	"	$0.430 \pm .01$	0.195		
	Raffinose	"	$0.290 \pm .01$	0.132		
PEO-1540	Urea	$3.305 \pm .01$	$1.29 \pm .01$ (5)	0.899	4.044	1.31 (2)
	Glucose	$3.260 \pm .005$	$0.655 \pm .01$	0.457	$4.01 \pm .02$	0.64 (2)
	Sucrose	"	$0.58 \pm .015$	0.404	"	0.58 (2)
	Raffinose	"	$0.435 \pm .01$	0.303	"	0.44 (2)

(1) ± 0.5°C (2) Single Measurement (3) 50 hour value (4) Not corrected for weight change on swelling in urea solution (5) Could be 1.15, color indicator not noted.

TABLE 3.10

Solute Reflection Coefficient σ and Film Hydaulic Permeability L_p

Polymer Designation	Solute	Stretch Ratio Referred to Unswollen Dimensions λ_w	λ_1	Weighted Swollen Film Thickness cm x 10^3	Hydraulic* Permeability L_p - ml/atm hr	Osmotic Flux - ml Vpredicted	Vobserved	σ
PEO-600	Glucose	1.0	1.0	$7.42^{\pm}.4$	$0.0408^{\pm}.0005$	.473	.483	$0.929^{\pm}.015$
		1.230	1.0	$6.14^{\pm}.4$	$0.0781^{\pm}.0005$	.399	.397	$0.656^{\pm}.01$
		1.225	1.170	$5.39^{\pm}.4$	$0.116^{\pm}.001$	.527	.520	$0.592^{\pm}.01$
	Sucrose	1.0	1.0			.363	.373	$0.955^{\pm}.015$
		1.230	1.0	same as glucose		.470	.475	$0.752^{\pm}.02$
		1.225	1.170			.620	.625	$0.672^{\pm}.02$
PEO-1000	Glucose	1.0	1.0	$10.15^{\pm}.4$	$0.222^{\pm}.001$	.420	.426	$0.442^{\pm}.01$
		1.235	1.0	$8.43^{\pm}.4$	$0.343^{\pm}.001$	.606	.604	$0.397^{\pm}.01$
		1.235	1.225	$7.02^{\pm}.4$	$0.518^{\pm}.001$	.695	.693	$0.311^{\pm}.01$
	Sucrose	1.0	1.0			.583	.590	$0.574^{\pm}.02$
		1.235	1.0	same as glucose		.768	.775	$0.483^{\pm}.02$
		1.235	1.225			.975	.979	$0.413^{\pm}.02$

*Observed water flux through a membrane area of 25.65 cm^2

TABLE 3.10 continued

Solute Reflection Coefficient σ and Film Hydraulic Permeability L_p

Polymer Designation	Solute	Stretch Ratio Referred to Unswollen Dimensions λ_w	λ_1	Weighted Swollen Film Thickness cm x 10^3	Hydraulic* Permeability L_p - ml/atm hr	Osmotic Flux - ml Vpredicted	Vobserved	σ
PEO-1000	Raffinose	1.0	1.0	$10.15^{\pm}.4$	$0.222^{\pm}.001$	.399	.398	$.752^{\pm}.01$
		1.235	1.0	$8.43^{\pm}.4$	$0.343^{\pm}.001$	.544	.539	$.663^{\pm}.01$
		1.235	1.225	$7.02^{\pm}.4$	$0.518^{\pm}.001$	.700	.690	$.568^{\pm}.01$
PEO-1500	Glucose	1.0	1.0	$9.12^{\pm}.5$	$0.223^{\pm}.001$	.271	.267	$.391^{\pm}.01$
		1.157	1.0	$7.97^{\pm}.5$	$0.311^{\pm}.001$	.330	.326	$.347^{\pm}.01$
		1.157	1.143	$7.04^{\pm}.5$	$0.495^{\pm}.001$	.236	.232	$.309^{\pm}.01$
	Sucrose	1.0	1.0			.286	.290	$.488^{\pm}.01$
		1.157	1.0	same as glucose		.350	.355	$.434^{\pm}.01$
		1.157	1.143			.530	.535	$.377^{\pm}.01$
	Raffinose	1.0	1.0			.203	.200	$.682^{\pm}.01$
		1.157	1.0	same as glucose		.257	.253	$.625^{\pm}.01$
		1.157	1.143			.372	.370	$.577^{\pm}.01$

*Observed Water Flux through 25.65 cm^2 of membrane

TABLE 3.10 continued

Solute Reflection Coefficient σ and Film Hydraulic Permeability L_p

Polymer Designation	Solute	Stretch Ratio Referred to Unswollen Dimensions λ_w	λ_1	Weighted Swollen Film Thickness cm x 10^3	Hydraulic* Permeability L_p - ml/atm hr	Osmotic Flux - ml Vpredicted	Vobserved	σ
PEO-1540	Glucose	1.0	1.0	$14.74\pm.5$	$0.441\pm.001$	.256	.252	$.321\pm.01$
		1.235	1.0	$12.10\pm.5$	$0.669\pm.001$	.330	.325	$.276\pm.01$
		1.249	1.228	$9.88\pm.5$	$0.902\pm.001$	.397	.389	$.250\pm.01$
	Sucrose	1.0	1.0			.321	.322	$.395\pm.01$
		1.235	1.0	same as glucose		.435	.442	$.361\pm.01$
		1.249	1.228			.520	.530	$.318\pm.01$
	Raffinose	1.0	1.0			.243	.243	$.591\pm.01$
		1.235	1.0	same as glucose		.322	.317	$.520\pm.01$
		1.249	1.228			.347	.345	$.485\pm.01$

*Observed water flux through a membrane area of 25.65 cm^2

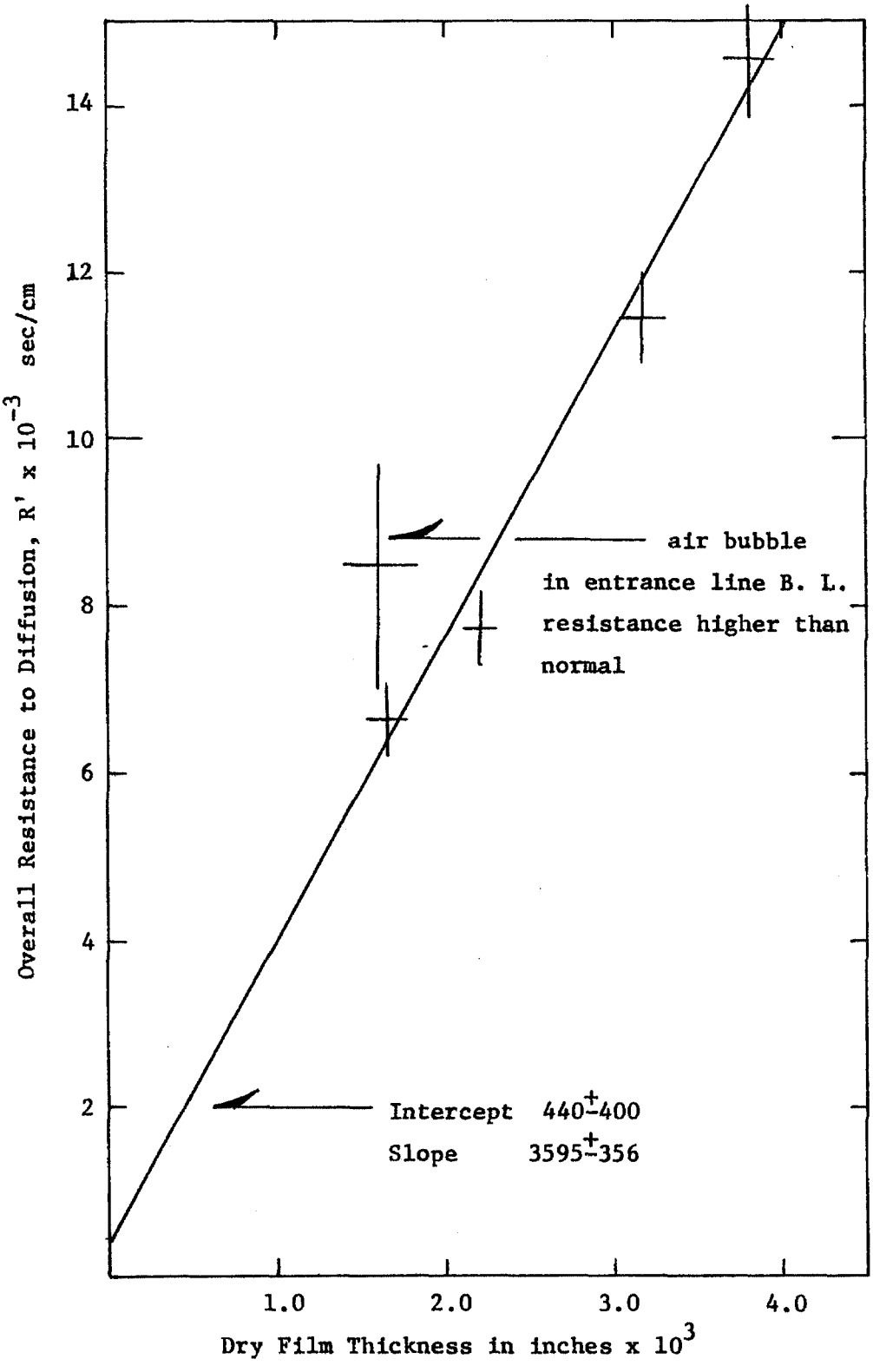

Figure 3.1. Overall Resistance to Diffusion for PEO-1000 Films.

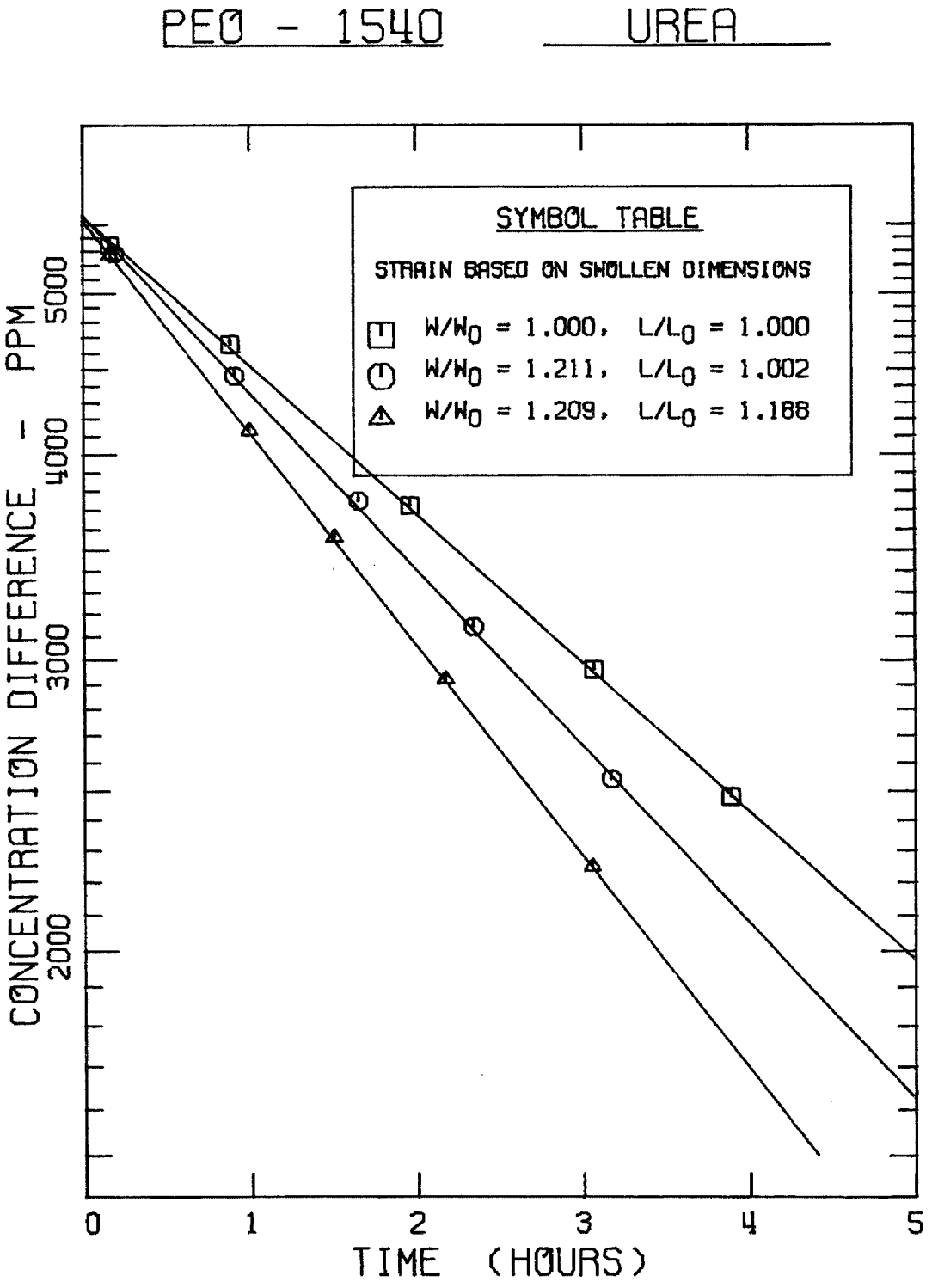

Figure 3.2. Concentration difference versus time for a PEO-1540 film. Weighted average film thickness 0.00482 cm. Curves theoretical (equation 3.10).

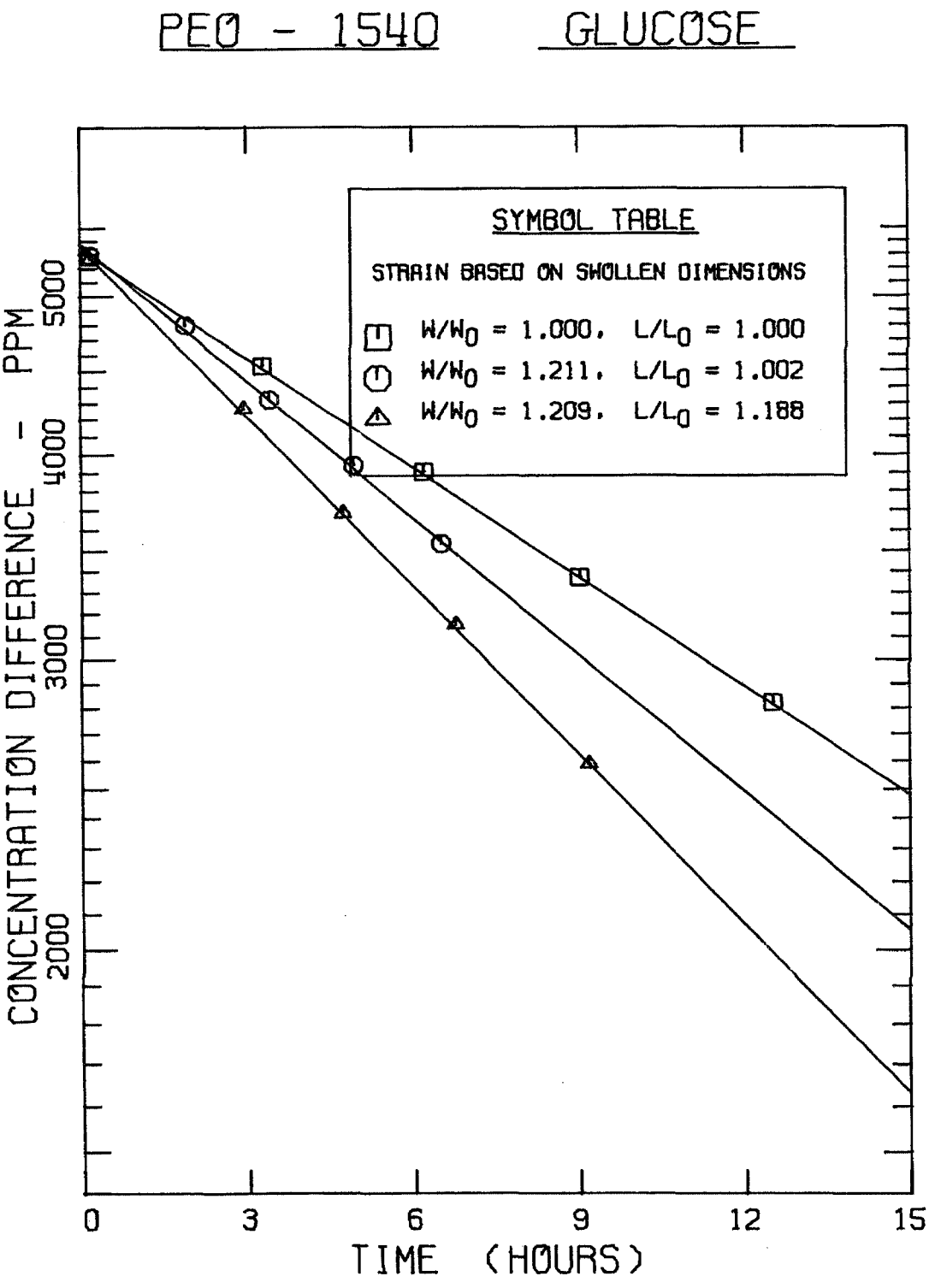

Figure 3.3. Concentration difference versus time for a PEO-1540 film. Weighted average film thickness 0.00482 cm for the dry unstrained film. Curves theoretical (eqn. 3.10).

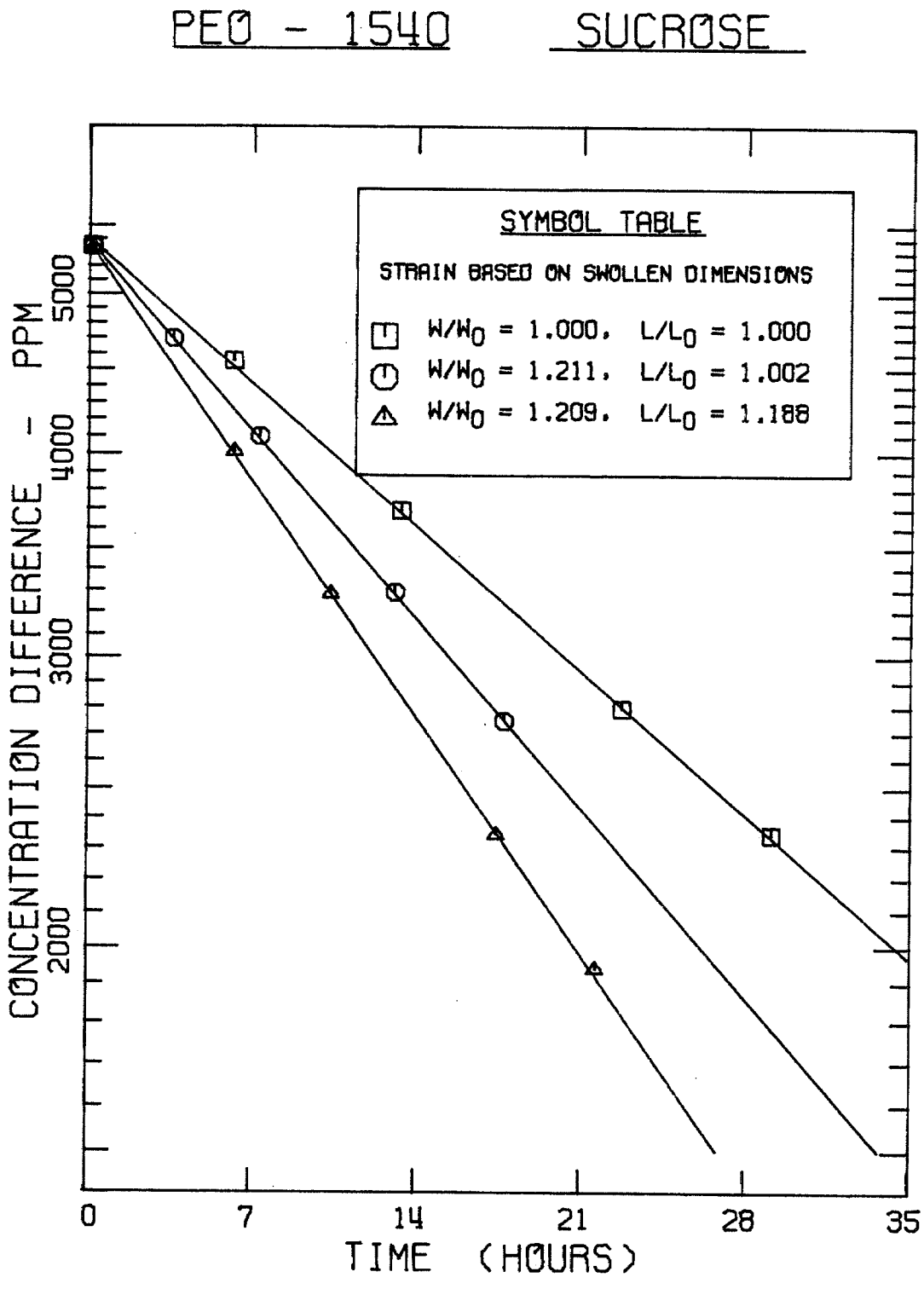

Figure 3.4. Concentration difference versus time for a PEO-1540 film. Weighted average film thickness 0.00482 cm for the dry unstrained film. Curves theoretical (eqn.3.10).

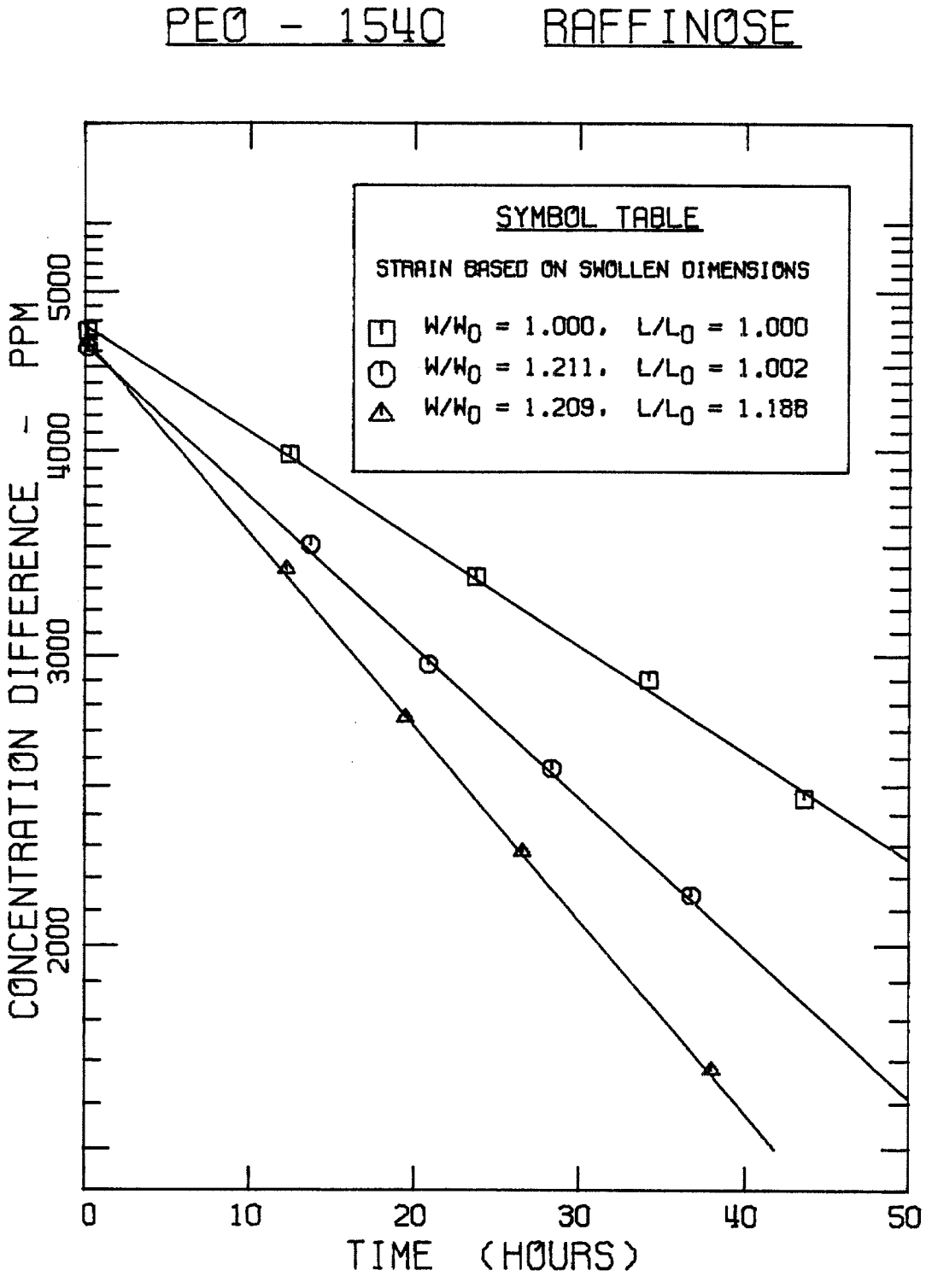

Figure 3.5. Concentration difference versus time for a PEO-1540 film. Weighted average film thickness 0.00482 cm for the dry unstrained film. Curves theoretical (eqn. 3.10).

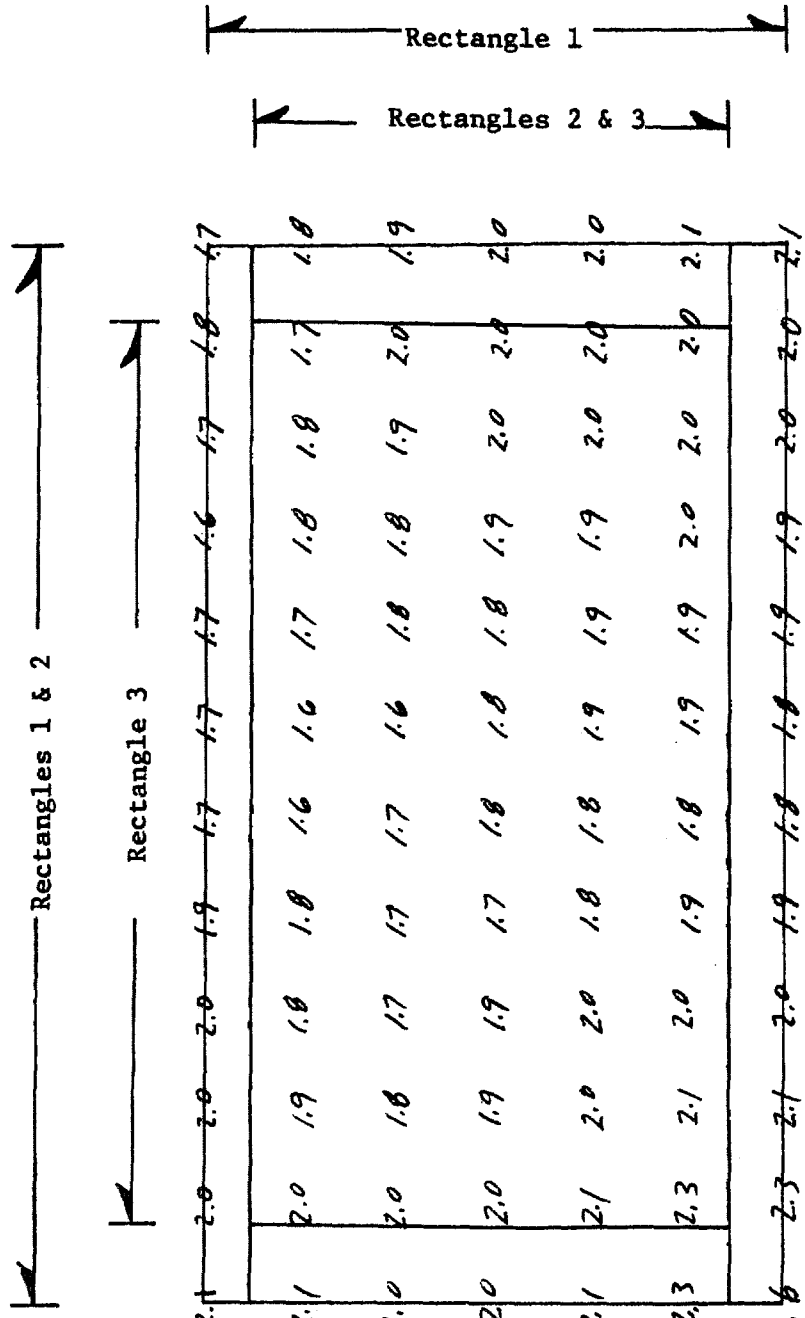

Rectangle 1 - exposed membrane area when $l_w = 1.0$ and $l_1 = 1.0$.

Rectangle 2 - exposed membrane area when $l_w = 1.211$ and $l_1 = 1.002$

Rectangle 3 - exposed membrane area when $l_w = 1.209$ and $l_1 = 1.188$

Figure 3.6. Thickness of a PEO-1540 film formed 12-20-75. Thickness measurements given in inches x 10^3.

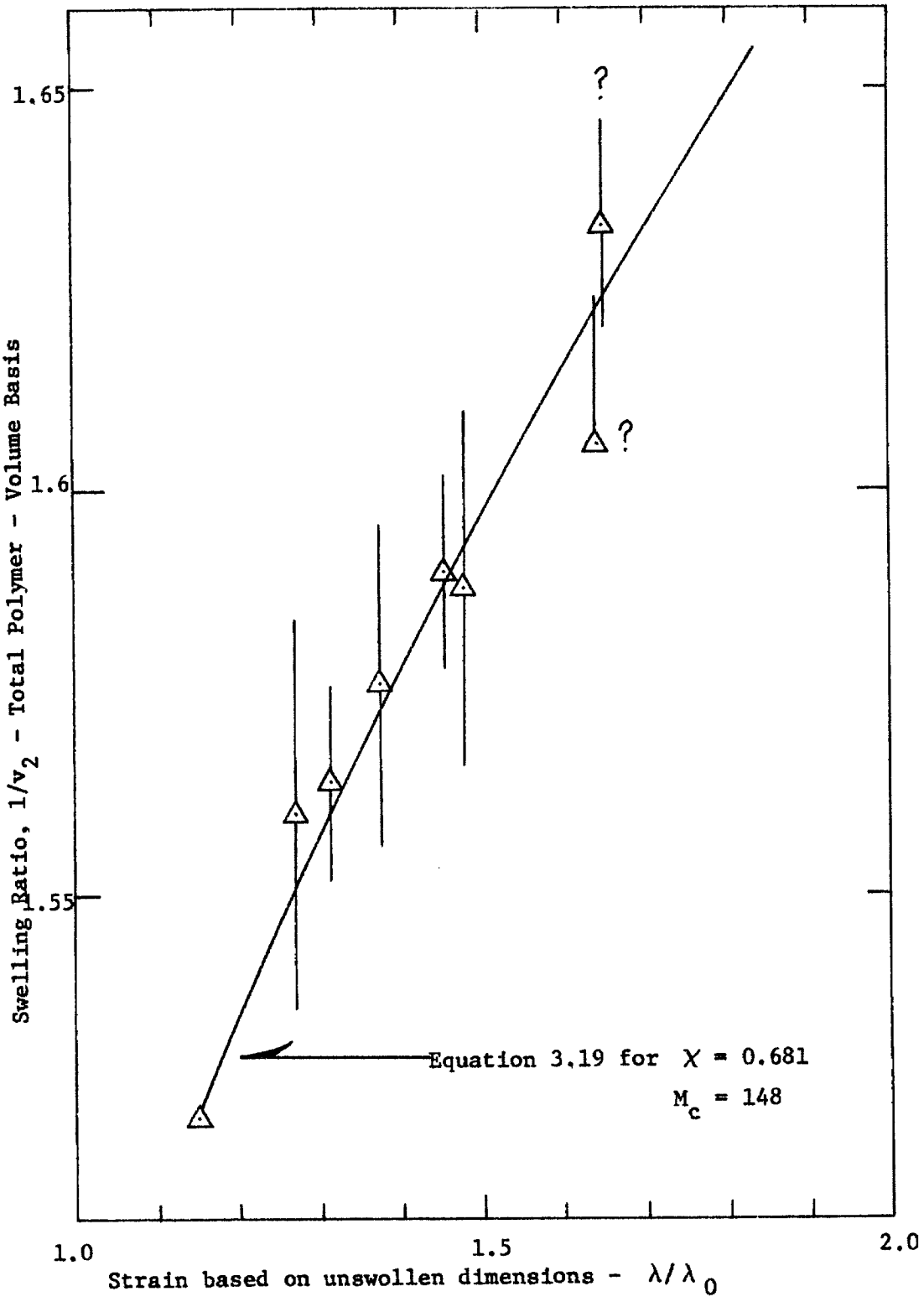

Figure 3.7. Dependence of swelling on strain. PEO-600 Film. Simple elongation. Curve theoretical (equation 3.19).

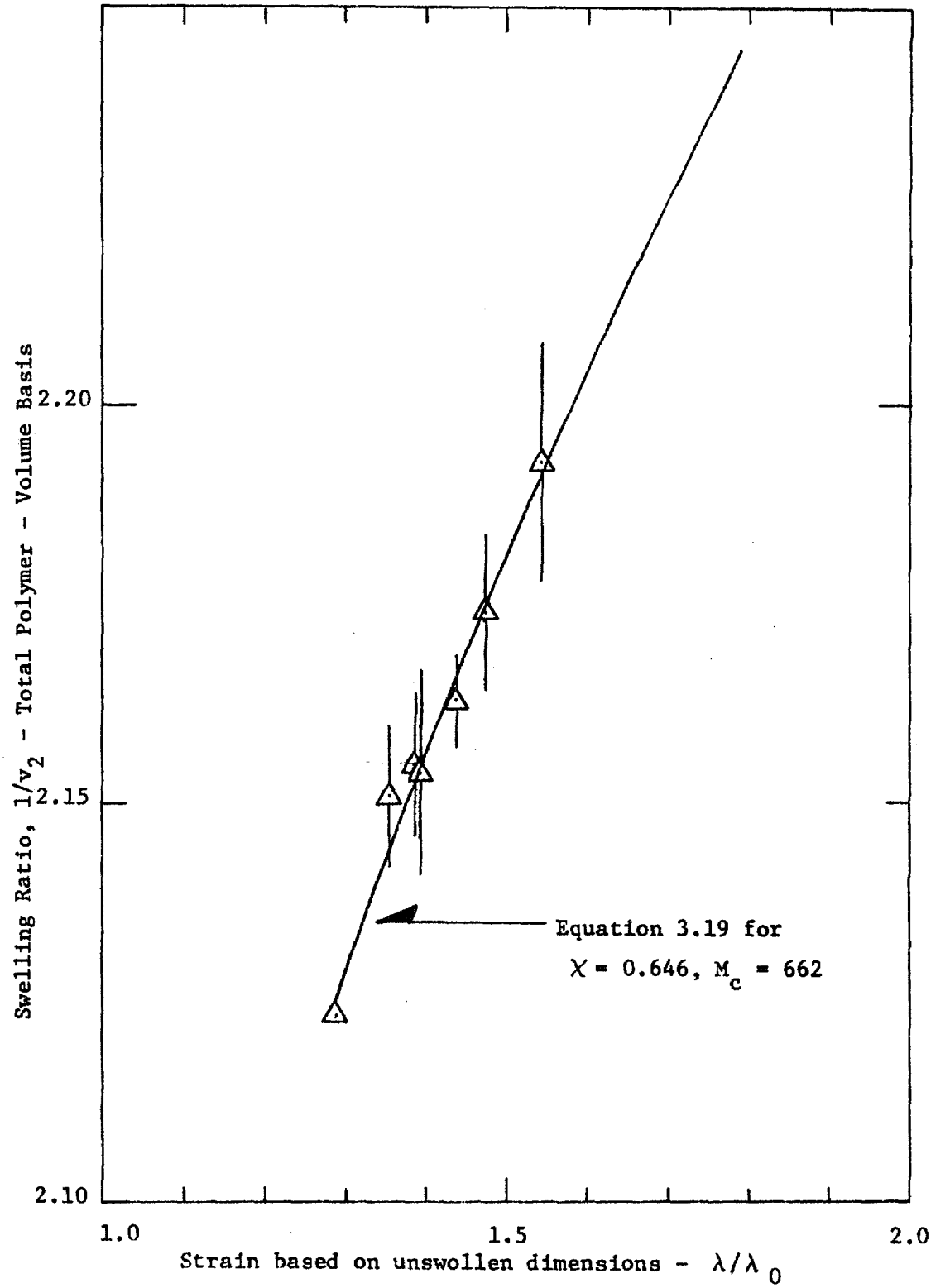

Figure 3.8. Dependence of swelling on strain. PEO-1000 film. Simple elongation. Curve theoretical (equation 3.19).

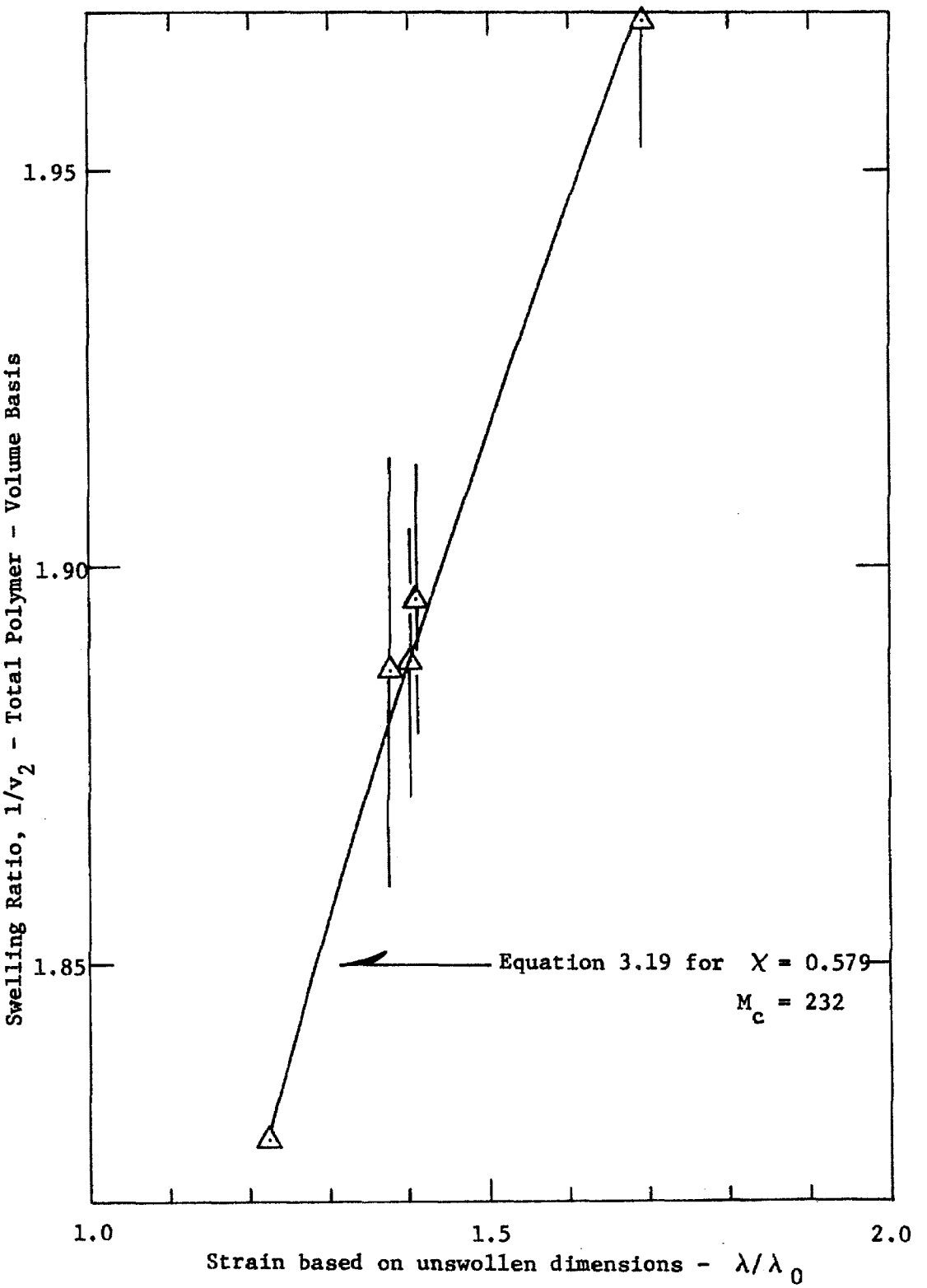

Figure 3.9. Dependence of swelling on strain. PEO-1500 film. Simple elongation. Curve theoretical (equation 3.19).

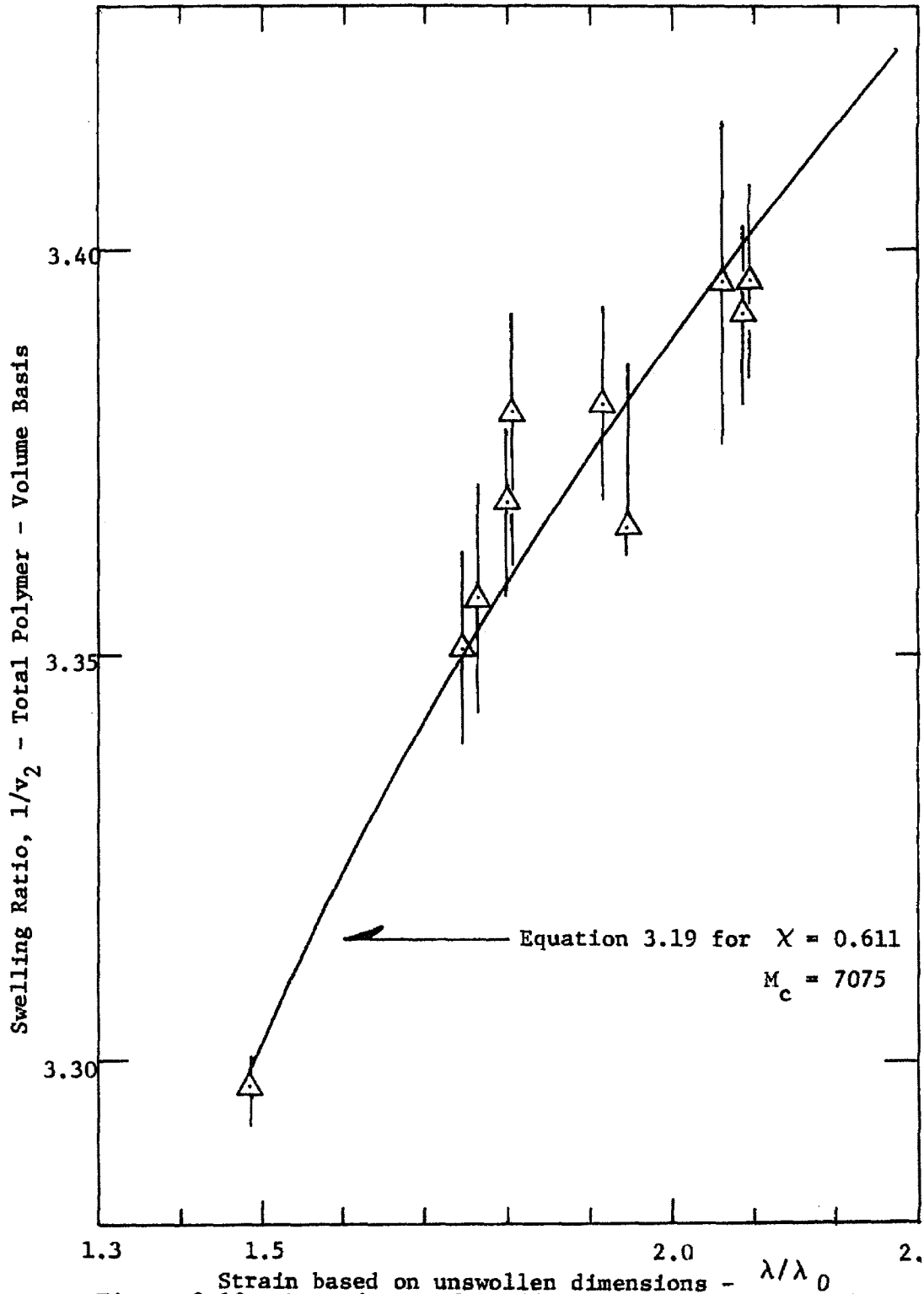

Figure 3.10. Dependence of swelling on strain. PEO-1540 film. Simple elongation. Curve theoretical (equation 3.19)

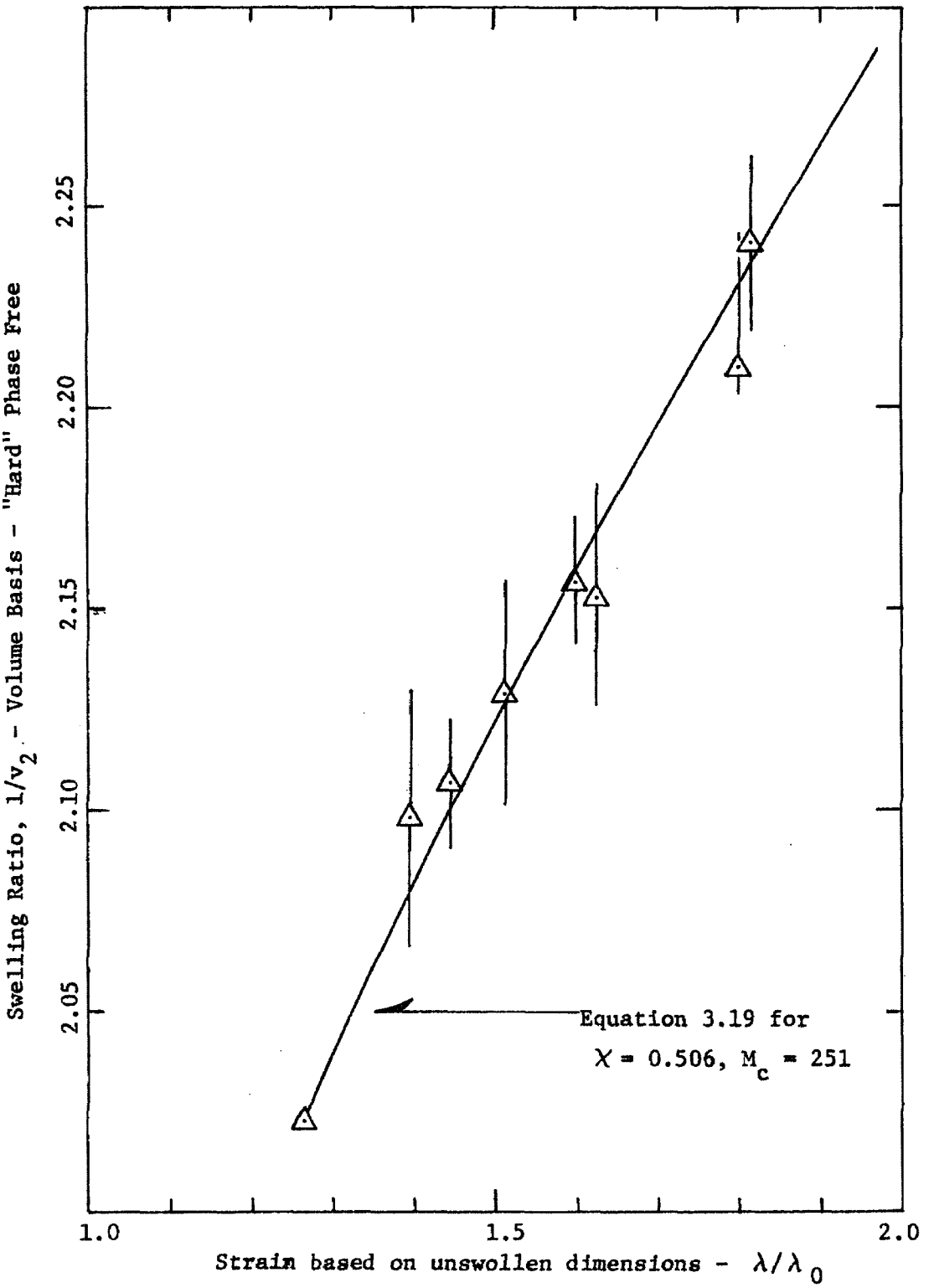

Figure 3.11. Dependence of swelling on strain. PEO-600 film. Simple elongation. Curve theoretical (equation 3.19)

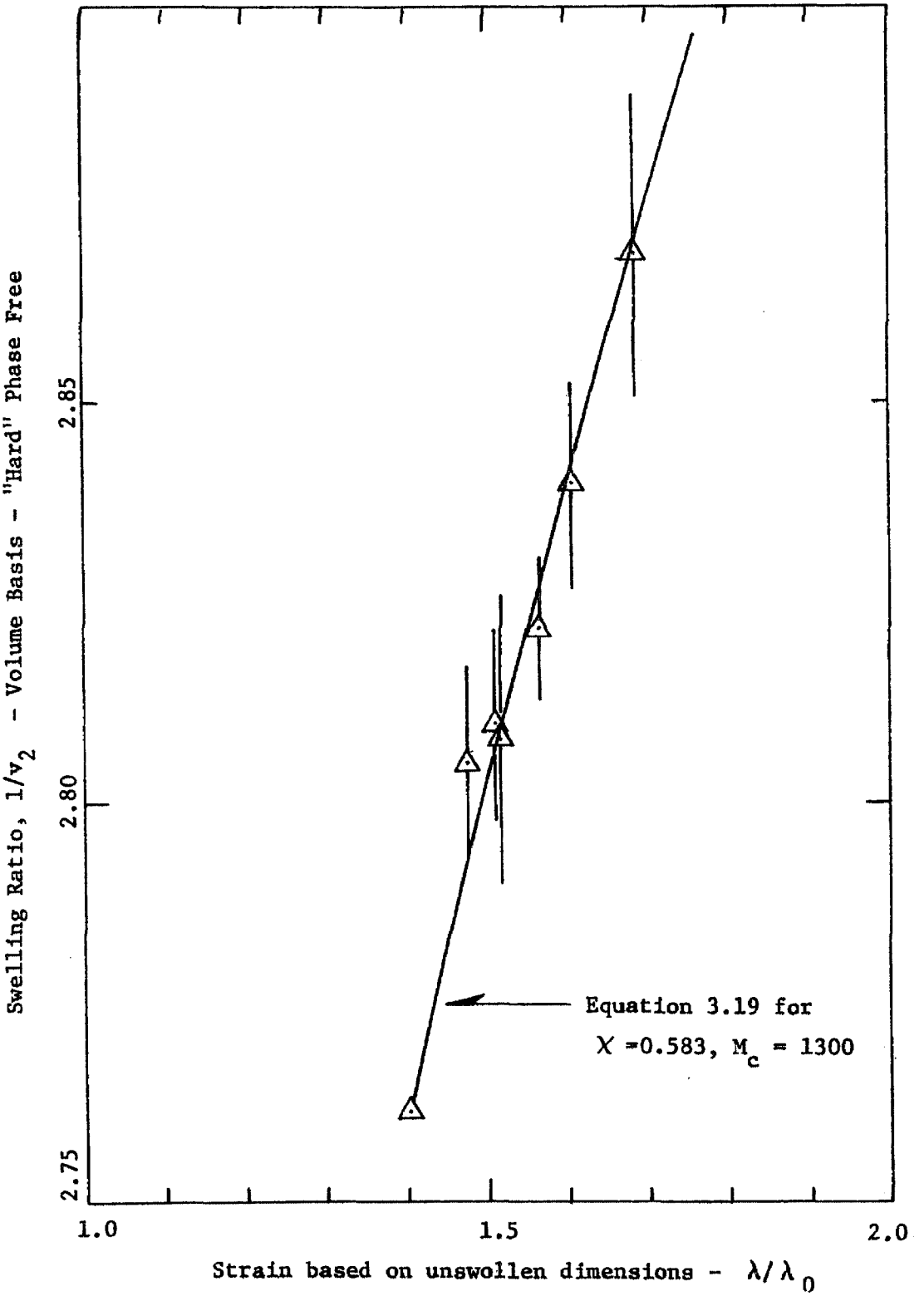

Figure 3.12. Dependence of swelling on strain. PEO-1000 film. Simple elongation. Curve theoretical (equation 3.19)

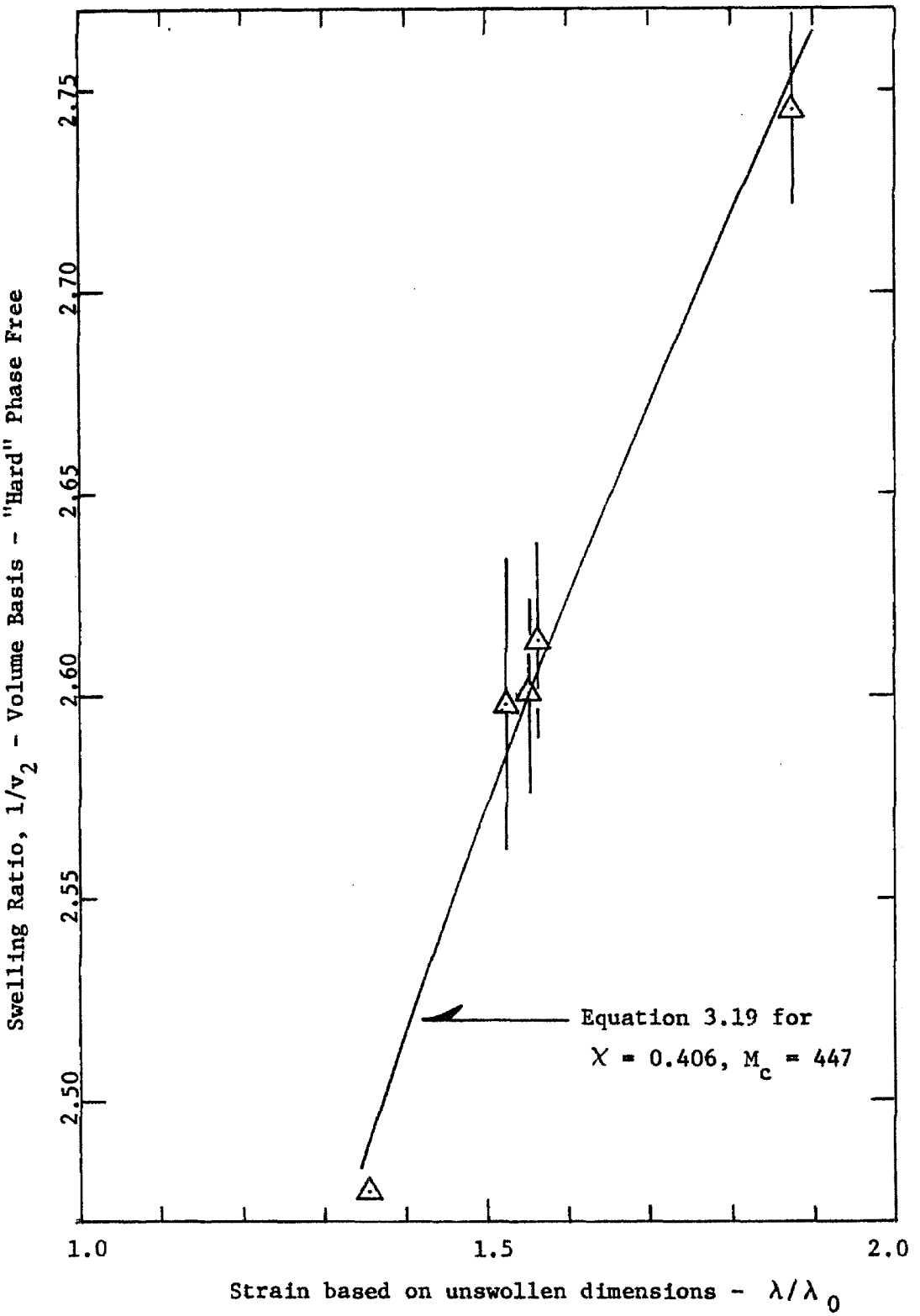

Figure 3.13. Dependence of swelling on strain. PEO-1500 film. Simple elongation. Curve theoretical (equation 3.19)

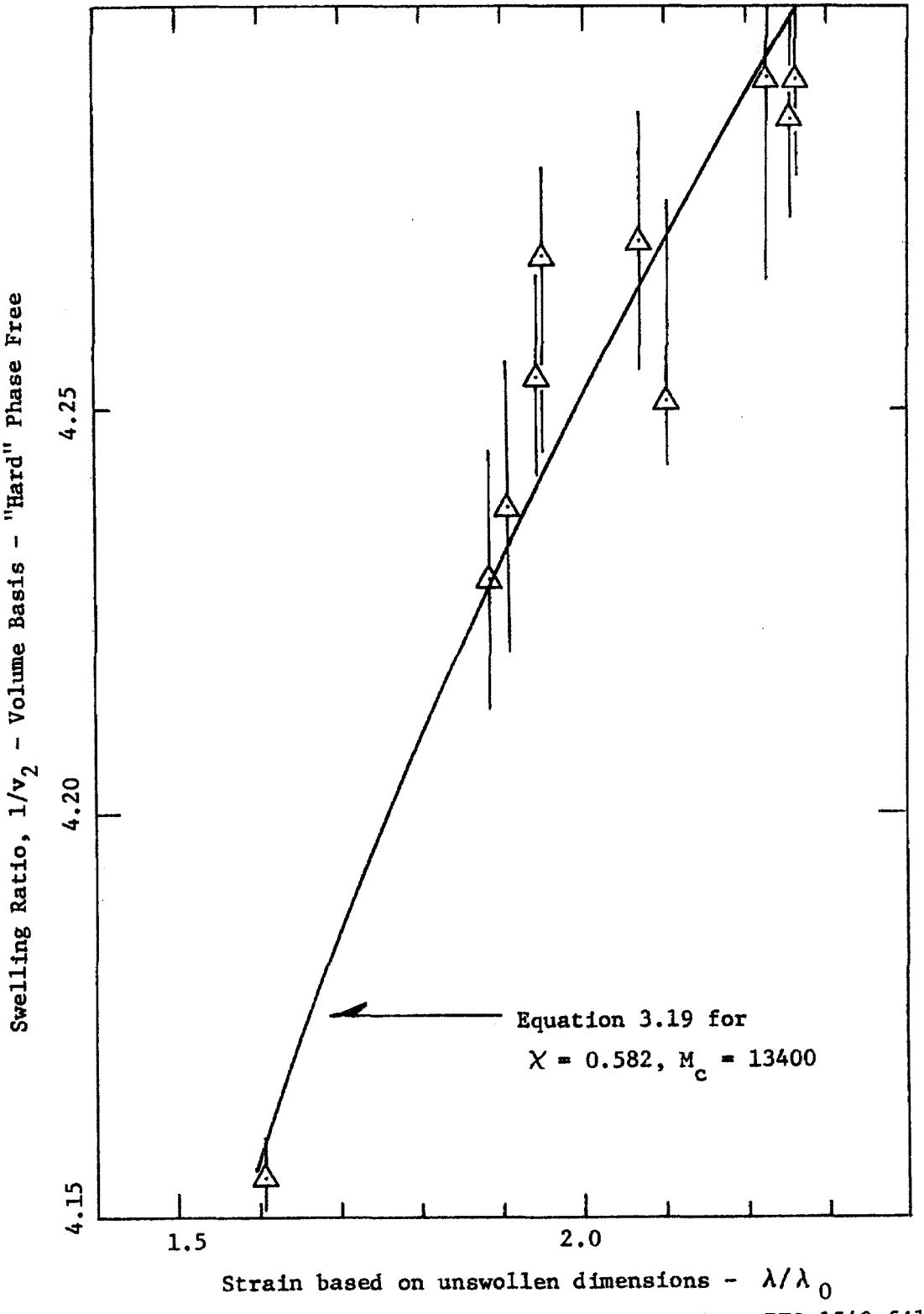

Figure 3.14. Dependence of swelling on strain. PEO-1540 film. Simple elongation. Curve theoretical (equation 3.19)

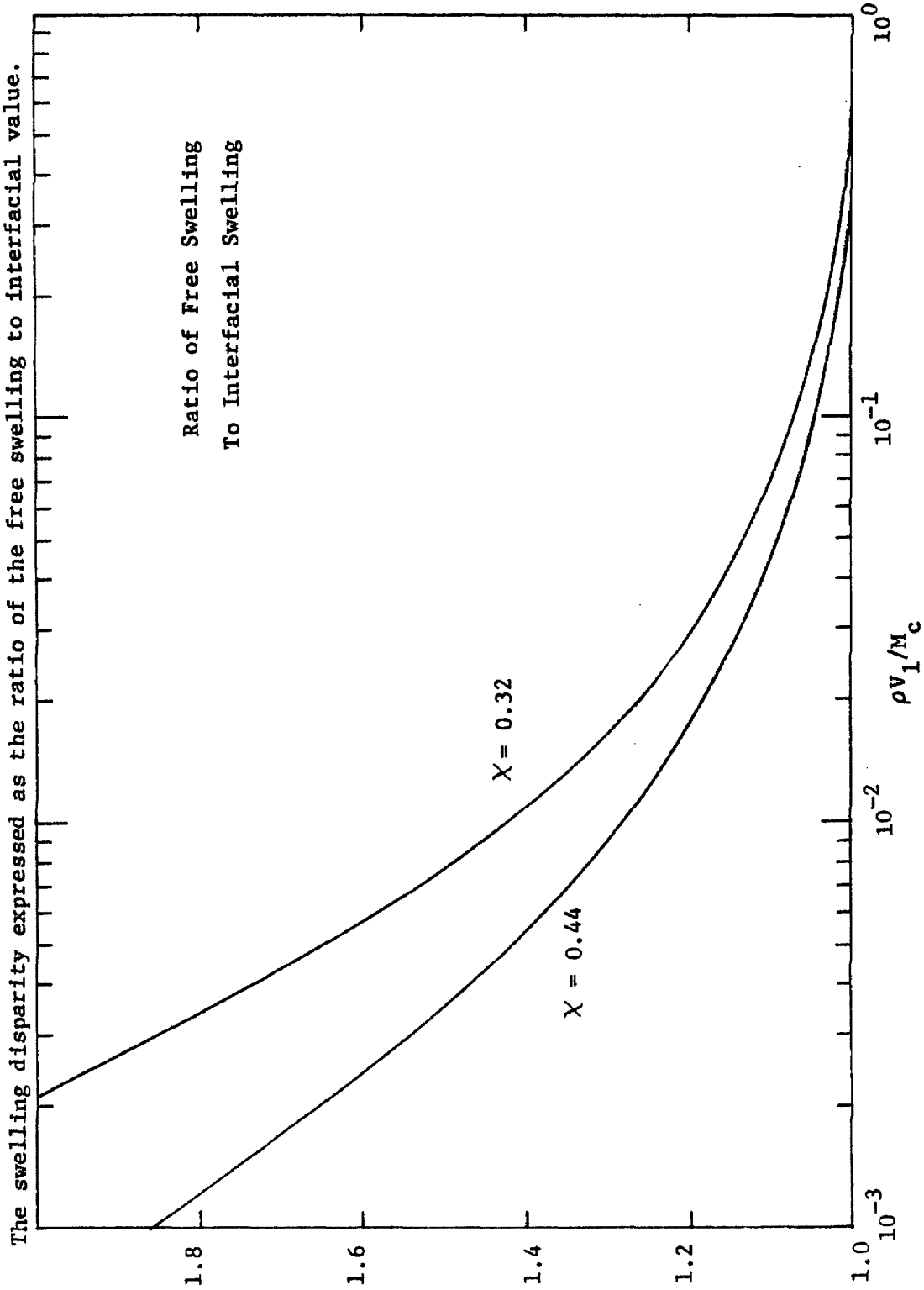

Figure 3.15. Sternstein's Figure 8 (see reference 17).
The swelling disparity expressed as the ratio of the free swelling to interfacial value.

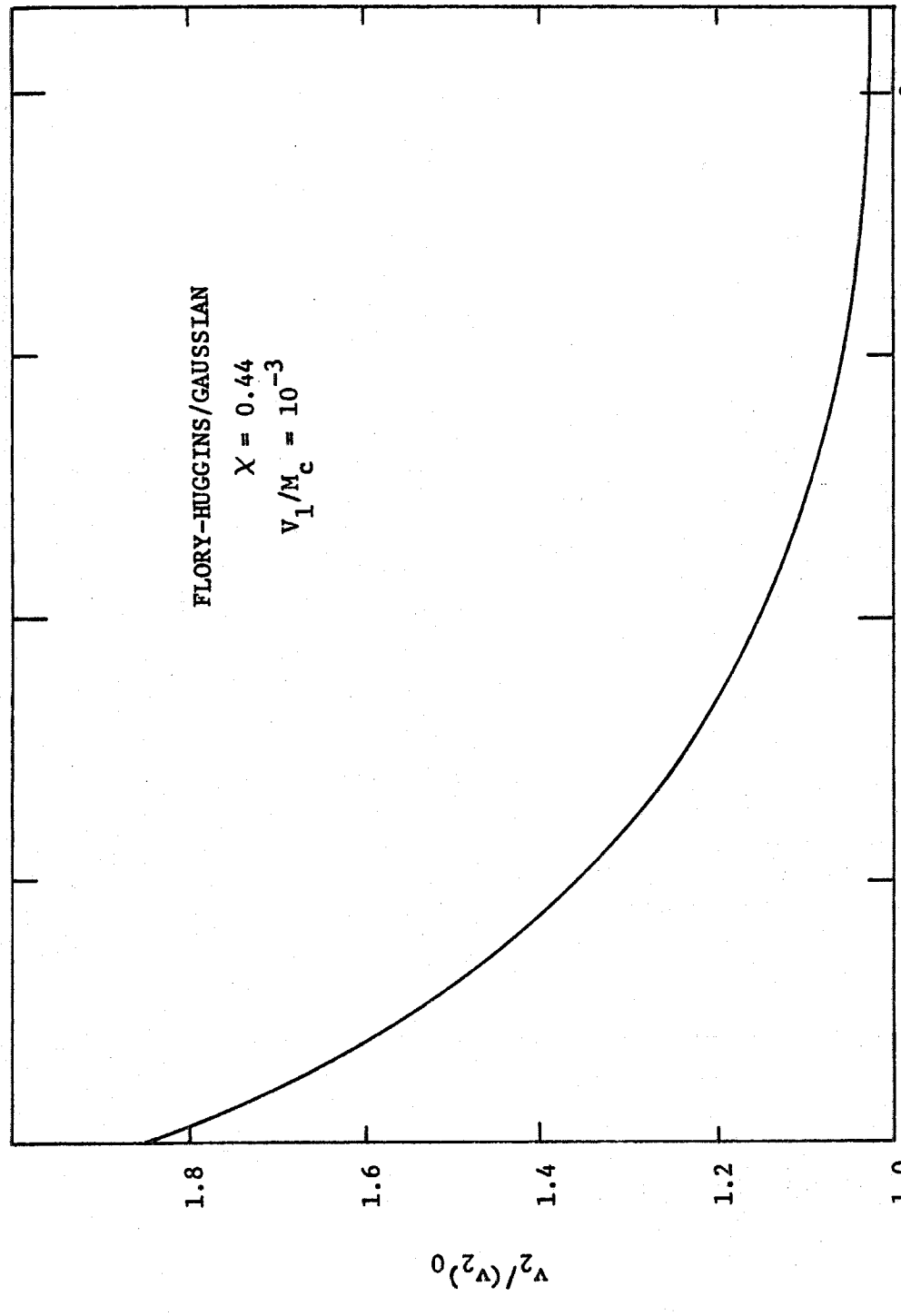

Figure 3.16. Sternstein's Figure 5 (see reference 17). The volume fraction of elastomer relative to the free swelling value as a function of reduced distance from the inclusion.

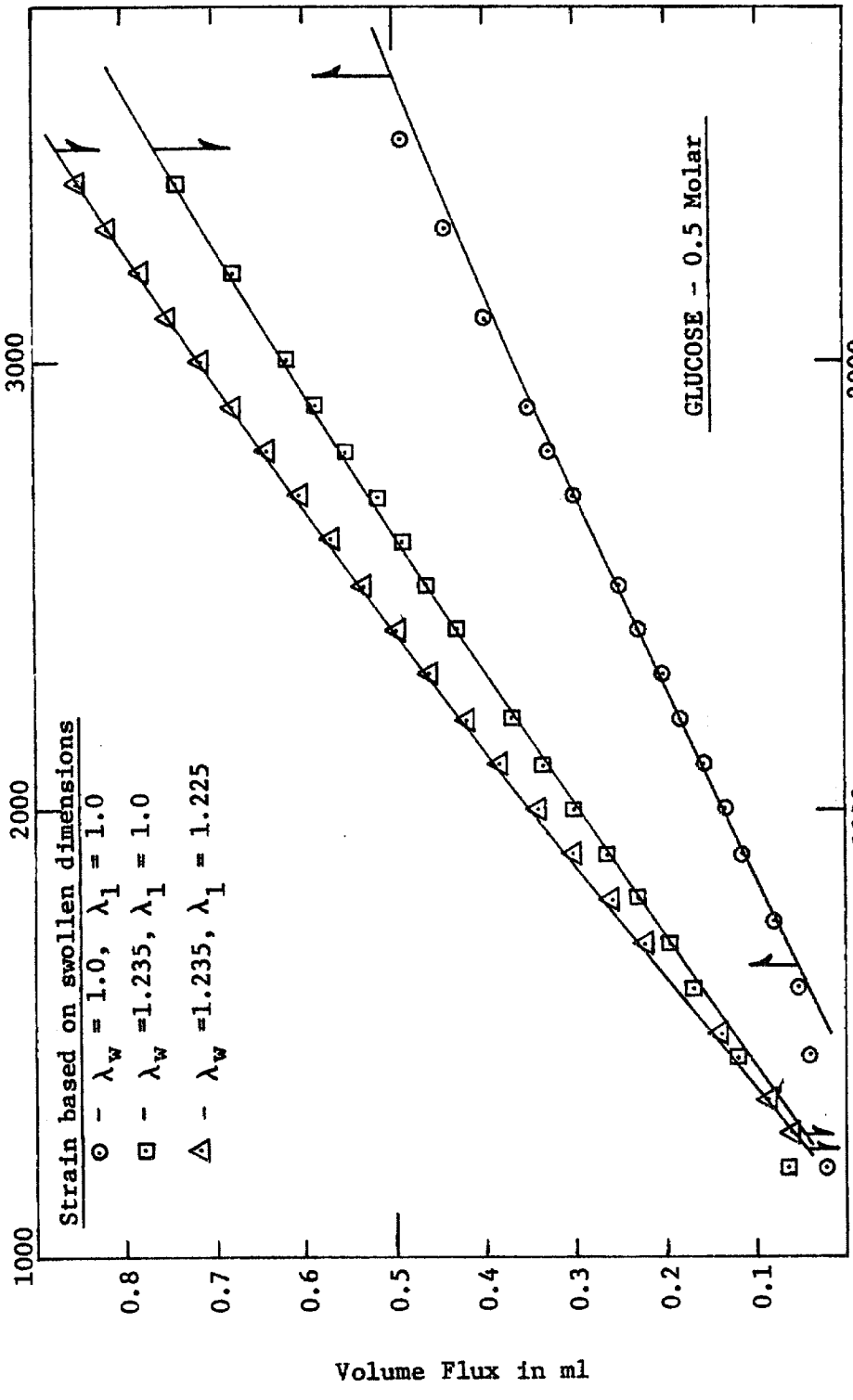

Figure 3.18. Net volume flow across a PEO-1000 membrane with glucose solution (0.5 M) in one half cell and deionized water in the other. Curves theoretical.

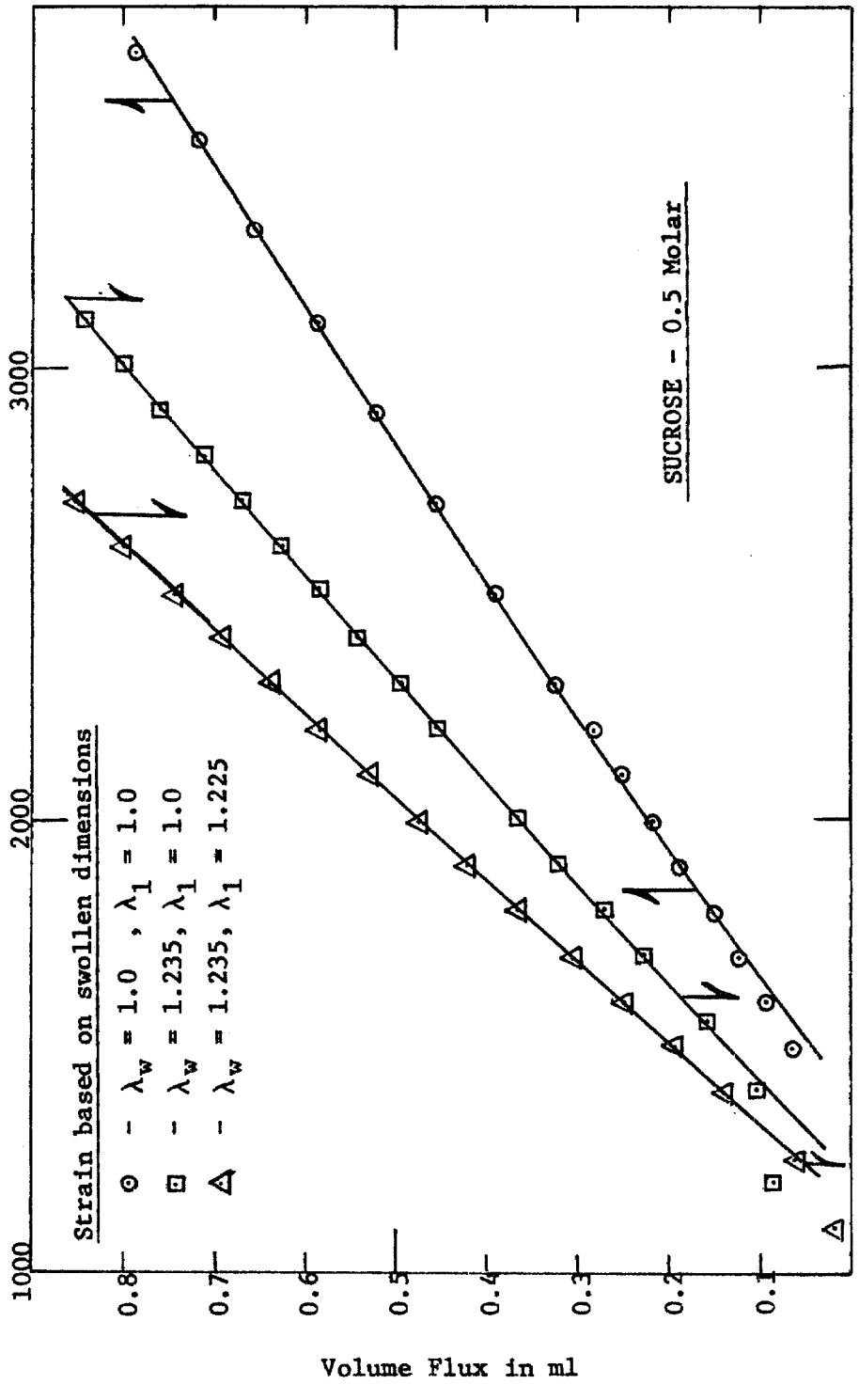

Figure 3.19. Net volume flow across a PEO-1000 membrane with sucrose solution (0.5 M) in one half cell and deionized water in the other. Curves theoretical.

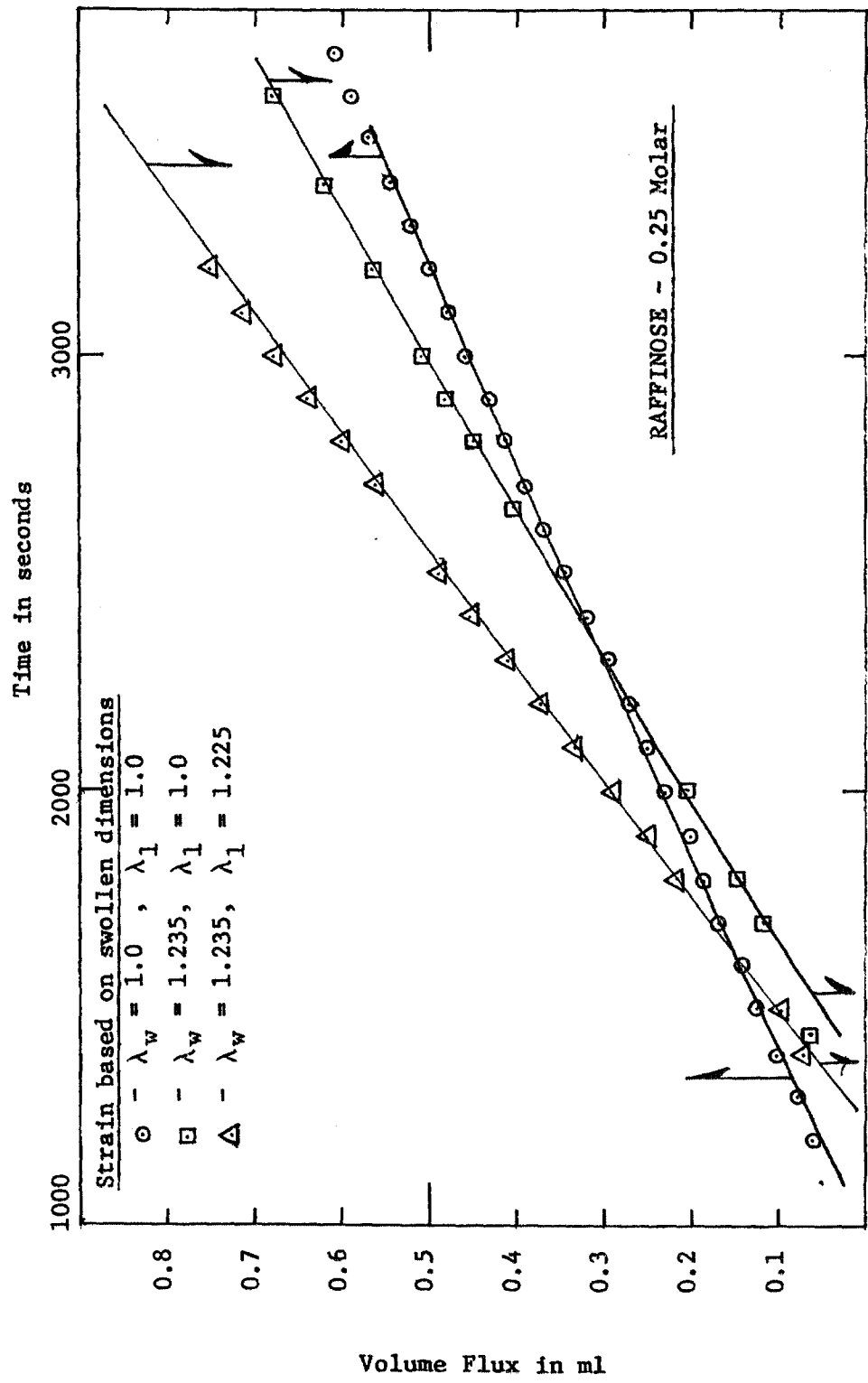

Figure 3.20. Net volume flow across a PEO-1000 membrane with raffinose solution (0.25 M) in one half cell and deionized water in the other.

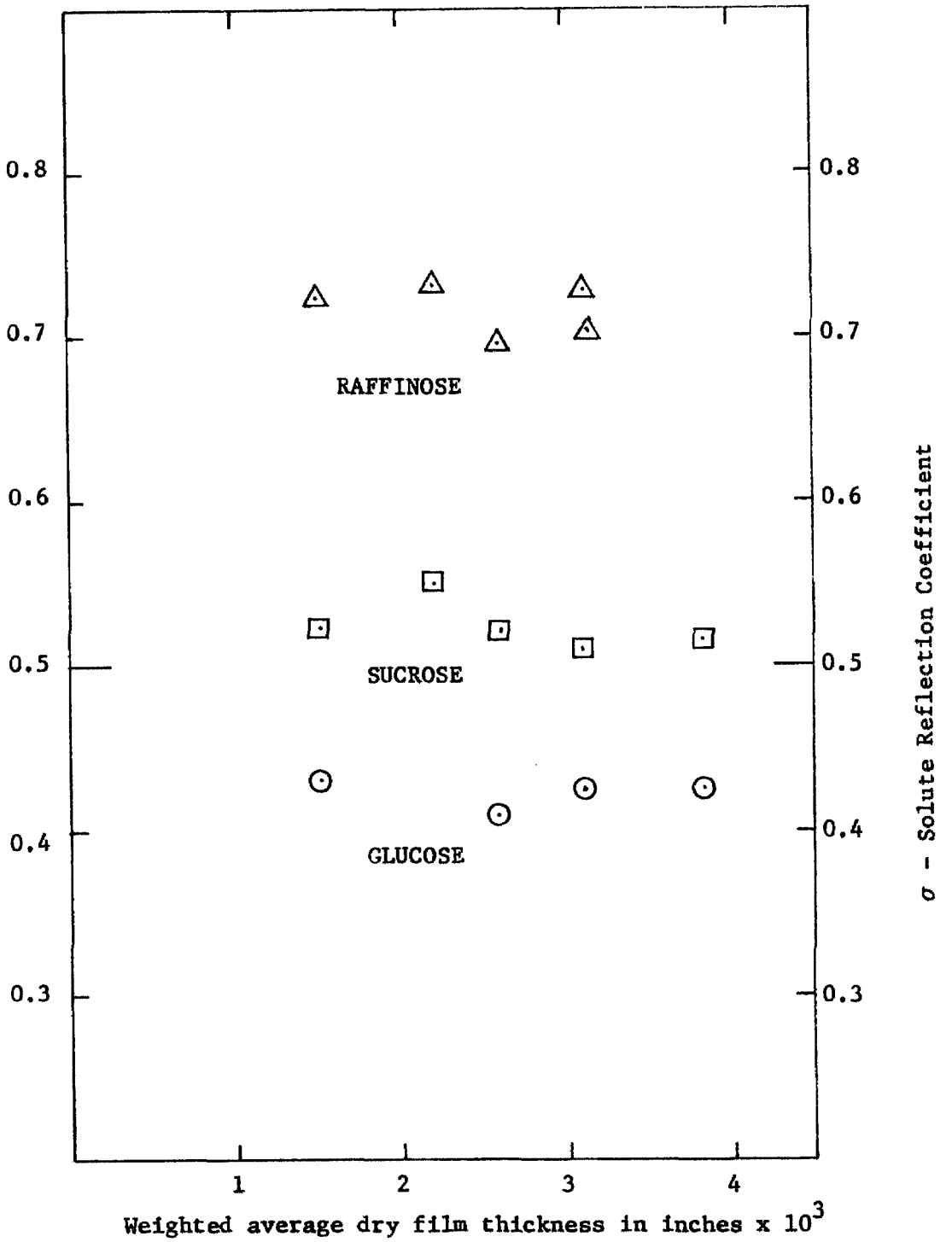

Figure 3.21. Solute reflection coefficient for several PEO-1000 films.

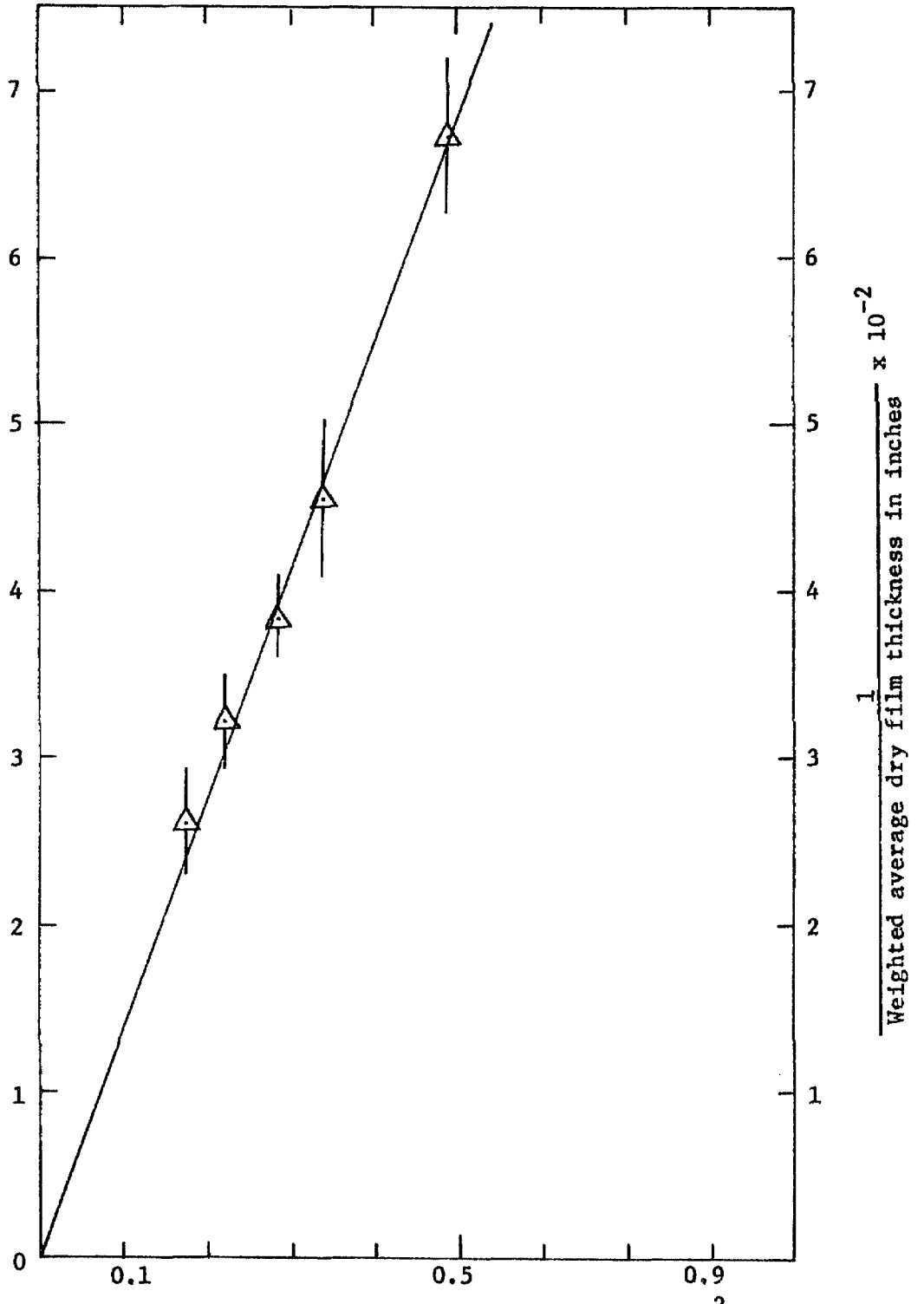

Volume flux through a membrane area of 25.65 cm^2 - ml/atm-hr

Figure 3.22. Film hydraulic permeability L_p versus the inverse film thickness.

CHAPTER 4

DISCUSSION

The data obtained during the course of this investigation are given in the tables of Chapter 3. The data which are most pertinent to the discussion which follows are summarized in Table 4.1. All of the information in Table 4.1 should be self-evident except for the entries in the column headed "Solute Diffusivity in the Swollen Film". These values are best estimates based on a consideration of all the data gathered for each type of film. In the case of the PEO-1000 film dated 8-30-74 for example, an air bubble that was trapped in the top half cell entrance port on startup was not removed. The presence of the bubble caused poor flow distribution near the entrance of the top half cell flow channel resulting in a lower film permeability.

4.1 Structure of the Polymers

All polymers used in this study belong to the class of materials known as segmented polyurethanes. Because of the manner in which these polymers are prepared, they consist of long chain molecules composed of alternating "soft" and "hard" blocks. The hydrophilic "soft" block is composed of a poly(oxyethylene glycol), the molecular weight of which varies from 300 to 1600. The "hard" block has a molecular weight of 584 and is composed of two molecules of 4,4'-dicyclohexylmethane diisocyanate, connected by urethane linkages to a molecule of ethylene

diamine. A "hard" block will under suitable conditions form strong interchain hydrogen bonds with other "hard" blocks, resulting in a physical crosslink (1-5). These physical crosslinks are not hydrated by water. Samples stored in room-temperature deionized water for two years are strong, optically clear, and show no signs of deterioration.

The structure of these polymers has been discussed elsewhere (1-3) and will not be considered further here. Figure 4.1a,b depicts the polymer structure schematically.

4.2 Application of the Molecular Sieve Theory to the Data

The principal result of the molecular sieve theory is the Pappenheimer Renkin equation (see Chapter 1).

$$\frac{D_m}{D_o} = \left(1 - \frac{R_s}{R_p}\right)^2 \left(1 - \frac{R_s}{R_p} + 2.09\left\{\frac{R_s}{R_p}\right\}^3 - 6.95\left\{\frac{R_s}{R_p}\right\}^5\right) \qquad (4.1)$$

This equation has been found to work well for systems where the solute diffuses through discrete solvent-filled pores. It would not be expected to give useful results for the homogeneously swollen elastomers used in this study. Nonetheless, it is possible to calculate the ratio of the solute radius to the pore radius, R_s/R_p, from the observed values of D_m/D_o and equation (4.1). The result of this calculation is reported in Table 4.2.

The striking thing about the values of R_s/R_p and R_p is that they suggest that each molecule, in diffusing through the membrane, finds a pore that is two to four times its own molecular size. This is exactly what would be expected if cooperative motion of the macromolecule chains is required to form a hole for the solute molecule to diffuse through.

4.3 The Effect of Strain on the Permeability

Figures 4.2 - 4.5 show plots of the concentration difference across a PEO-1000 film versus time. One effect of stretching the membrane is to reduce its thickness. If the change in swelling when the film is stretched is ignored momentarily and the assumption made that the film is incompressible, then it is possible to remove the effect of thinning the membrane by a simple time shift of the data. The film permeability, and therefore the time rate of change of the concentration difference across the film, is inversely proportional to the film thickness. For an incompressible membrane the volume must remain constant when the membrane is stretched and hence the film thickness is related to λ_w and λ_1 by $x = 1/\lambda_w\lambda_1$ where λ_w and λ_1 are the widthwise and lengthwise stretch ratios referred to the swollen dimensions of the film. To remove the effect of thinning the membrane, the data need only to be normalized to some reference thickness. This can be done by multiplying the time at which each data point is taken by the inverse of the film thickness and plotting the data point at the new time. The

relationship between the new and the old time is given by

$$t_{new} = t_{old}/x = t_{old}/(1/\lambda_w \lambda_1) = \lambda_w \lambda_1 t_{old} \quad (4.2)$$

Application of (4.2) to the data will not have any effect on the data for the unstretched films ($\lambda_w = \lambda_1 = 1$) but will shift the data for stretched films to longer times. Figures 4.6 - 4.9 show the data of Figures 4.2 - 4.5 replotted to remove the effect of thinning the membrane. It is apparent that the change in film thickness is one of the major causes of the change in film permeability on stretching. In the above the effect of thinning the membrane has been slightly overstated because the swelling of the membrane on stretching results in a smaller change in the film thickness and, therefore, a smaller time shift than that shown in Figures 4.6 - 4.9.

4.4 The Partition Coefficient

The partition coefficient data were presented in Table 3.9. These data were taken at two temperatures rather than as a function of strain because of the large uncertainty observed in the data determined as a function of strain. This uncertainty is due in part to contamination of the elution fluid by the sample stretching frame and in part to the uncertainty in the weight of the swollen polymer sample. For the experiments conducted, no systematic variation of K* with strain was observed. Data taken at two temperatures confirm that K* is independ-

ent of film hydration, H, for the range of hydrations important in this study.

4.5 Application of the Theory of Thermodynamics of Irreversible Processes

The film permeability ω reported in Table 3.3 has not been determined under conditions of zero volume flow through the membrane. For most experiments, 1 - 2 grams out of a 900 gram charge traverse the membrane during an experiment. The effect of this small flow on ω is negligible.

The theory of the thermodynamics of irreversible processes, as presented in Chapter 1, primarily makes statements about σ and what σ might mean. In Table 4.3 the data necessary for the discussion below are summarized.

It was shown in Chapter 1 that for a completely nonselective film $\sigma = 0$ and for an ideally semipermeable membrane $\sigma = 1$. For films which are partially selective σ is given by

$$\sigma = 1 - \frac{\omega \bar{V}_s}{L_p} - \frac{A_s}{A_w} = 1 - \frac{\omega \bar{V}_s}{L_p} - \frac{\omega RT}{D\nu\phi_w/\Delta x} \qquad (4.3)$$

where A_s/A_w is the ratio of the area available for diffusion of the solute relative to the area available for diffusion of water. Values for the area ratio A_s/A_w are given in Table 4.3.

The change in A_s/A_w does not correlate with the change in the film permeability. In some cases the area ratio changes by a factor

of twenty while the film permeability doubles. Similarly, unreasonable changes are predicted for the film tortuosity ν. Apparently the concept of an available area or a film tortuosity is not useful for these swollen films. Indeed, one would expect from the free volume theory that all of the solvent would be equally available to the solute for diffusion and hence that A_s/A_w should be nearly one.

It is proposed here that the film permeability ω and the solute reflection coefficient σ are related in such a way that $\sigma\omega$ is a constant for a given solute and a given film. Assuming that small differences in the strain states cause small linear changes in σ and ω and that σ is independent of film thickness then the proposed correlation takes the form

$$C = \sigma_i \frac{\omega_i \left(\lambda_w \lambda_1\right)_{\sigma_i}}{\omega_o \left(\lambda_w \lambda_1\right)_{\omega_i}} \tag{4.4}$$

where C is a constant, σ_i is the solute reflection coefficient for the ith pull, ω_i is the normalized film permeability for the ith pull, and $\left(\lambda_w \lambda_1\right)_{\sigma_i}$ and $\left(\lambda_w \lambda_1\right)_{\omega_i}$ are stretch ratio products based on the swollen film dimensions for the ith solute reflection coefficient experiment and the ith permeability experiment, respectively. The necessary data and the correlation C calculated from (4.4) appear in Table 4.4.

For low molecular weight solutes the correlation appears to hold. Most of the error in the correlation C is due to the error in the film permeability, ω, which in turn is due to uncertainty in the film thickness. The correlation appears to be valid for glucose for all films and for sucrose for PEO-1000 and PEO-1540 films. Additionally the correlation may be valid for sucrose and PEO-1500 and raffinose

and PEO-1540. The correlation fails for raffinose with either PEO-1000 or PEO-1500 films.

This correlation implies that for some range of solute size and film hydration σ is inversely proportional to ω. As ω is a measure of the ease with which a solute traverses the membrane and σ is a measure of the difficulty with which the solute traverses the membrane (or, in other words, the ease with which the solvent traverses the film relative to the solute), it is not surprising that over some range changes in σ and ω are proportional. Presumably, as the film becomes progressively more permeable, the correlation would fail just as it does when the film becomes too restrictive. If this occurred it would be expected that there would be a drop in the value of the correlation constant C as the film was stretched to higher and higher strains. This may be occurring with glucose and PEO-1540 films.

The data presented here are insufficient to determine the range in σ for which the correlation is valid. The data suggest that for $0.3 < \sigma < 0.7$ the correlation is at least approximately correct. If further experiments confirmed the validity of the correlation it could be used to estimate changes in film permeability caused by changes in swelling.

Consider the problem of implanting a pharmaceutical impregnated hydrogel in the body. Implants of this type are being studied as a method of administering controlled amounts of drug over long periods of time or as a method of localizing the drug at the site where it is needed. The hydrogel selected must be compatible with the drug as

well as with body tissues and fluids, have adequate mechanical integrity, and be sufficiently permeable to the pharmaceutical. The proposed correlation between σ and ω should be useful in screening materials for implants and, once a candidate material has been selected, in quality control programs to assure that the implant performs as desired.

The correlation between σ and ω that is proposed here is based on an analysis of changes in membrane permeability caused by stretching the membrane. In the last section of this chapter it will be shown that it is not the stretching of the membrane that is important in changing the permeability of the membrane but rather the change in the degree of swelling that occurs because the membrane is stretched. Therefore the correlation between σ and ω should be valid when the degree of swelling changes, regardless of whether the change occurs because the membrane is strained or because of some other reason, for example, a change in temperature.

4.6 Application of the Free Volume Theory

The free volume theory (see Chapter 1) suggests that the diffusion of a solute in a swollen membrane should be inversely proportional to the free volume of the swollen membrane. When the solute cannot diffuse through the membrane matrix or when the membrane is highly swollen, then the free volume of the unswollen membrane makes a negligible contribution to the overall free volume of the membrane swelling-solvent

system. In this case the diffusion coefficient of the solute in a swollen membrane becomes inversely proportional to the free volume of the solvent contained in the membrane and

$$D_m \propto \frac{1}{H} \qquad (4.5)$$

where H is the volume fraction of solvent in the swollen membrane.

Figure 4.10 is a plot of the diffusion coefficient of the various solutes through unstretched poly(oxyethylene glycol) based segmented polyurethanes. For a homologous series of polymers the data would be expected to fall on a straight line. With the exception of the PEO-1500 data, this is seen to be true. The PEO-1500 material was synthesized improperly (see Chapter 2) and it is not surprising that data for this material do not fall on the line. Data for PEO-1500 films are included in Figure 4.10 and subsequent plots for completeness.

It would be expected that in the limit as $H \longrightarrow 1$, the data should extrapolate to the free diffusion coefficient of the solute in water, D_o. In Figure 4.10 the lines through the data do not extrapolate to D_o. The extrapolation fails because no diffusion occurs through the "hard" phase. Two corrections are necessary to account for the presence of the "hard" phase. First, the diffusion coefficient of the solute in the membrane D_m must be increased according to

$$D_m = D_m(1/(1 - v_{hard})) \qquad (4.6)$$

where v_{hard} is the volume fraction of the "hard" phase in the swollen film. Second, the hydration H must be stated on a filler-free basis (glycol basis in Table 4.1). The necessary data are shown in Table 4.1 and plotted in Figure 4.11.

In Figure 4.11 the lines through the data for PEO-600 and PEO-1000 extrapolate to the proper D_o, but the PEO-1540 data which lay on the lines in Figure 4.10 fall below the lines in Figure 4.11. What has happened is that the effect of the "hard" phase has been greatly overstated for PEO-1540. The strain-swelling data reported in Chapter 3 (see Table 3.6) suggest a M_c of around 10,000 instead of the expected value of 1500. This implies that perhaps only one out of every five "hard" segments is participating in a "hard" domain. If this is the case then the effect is to reduce the corrections made when plotting Figure 4.11 and leave the PEO-1540 data essentially where they appear in Figure 4.10. In Figure 4.12 the PEO-1540 diffusion data are replotted to reflect the smaller effective filler concentration.

There are several reasons why it is probable that the PEO-1540 membranes would have a relatively low proportion of the "hard" blocks participating in "hard" domains. First, the concentration of the "hard" phase is less than 30% in the unswollen polymer, lowering the probability of a "hard" segment finding a "hard" domain to imbed itself in as the film forms. Second, the longer glycol chain would make it less energetically unfavorable for the "hard" segment to be surrounded by other glycol chains. Third, with a low concentration of "hard" phase, smaller domains would be expected to form, some of which might be small enough to be torn apart by forces acting on the polymer matrix

when the film swells. When the swollen weight of a PEO-1540 sample immersed in water is measured as a function of time after immersion, it takes longer to achieve an equilibrium weight (24-48 hours) than do other polyurethanes used in this study (6-12 hours).

Figures 4.13 - 4.16 are plots of the solute diffusion coefficient in the various films as a function of strain. Filled symbols represent unstretched membranes and open symbols represent stretched membranes. Since the diffusion coefficients used in Figures 4.10 - 4.16 are normalized by the film thickness, thinning of the membrane on stretching has already been compensated for.

With the exception of PEO-600 films and the plot of D_m versus 1/H for urea (Figure 4.13), the change in film hydration on stretching adequately accounts for the observed changes in D_m. Excluding these two cases the data for stretched and unstretched films fall on the same line and extrapolate to the free diffusion coefficient of the solute in water at H = 1. In the next several paragraphs the reasons for the deviation of the data for PEO-600 films and for urea are presented.

Hydrations used in Figures 4.13 - 4.16 for the stretched films are calculated from equation (3.21) using as values for χ and M_c the values determined from the strain-swelling experiments as reported in Table 3.6. These experiments are difficult to perform on PEO-600 films because of the high modulus and low degree of swelling for this material. If the two questionable data points at high strains are excluded (see Figure 3.11) then the "hard" phase free data can be fit equally well with $\chi = 0.601$ and $M_c = 400$. The predicted values for

1/H become 1.970, 1.833, 1.733, and 1.661 instead of 1.975, 1.807, 1.690, and 1.610 used in plotting Figures 4.10 - 4.16. Using the new 1/H values would bring the PEO-600 data closer to the line, but a noticeable difference would still exist.

One of three possible conclusions could be drawn from the PEO-600 data. First, the free volume theory could break down for PEO-600 films but this is unlikely in view of the fact that data for the unstretched PEO-600 film are properly predicted. Second, the Flory-Huggins equation (3.21) may not accurately predict changes in the polymer volume fraction and 1/H when the film is stretched. Third, the PEO-600 strain-swelling data are inaccurate. The most logical explanation for the discrepancy between D_m for stretched PEO-600 films and the lines through the rest of the data is that the PEO-600 strain-swelling data, which are available for a limited range of strains, are unreliable.

Figure 4.13 showing the plot of D_m for urea versus 1/H will now be considered. The free volume theory does not predict changes in D_m for urea as well as it does for other solutes. Partition coefficient data (see Table 3.9) indicate an attractive interaction between urea and the polymer. For PEO-600 films the maximum K* expected in the absence of this interaction would be a few times that of glucose, $K^* < 1.0$. The observed K* of 1.5 suggests that a third, and perhaps more, of the urea in the membrane is there because of an attractive interaction between urea and the membrane material. Similar interactions have been noted by Gary-Bobo et al. (6) and Yasuda et al. (7).

Because of this urea-polymer interaction, increases in the film hydration would not be as effective in increasing D_m for urea as for the other solutes, since part of the total urea flux occurs by diffusion through the polymer matrix and is unaffected by changes in film hydration. If the explanations offered for the discrepancy between the PEO-600 data and the stretched film urea data and the lines through the remainder of the data are correct, then the free volume theory adequately describes the changes in film permeability that occur when the membrane is strained.

Meares et al. (8,9) have proposed that for uniformly swollen polymers the ratio D_m/D_o is given by

$$\frac{D_m}{D_o} = \left(\frac{1 - v_2}{1 + v_2}\right)^2 \qquad (4.7)$$

Paul, Garcin, and Garmon (10) have shown that for highly swollen natural rubber membranes ($0.5 > v_2$), equation (4.7) adequately describes the diffusion of the red dye Sudan IV. They point out four other sets of data in the literature of which only one is described satisfactorily by (4.7). Data from this study are shown along with equation (4.7) in Figures 4.17 and 4.18. Of the two plots Figure 4.18 is the more meaningful as in that plot a correction was made for the presence of the "hard" phase. Even in Figure 4.17 the fit between the data and equation (4.7) is not good. While (4.7) predicts that D_m/D_o will be independent of the size of the solute, the free volume theory predicts that D_m/D_o will depend on molecular size. Vrentas

and Duda (11,12) have shown that in concentrated polymer solutions not only is the molecular size important but also the ratio of the molecular size to the size of a "jumping unit" (approximately a monomeric unit) for the polymer is important. It is not clear how the approach of Vrentas and Duda would apply to highly swollen systems such as those considered here. It appears that the importance of the size of the "jumping unit" becomes negligible for highly swollen polymers but that the importance of the solute size remains. It is likely that the Meares approach fails because of a failure to consider the size of the solute.

4.7 Importance of Polymer Microstructure

The microstructure of the segmented polyurethanes used in this study controls the physical and permeability properties of these polymers. The microstructure of a typical segmented polyurethane is shown schematically in Figure 4.1 a,b.

Segmented polyurethanes are elastomers because microphase separation of the "hard" blocks into discrete "hard" domains occurs. The domains that are formed are smaller but far stronger than the domains formed in the styrene-butadiene-styrene tri-block elastic polymers (13). In the S-B-S tri-block polymers physical crosslinking occurs below

the glass transition temperature of the styrene phase due to the separation of the butadiene and styrene blocks into domains. The styrene domains are held together by van der Waal's forces and so the styrene molecular weight required for domain formation is relatively high (14) (approximately 10,000) and the domains formed are generally larger than 100 Å. Segmented polyurethanes are capable of forming strong hydrogen bonds between the "hard" blocks (see Figure 4.19) and thus can form stable physical crosslinks even though the "hard" block molecular weight is only 584. Perfect allignment of the "hard" blocks as shown in Figure 4.19 is not required in order for the "hard" domain to exist. Bonart (15) gives a number of other configurations that are stable as well as X-ray data which confirm the formation of "hard" domains. Shimannski et al. (16) also have reported X-ray interferences due to "hard" domains. Little is known about the actual structures of the "hard" domains except that they are quite narrow ($\sim$25 Å) and lamellar rather than spherical in shape.

The modulus of segmented polyurethanes is controlled by the "hard" phase which acts not only as a physical crosslink but also as a filler. The modulus of these polymers may be increased by increasing the "hard" phase concentration or by using bulkier diisocyanates and diamines which tend to form more rigid "hard" domains (17). The "soft" polyether segment influences the elongation at break and

the degree of swelling. The relative amounts of "hard" phase and "soft" phase may be varied by changing the polyether molecular weight or by using a different diisocyanate or diamine. For a given "hard" segment, increasing the polyether molecular weight decreases the "hard" phase concentration in the final polymer, increases the degree of swelling in water, decreases the modulus, and increases the elongation at break. Additionally, the film permeability increases and the film selectivity, the ability of the swollen film to discriminate between solutes, decreases. These trends are shown in Figure 4.20.

The size of the polyether segment determines not only the degree to which the polymer swells but also the molecular weight range of the solutes that can diffuse through the film. The poly(oxyethylene glycol) 600 based polyurethane is essentially impermeable to raffinose, molecular weight 504. Cutoff molecular weights, the molecular weight above which the film is impermeable, were not determined for the other polyurethanes. Since the polyether molecule determines the spacing of the "hard" blocks in the polymer it is probable that the cutoff molecular weight is strongly correlated with the molecular weight of the polyether segment.

Figure 4.21 shows how the diffusion coefficient of each solute in the swollen films varies with changes in the the weight-average molecular weight of the "soft" segment. The dotted curves through the data are shown to emphasize the

similarity in the changes. As M_w increases, each curve asymptotically approaches D_o, the free diffusion coefficient for its solute. As M_w decreases each curve becomes steeper as the films become more restrictive and eventually unable to pass the solute. The similarity in the shape of the curves further suggests that each solute finds a similar environment when diffusing through a film and that the important parameters are the size of the solute and the number and size of the regions through which the solute may diffuse.

No attempt has been made to account for changes in film permeability that might be due to changes in the film tortuosity. For the polymers studied here, little if any, change in the film tortuosity would be expected when the films are stretched but there may be small differences between the tortuosities of the films made from different polyethers.

Throughout this discussion no reference has been made to free chain ends or to the number of blocks per polymer molecule. Other studies have shown that there is little change in polymer properties when the number of blocks in the main chain increases above five. The actual number of blocks per molecule for the polyurethanes studied here is unknown but it is certainly greater than five. The intrinsic viscosities for the polymers synthesized in this study are given in Table 4.5 along with estimates of the Mark-Howink parameters and the number of blocks per molecule.

Mark-Howink parameters for the polyurethanes studied here are not available in the literature. The molecular weight of the polymers and the number of blocks per molecule were calculated from the Mark-Howink equation. Based on the

$$[\eta] = KM^a \qquad (4.8)$$

estimates for the molecular weight of these polymers it is believed that the effect of free chain ends and the number of blocks per molecule is negligible.

4.8 Conclusions and Recommendations

This thesis represents the first determination of the permeability of segmented polyurethane films for the solutes urea, glucose, sucrose, and raffinose. The usefulness of the free-volume theory for explaining permeability data for systems where strong solute-membrane interactions are absent is confirmed. Some reasons for the failure of Meares' approach to explain data for solute diffusion through swollen membranes are suggested. The work of Tobolsky and co-workers on the NaCl and water permeability of segmented polyurethane films is extended to include other solutes. Changes in film permeability which occur when the film is deformed are shown to be due in part to changing the film thickness and in part to changing the degree of swelling of the film, the sum of these two effects being sufficient

to explain the total observed change in the film permeability. Finally, more time efficient methods of screening polymers for use as membranes in certain applications and for evaluating the performance and quality of the membranes are suggested.

The permeability of segmented polyurethanes based on four poly(oxyethylene glycol)s of different molecular weights for the solutes urea, glucose, sucrose, and raffinose has been determined. These data suggest another approach, besides that of Tobolsky and co-workers, to obtain reverse osmosis membranes using segmented polyurethanes.

Tobolsky and co-workers determined the water and NaCl permeability of a large number of segmented polyurethanes. They varied the hydrophilic properties of their membranes by using varying ratios of poly(oxyethylene glycol) and poly(oxypropylene glycol) in the polymer in an attempt to achieve membranes with both high water flux and high salt rejection. They did not succeed although some of their films did give either high water flux or high salt rejection but not both.

Instead of increasing salt rejection by providing a poor environment for water to diffuse (by increasing the poly(oxyethylene glycol) content), one could retain in the polymer strong hydrophilic domains but restrict their size. This may be done by reacting a low molecular weight (86 to 300) poly(oxyethylene glycol) with a diisocyanate to produce

a polymer similar to the ones studied in this thesis but with "hard" and "soft" blocks of lower molecular weight. Such a polymer should be tough and provide a good environment for water diffusion but a poor environment for salt diffusion. It must be remembered that what is being sought both here and by Tobolsky, is a polymer in which the water dissolves in and diffuses through an essentially "solid" material. There is evidence that this happens in the asymmetric cellulose-acetate reverse-osmosis membranes in the skin layer. Neither the approach of Tobolsky nor the approach suggested here is likely to give useful membranes unless they can be formed with a dense thin skin over a macroporous supporting layer as in the cellulose-acetate reverse-osmosis membranes.

The data taken during the course of this investigation confirm the validity of the free-volume theory for diffusion through swollen polymers in the absence of strong solute-membrane interactions. The free-volume theory states that the permeability of a polymer film to a solute depends on the degree to which the polymer is swollen and the size of the solute. For a given solute, as the free volume of the membrane (degree of swelling) increases, the diffusion coefficient of the solute in the membrane should approach that of the solute in pure solvent at the same concentration and temperature. For a homologous family of polymers, a plot of the logarithim of the ratio of the diffusion coefficient

of the solute in the membrane to that in solution, $\log(D_m/D_o)$, versus the inverse of the film degree of swelling, $(1/H)$, should be linear and extrapolate to D_o at $H = 1$.

When a membrane is deformed, the film permeability changes. Part of this change is due to a change in the film thickness, and the remainder is due to a change in the degree of swelling of the film. If the data are normalized to remove the effect of the changing film thickness, the remaining change in the film permeability (solute diffusion coefficient in the film) is explained by the change in the free volume (degree of swelling) that occurs when the film is stretched. Thickness-normalized data for stretched films at different total stretch ratios (different degrees of swelling) fall on the same line as data for a homologous family of polymers in a $\log(D_m/D_o)$ versus $1/H$ plot.

If there is a strong interaction between the polymer and the solute, the free-volume theory may fail to predict diffusion data accurately. When more than one diffusion path is involved, for example diffusion through a swollen membrane and absorption on and surface diffusion along the membrane matrix, the free-volume theory will in general fail, and the magnitude of the difference between the predictions of the theory and the actual data will depend on the relative importance of each of the diffusion paths.

The free-volume theory predicts that the ability of a polymer or family of polymers to discriminate between

solutes decreases as the degree of swelling increases. Data from this study confirm this prediction. For a pair of solutes, the ability of a membrane to discriminate between them is infinite when only one of the solutes can permeate the film. As the membrane becomes more and more highly swollen, the diffusion coefficient of each solute in the film approaches the solute free-diffusion coefficient. Depending on the partition coefficient of each solute between the solution and the film, it is possible for a family of polymers to be impermeable to one of a pair of solutes at low degrees of swelling and more permeable to it than the second of the pair at high degrees of swelling.

This study suggests an explanation for the failure of Meares' approach to account accurately for permeability data. Meares' approach does not consider molecular size of the solute as a variable influencing the permeability of a polymer. The free-volume theory, other experimental data, and this study all indicate that membrane permeability is related to solute size. Meares' approach predicts that all data for all solutes and all polymers will fall on a single curve. The Meares' approach does fit data for one or two systems reported in the literature but fails to predict properly the vast majority of the data available in the literature. At this point the fit between Meares' theory and the data from the two systems that it does fit should be regarded as coincidental.

This study suggests the possibility of a correlation between two parameters which appear in the theory of thermodynamics of irreversible processes. The correlation states that for a limited range in the solute reflection coefficient σ, σ and the film permeability coefficient ω are inversely proportional. The data from this study are insufficient to determine the range in σ for which the correlation is valid but suggest that for $0.3 \leq \sigma \leq 0.7$, the correlation will hold. Since it is much easier and faster to determine σ for a polymer-solute system than it is to determine ω, further work should be done to determine the range in σ for which the correlation is valid. It is known that the correlation must fail for both sufficiently low and high values of σ but the range over which the correlation appears to be valid is quite wide. The correlation should prove useful as a method of screening membranes to select the most likely candidates for a given application for further testing and as a quality control test in critical applications such as drug impregnated polymeric implants.

Finally, many membrane applications involve the use of membrane supports which may be needed to prevent either damage or deformation of the membrane. For economic reasons it is desirable to balance the need for membrane support against the deterioration of the membrane performance that may occur because of inadequate support. It is relatively easy to design membrane supports to ensure mechanical

integrity of the membrane, but it is not as easy to design supports that give optimum performance of the membrane as a separator. For example, up to 30% of the total salt flux through reverse-osmosis membranes occurs because of deformation of the membrane in the vicinity of the perforations in the supporting plate. In areas such as combustion gas cleanup, solvent vapor recovery, and purification of waste waters, the design of the membrane support may be as important as the selection of the membrane in determining the success or failure of the membrane system. This study points out the necessity of considering deformation of the membrane when designing membrane systems and suggests that for membranes which may be regarded as swollen elastomers, the free-volume theory will be useful in matching the membrane and its support to achieve optimum performance.

TABLE 4.1

Summary of Diffusion Coefficient and Film Hydration Data

Polymer Designation	Stretch Ratio referred to swollen dimensions λ_w	λ_1	Solute	Solute Diffusivity in the Swollen Film $D_m \times 10^7$	1/H	Glycol Basis 1/H	Glycol Basis $D_m \times 10^7$ cm^2/sec
PEO-600	1	1	Urea	8.72 ± 2.2	2.912	1.975	12.9 ± 3.4
	1.259	0.998		10.0 ± 2.3	2.58	1.807	14.8 ± 3.7
	1.247	1.242		10.3 ± 2.4	2.36	1.690	15.2 ± 3.6
	1.250	1.485		10.3 ± 2.4	2.21	1.611	15.2 ± 4.3
	1	1	Glucose	$3.30 \pm .73$	- see urea-		4.87 ± 1.3
	1.259	0.998		$3.83 \pm .80$			5.65 ± 1.4
	1.247	1.242		4.48 ± 1.0			6.61 ± 1.6
	1.250	1.485		4.84 ± 1.0			7.14 ± 2.0
	1	1	Sucrose	$1.34 \pm .29$	-see urea-		1.98 ± 0.6
	1.259	0.998		$1.65 \pm .34$			2.43 ± 0.7
	1.247	1.242		$2.23 \pm .50$			3.29 ± 1.0
	1.250	1.485		$2.56 \pm .51$			3.78 ± 1.1

TABLE 4.1 - continued

Summary of Diffusion Coefficient and Film Hydration Data

Polymer Designation	Stretch Ratio referred to swollen dimensions λ_w	λ_1	Solute	Solute Diffusivity in the Swollen Film $D_m \times 10^7$	1/H	Glycol Basis 1/H	Glycol Basis $D_m \times 10^7$ cm^2/sec
PEO-1000	1	1	Urea	27.3	1.89	1.568	33.4 ± 7.0
	1.246	0.996		33.1	1.807	1.510	39.9 ± 8.4
	1.239	1.249		35.2	1.729	1.461	$42.4 \pm 10.$
	1	1	Glucose	12.4	-see urea-		15.0 ± 3.0
	1.246	0.996		14.5			16.8 ± 2.9
	1.239	1.249		17.0			20.4 ± 4.1
	1	1	Sucrose	6.60	-see urea-		7.95 ± 1.3
	1.246	0.996		7.92			9.54 ± 1.6
	1.239	1.249		8.88			10.7 ± 2.0
	1	1	Raffinose	4.70	-see urea-		5.66 ± 1.0
	1.246	0.996		6.55			7.89 ± 1.1
	1.239	1.249		7.88			9.50 ± 1.7

TABLE 4.1 - continued

Summary of Diffusion Coefficient and Film Hydration Data

Polymer Designation	Stretch Ratio referred to swollen dimensions λ_w	λ_l	Solute	Solute Diffusivity in the Swollen Film $D_m \times 10^7$	1/H	Glycol Basis 1/H	Glycol Basis $D_m \times 10^7$ cm^2/sec
PEO-1500*	1	1	Urea	22.5	2.208	1.671	25.6 ± 4.0
	1	1.151		23.5	2.08	1.600	26.7 ± 4.7
	1.141	1.152		25.0	1.976	1.541	28.4 ± 5.5
	1	1	Glucose	11.7	-see urea-		13.3 ± 2.0
	1	1.151		12.9			14.6 ± 2.2
	1.141	1.152		15.6			17.7 ± 2.7
	1	1	Sucrose	6.84	-see urea-		7.77 ± 1.1
	1	1.151		8.23			9.35 ± 1.4
	1.141	1.152		11.0			12.5 ± 1.7
	1	1	Raffinose	4.61	-see urea-		5.24 ± 0.8
	1	1.151		6.72			7.63 ± 1.3
	1.141	1.152		9.25			10.5 ± 1.3

*It is assumed that half of the non-glycol material is in the "hard" domains. (see Chapter 2)

TABLE 4.1 - continued

Summary of Diffusion Coefficient and Film Hydration Data

Polymer Designation	Stretch Ratio referred to swollen dimensions λ_w	λ_1	Solute	Solute Diffusivity in the Swollen Film $D_m \times 10^7$	1/H	Glycol Basis 1/H	Glycol Basis $D_{m_2} \times 10^7$ cm^2/sec	Corrected Glycol Basis 1/H	Corrected Glycol Basis $D_m \times 10^7$ cm^2/sec
PEO-1540	1	1	Urea	44.3 ± 7.3	1.435	1.317	48.2	1.42	45.0 ± 7.3
	1.211	1.002		44.1 ± 8.4	1.415	1.303	48.2	1.395	44.8 ± 8.4
	1.209	1.188		45.2 ± 9.0	1.398	1.292	49.2	1.38	46.0 ± 9.0
	1	1	Glucose	20.4 ± 2.2	-see urea-		22.3	1.42	20.7 ± 2.2
	1.211	1.002		21.3 ± 2.8			23.2	1.395	21.7 ± 2.8
	1.209	1.188		22.3 ± 3.0			24.2	1.38	22.7 ± 3.0
	1	1	Sucrose	12.9 ± 1.3	-see urea-		14.0	1.42	13.1 ± 1.3
	1.211	1.002		14.0 ± 1.5			15.3	1.395	14.2 ± 1.5
	1.209	1.188		14.8 ± 1.6			16.1	1.38	15.0 ± 1.6
	1	1	Raffinose	8.79 ± 0.9	-see urea-		9.57	1.42	8.94 ± 0.9
	1.211	1.002		10.3 ± 1.1			11.2	1.395	10.5 ± 1.1
	1.209	1.188		11.1 ± 1.4			12.1	1.38	11.3 ± 1.4

TABLE 4.2

Molecular Sieve Theory predicted Pore Size, R_p

Polymer Designation	Solute	10 x (D_m/D_o)	R_s/R_p	R_p in Å
PEO-600	Urea	0.906	0.3889	6.8
	Glucose	o.705	0.4092	10.9
	Sucrose	0.370	0.4473	12.4
PEO-1000	Urea	2.352	0.2770	9.5
	Glucose	2.171	0.2886	15.4
	Sucrose	1.486	0.3379	16.4
	Raffinose	1.269	0.3558	18.5
PEO-1500	Urea	1.803	0.3138	8.4
	Glucose	1.925	0.3052	14.6
	Sucrose	1.452	0.3406	16.3
	Raffinose	1.175	0.3639	18.0
PEO-1540	Urea	3.120	0.2333	11.3
	Glucose	2.952	0.2337	18.3
	Sucrose	2.411	0.2734	20.3
	Raffinose	1.971	0.3020	21.7

TABLE 4.3

Available Area Ratio - A_s/A_w

Polymer Designation	Solute	Total Strain in the σ expt.	σ	$1 - \frac{\omega \bar{V}_s}{L_p}$	A_s/A_w	$(A_s/A_w)/(A_s/A_w)_o$	ω/ω_o
PEO-600	Glucose	1	0.929	0.946	0.017	1	1
		1.23	0.656	0.936	.280	16.5	1.3
		1.43	0.592	0.885	.293	17.2	1.65
	Sucrose	1	0.955	0.969	.014	1	1
		1.23	0.752	0.953	.201	14.4	1.38
		1.43	0.672	0.897	.225	16.1	2.03
PEO-1000	Glucose	1	0.442	0.942	.500	1	1
		1.235	0.392	0.939	.567	1.13	1.17
		1.513	0.311	0.926	.615	1.23	1.5
	Sucrose	1	0.574	0.947	.373	1	1
		1.235	0.483	0.945	.462	1.24	1.27
		1.513	0.413	0.931	.518	1.39	1.47
	Raffinose	1	0.752	0.966	0.214	1	1
		1.235	0.663	0.959	.296	1.38	1.46
		1.513	0.568	0.942	.374	1.75	1.83

TABLE 4.3 - continued

Available Area Ratio - A_s/A_w

Polymer Designation	Solute	Total Strain in the σ expt.	σ	$1 - \frac{\omega \bar{V}_s}{L_p}$	A_s/A_w	$(A_s/A_w)/(A_s/A_w)_o$	ω/ω_o
PEO-1500	Glucose	1	0.391	0.955	.564	1	1
		1.157	0.347	0.957	.610	1.08	1.17
		1.322	0.309	0.961	.652	1.16	1.48
	Sucrose	1	0.488	0.960	.472	1	1
		1.157	0.434	0.958	.524	1.11	1.28
		1.322	0.377	0.958	.581	1.23	1.79
	Raffinose	1	0.682	0.975	.293	1	1
		1.157	0.625	0.971	.346	1.18	1.42
		1.322	0.577	0.967	.390	1.33	2.33
PEO-1540	Glucose	1	0.321	0.940	.619	1	1
		1.235	0.276	0.949	.673	1.09	1.06
		1.534	0.250	0.956	.706	1.14	1.12
	Sucrose	1	0.395	0.937	.542	1	1
		1.235	0.361	0.944	.583	1.08	1.10
		1.534	0.318	0.946	.628	1.16	1.18
	Raffinose	1	0.591	0.953	.362	1	1
		1.235	0.520	0.955	.435	1.2	1.18
		1.534	0.485	0.956	.471	1.3	1.29

TABLE 4.4

Data for and the Calculation of the Correlation between σ and ω

Polymer Designation	Solute	Permeability Experiment		Solute Reflection Experiment		Correlation
		Total strain $\lambda_w\lambda_1$	$\omega \times 10^{18}$ mol-cm/dyne-sec	Total Strain $\lambda_w\lambda_1$	σ	C
PEO-600	Glucose	1	$1.548 \pm .341$	1	$.929 \pm .015$	$.929 \pm .20$
		1.256	$2.027 \pm .426$	1.230	$.656 \pm .01$	$.841 \pm .20$
		1.549	$2.592 \pm .557$	1.433	$.592 \pm .01$	$.917 \pm .22$
	Sucrose	1	$0.475 \pm .105$	1	$.955 \pm .015$	$.955 \pm .21$
		1.256	$0.654 \pm .137$	1.230	$.752 \pm .02$	$1.014 \pm .21$
		1.549	$0.965 \pm .217$	1.433	$.672 \pm .02$	$1.263 \pm .27$
PEO-1000	Glucose	1	9.488 ± 1.57	1	$.442 \pm .01$	$.442 \pm .06$
		1.241	11.08 ± 1.74	1.235	$.397 \pm .01$	$.461 \pm .07$
		1.548	14.21 ± 2.42	1.513	$.311 \pm .01$	$.455 \pm .07$
	Sucrose	1	$5.010 \pm .716$	1	$.574 \pm .01$	$.574 \pm .06$
		1.241	$6.296 \pm .944$	1.235	$.483 \pm .01$	$.604 \pm .08$
		1.548	7.382 ± 1.23	1.513	$.413 \pm .01$	$.595 \pm .09$
	Raffinose	1	$1.678 \pm .227$	1	$.752 \pm .01$	$.752 \pm .11$
		1.241	$2.446 \pm .311$	1.235	$.663 \pm .01$	$.962 \pm .13$
		1.548	$3.076 \pm .431$	1.513	$.568 \pm .01$	$1.018 \pm .15$

TABLE 4.4 - continued

Data for and the Calculation of the Correlation between σ and ω

Polymer Designation	Solute	Permeability Experiment		Solute Reflection Experiment		Correlation
		Total Strain λ_w λ_1	$\omega \times 10^{18}$ mol-cm/dyne-sec	Total Strain λ_w λ_1	σ	C
PEO-1500	Glucose	1	8.732 ± 1.17	1	$0.391 \pm .01$	$.391 \pm .05$
		1.151	10.19 ± 1.30	1.157	$.347 \pm .01$	$.407 \pm .05$
		1.314	12.96 ± 1.65	1.322	$.309 \pm .01$	$.461 \pm .06$
	Sucrose	1	$4.107 \pm .485$	1	$.488 \pm .01$	$.488 \pm .06$
		1.151	$5.251 \pm .651$	1.157	$.434 \pm .01$	$.558 \pm .06$
		1.314	$7.370 \pm .855$	1.322	$.377 \pm .01$	$.681 \pm .08$
	Raffinose	1	$1.781 \pm .235$	1	$.682 \pm .01$	$.682 \pm .09$
		1.151	$2.527 \pm .361$	1.157	$.625 \pm .01$	$.891 \pm .12$
		1.314	$3.974 \pm .990$	1.322	$.577 \pm .01$	$1.29 \pm .25$
PEO-1540	Glucose	1	37.19 ± 3.44	1	$.321 \pm .01$	$.321 \pm .03$
		1.213	39.58 ± 4.87	1.235	$.276 \pm .01$	$.299 \pm .04$
		1.436	41.72 ± 4.92	1.534	$.250 \pm .01$	$.300 \pm .04$
	Sucrose	1	20.85 ± 1.69	1	$.395 \pm .01$	$.395 \pm .04$
		1.213	23.00 ± 2.23	1.235	$.361 \pm .01$	$.405 \pm .05$
		1.436	24.50 ± 2.48	1.534	$.318 \pm .01$	$.399 \pm .05$
	Raffinose	1	$10.69 \pm .88$	1	$.591 \pm .01$	$.591 \pm .06$
		1.213	12.65 ± 1.14	1.235	$.520 \pm .01$	$.626 \pm .08$
		1.436	13.79 ± 1.15	1.534	$.485 \pm .01$	$.668 \pm .08$

Table 4.5

Intrinsic Viscosity and Estimated Molecular Weight of Segmented Polyurethanes

Polymer Designation	Estimated[1] Mark-Howink Parameters a	K	Intrinsic Viscosity	Predicted Molecular Weight	Average Molecular Weight of a "Hard" - "Soft" Block Pair	Approximate Number of Block Pairs per Molecule
PE0-600	0.8	$1x10^{-4}$	0.71	$1.16x10^{5}$	1180	98
PE0-1000	0.8	$1x10^{-4}$	0.67	$1.08x10^{5}$	1580	68
PE0-1500	0.8	$1x10^{-4}$	1.35	$2.59x10^{5}$	1150	225
PE0-1540	0.8	$1x10^{-4}$	2.16	$4.66x10^{5}$	2000	230

(1) Mark-Howink parameters were estimated from data for similar polyurethanes. Estimates are believed to be conservative, i.e. the predicted molecular weight should be lower than the actual molecular weight.

Segmented Polyurethane

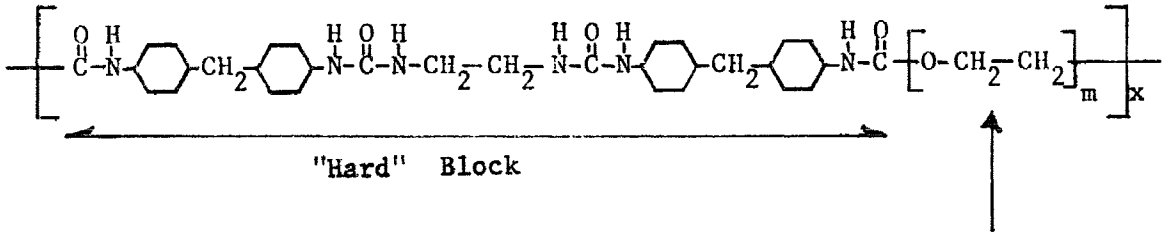

Figure 4.1a

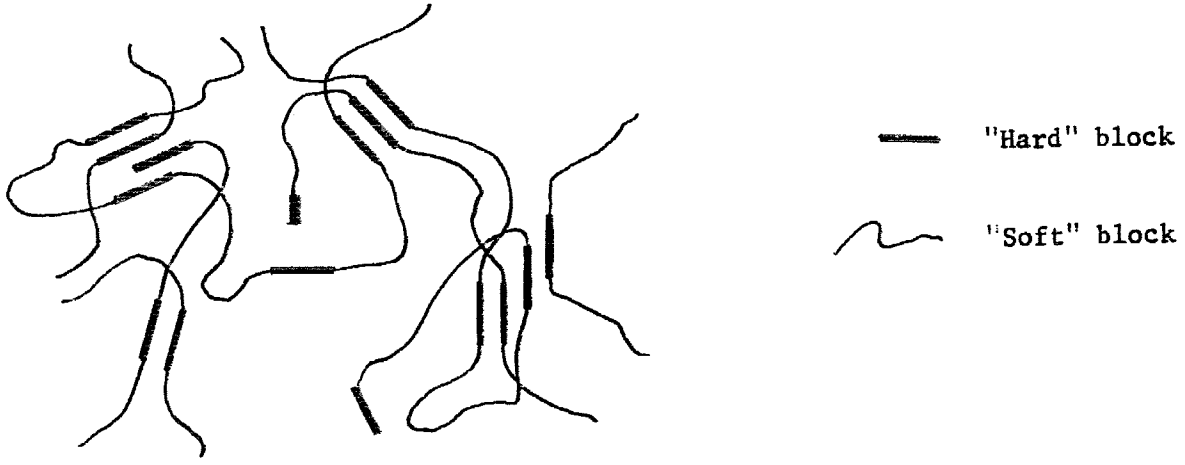

Figure 4.1b

Figure 4.1a,b. Schematic representation of the structure of segmented polyurethanes.

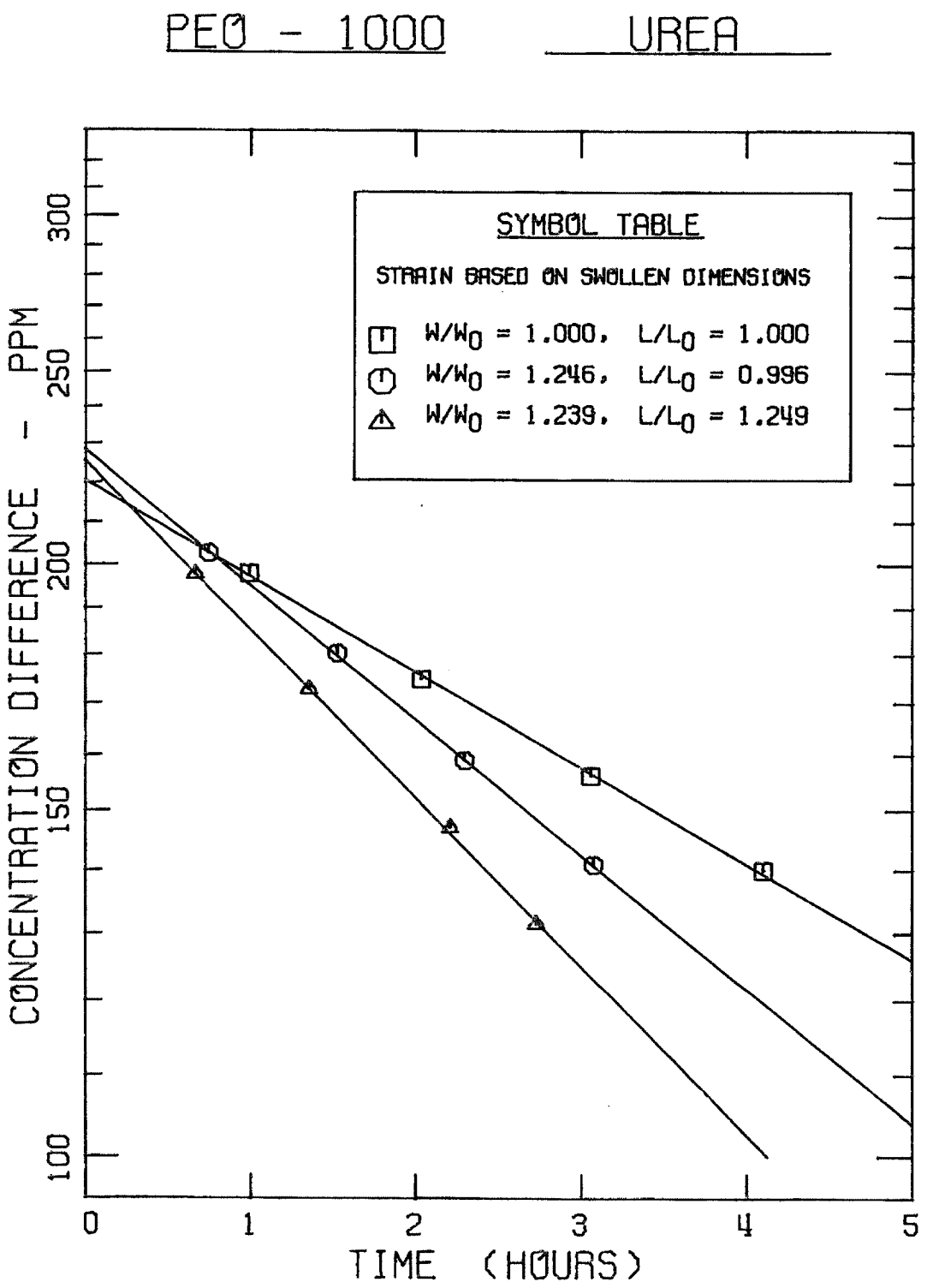

Figure 4.2. Concentration difference versus time for a PEO-1000 film. Weighted average film thickness 0.00402 cm for the dry unstrained film. Curves theoretical (eqn. 3.10).

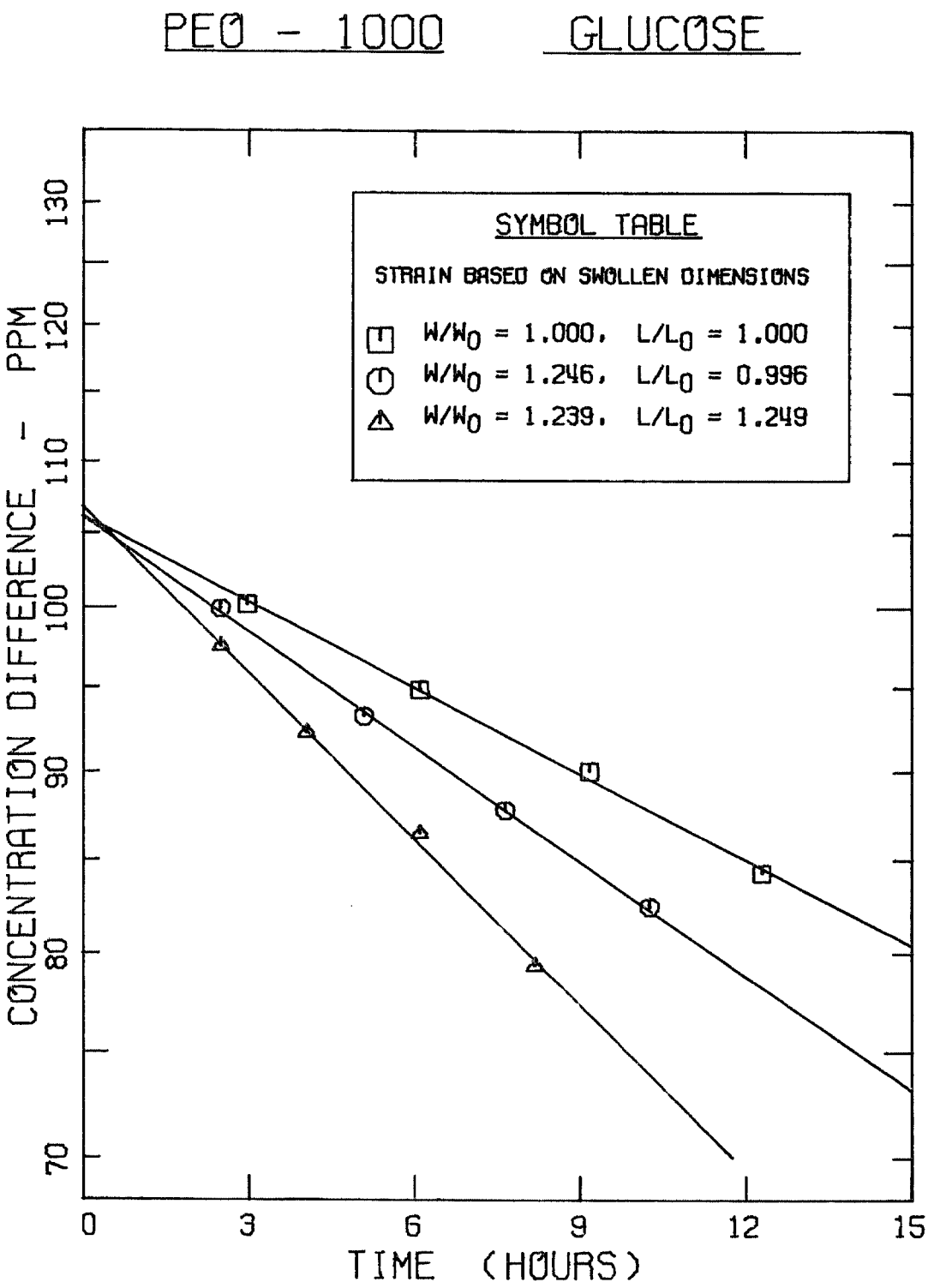

Figure 4.3. Concentration difference versus time for a PEO-1000 film. Weighted average film thickness 0.00402 cm for the dry unstrained film. Curves theoretical (eqn. 3.10).

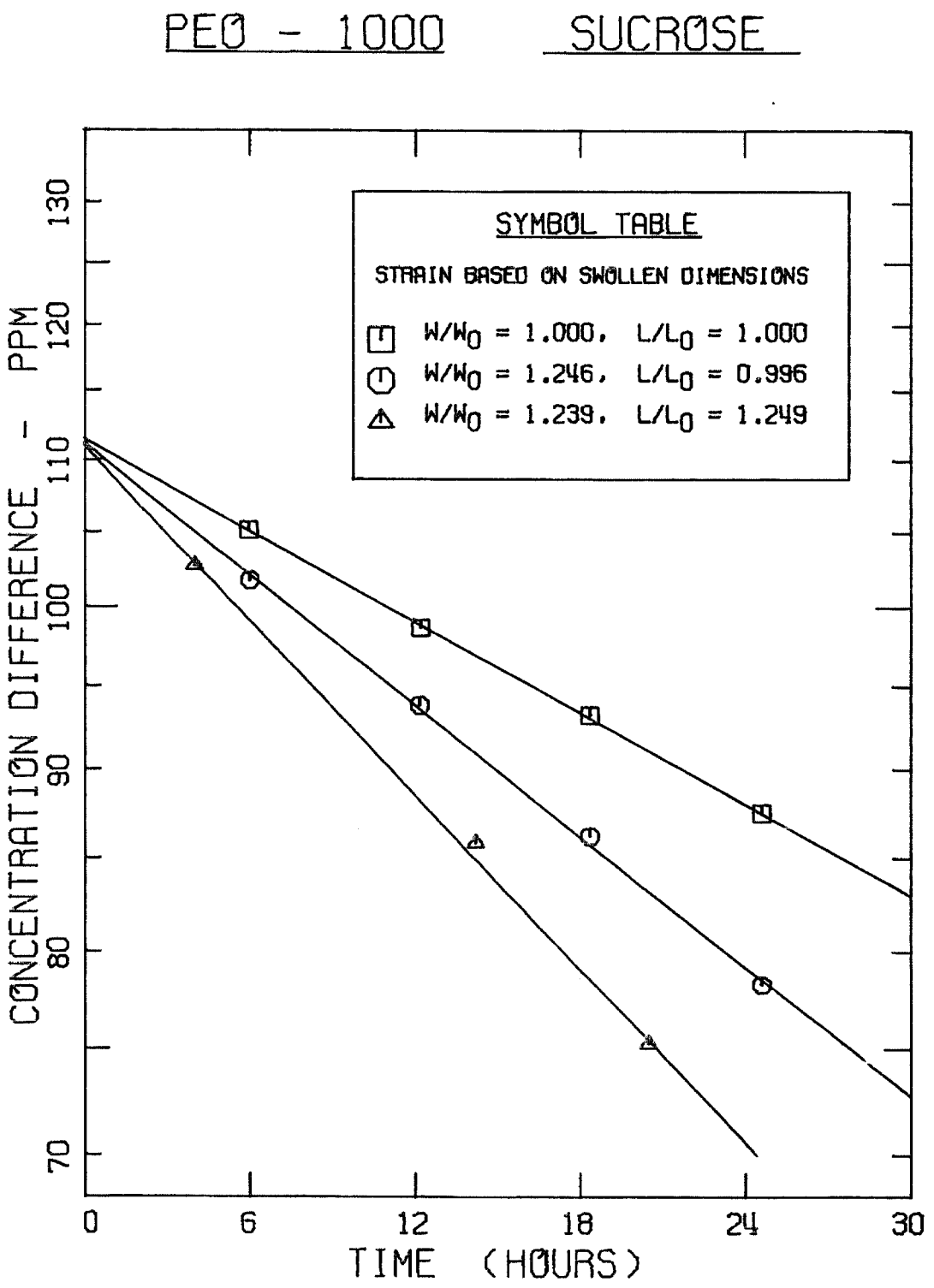

Figure 4.4. Concentration difference versus time for a PEO-1000 film. Weighted average film thickness 0.00402 cm for the dry unstrained film. Curves theoretical (eqn. 3.10).

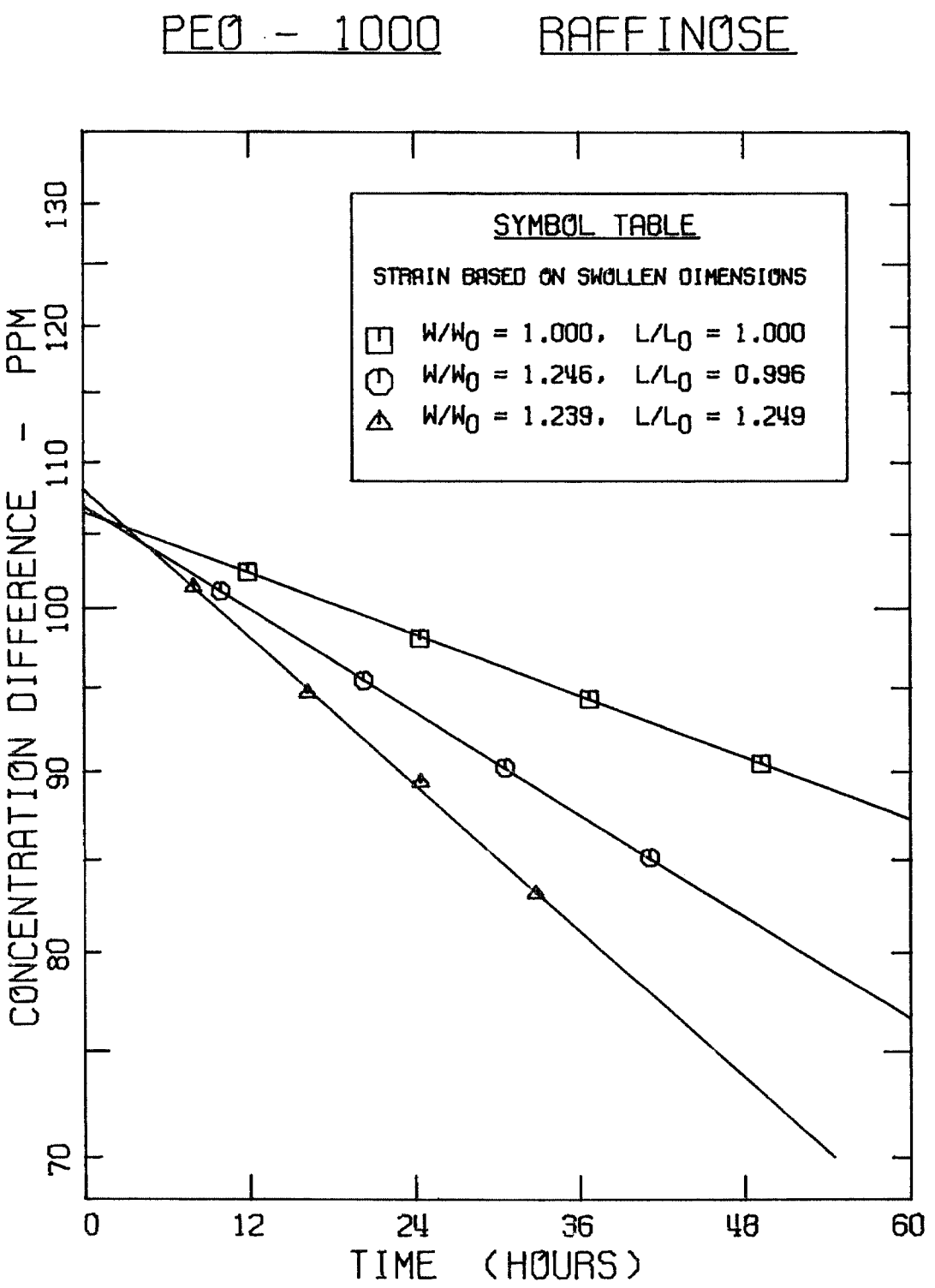

Figure 4.5. Concentration difference versus time for a PEO-1000 film. Weighted average film thickness 0.00402 cm for the dry unstrained film. Curves theoretical (eqn. 3.10).

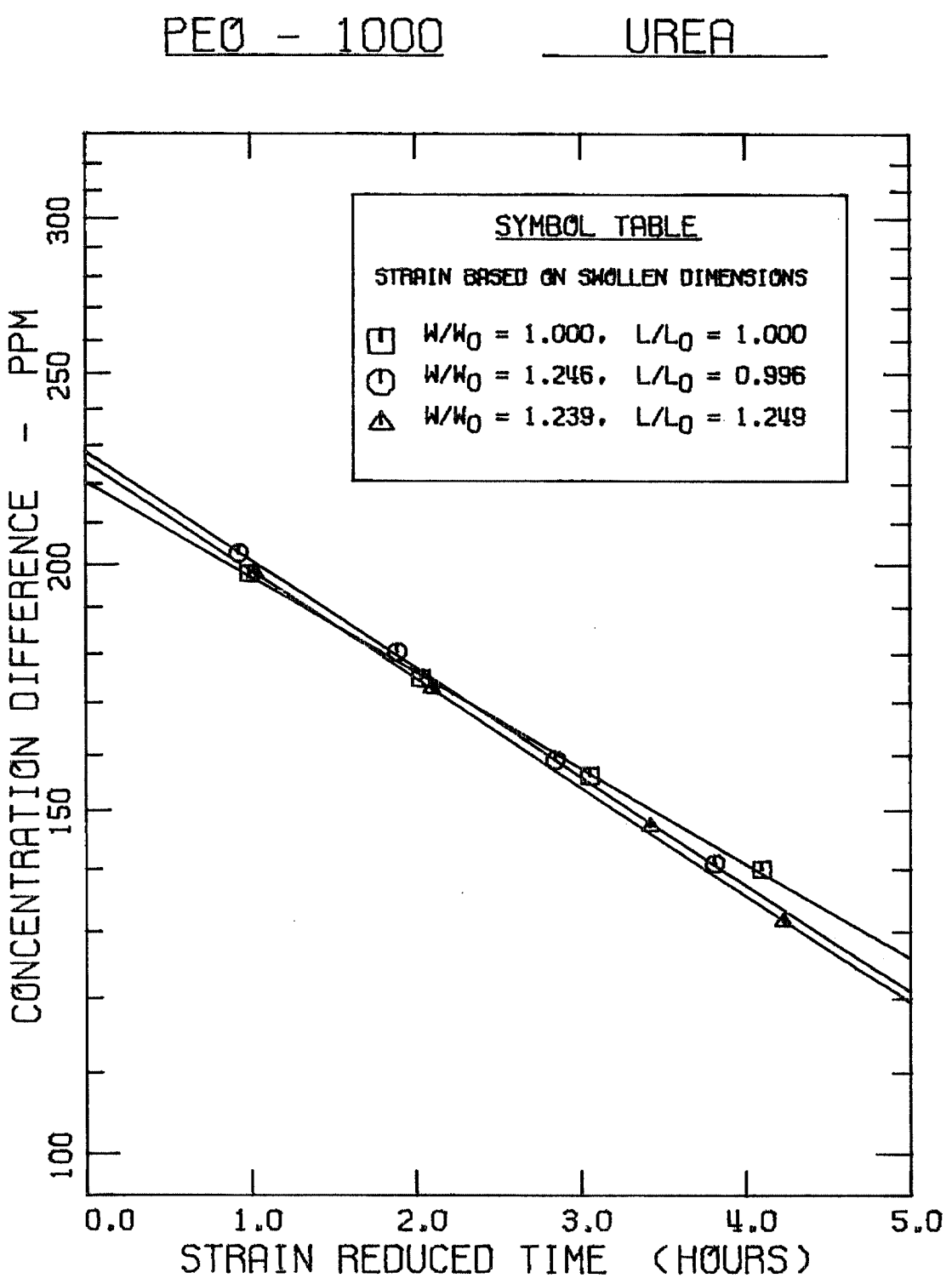

Figure 4.6. Concentration difference versus time for a PEO-1000 film. Weighted average film thickness 0.00402 cm for the dry unstrained film. Curves theoretical (eqn. 3.10).

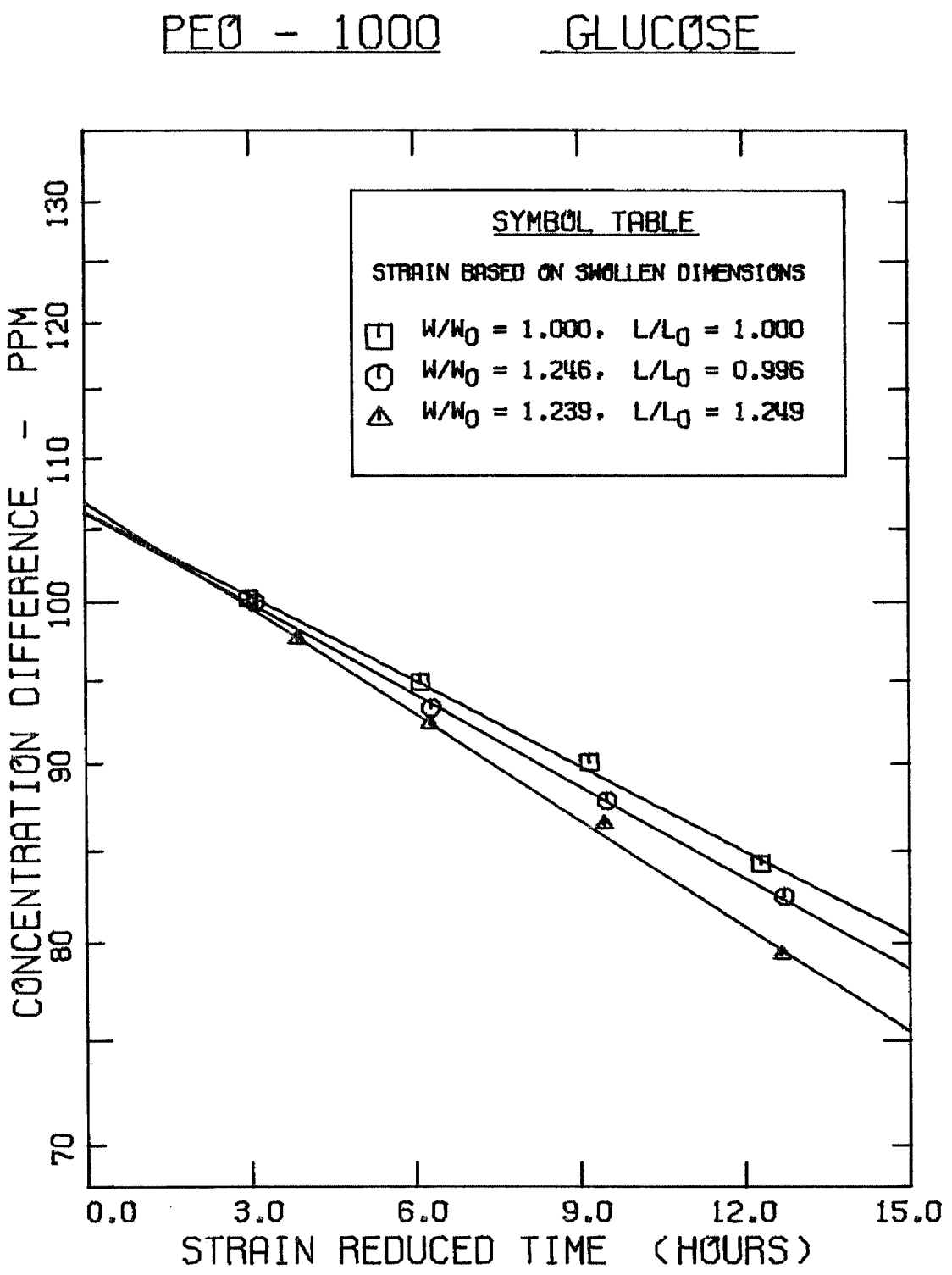

Figure 4.7. Concentration difference versus time for a PEO-1000 film. Weighted average film thickness for the dry unstrained film 0.00402 cm. Curves theoretical (eqn. 3.10).

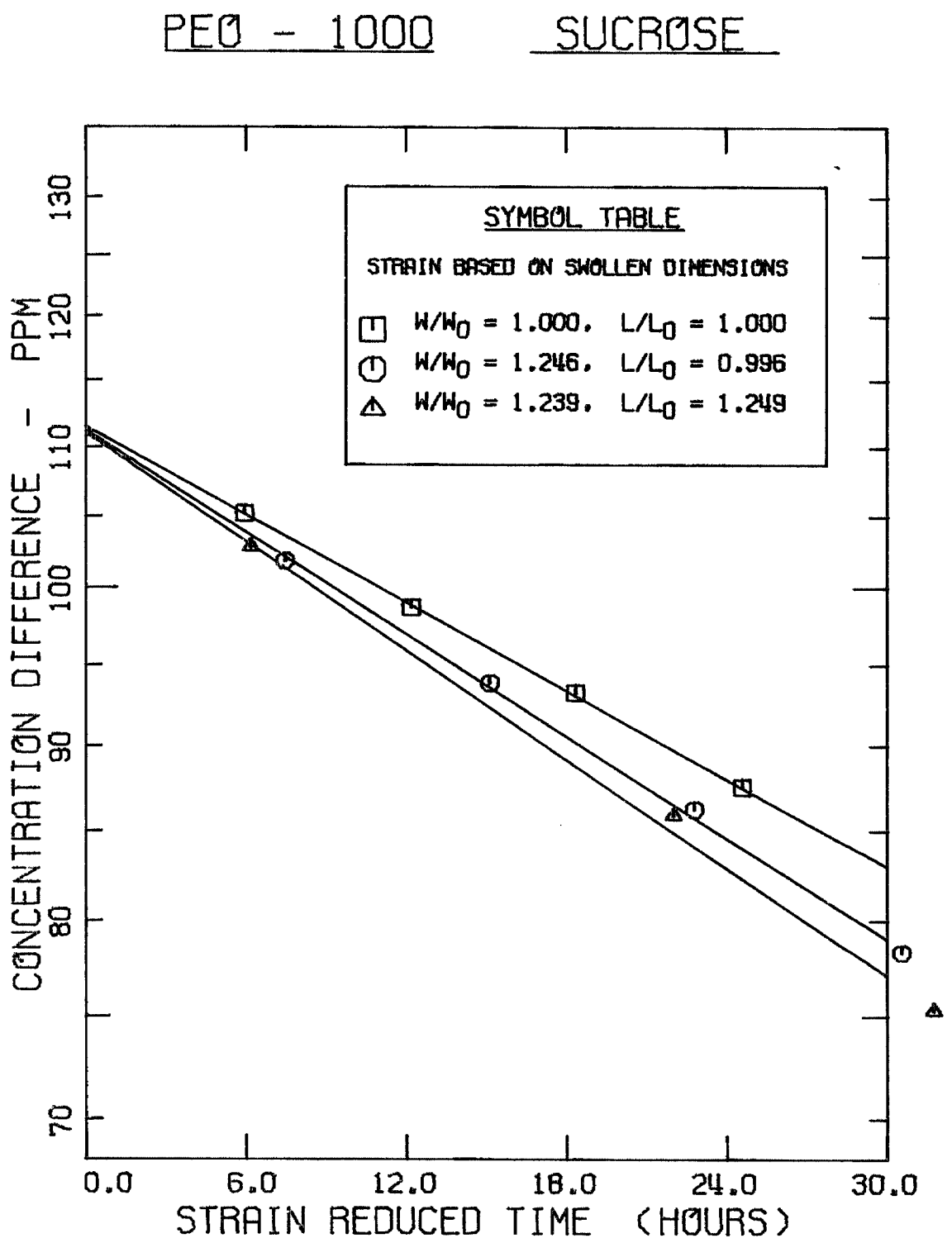

Figure 4.8. Concentration difference versus time for a PEO-1000 film. Weighted average film thickness 0.00402 cm for the dry unstrained film. ~~Curves~~ theoretical (eqn. 3.10).

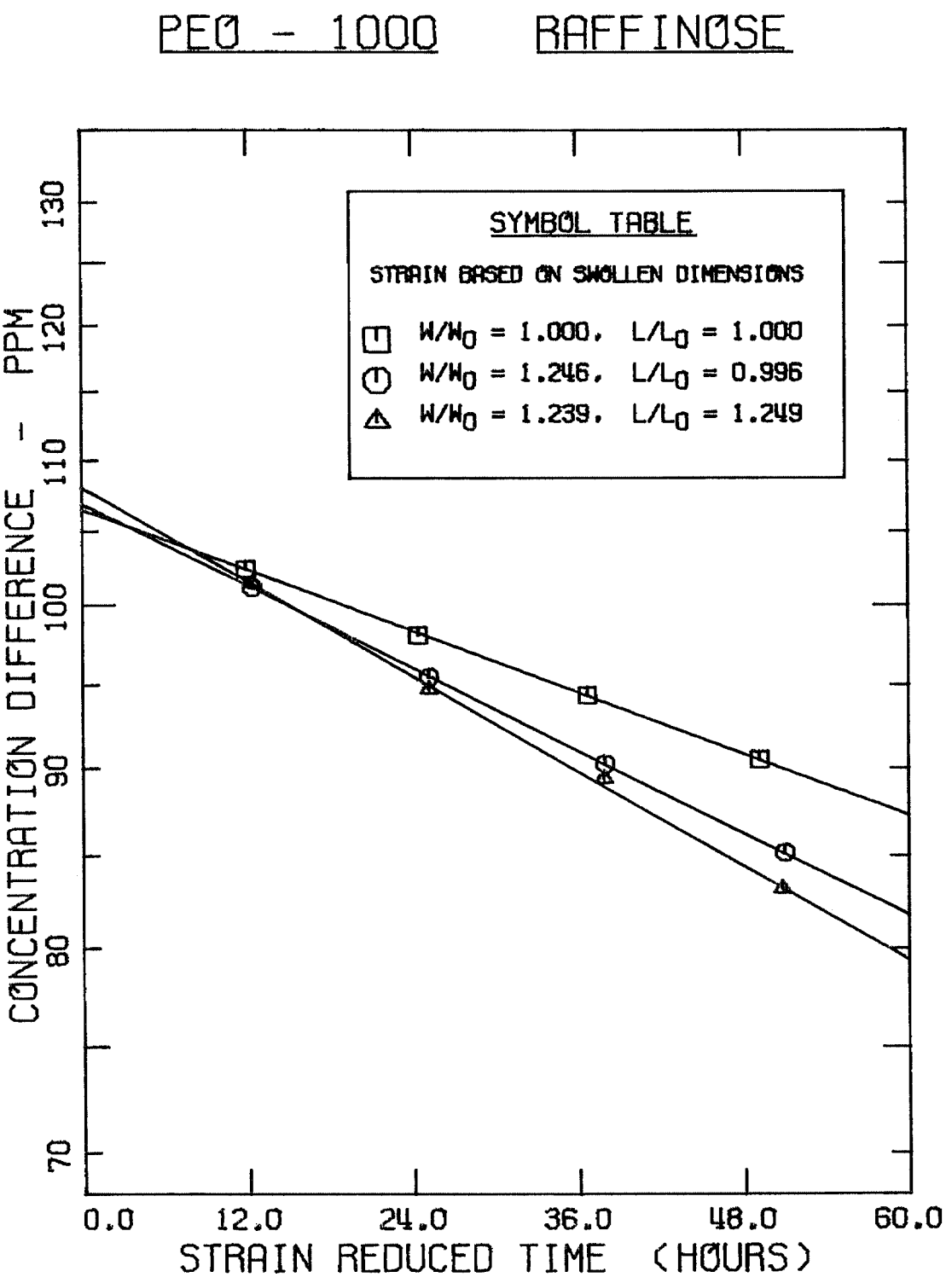

Figure 4.9. Concentration difference versus time for a PEO-1000 film. Weighted average film thickness 0.00402 cm for the dry unstrained film. Curves theoretical (eqn. 3.10).

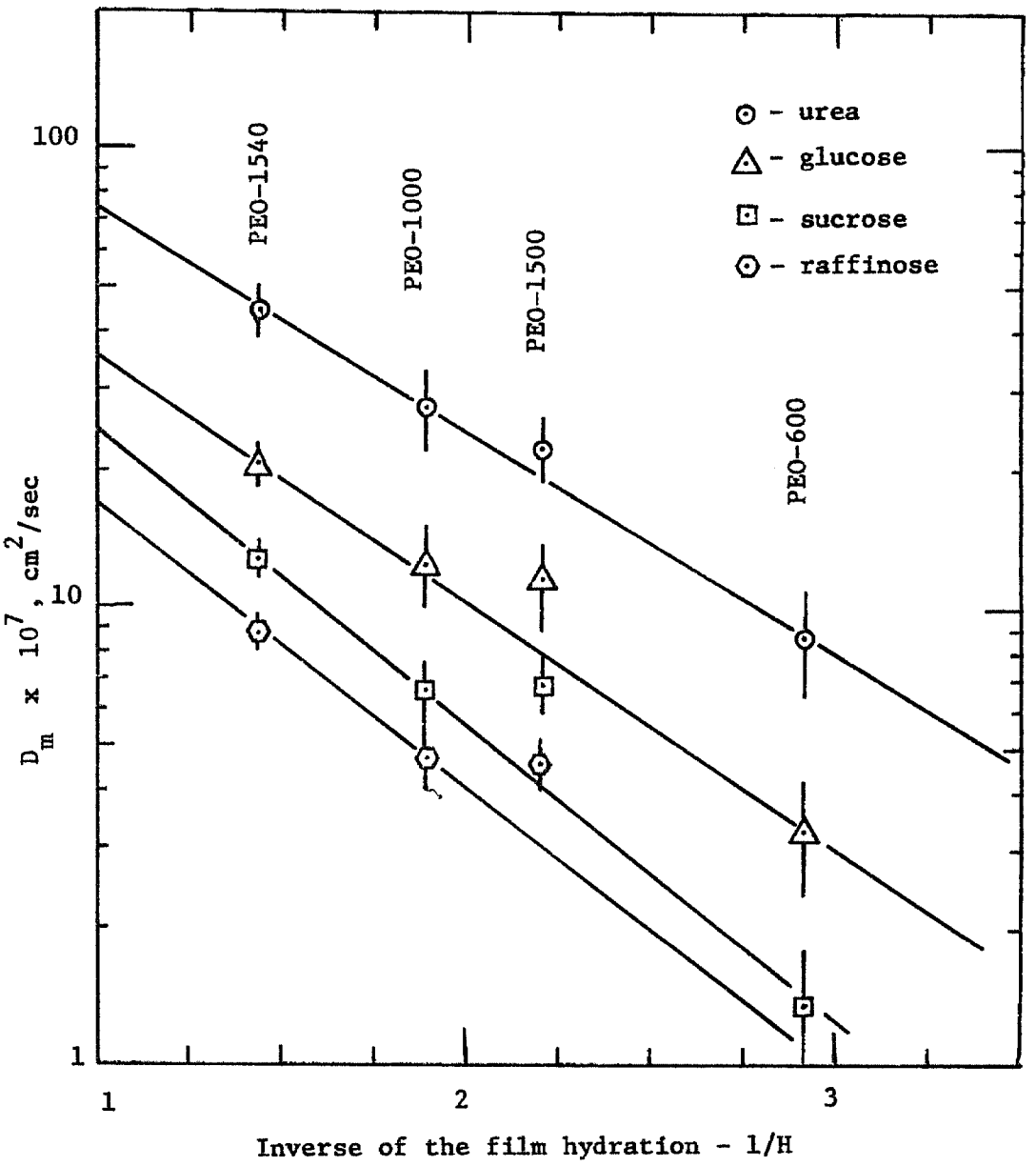

Figure 4.10. The diffusion coefficient of several solutes in a series of segmented polyurethanes as a function of the inverse of the film hydration.

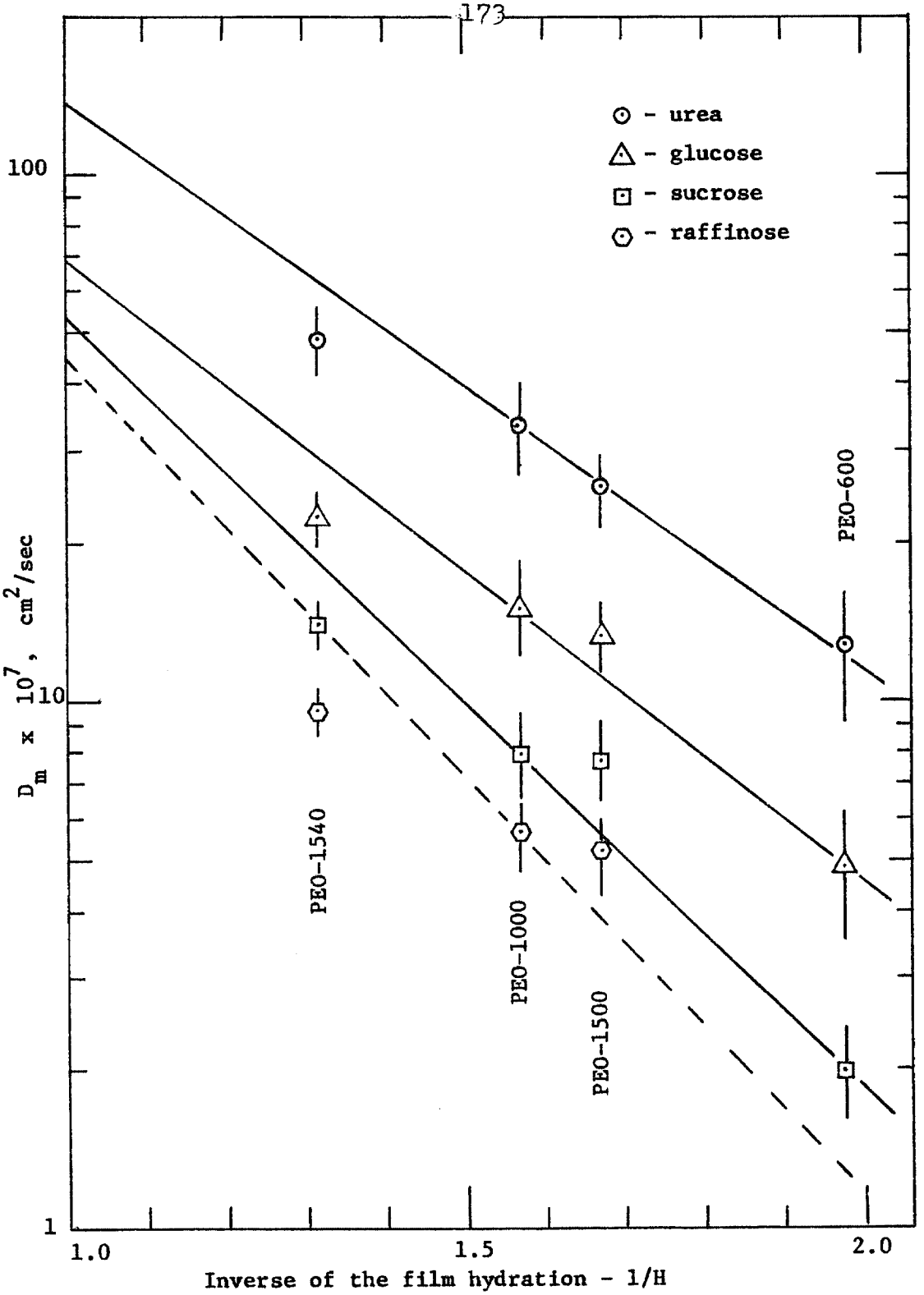

Figure 4.11. The diffusion coefficient of a series of solutes in several segmented polyurethanes as a function of 1/H. Partial correction for the presence of the "hard" phase applied.

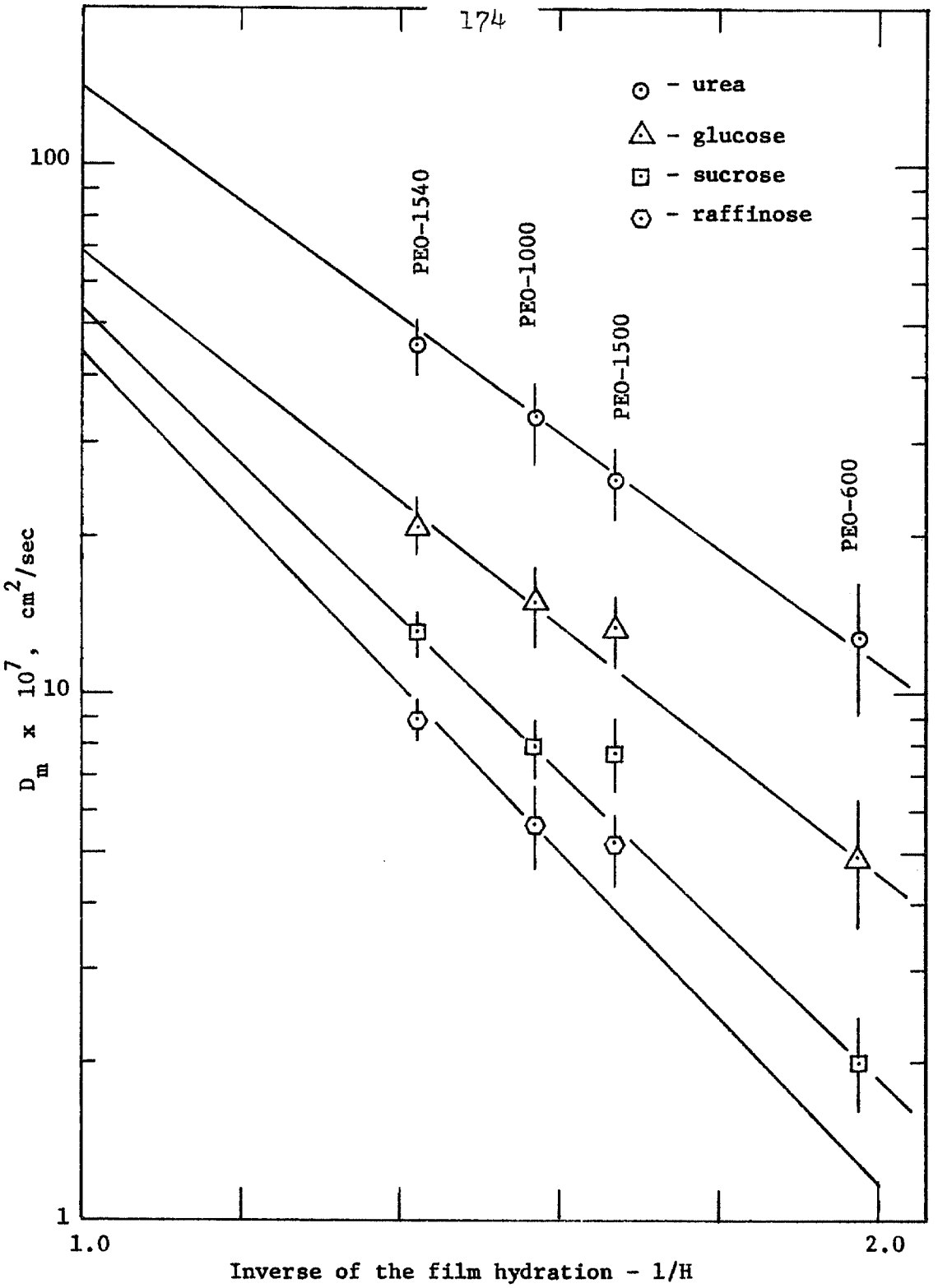

Figure 4.12. The diffusion coefficient of several solutes in a series of segmented polyurethanes as a function of 1/H. Full correction for the presence of the "hard" phase applied.

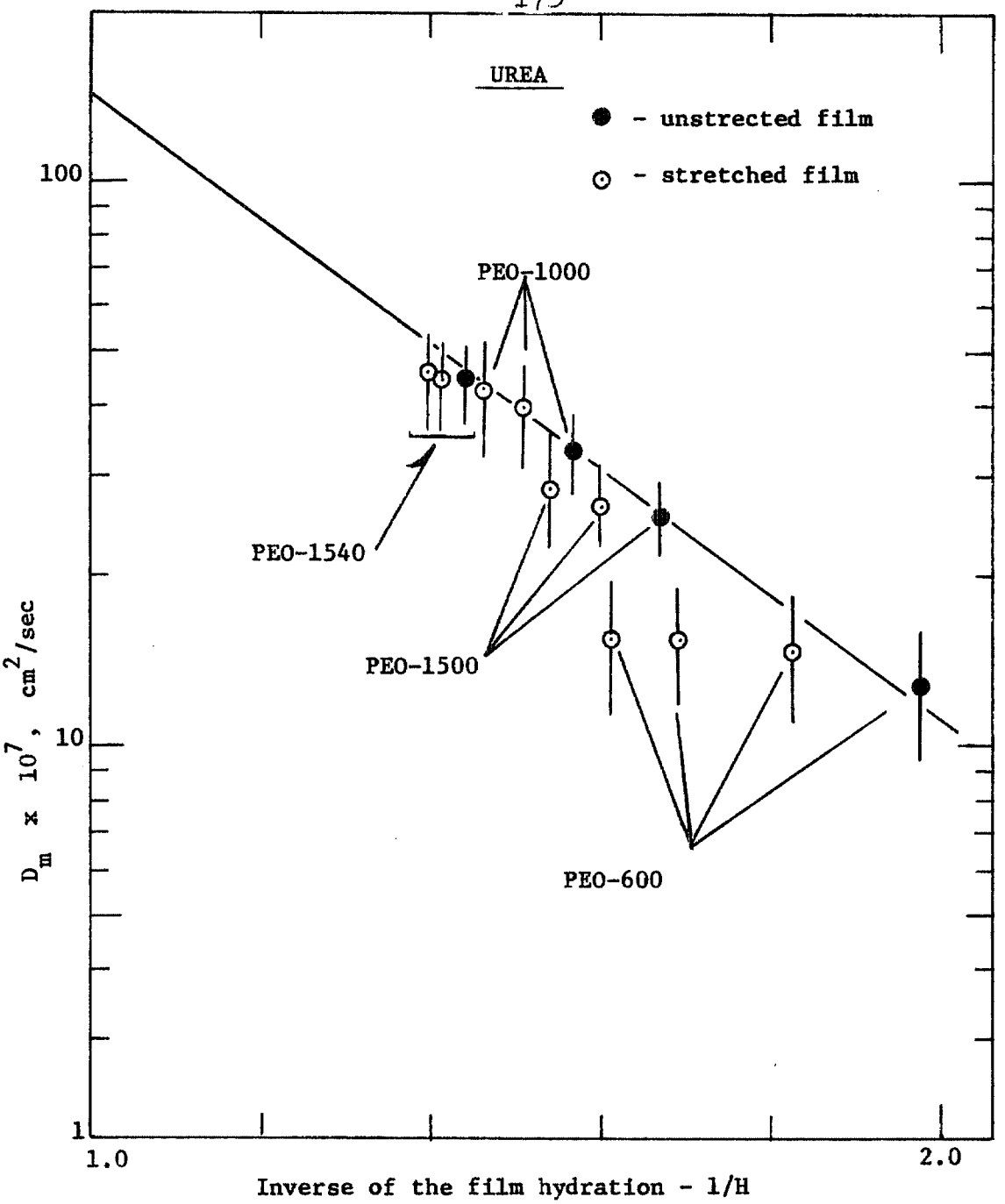

Figure 4.13. The diffusion coefficient for urea in a series of segmented polyurethanes. Full correction for the presence of the "hard" phase applied.

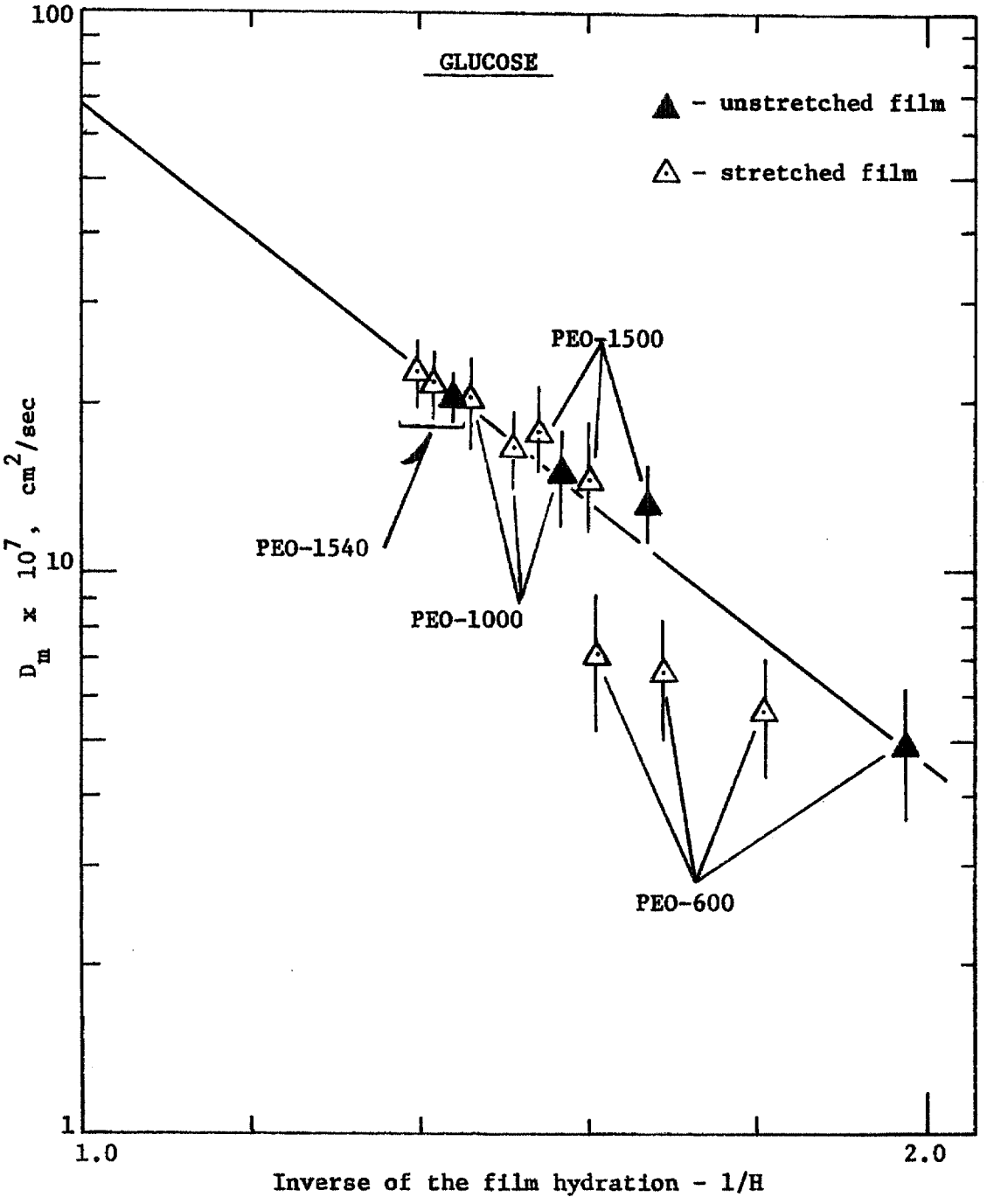

Figure 4.14. The diffusion coefficient of glucose in a series of segmented polyurethanes. Full correction for the presence of the "hard" phase applied.

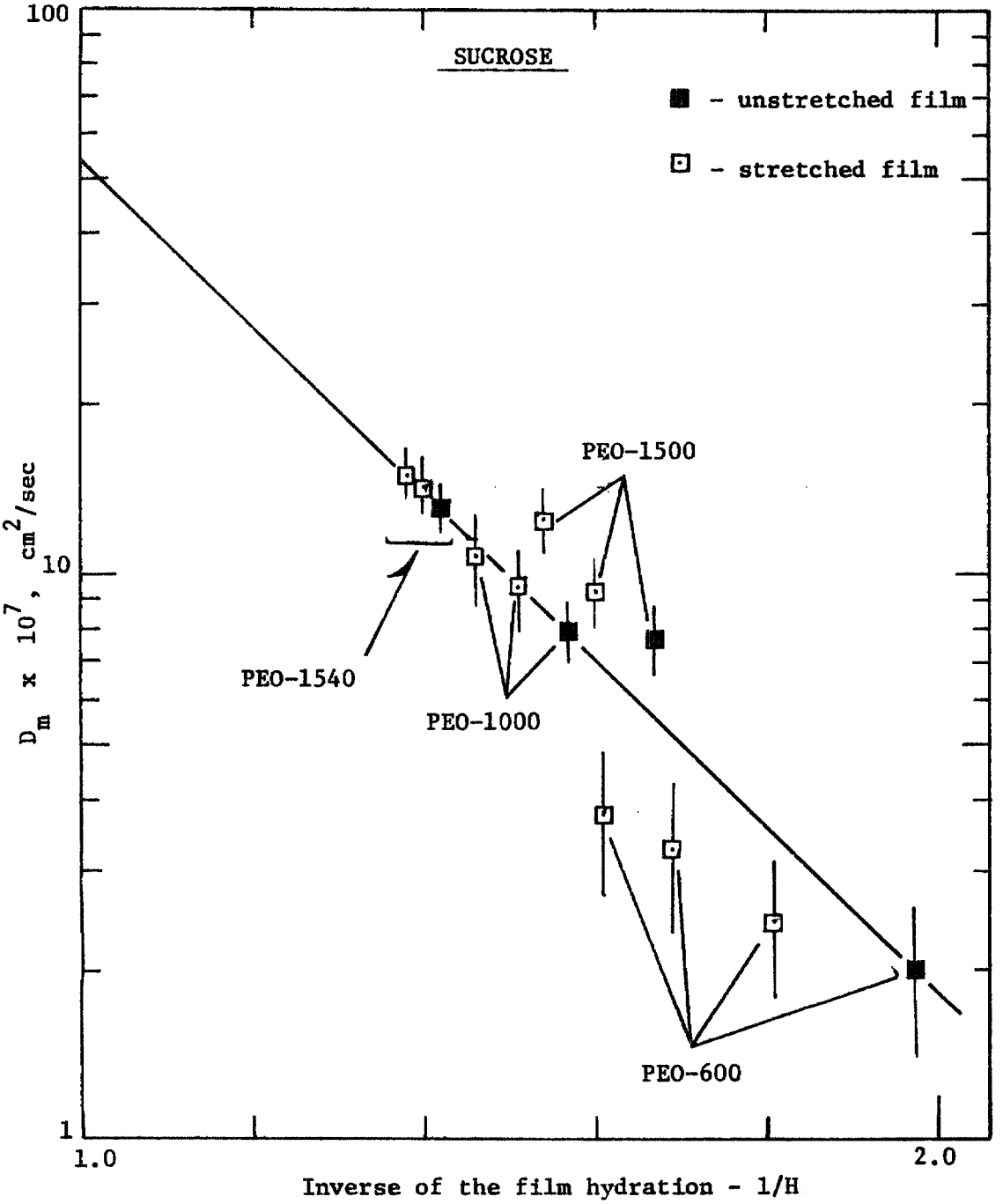

Figure 4.15. The diffusion coefficient of sucrose in a series of segmented polyurethanes. Full correction for the presence of the "hard" phase applied.

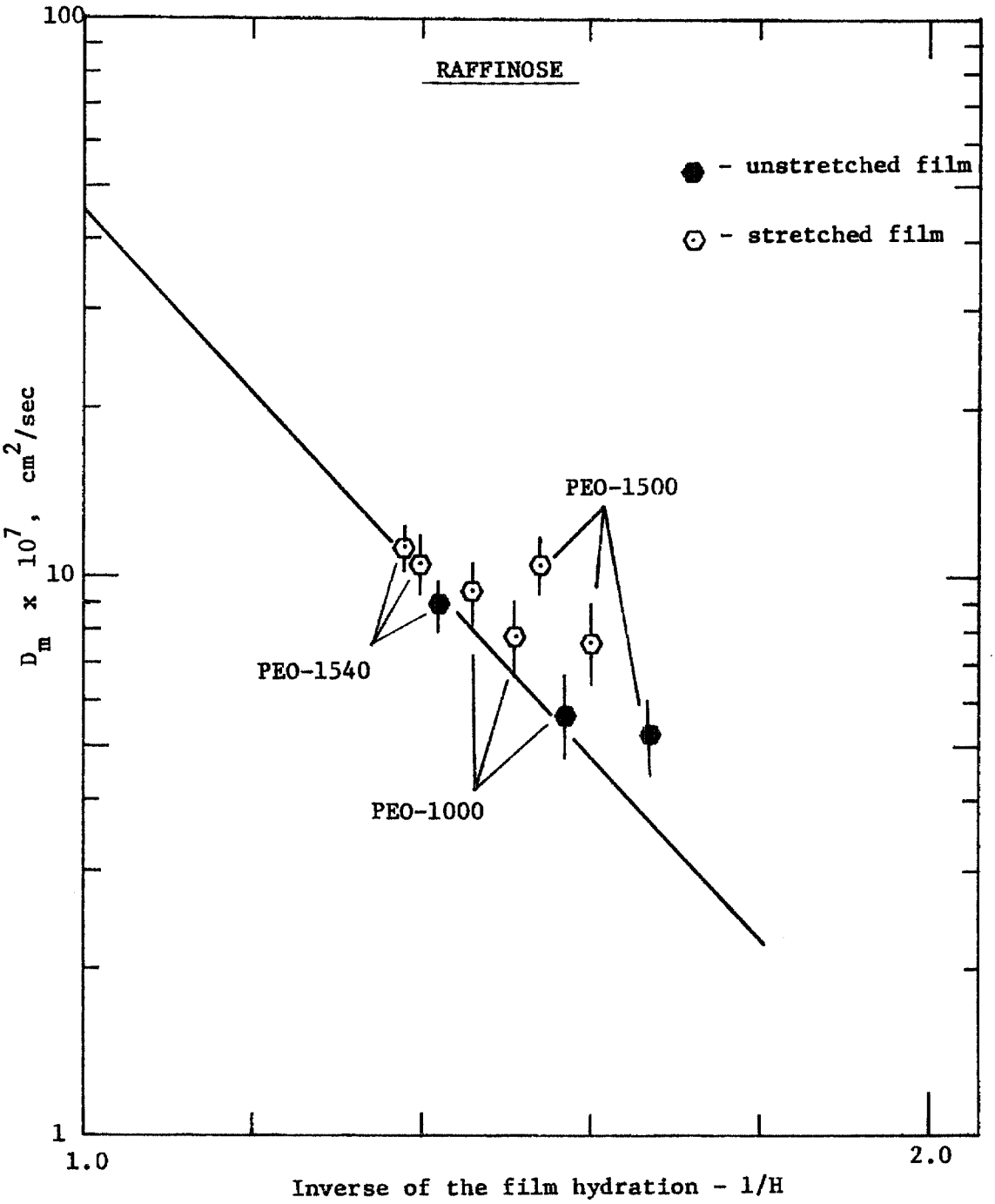

Figure 4.16. The diffusion coefficient of raffinose in a series of segmented polyurethanes. Full correction for the presence of the "hard" phase applied.

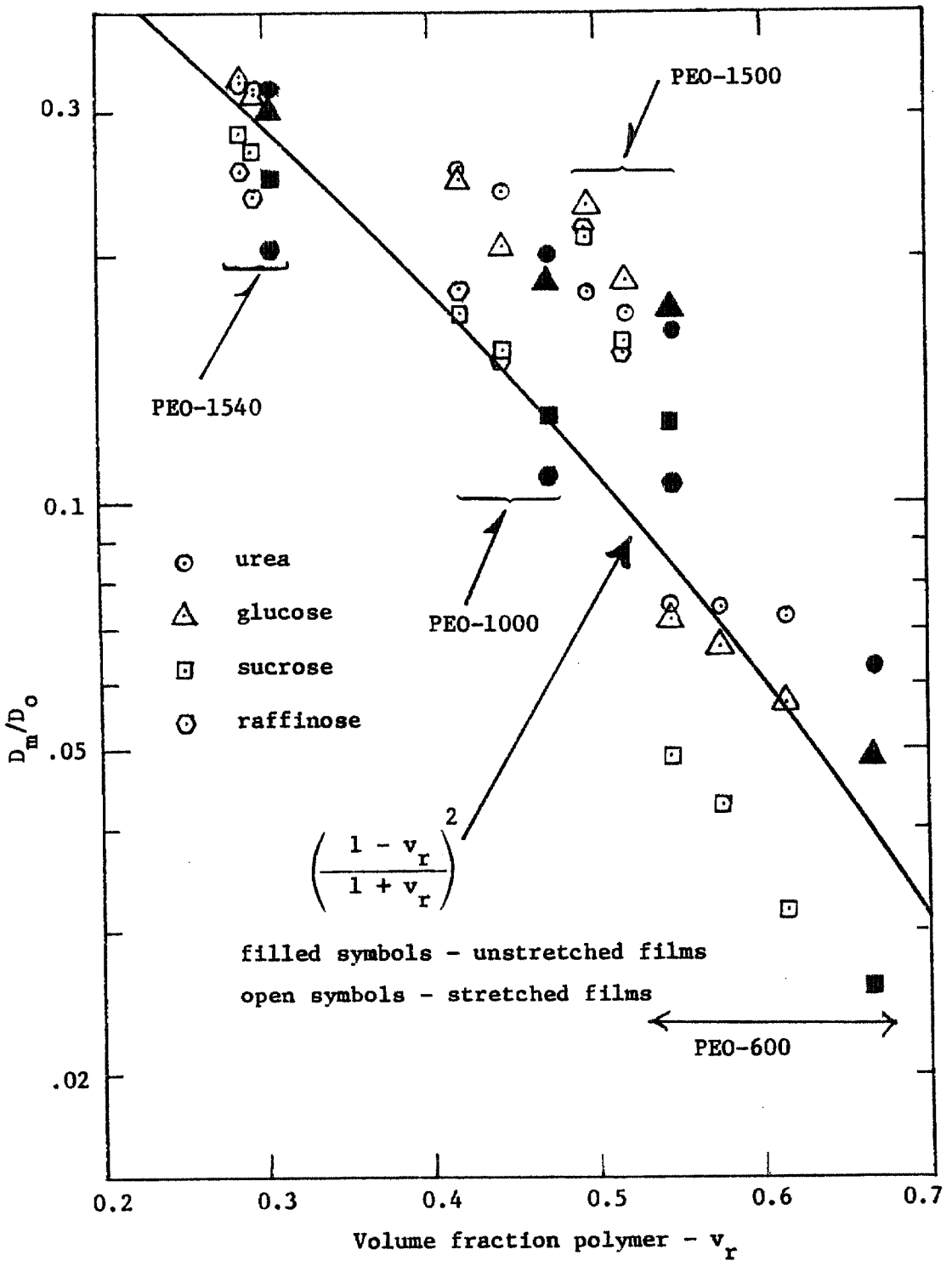

Figure 4.17. The ratio of the film diffusion coefficient to the free diffusion coefficient versus the volume fraction polymer. Curve theoretical (Meares).

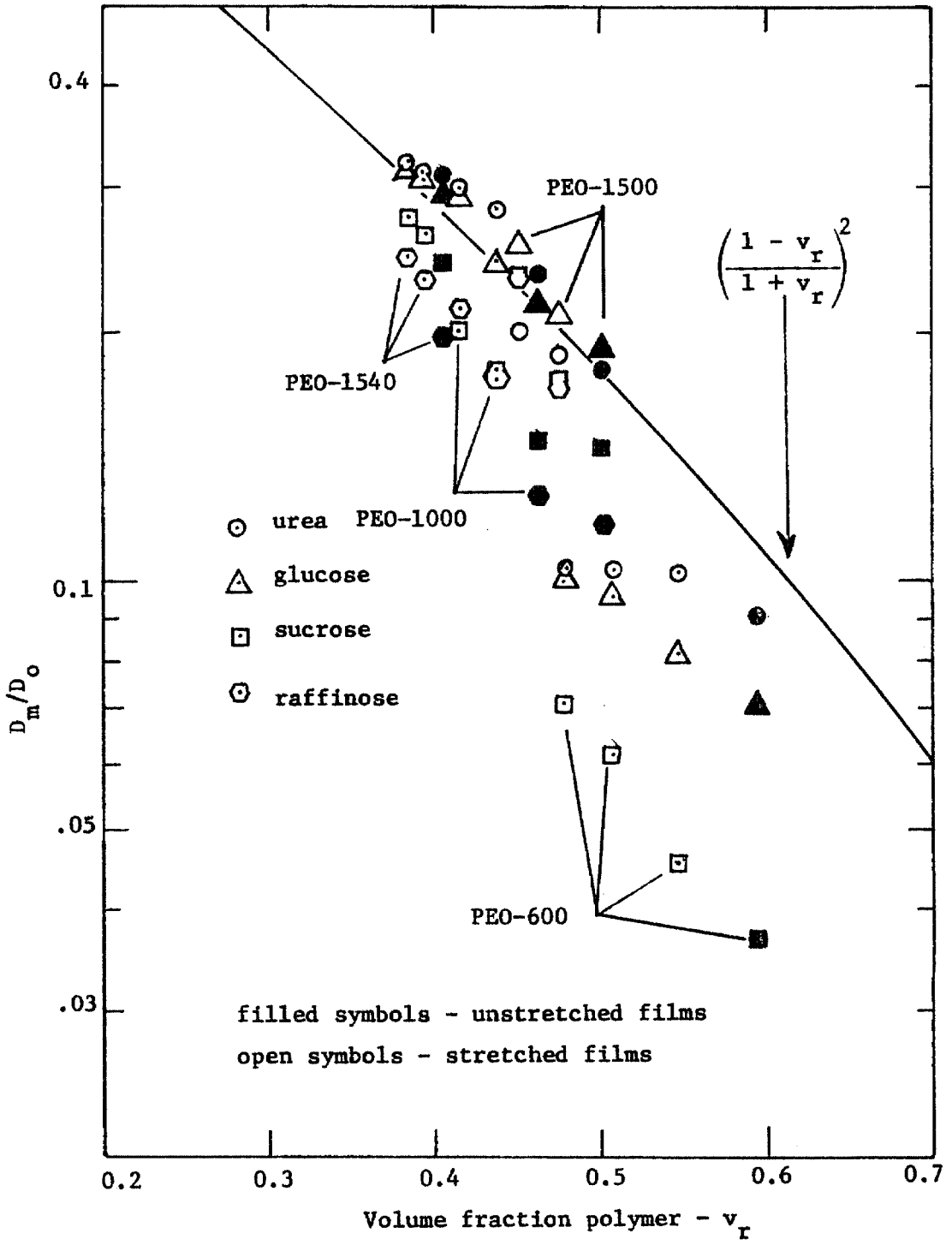

Figure 4.18. D_m/D_o versus v_r. Full correction for the presence of the "hard" phase applied to both D_m and v_r.

Curve theoretical (Meares).

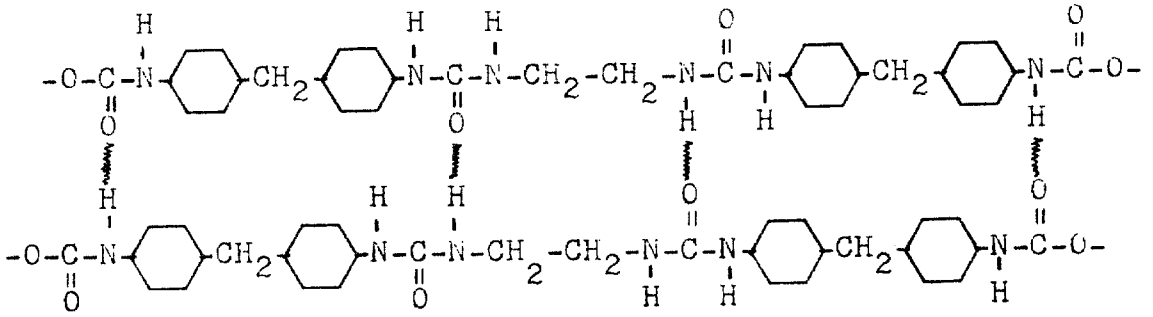

Figure 4.19. Interchain hydrogen bonds between "hard" blocks. One of many possible stable configurations.

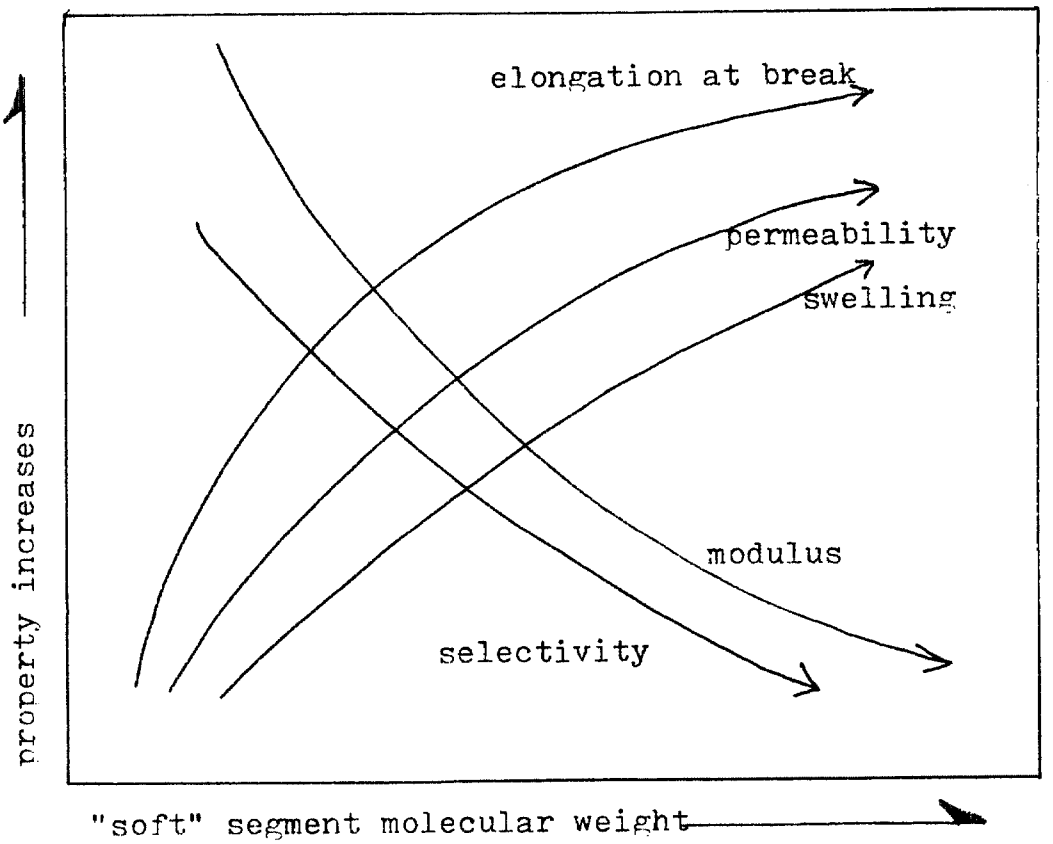

Figure 4.20. Film properties as a function of "soft" segment molecular weight.

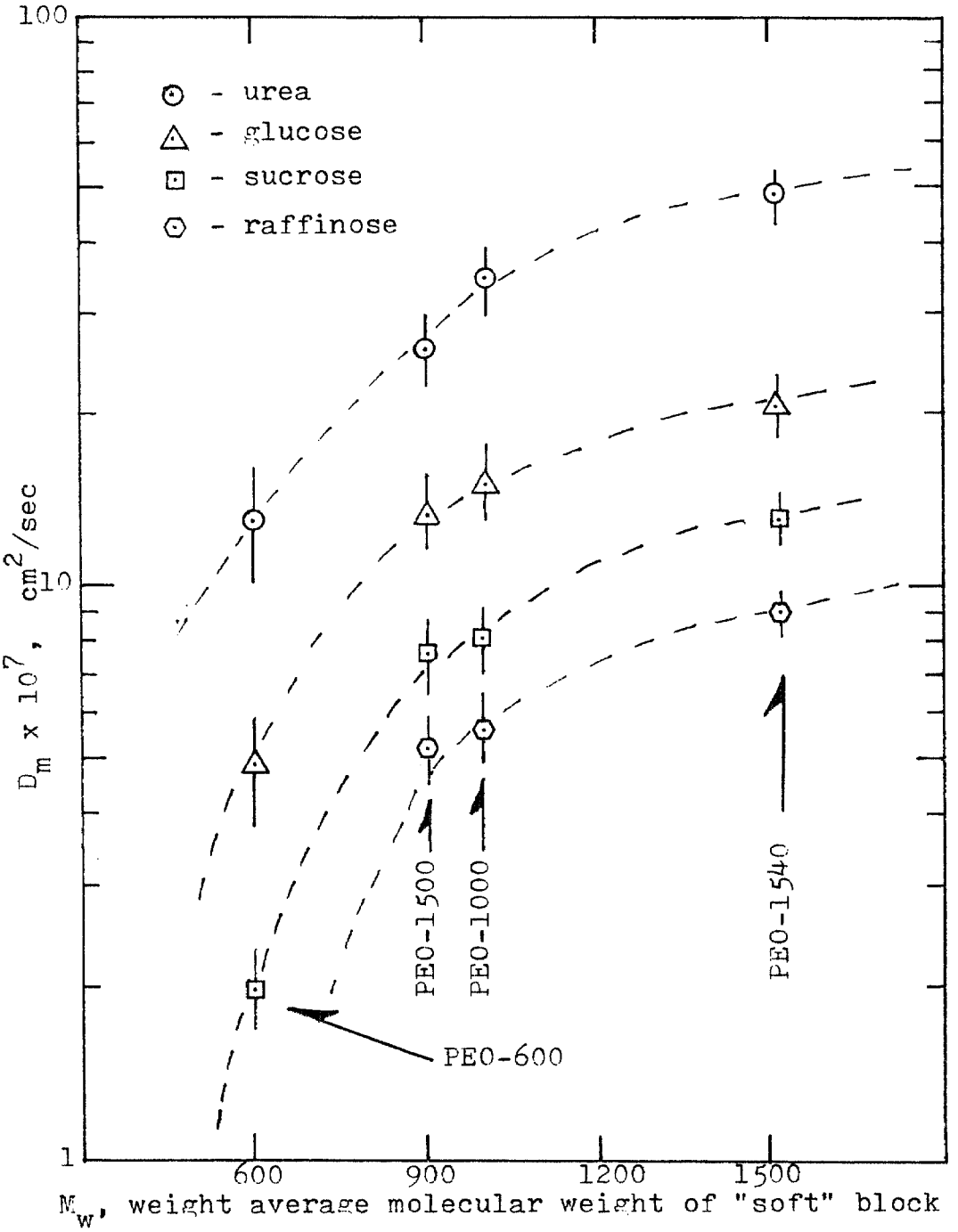

Figure 4.21. Diffusion coefficient of solutes in the membranes versus the "soft" segment weight average molecular weight.

APPENDIX I

Additional Figures

Additional figures that were prepared but not referred to in the text are presented here.

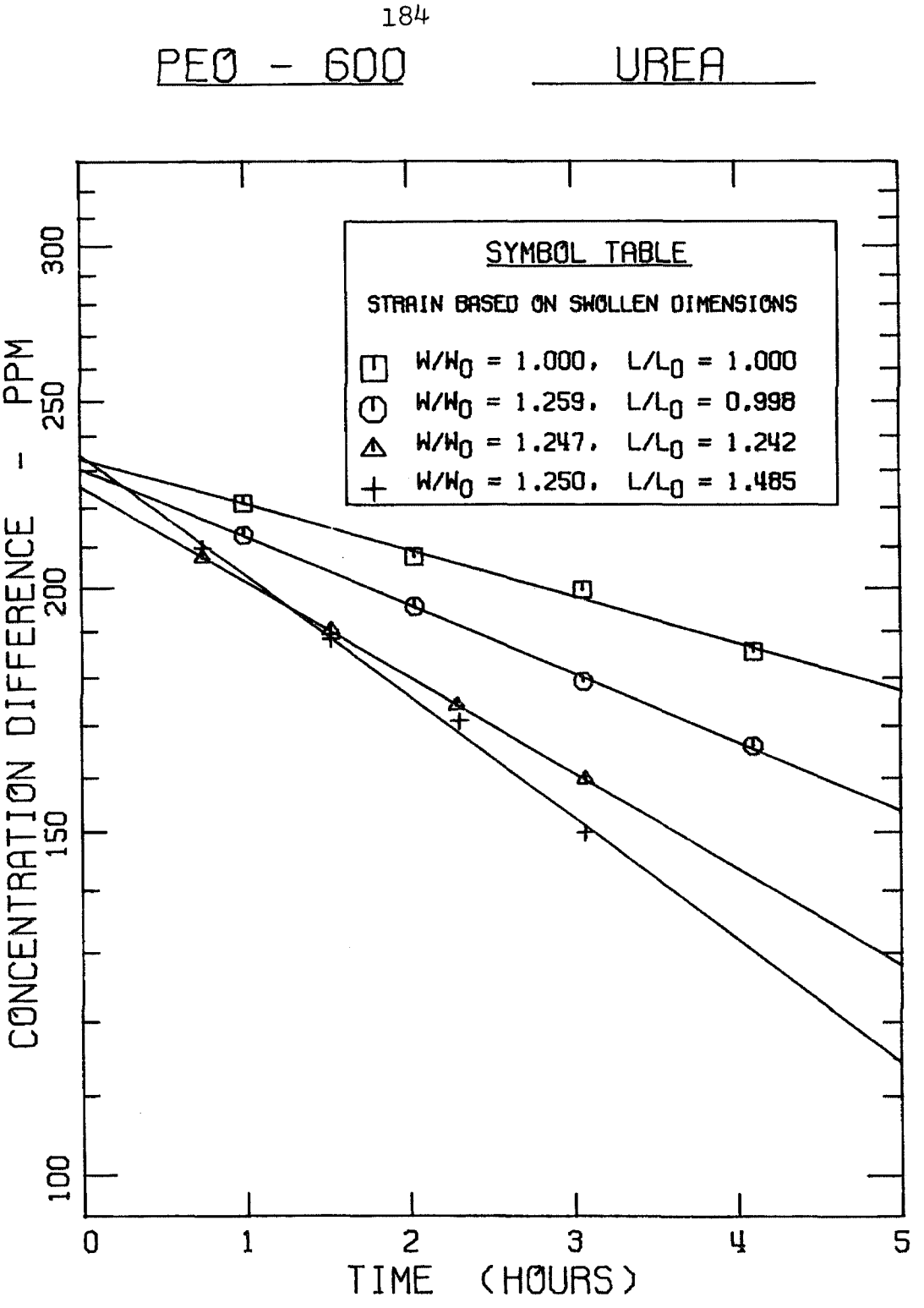

Figure A-1. Concentration difference versus time for a PEO-600 film. Weighted average film thickness 0.00281 cm for the dry unstrained film. Curves theoretical (eqn. 3.10).

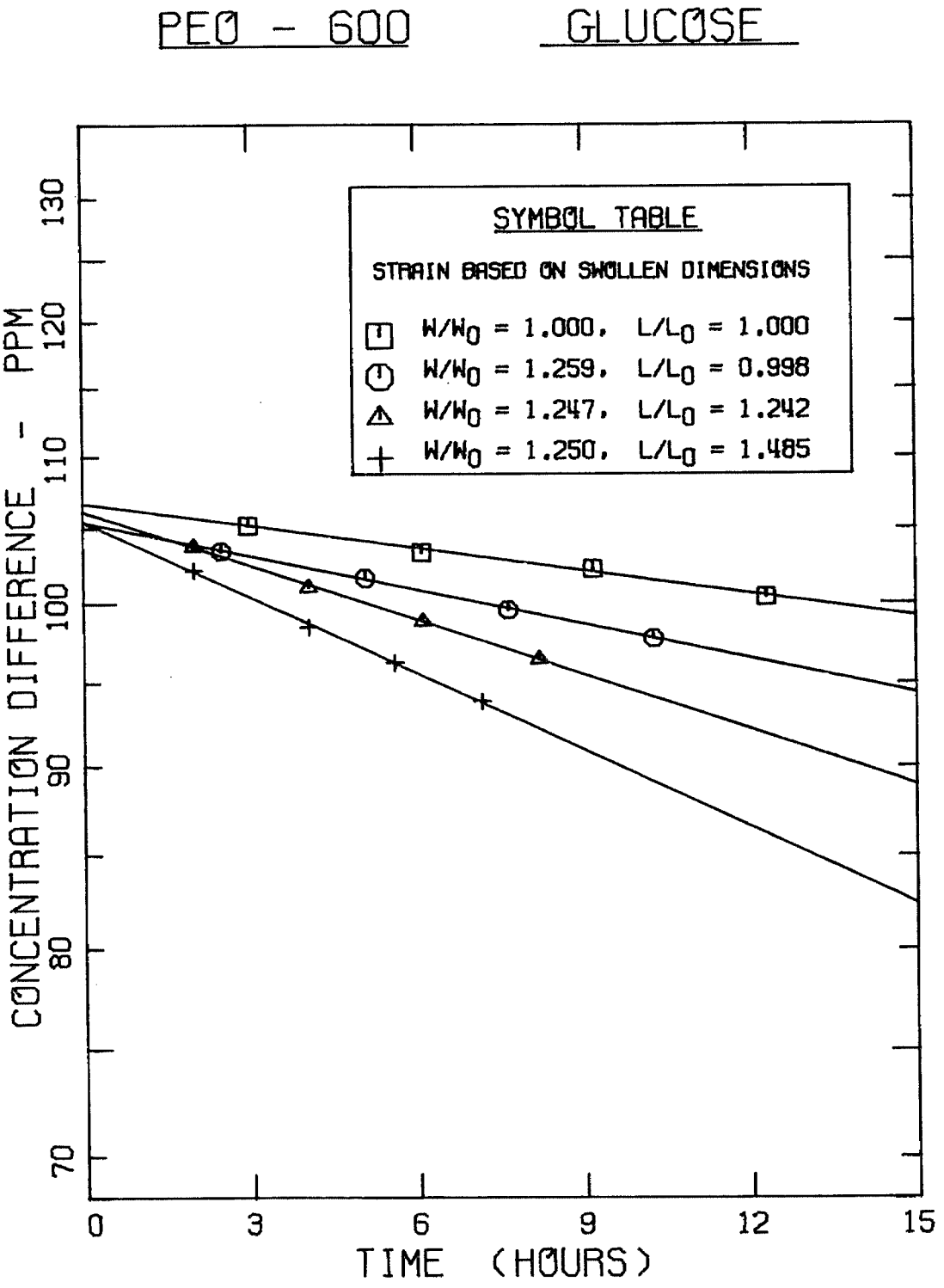

Figure A-2. Concentration difference versus time for a PEO-600 film. Weighted average film thickness 0.00281 cm for the dry unstrained film. Curves theoretical (eqn. 3.10).

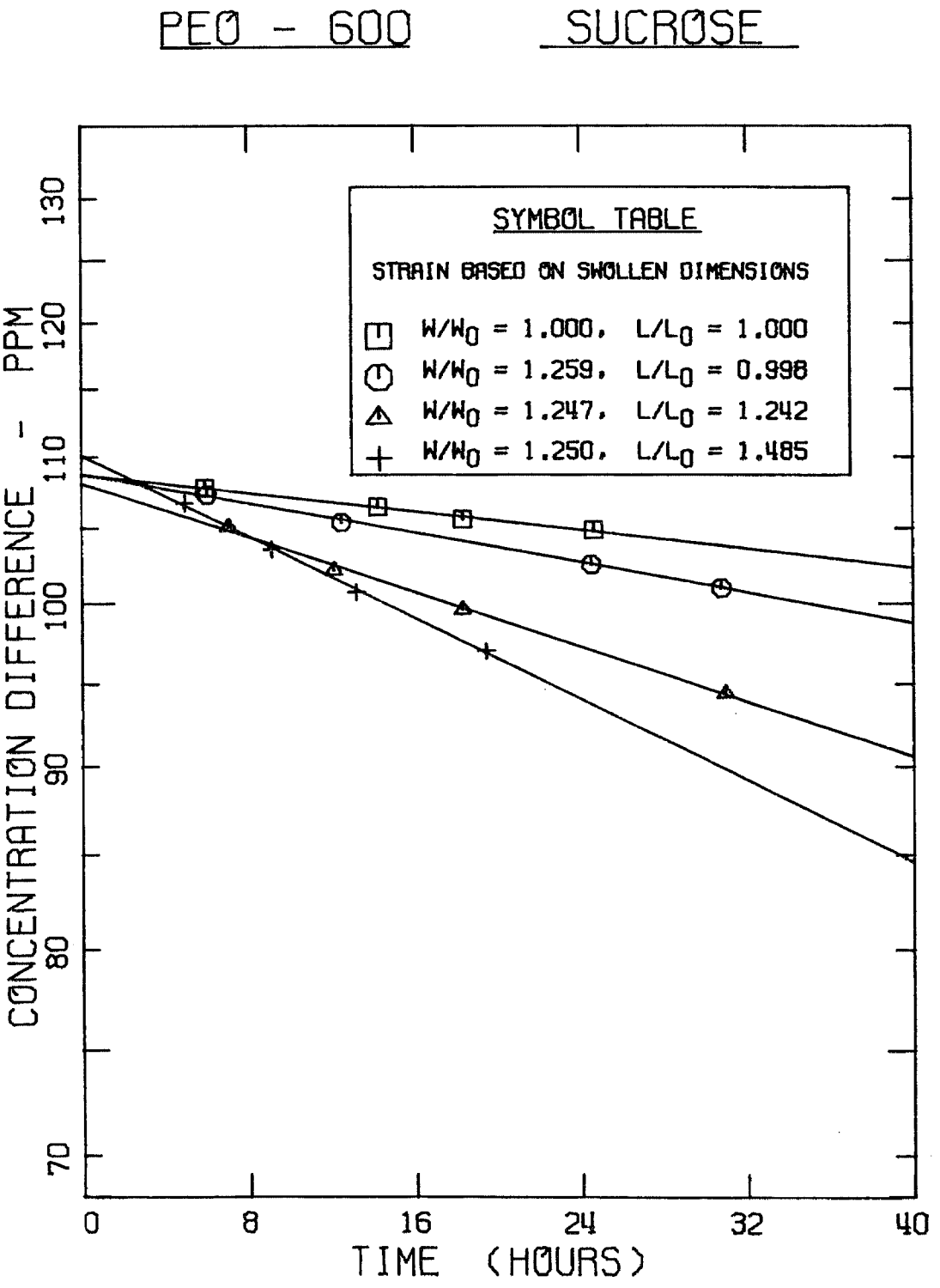

Figure A-3. Concentration difference versus time for a PEO-600 film. Weighted average film thickness 0.00281 cm for the dry unstrained film. Curves theoretical (eqn. 3.10).

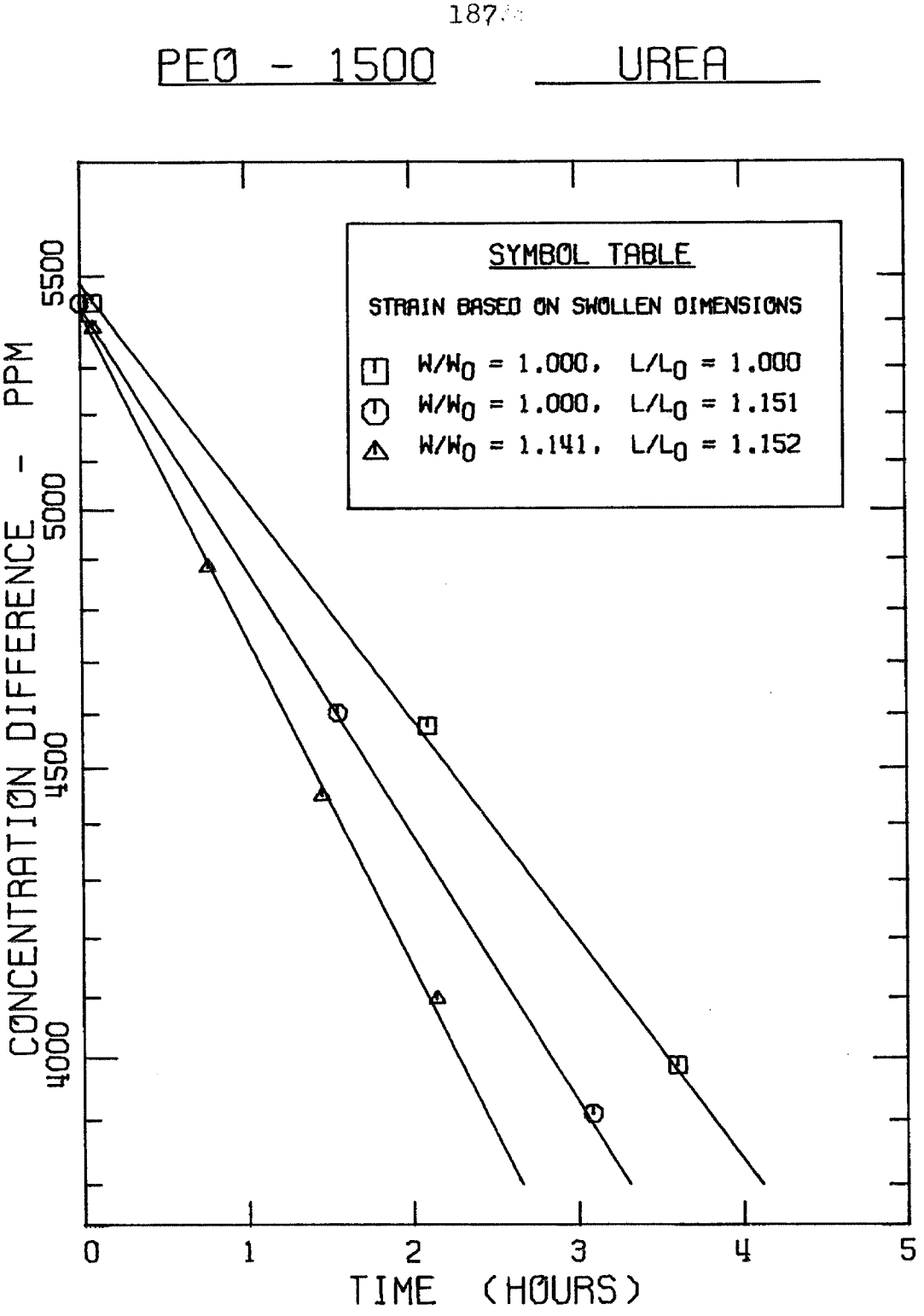

Figure A-4. Concentration difference versus time for a PEO-1500 film. Weighted average film thickness 0.00453 cm for the dry unstrained film. Curves theoretical (eqn. 3.10).

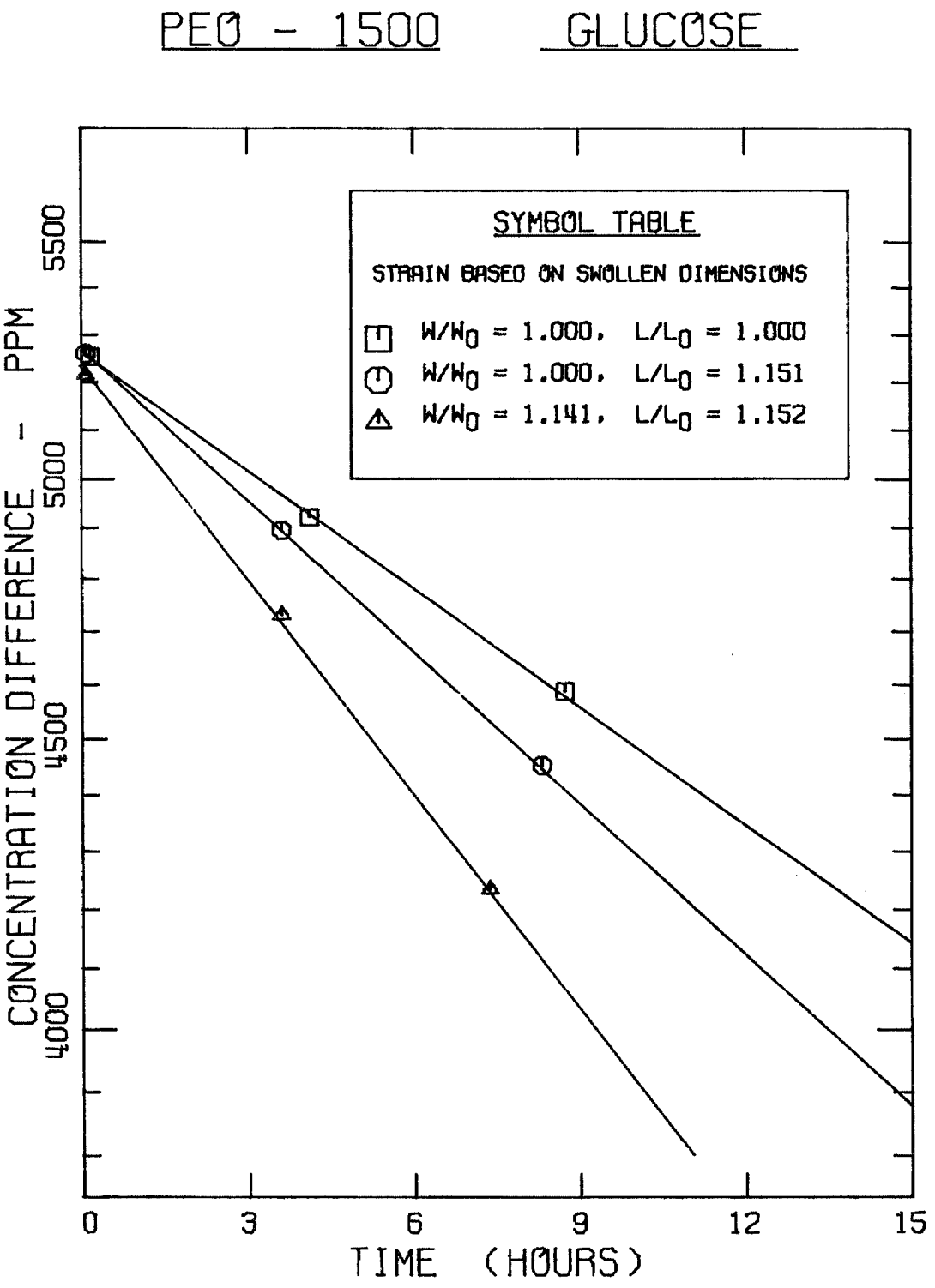

Figure A-5. Concentration difference versus time for a PEO-1500 film. Weighted average film thickness 0.00453 cm for the dry unstrained film. Curves theoretical (eqn. 3.10).

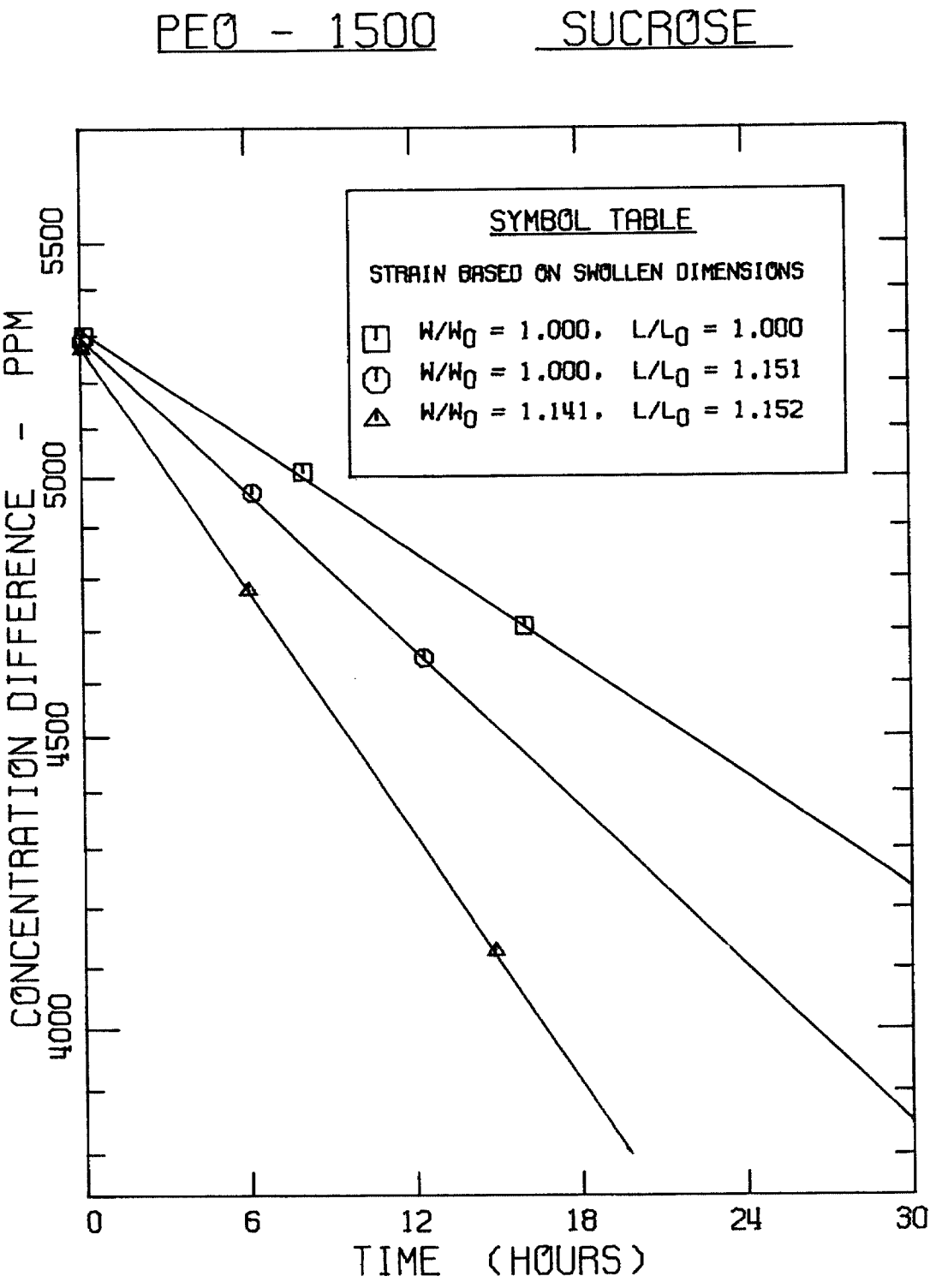

Figure A-6. Concentration difference versus time for a PEO-1500 film. Weighted average film thickness 0.00453 cm for the dry unstrained film. Curves theoretical (eqn. 3.10).

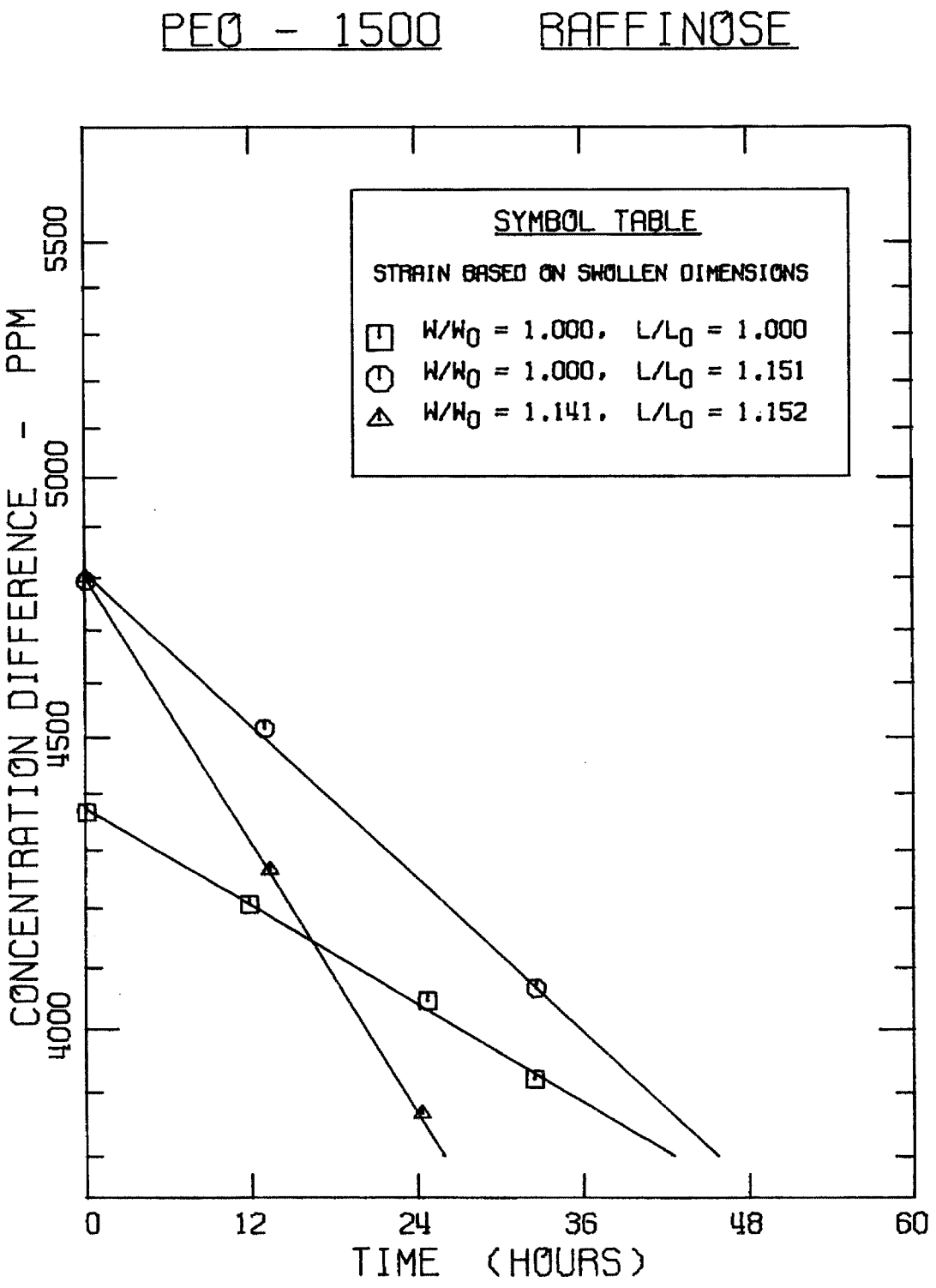

Figure A-7. Concentration difference versus time for a PEO-1500 film. Weighted average film thickness 0.00453 cm for the dry unstrained film. Curves theoretical (eqn. 3.10).

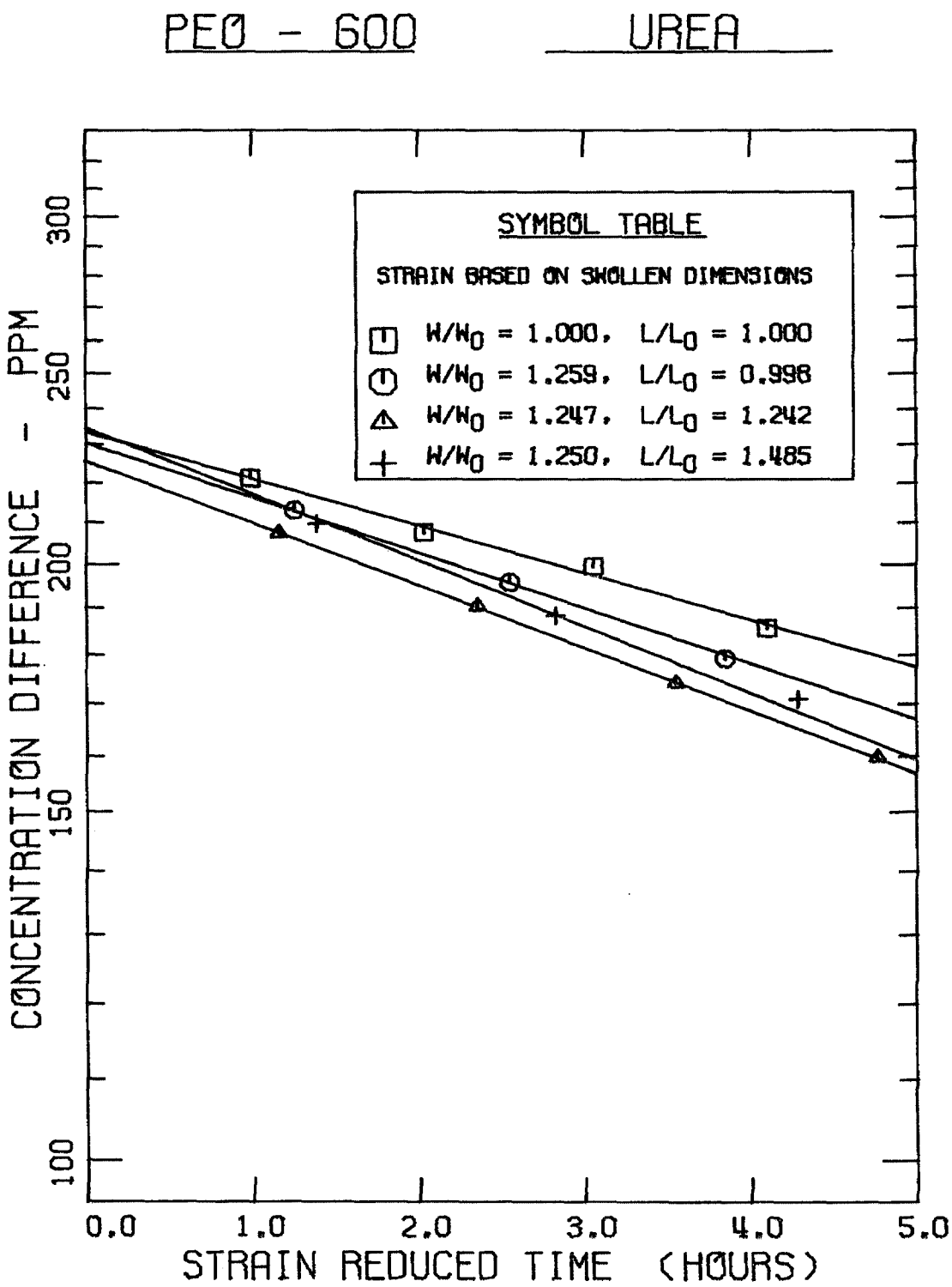

Figure A-8. Concentration difference versus time for a PEO-600 film. Weighted average film thickness 0.00281 cm for the dry unstrained film. Curves theoretical (eqn. 3.10).

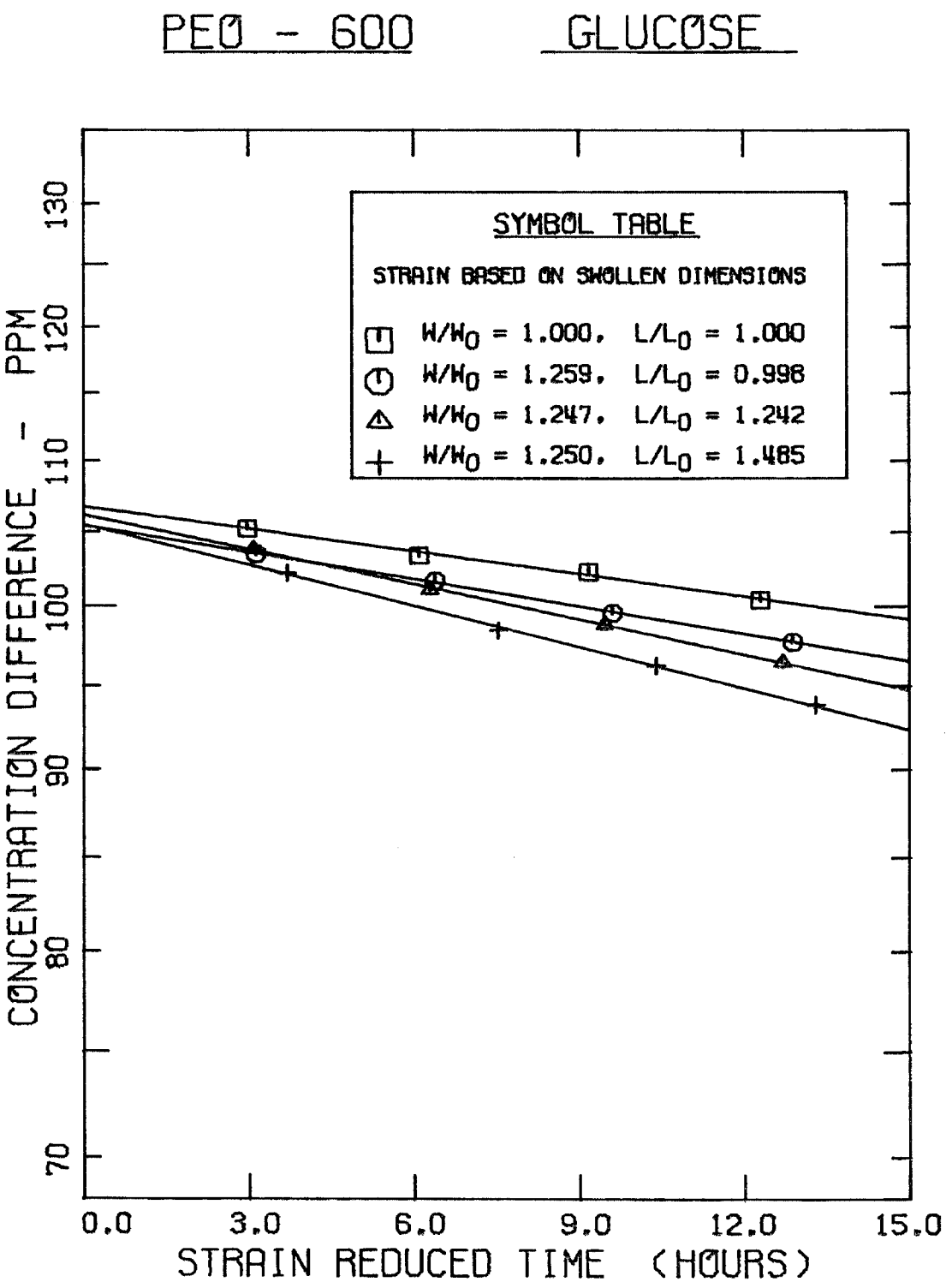

Figure A-9. Concentration difference versus time for a PEO-600 film. Weighted average film thickness 0.00281 cm for the dry unstrained film. Curves theoretical (eqn. 3.10).

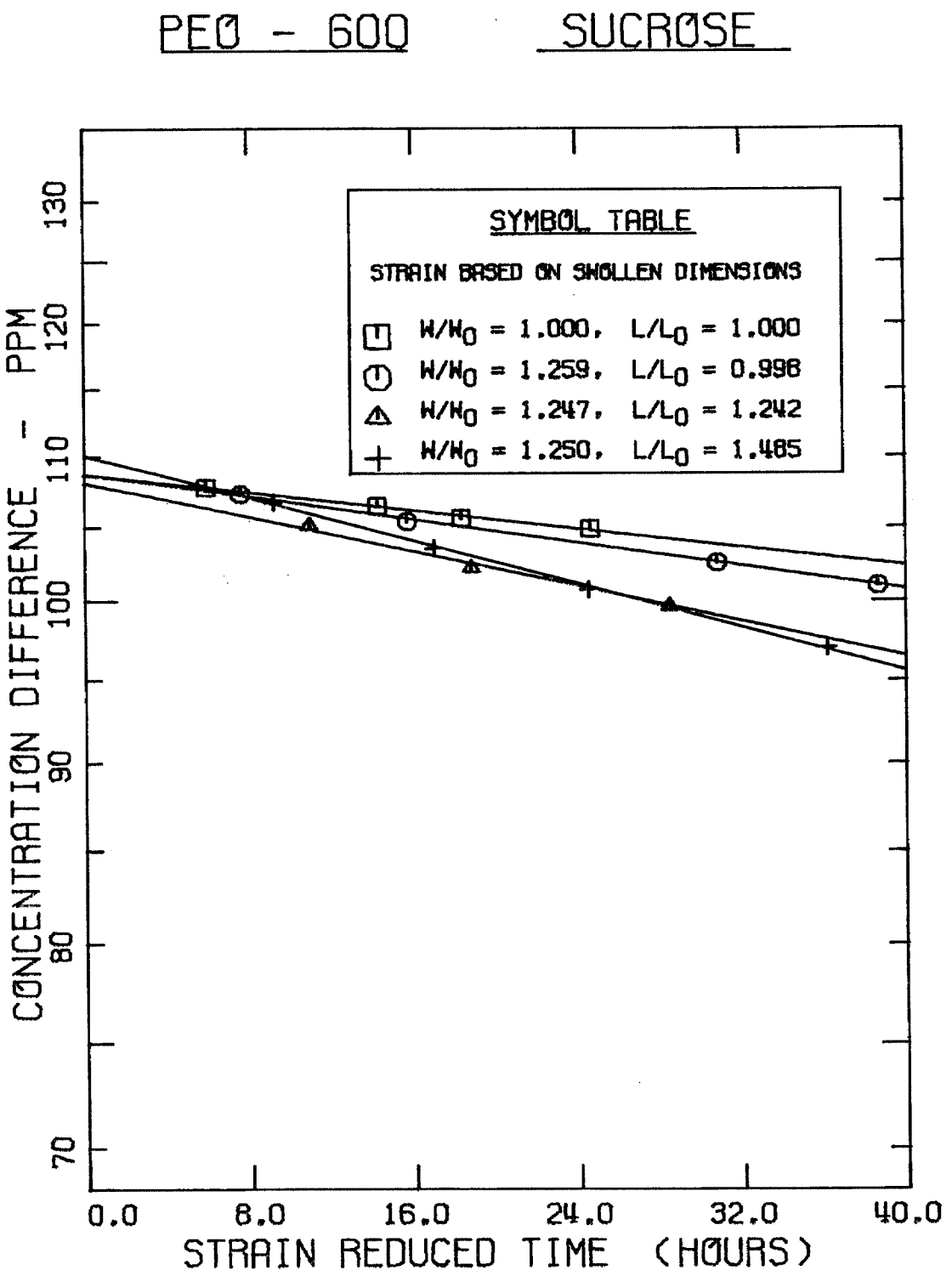

Figure A-10. Concentration difference versus time for a PEO-600 film. Weighted average film thickness 0.00281 cm for the dry unstrained film. Curves theoretical (eqn. 3.10).

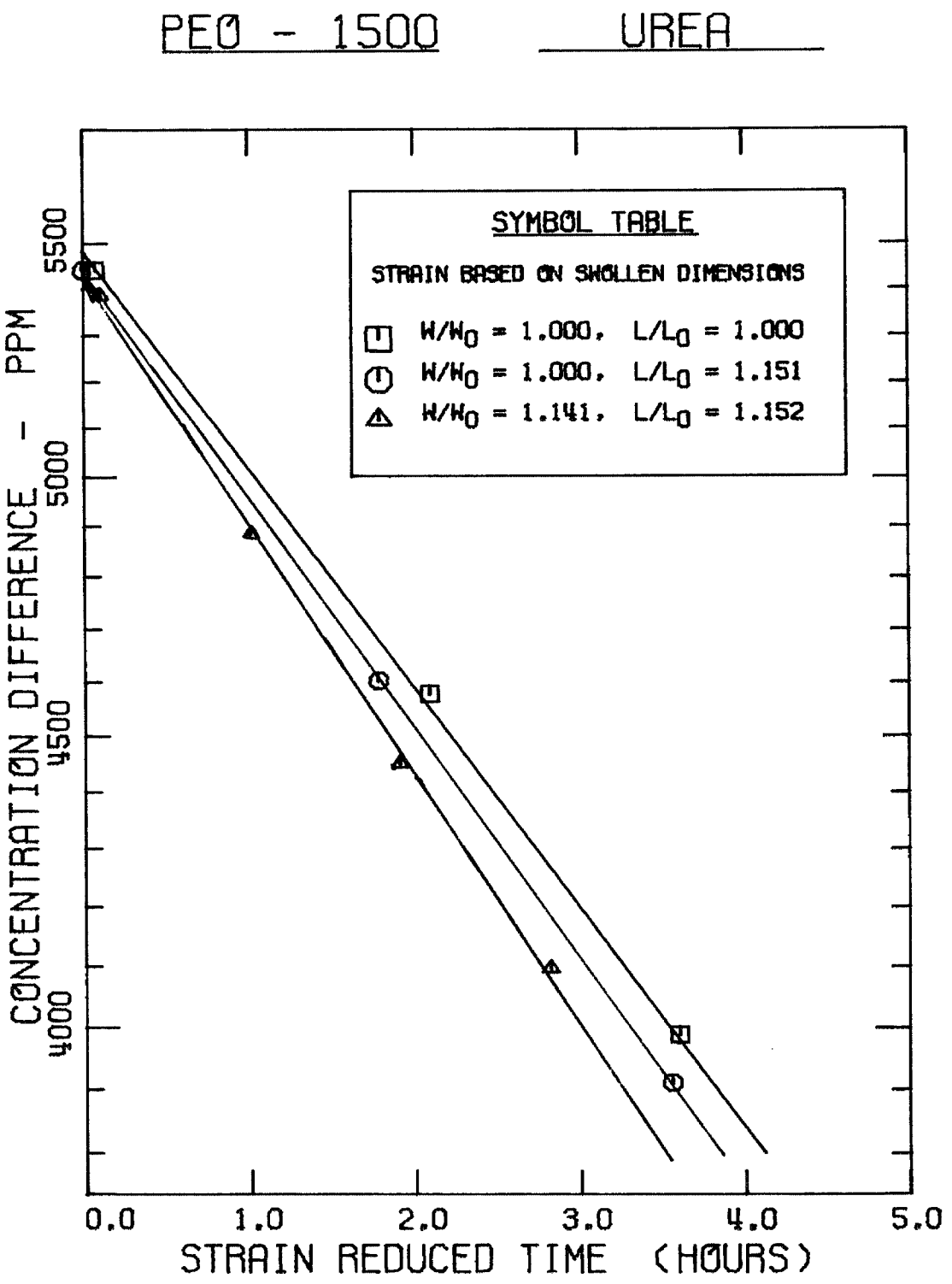

Figure A-11. Concentration difference versus time for a PEO-1500 film. Weighted average film thickness 0.00453 cm for the dry unstrained film. Curves theoretical (eqn. 3.10).

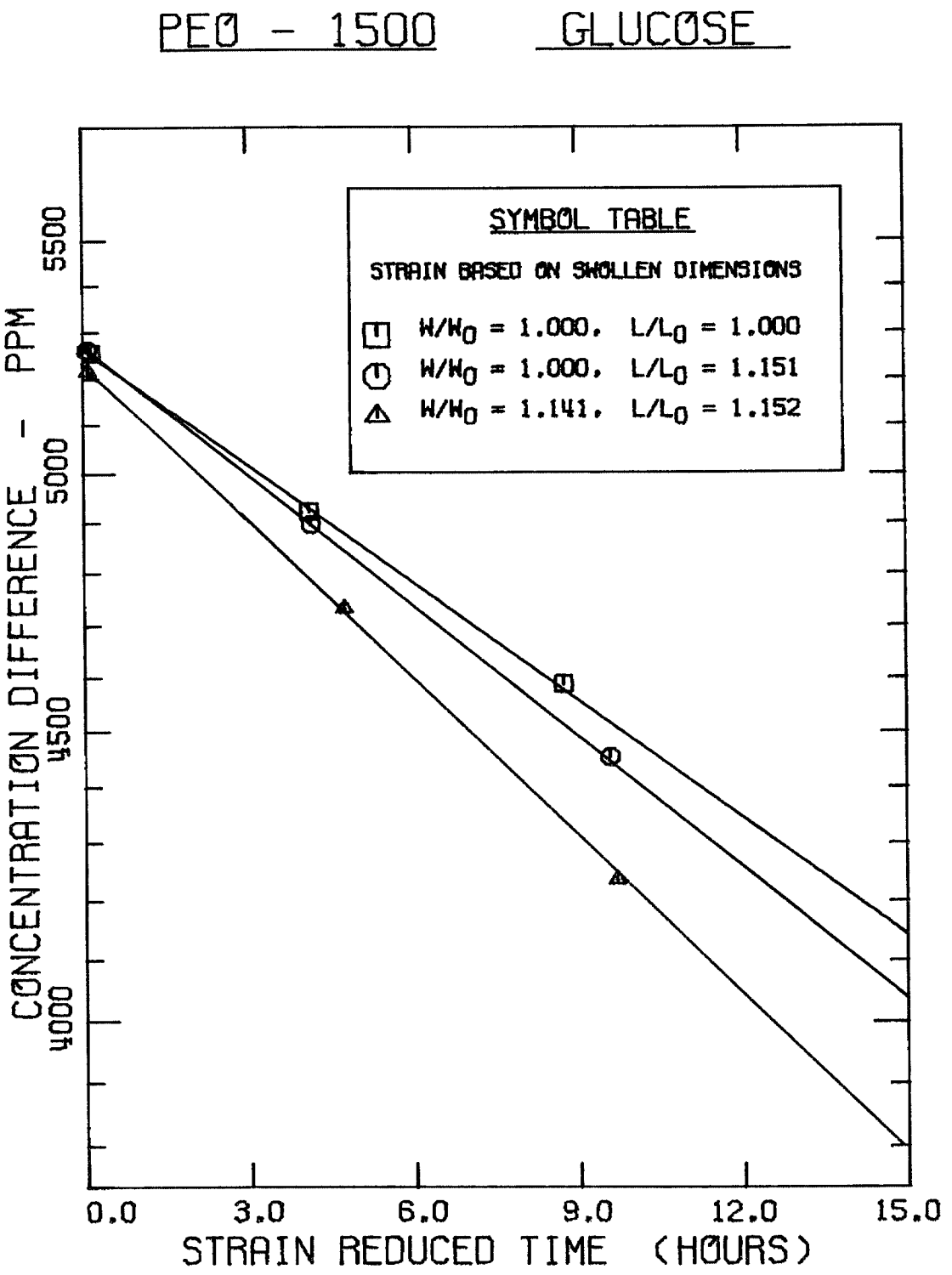

Figure A-12. Concentration difference versus time for a PEO-1500 film. Weighted average film thickness 0.00453 cm for the dry unstrained film. Curves theoretical (eqn. 3.10).

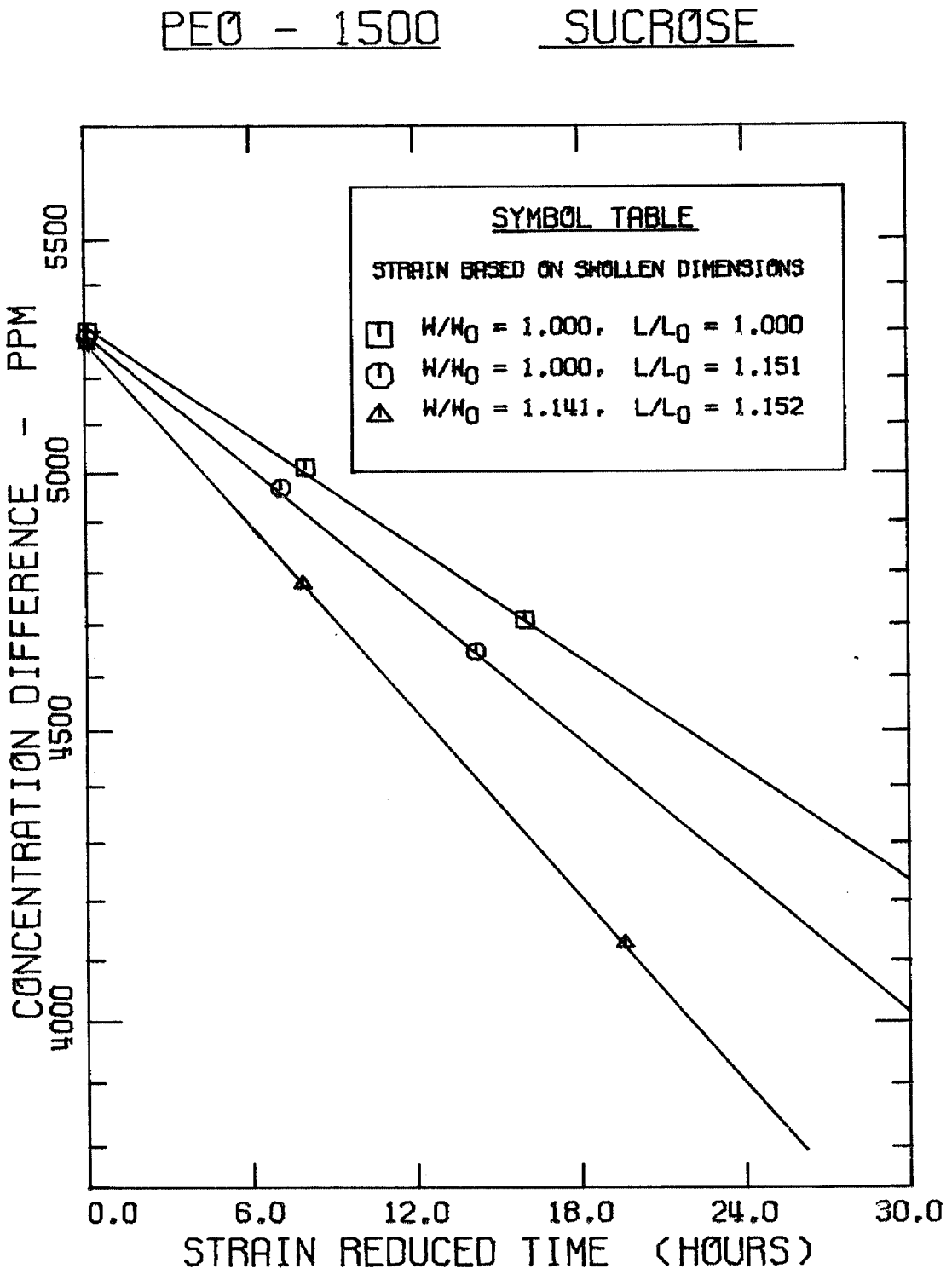

Figure A-13. Concentration difference versus time for a PEO-1500 film. Weighted average film thickness 0.00453 cm for the dry unstrained film. Curves theoretical (eqn. 3.10).

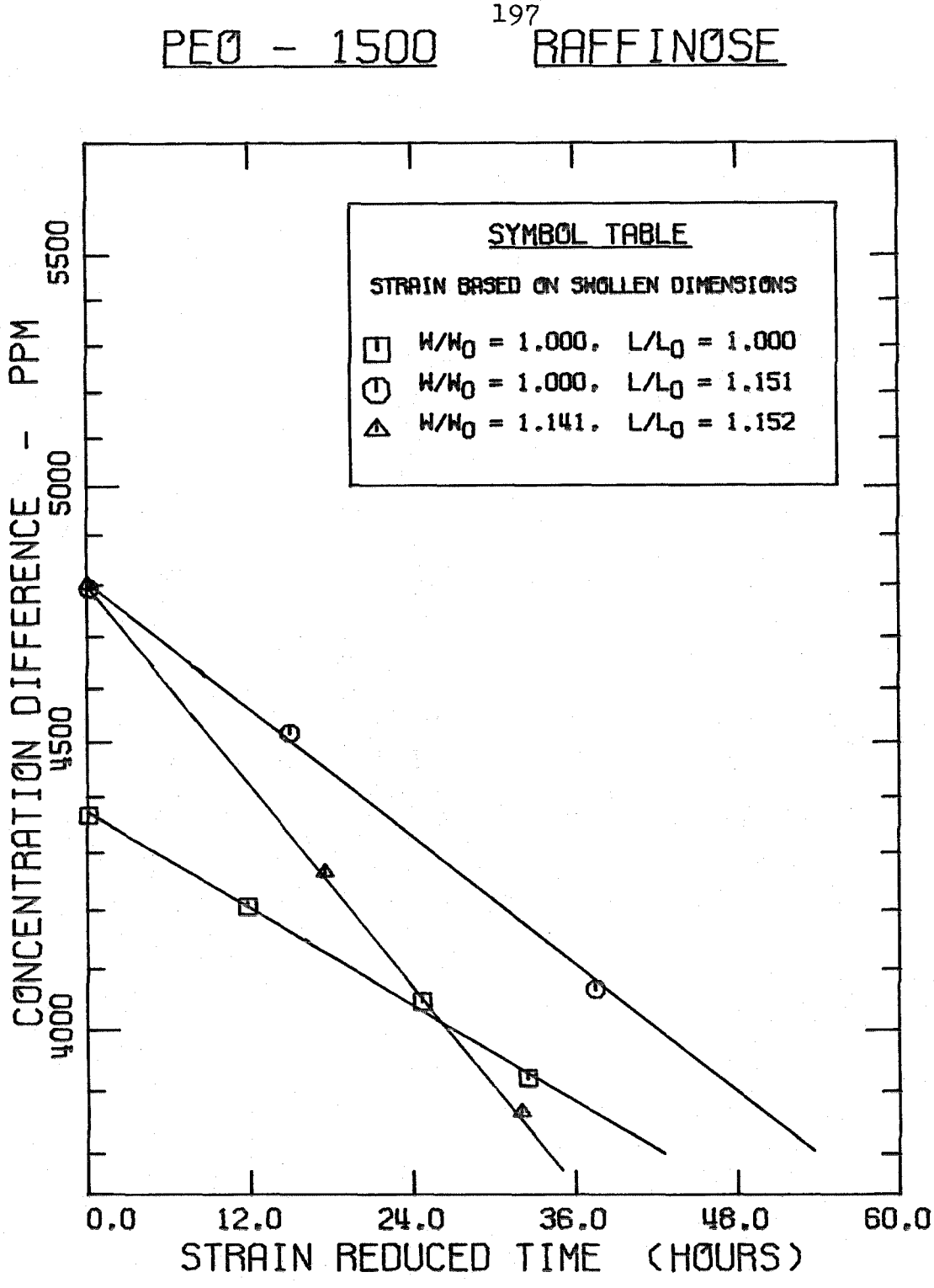

Figure A-14. Concentration difference versus time for a PEO-1500 film. Weighted average film thickness 0.00453 cm for the dry unstrained film. Curves theoretical (eqn. 3.10).

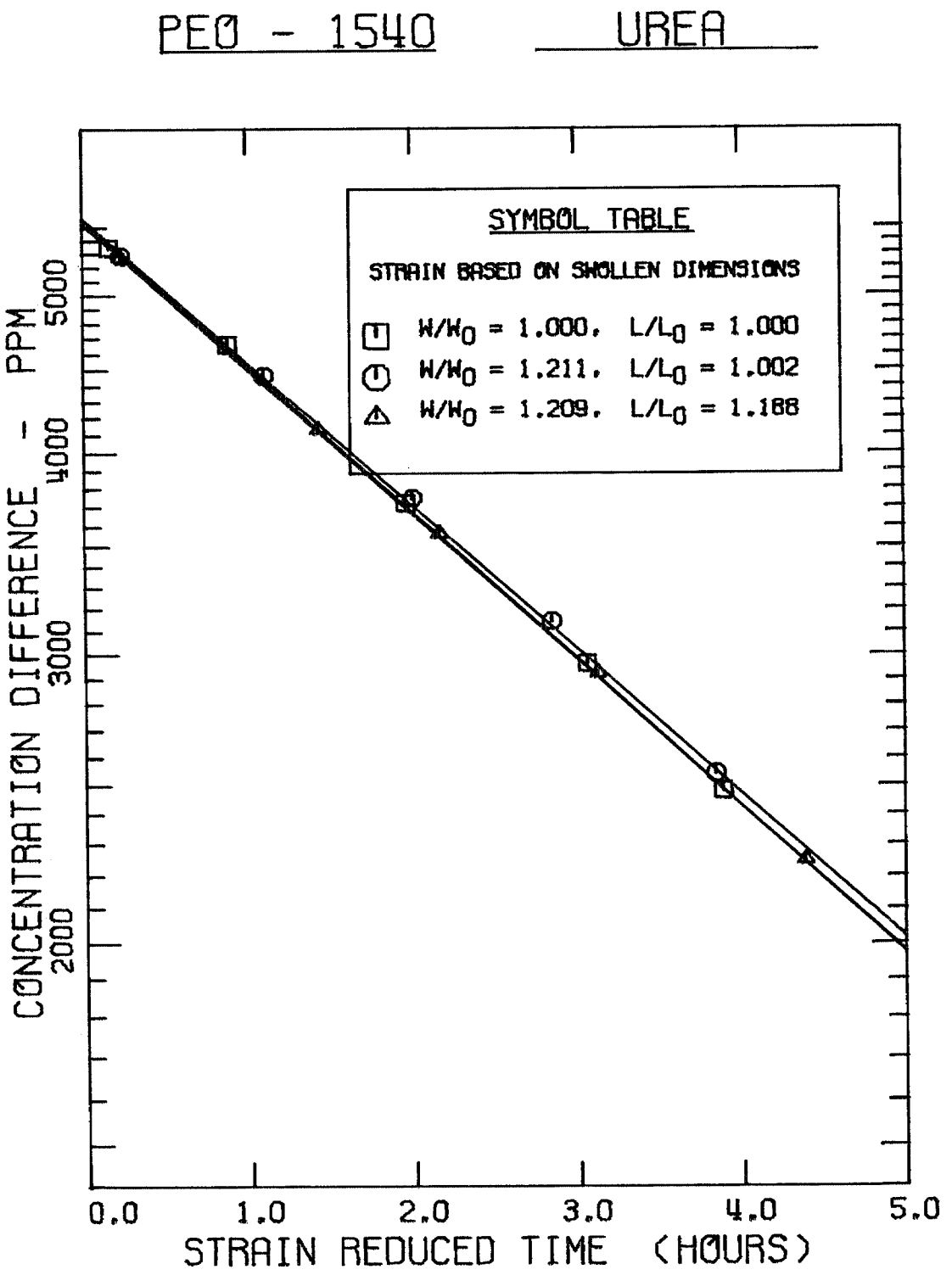

Figure A-15. Concentration difference versus time for a PEO-1540 film. Weighted average film thickness 0.00482 cm for the dry unstrained film. Curves theoretical (eqn. 3.10).

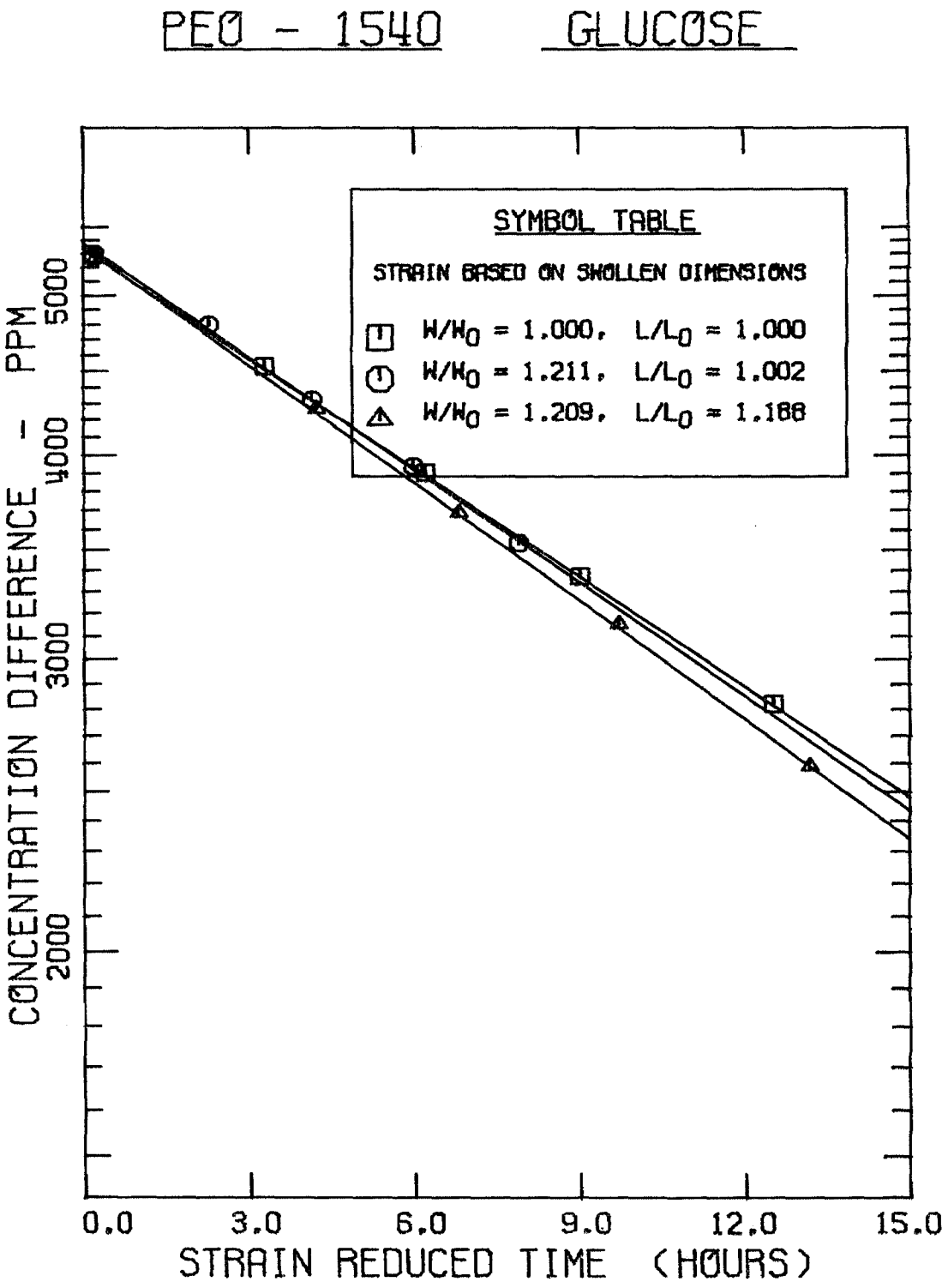

Figure A-16. Concentration difference versus time for a PEO-1540 film. Weighted average film thickness 0.00482 cm for the dry unstrained film. Curves theoretical (eqn. 3.10).

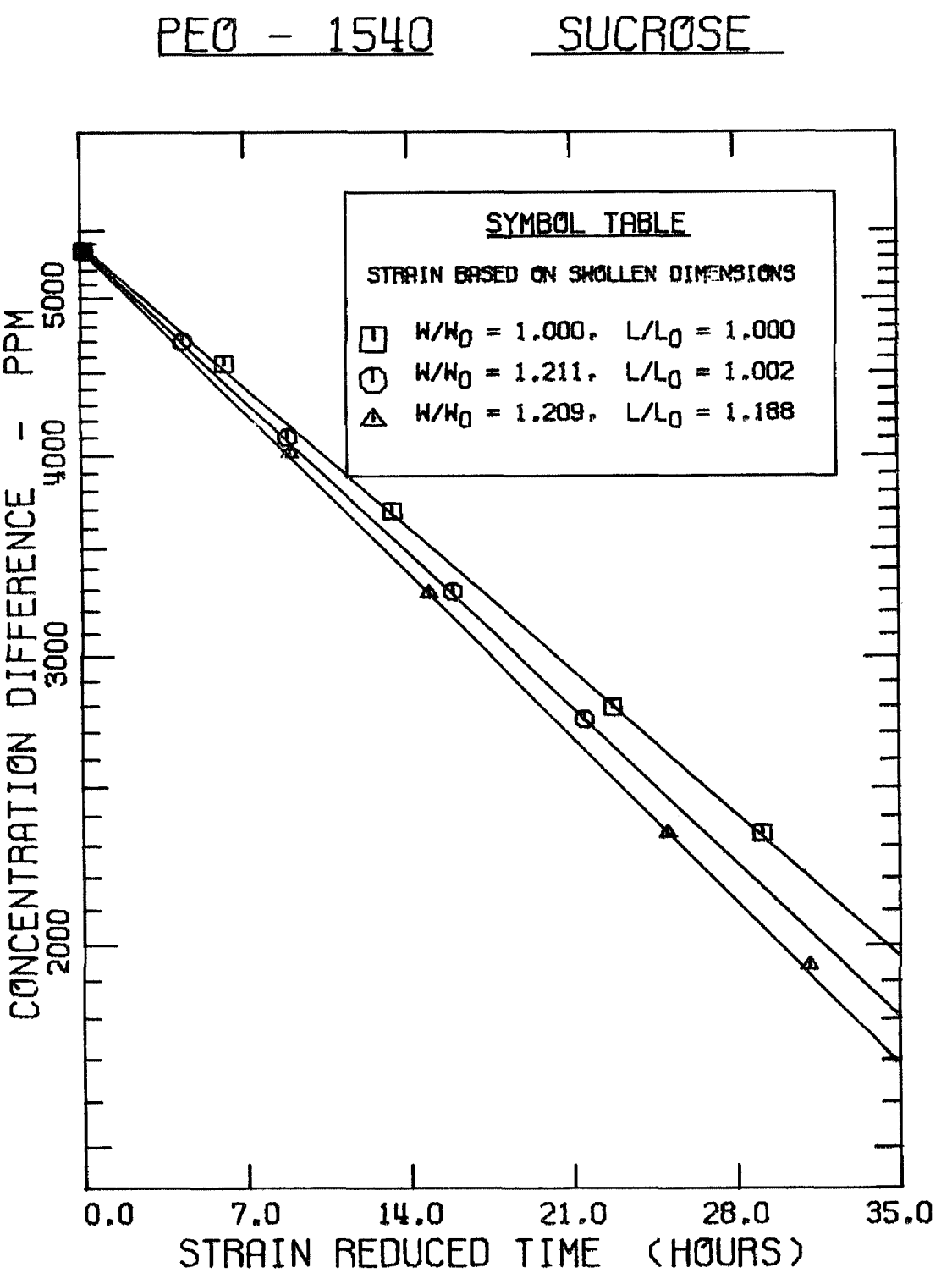

Figure A-17. Concentration difference versus time for a PEO-1540 film. Weighted average film thickness 0.00482 cm for the dry unstrained film. Curves theoretical (eqn. 3.10).

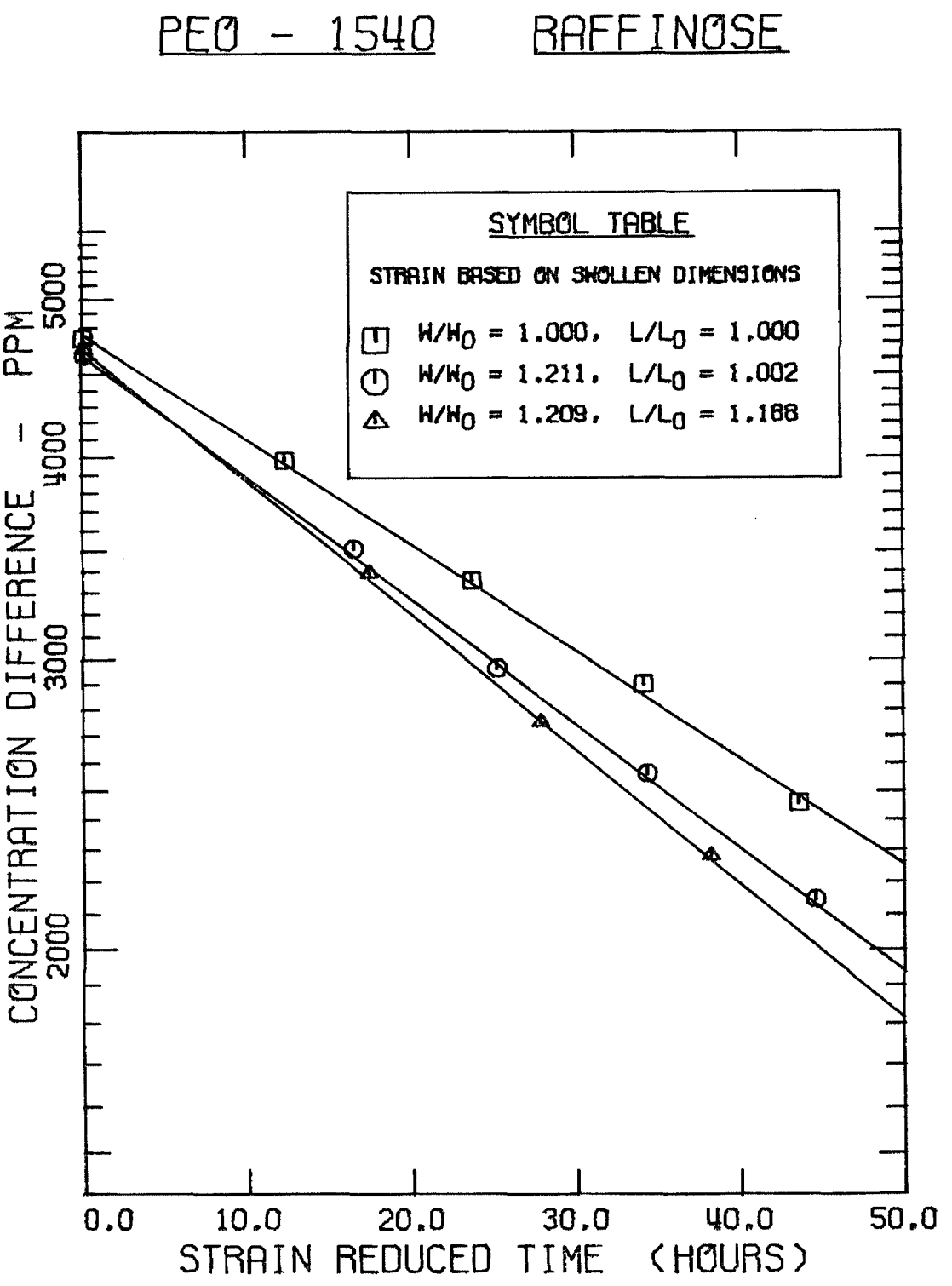

Figure A-18. Concentration difference versus time for a PEO-1540 film. Weighted average film thickness 0.00482 cm for the dry unstrained film. Curves theoretical (eqn. 3.10).

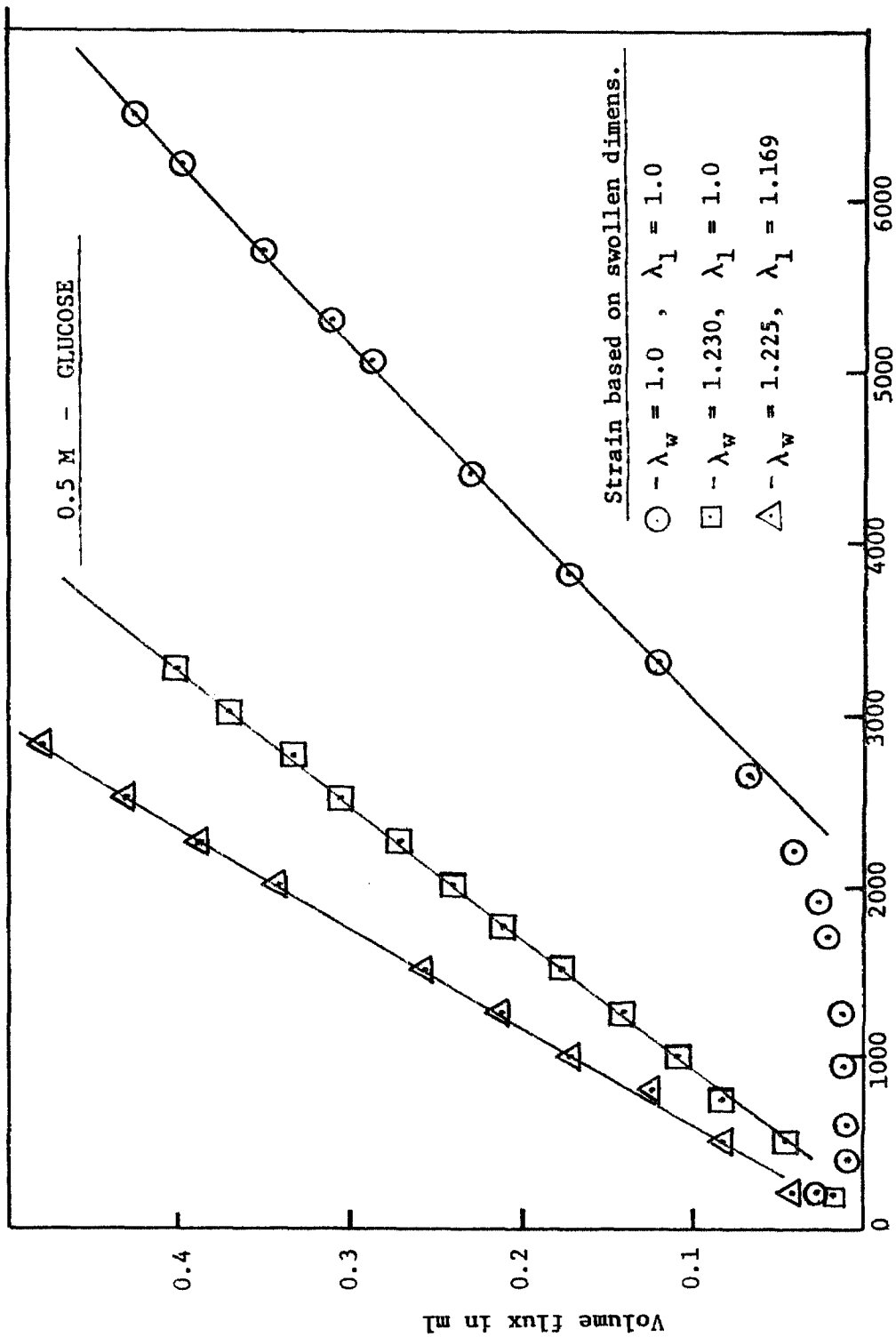

Figure A-19. Net volume flow across a PEO-600 membrane with glucose solution (0.5 M) in one half cell and deionized water in the other.

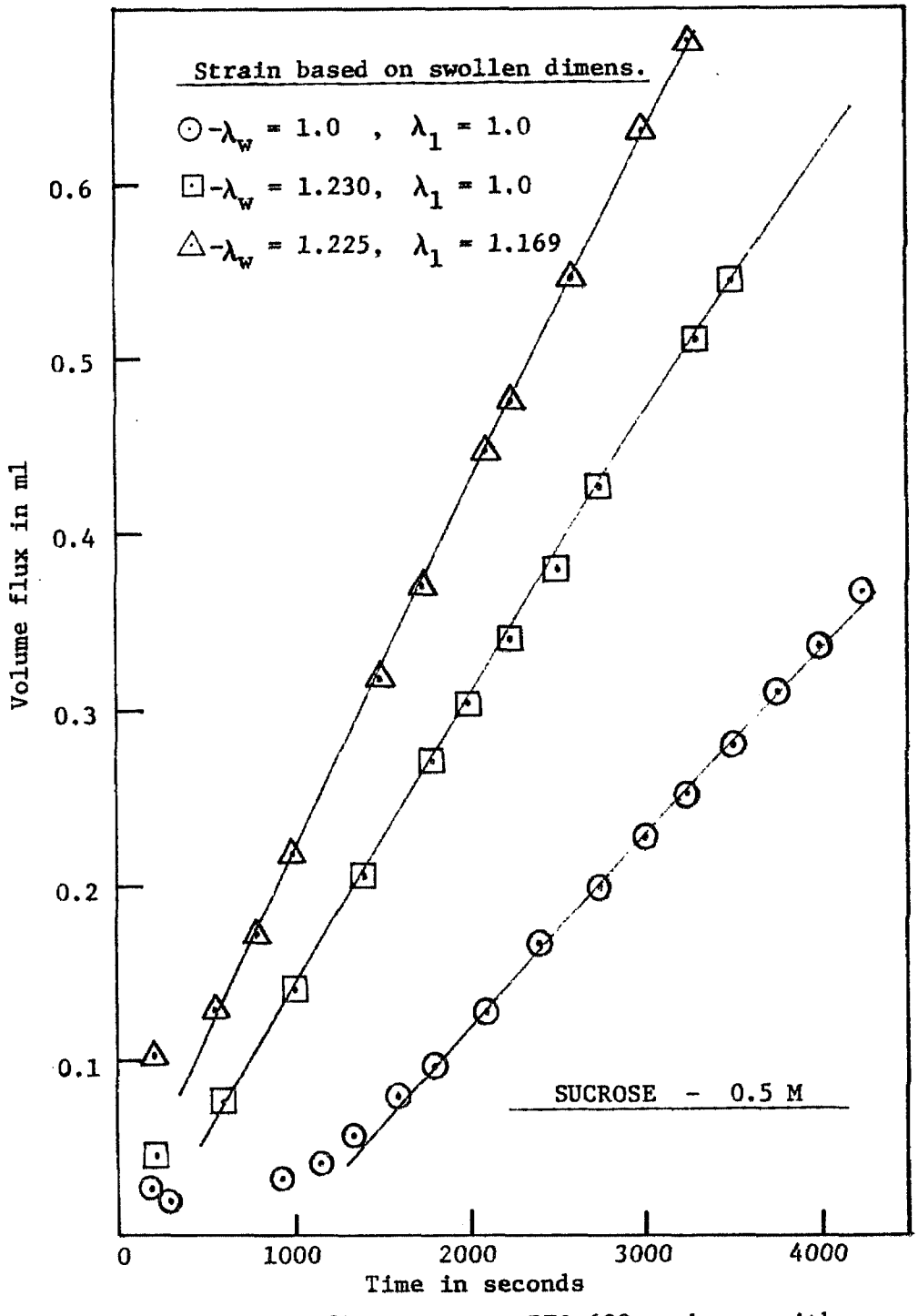

Figure A-20. Net volume flow across a PEO-600 membrane with sucrose solution in one half-cell and deionized water in the other.

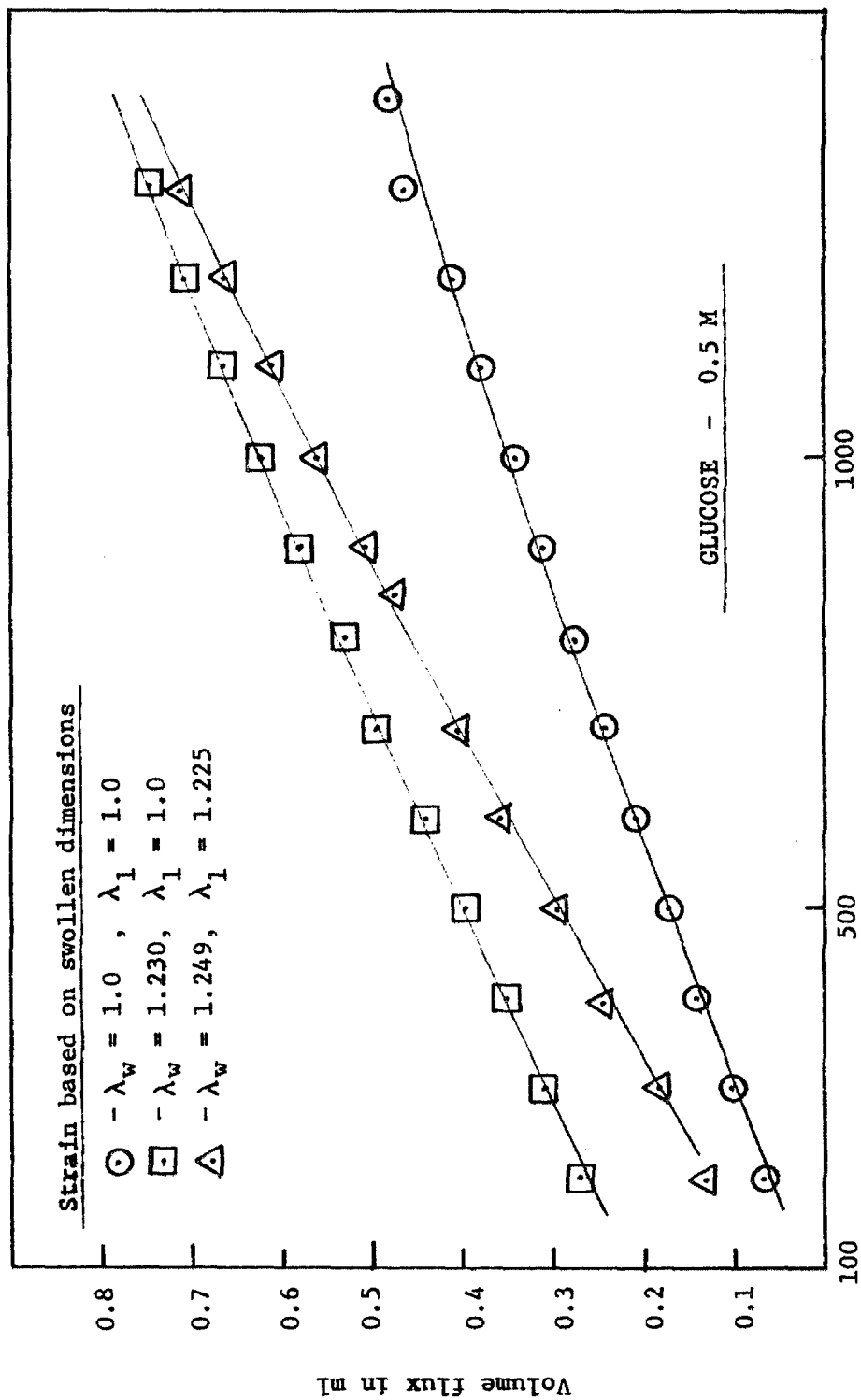

Figure A-21. Net volume flow across a PEO-1540 membrane with glucose solution (0.5 M) in one half cell and deionized water in the other.

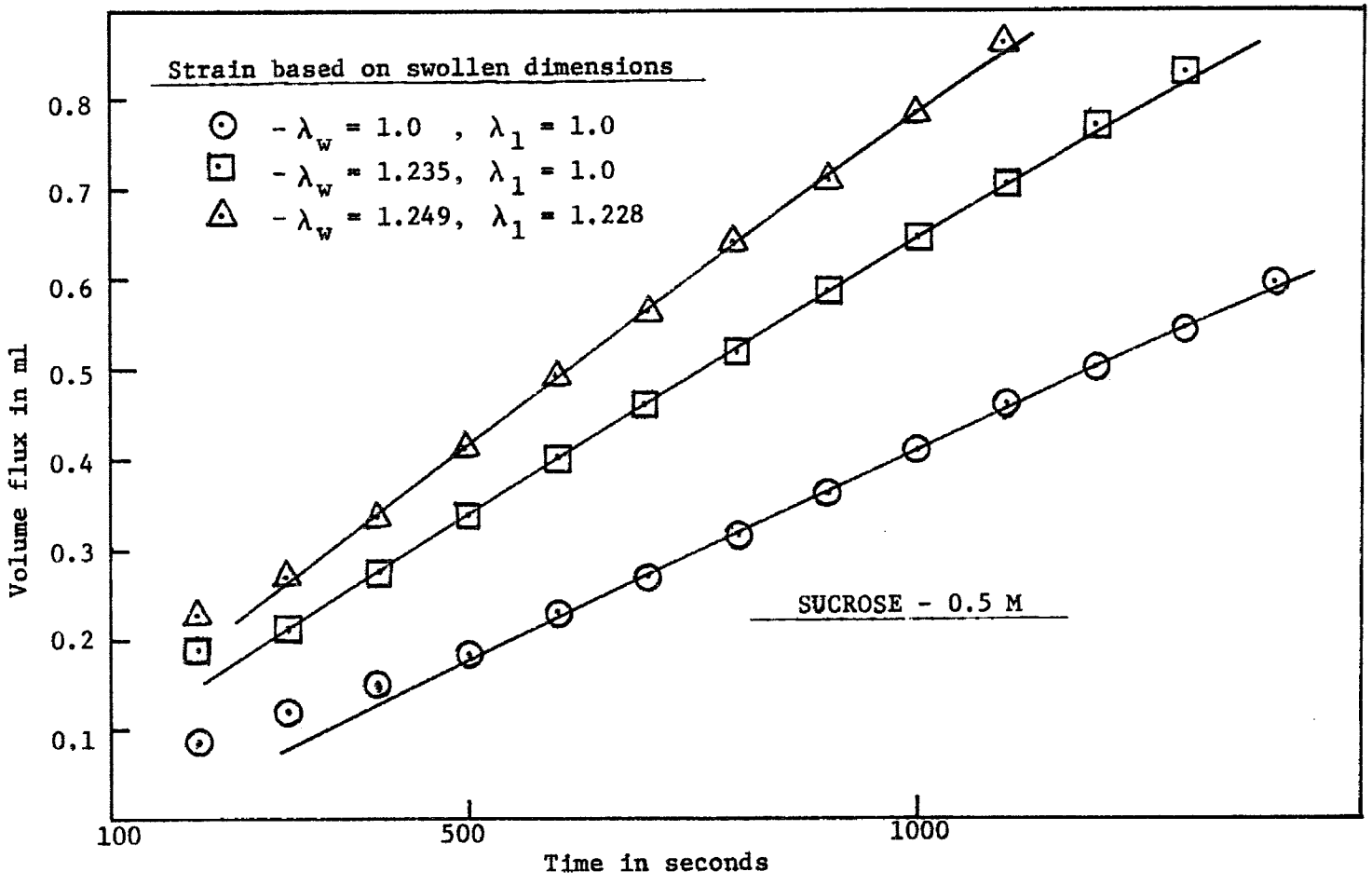

Figure A-22. Net volume flow across a PEO-1540 membrane with sucrose solution (0.5 M) in one half-cell and deionized water in the other.

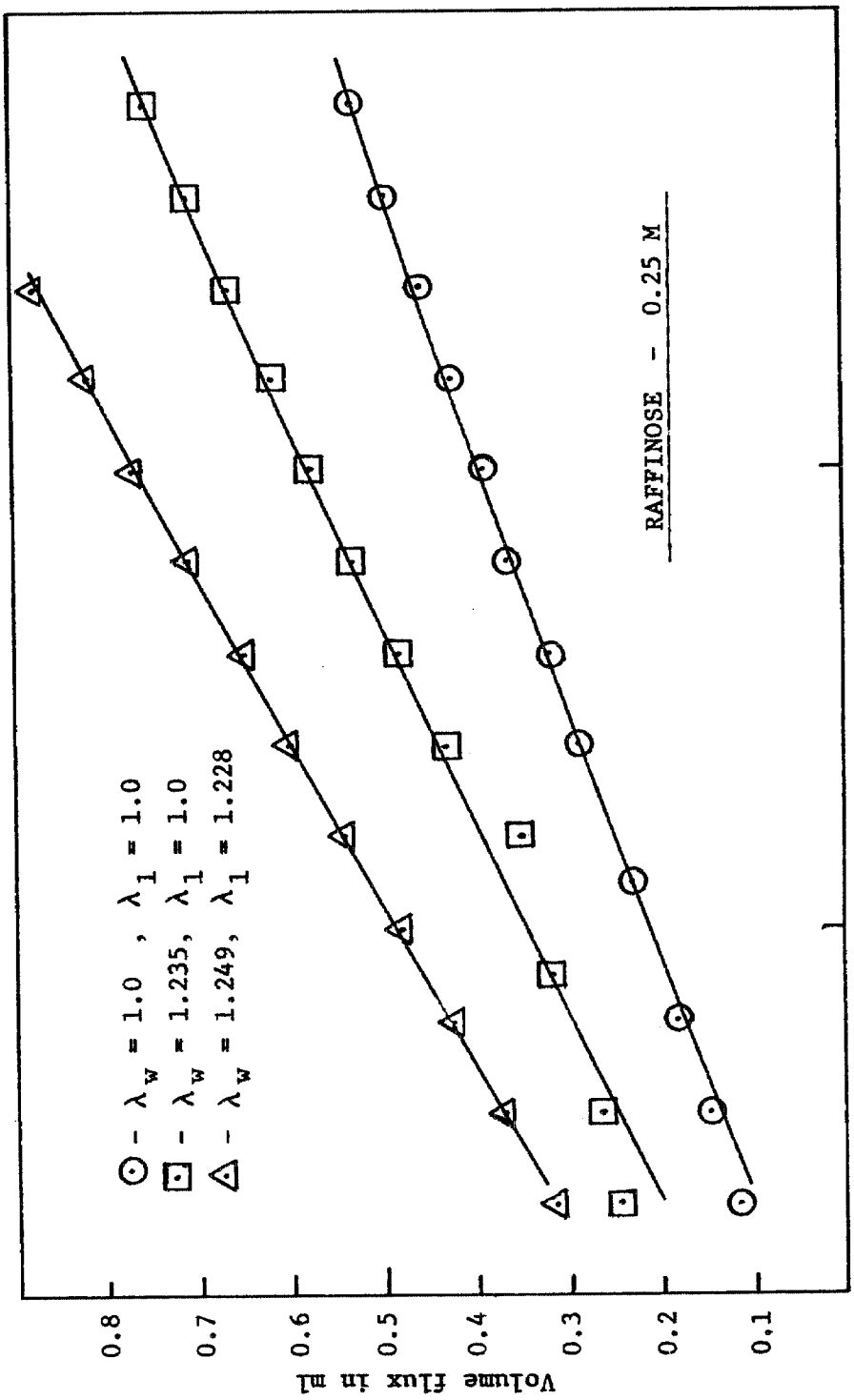

Figure A-23. Net volume flow across a PEO-1540 membrane with raffinose solution (0.25 M) in one half-cell and deionized water in the other.

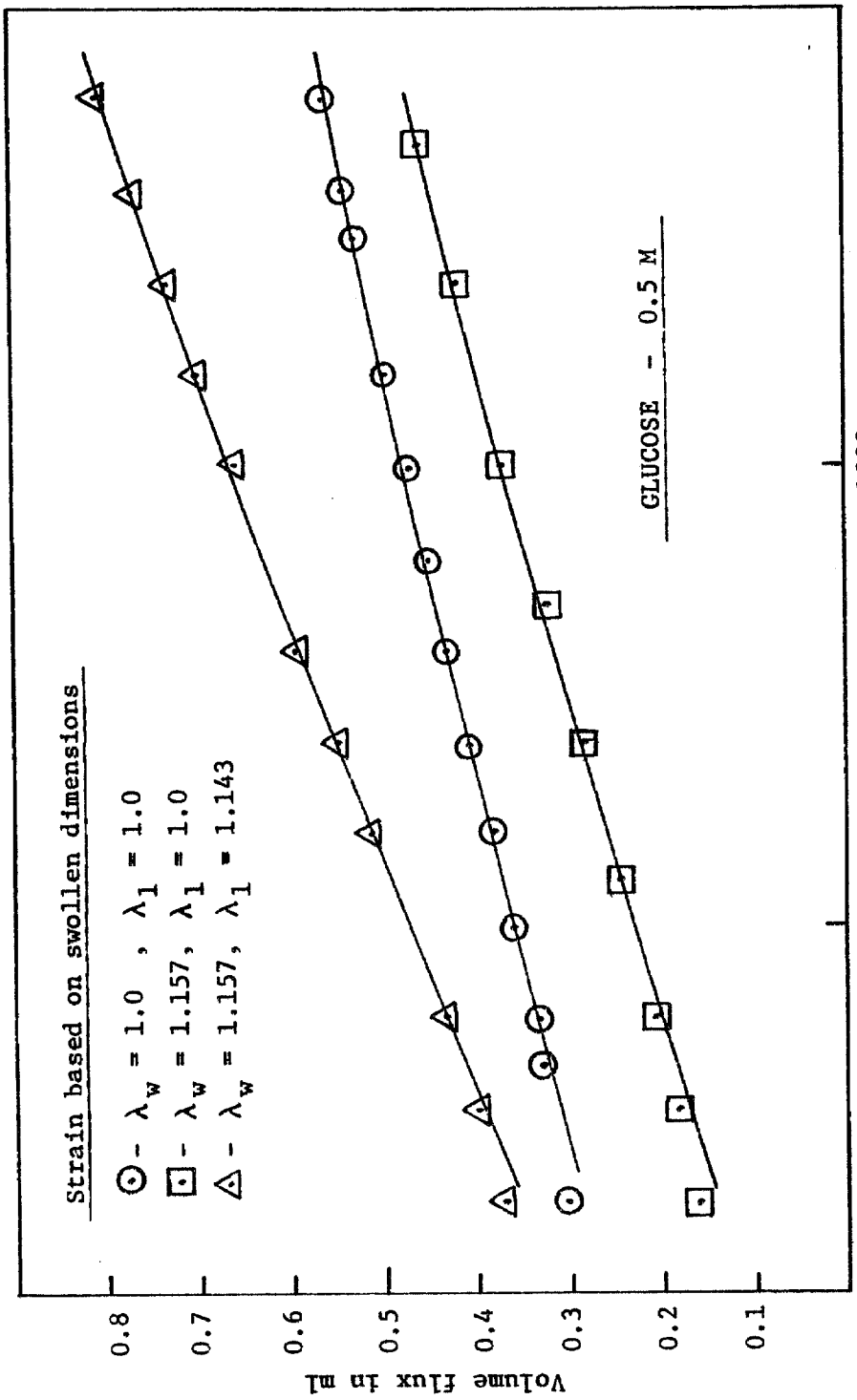

Figure A-24. Net volume flow across a PEO-1500 membrane with glucose solution (0.5 M) in one half-cell and deionized water in the other.

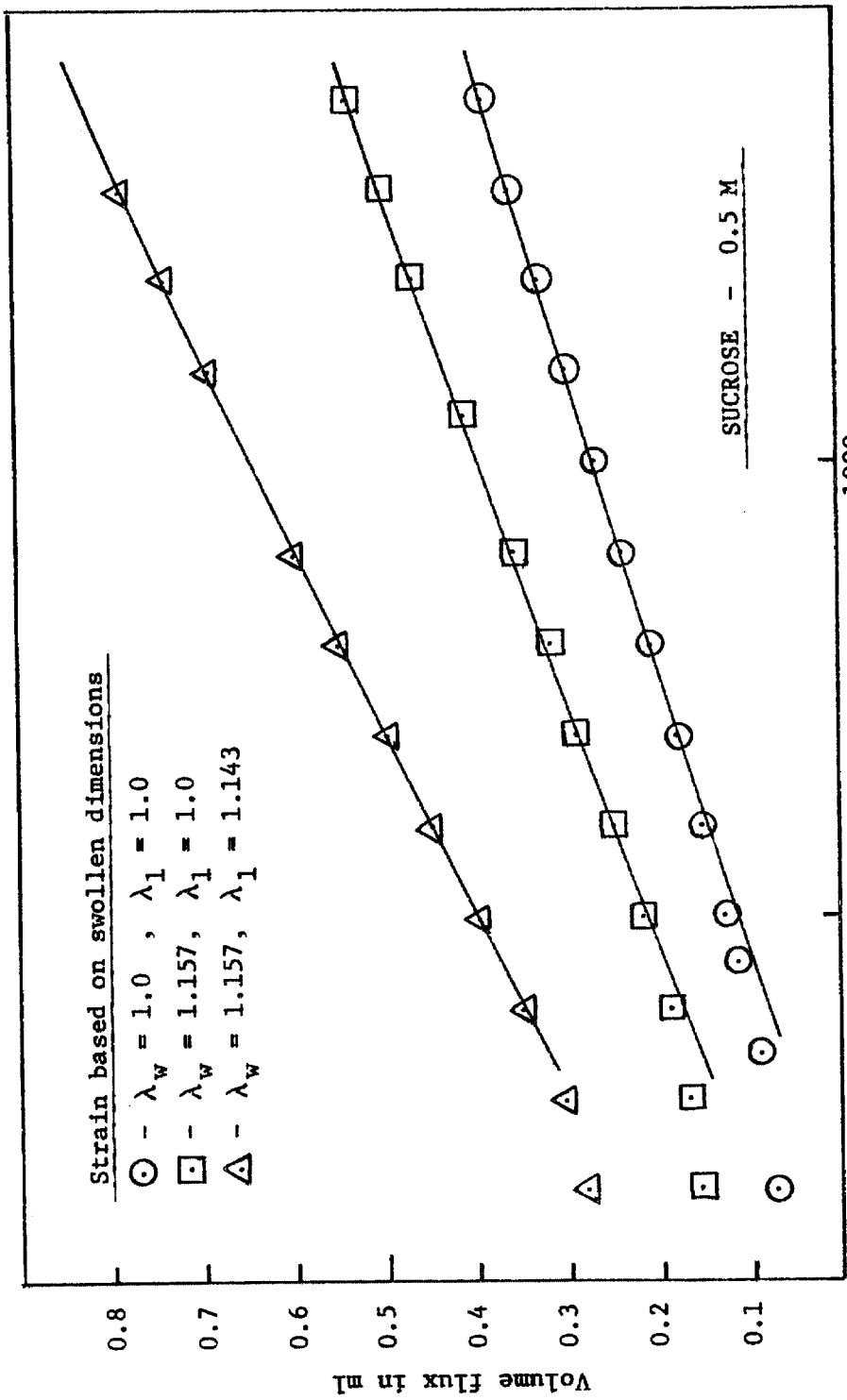

Figure A-25. Net volume flow across a PEO-1500 film with sucrose solution (0.5 M) in one half-cell and deionized water in the other.

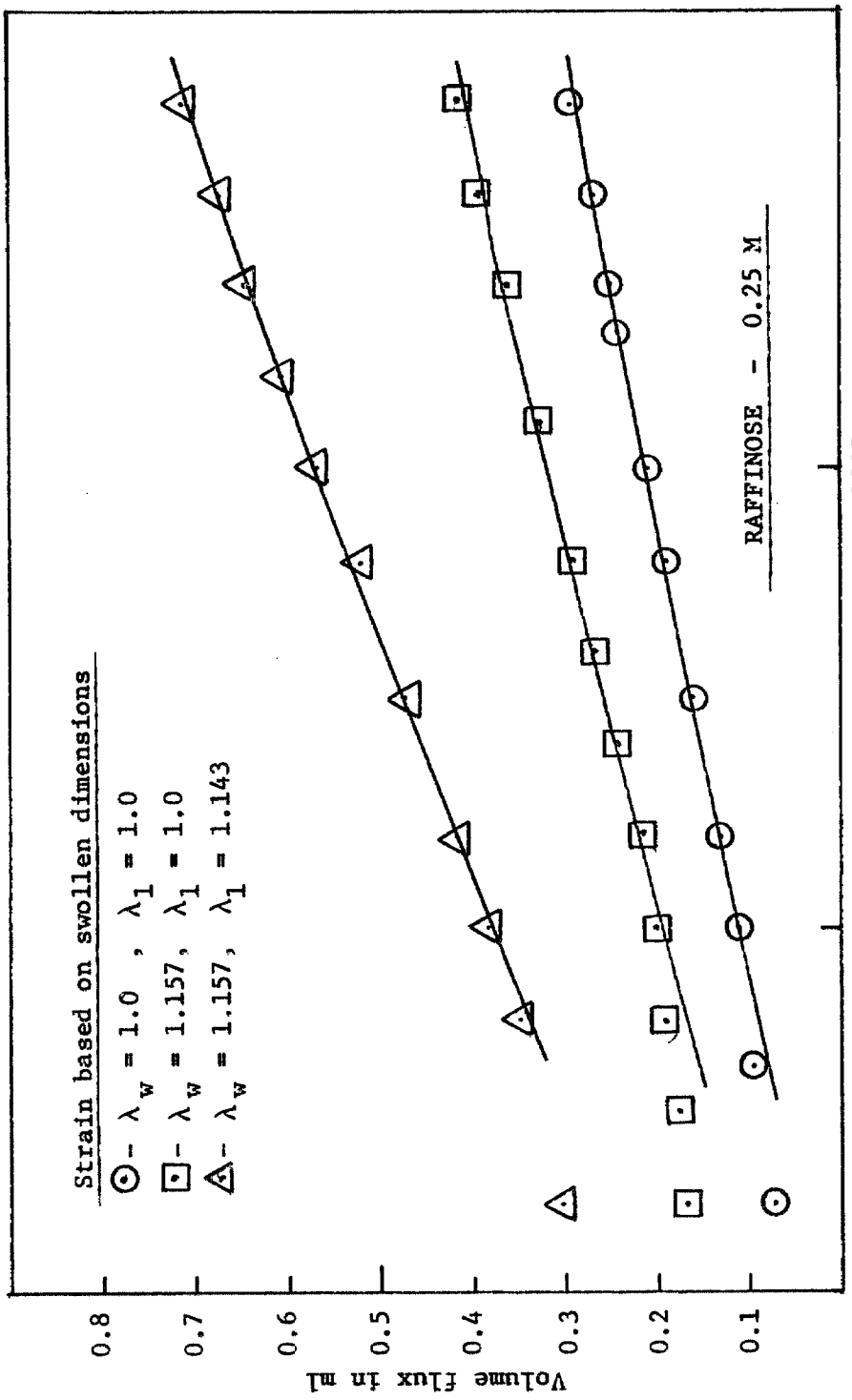

Figure A-26. Net volume flow across a PEO-1500 membrane with raffinose solution (0.25 M) in one half-cell and deionized water in the other.

APPENDIX II

Computer Programs

Three computer programs and samples of their output appear in this Appendix. The program used to determine the slope S in equation (3.10) appears on pages 198-205 . The program used to determine χ and M_c from strain-swelling data is given on pages 206-209 . The program used to fit the solute reflection coefficient data is located on pages 210-213 .

```
      REAL LGMEAN
      DIMENSION X(500,1),Y(500),B(2),IB(2),AHIGH(10),ALOW(10)
C
C
C     READ IN INITIALIZING PARAMETERS
C        NDATAS.....NUMBER OF DATA SETS
C        B(1),B(2).....INITIAL GUESSES FOR LSQENP
C        SLOPE1,SLOPE2.....SLOPES FROM CALIBRATION CURVE
C        BRANCH.....POINT AT WHICH SWITCH FROM SLOPE1 TO SLOPE2 OCCURS
C
C
      READ(5,100) NDATAS,B(1),B(2)
      DO 10 I=1,NDATAS
C
C
C     READ IN NTIMES AND NSUBST
C        NTIMES.....THE NUMBER OF TIMES FOR A GIVEN EXPERIMENT
C        NSUBST.....SOLUTE DESIGNATION CODE
C
C
      READ(5,101) NTIMES,NSUBST
C
C
C     EXMEAN = MEAN FOR AN EXPERIMENT
C     TMEAN = MEAN FOR ALL EXPERIMENTS ON THAT SOLUTE
C
C
      XSCALE=1.0
      M=1
C
C
C     PRINT HEADING
C
C
      WRITE(6,107)
      WRITE (6,103)
```

```
C
C
C     READ IN DATA
C
C
      DO 20 J=1,NTIMES
      READ(5,102) TIME,TSCALE
      READ(5,105) NHIGH,NLOW,NSUBST,SLOPE1,SLOPE2,BRANCH
      READ(5,102) (AHIGH(K),K=1,NHIGH)
      READ(5,102) (ALOW(K),K=1,NLOW)
C
C
C     SCALE DATA IF NECESSARY
C
C
      AXSQR=0.0
      AXMEAN=0.0
      IF(NSUBST.NE.3)  GO TO 16
      BRANCH=10000.0
      DO 15 K=1,NHIGH
      IF (AHIGH(K)-BRANCH) 15,15,17
17    AHIGH(K)=(AHIGH(K)-BRANCH)*SLOPE1/SLOPE2 + BRANCH
15    CONTINUE
C
C
C     CALCULATE COORDINATES OF POINT
C
C
16    DO 30 K=1,NHIGH
      DO 31 L=1,NLOW
      ZA=AHIGH(K)-ALOW(L)
      Z=ZA/SLOPE1
      ZN=Z*XSCALE
      AXMEAN=AXMEAN+ZN
      AXSQR=AXSQR+ZN*ZN
```

```
      X(M,1)=TIME*TSCALE
      Y(M)=ALOG10(ZN)
C
C
C     PRINT THE RESULTS
C
C
      WRITE(6,104) X(M,1),ZA,Z,ZN,Y(M)
31    M=M+1
30    CONTINUE
      AXMEAN=AXMEAN/(NHIGH*NLOW)
      STDDEV=SQRT((AXSQR/(NHIGH*NLOW))-(AXMEAN)**2)
      LGMEAN=ALOG10(AXMEAN)
      WRITE(6,106) AXMEAN,STDDEV,LGMEAN
20    CONTINUE
      M=M-1
C
C
C     USE LSQENP TO FIT A LINE TO THE DATA
C
C
      CALL LSQENP(M,2,1,Y,X,B,0,IB,0,0,100,0)
10    CONTINUE
100   FORMAT(I5,5F10.5)
101   FORMAT(2I5)
102   FORMAT (F10.4)
103   FORMAT('1',11X,'TIME',10X,'DELTA ABSORB.',10X,'DELTA CONC.',10X,'N
     1ORM. DELTA CONC.',10X,'LOG DELTA CONC. NORM')
104   FORMAT(' ',11X,F8.1,8X,F10.4,13X,F10.4,13X,F10.4,13X,F10.7)
105   FORMAT(3I5,3F10.5)
106   FORMAT(' THE ABOVE DATA SET MEAN CONCENTRATION = ',F10.4,'    STAN
     1DARD DEVIATION = ',F10.4,'     AND LOG MEAN CONCENTRATION = ',F10.
     17)
107   FORMAT( ////////)
108   FORMAT(2F10.5)
      END
```

```
C
C
C     SUBROUTINES REQUIRED BY LSQENP
C
C
      SUBROUTINE FCODE(Y,X,B,F,I)
      DIMENSION Y(1),X(500,1),B(1)
      F=B(1)+B(2)*X(I,1)
      RETURN
      ENC



      SUBROUTINE PCODE(P,X,B,F,I)
      DIMENSION P(1),X(500,1),B(1)
      P(1)=1.0
      P(2)=X(I,1)
      RETURN
      END
```

TIME	DELTA ABSORB.	DELTA CONC.	NORM. DELTA CONC.	LOG DELTA CONC. NORM
600.0	798.0000	5320.0000	5320.0000	3.7259121
600.0	799.0000	5326.6641	5326.6641	3.7264557
600.0	799.0000	5326.6641	5326.6641	3.7264557
600.0	799.0000	5326.6641	5326.6641	3.7264557
600.0	799.0000	5326.6641	5326.6641	3.7264557
600.0	801.0000	5340.0000	5340.0000	3.7275410
600.0	802.0000	5346.6641	5346.6641	3.7280827
600.0	802.0000	5346.6641	5346.6641	3.7280827
600.0	802.0000	5346.6641	5346.6641	3.7280827
600.0	802.0000	5346.6641	5346.6641	3.7280827
600.0	802.0000	5346.6641	5346.6641	3.7280827
600.0	803.0000	5353.3320	5353.3320	3.7286243
600.0	803.0000	5353.3320	5353.3320	3.7286243
600.0	803.0000	5353.3320	5353.3320	3.7286243
600.0	803.0000	5353.3320	5353.3320	3.7286243
600.0	802.0000	5346.6641	5346.6641	3.7280827
600.0	803.0000	5353.3320	5353.3320	3.7286243
600.0	803.0000	5353.3320	5353.3320	3.7286243
600.0	803.0000	5353.3320	5353.3320	3.7286243
600.0	802.0000	5346.6641	5346.6641	3.7280827
600.0	803.0000	5353.3320	5353.3320	3.7286243
600.0	803.0000	5353.3320	5353.3320	3.7286243
600.0	803.0000	5353.3320	5353.3320	3.7286243
600.0	803.0000	5353.3320	5353.3320	3.7286243
THE ABOVE DATA SET MEAN CONCENTRATION = 5345.3164 STANDARD DEVIATION = 12.0000 AND LOG MEAN CONCENTRATION = 3.7279739				
3100.0	699.0000	4660.0000	4660.0000	3.6683855
3100.0	698.0000	4653.3320	4653.3320	3.6677637
3100.0	698.0000	4653.3320	4653.3320	3.6677637
3100.0	697.0000	4646.6641	4646.6641	3.6671410
3100.0	697.0000	4646.6641	4646.6641	3.6671410
3100.0	700.0000	4666.6641	4666.6641	3.6690063
3100.0	699.0000	4660.0000	4660.0000	3.6683855
3100.0	699.0000	4660.0000	4660.0000	3.6683855
3100.0	698.0000	4653.3320	4653.3320	3.6677637
3100.0	698.0000	4653.3320	4653.3320	3.6677637
3100.0	699.0000	4660.0000	4660.0000	3.6683855
3100.0	699.0000	4660.0000	4660.0000	3.6683855
3100.0	698.0000	4653.3320	4653.3320	3.6677637
3100.0	698.0000	4653.3320	4653.3320	3.6677637
3100.0	701.0000	4673.3320	4673.3320	3.6696262
3100.0	700.0000	4666.6641	4666.6641	3.6690063
3100.0	700.0000	4666.6641	4666.6641	3.6690063
3100.0	699.0000	4660.0000	4660.0000	3.6683855
3100.0	699.0000	4660.0000	4660.0000	3.6683855
3100.0	701.0000	4673.3320	4673.3320	3.6696262
3100.0	700.0000	4666.6641	4666.6641	3.6690063
3100.0	700.0000	4666.6641	4666.6641	3.6690063
3100.0	699.0000	4660.0000	4660.0000	3.6683855
3100.0	699.0000	4660.0000	4660.0000	3.6683855
THE ABOVE DATA SET MEAN CONCENTRATION = 4659.9883 STANDARD DEVIATION = 8.0000 AND LOG MEAN CONCENTRATION = 3.6683846				

6900.0	559.0000	3726.6672	3726.6672	3.5713205
6900.0	558.0000	3720.0005	3720.0005	3.5705433
6900.0	556.0000	3706.6672	3706.6672	3.5689840
6900.0	555.0000	3700.0005	3700.0005	3.5682020
6900.0	554.0000	3693.3337	3693.3337	3.5674181
6900.0	560.0000	3733.3337	3733.3337	3.5720968
6900.0	559.0000	3726.6672	3726.6672	3.5713205
6900.0	557.0000	3713.3337	3713.3337	3.5697641
6900.0	556.0000	3706.6672	3706.6672	3.5689840
6900.0	555.0000	3700.0005	3700.0005	3.5682020
6900.0	561.0000	3740.0005	3740.0005	3.5728712
6900.0	560.0000	3733.3337	3733.3337	3.5720968
6900.0	559.0000	3726.6672	3726.6672	3.5713205
6900.0	557.0000	3713.3337	3713.3337	3.5697641
6900.0	556.0000	3706.6672	3706.6672	3.5689840
6900.0	555.0000	3700.0005	3700.0005	3.5682020
6900.0	561.0000	3740.0005	3740.0005	3.5728712
6900.0	560.0000	3733.3337	3733.3337	3.5720968
6900.0	558.0000	3720.0005	3720.0005	3.5705433
6900.0	557.0000	3713.3337	3713.3337	3.5697641
6900.0	556.0000	3706.6672	3706.6672	3.5689840
6900.0	561.0000	3740.0005	3740.0005	3.5728712
6900.0	560.0000	3733.3337	3733.3337	3.5720968
6900.0	558.0000	3720.0005	3720.0005	3.5705433
6900.0	557.0000	3713.3337	3713.3337	3.5697641
6900.0	556.0000	3706.6672	3706.6672	3.5689840

THE ABOVE DATA SET MEAN CONCENTRATION = 3717.3250 STANDARD DEVIATION = 14.5602 AND LOG MEAN CONCENTRATION = 3.5702305

10700.0	443.0000	2953.3337	2953.3337	3.4703121
10700.0	442.0000	2946.6670	2946.6670	3.4693308
10700.0	441.0000	2940.0002	2940.0002	3.4683475
10700.0	441.0000	2940.0002	2940.0002	3.4683475
10700.0	440.0000	2933.3337	2933.3337	3.4673615
10700.0	444.0000	2960.0002	2960.0002	3.4712915
10700.0	443.0000	2953.3337	2953.3337	3.4703121
10700.0	442.0000	2946.6670	2946.6670	3.4693308
10700.0	442.0000	2946.6670	2946.6670	3.4693308
10700.0	441.0000	2940.0002	2940.0002	3.4683475
10700.0	446.0000	2973.3337	2973.3337	3.4732437
10700.0	445.0000	2966.6670	2966.6670	3.4722691
10700.0	444.0000	2960.0002	2960.0002	3.4712915
10700.0	444.0000	2960.0002	2960.0002	3.4712915
10700.0	443.0000	2953.3337	2953.3337	3.4703121
10700.0	446.0000	2973.3337	2973.3337	3.4732437
10700.0	445.0000	2966.6670	2966.6670	3.4722691
10700.0	444.0000	2960.0002	2960.0002	3.4712915
10700.0	444.0000	2960.0002	2960.0002	3.4712915
10700.0	443.0000	2953.3337	2953.3337	3.4703121
10700.0	449.0000	2993.3337	2993.3337	3.4761553
10700.0	448.0000	2986.6670	2986.6670	3.4751873
10700.0	447.0000	2980.0002	2980.0002	3.4742165
10700.0	447.0000	2980.0002	2980.0002	3.4742165
10700.0	446.0000	2973.3337	2973.3337	3.4732437

THE ABOVE DATA SET MEAN CONCENTRATION = 2959.9973 STANDARD DEVIATION = 15.7162 AND LOG MEAN CONCENTRATION = 3.4712915

13500.0	372.0000	2480.0002	2480.0002	3.3944521
13500.0	372.0000	2480.0002	2480.0002	3.3944521
13500.0	371.0000	2473.3335	2473.3335	3.3932829
13500.0	371.0000	2473.3335	2473.3335	3.3932829
13500.0	371.0000	2473.3335	2473.3335	3.3932829
13500.0	372.0000	2480.0002	2480.0002	3.3944521
13500.0	372.0000	2480.0002	2480.0002	3.3944521
13500.0	371.0000	2473.3335	2473.3335	3.3932829
13500.0	371.0000	2473.3335	2473.3335	3.3932829
13500.0	371.0000	2473.3335	2473.3335	3.3932829

13500.0	373.0000	2486.6670	2486.6670	3.3956175
13500.0	373.0000	2486.6670	2486.6670	3.3956175
13500.0	372.0000	2480.0002	2480.0002	3.3944521
13500.0	372.0000	2480.0002	2480.0002	3.3944521
13500.0	372.0000	2480.0002	2480.0002	3.3944521
13500.0	373.0000	2486.6670	2486.6670	3.3956175
13500.0	373.0000	2486.6670	2486.6670	3.3956175
13500.0	372.0000	2480.0002	2480.0002	3.3944521
13500.0	372.0000	2480.0002	2480.0002	3.3944521
13500.0	372.0000	2480.0002	2480.0002	3.3944521
13500.0	373.0000	2486.6670	2486.6670	3.3956175
13500.0	373.0000	2486.6670	2486.6670	3.3956175
13500.0	372.0000	2480.0002	2480.0002	3.3944521
13500.0	372.0000	2480.0002	2480.0002	3.3944521
13500.0	372.0000	2480.0002	2480.0002	3.3944521

THE ABOVE DATA SET MEAN CONCENTRATION = 2479.9990 STANDARD DEVIATION = 4.3990 AND LOG MEAN CONCENTRATION = 3.3944511
EPSILON TEST
N = 125 K = 2 IP = C M = 1
FF = 0.400E 01 T = 0.200E 01 E = C.5CCE-C4 TAU = 0.100E-02

PARAMETERS 0.37466097E 01 -0.25882866E-04

PHI	S E	LAMBDA	ANALYTIC PARTIALS USED
0.95079597E-03	0.27602956E-02	0.100E-03	

PTP INVERSE

1	0.25283724E-01	-0.24832934E-05
2	-0.24832934E-05	0.35679482E-09

PARAMETER CORRELATION MATRIX

1	1.0000	-0.8268
2	-0.8268	1.0000

	STD	ONE - PARAMETER		SUPPORT PLANE	
B	ERROR	LOWER	UPPER	LOWER	UPPER
1	0.44209044E-03	0.37457247E 01	0.37474937E 01	0.37453585E 01	0.37478600E 01
2	0.52516995E-07	-0.25987887E-04	-0.25777830E-04	-0.26031397E-04	-0.25734320E-04

NONLINEAR CONFIDENCE LIMITS

PHI CRITICAL = 0.10126340E-02

PARA	LOWER B	LOWER PHI	UPPER B	UPPER PHI
1	0.37459068E 01	0.10126054E-02	0.37473135E 01	0.10126524E-02
2	-0.25966423E-04	0.10129202E-02	-0.25799538E-04	0.10125309E-02

```
      DIMENSION WTS(12)
      DIMENSION X(500,1),Y(500),B(2),IB(2),SR(4)
1     READ(5,100) N,B(1),B(2)
      DO 10 I=1,N
      READ(5,101) SWELL,STRAIN,WTS(I)
      SWELLO=((SWELL-1.0)+0.8929)/0.8929
      V2=1.0/SWELLO
      SWELL=SWELLO
      WRITE(6,102) STRAIN,SWELL,V2,WTS(I)
      X(I,1)=V2
10    Y(I)=STRAIN
      CALL LSQENP(N,2,1,Y,X,B,0,IB,0,0,0,-1)
      GO TO 1
100   FORMAT (I5,2F10.4)
101   FORMAT (3F10.4)
102   FORMAT ('   STRAIN IS     ',F10.3,'   SWELL IS   ',F10.3,'   V2 IS
     1     ',F10.3,'   WEIGHTING FACTOR IS     ',F5.2)
      END

      SUBROUTINE FCODE(Y,X,B,F,I)
      DIMENSION Y(1),X(500,1),B(1)
      F=-20.16/(B(2)*(ALOG(1.0-X(I,1))+X(I,1)+B(1)*X(I,1)*X(I,1)))
      RETURN
      END

      SUBROUTINE PCODE(P,X,B,F,I)
      DIMENSION P(1),X(500,1),B(1)
      P(1)=20.16*X(I,1)*X(I,1)/(B(2)*(ALOG(1.0-X(I,1))+X(I,1)+B(1)*X(I,1
     1)*X(I,1))**2)
      P(2)=20.16/(B(2)*B(2)*(ALOG(1.0-X(I,1))+X(I,1)+B(1)*X(I,1)*X(I,1))
     1)
      RETURN
      END
```

```
 STRAIN IS          1.136   SWELL IS        1.523   V2 IS          0.657   WEIGHTING FACTOR IS      1.00
 STRAIN IS          1.136   SWELL IS        1.522   V2 IS          0.657   WEIGHTING FACTOR IS      1.00
 STRAIN IS          1.136   SWELL IS        1.521   V2 IS          0.658   WEIGHTING FACTOR IS      1.00
 STRAIN IS          1.359   SWELL IS        1.576   V2 IS          0.635   WEIGHTING FACTOR IS      1.00
 STRAIN IS          1.297   SWELL IS        1.564   V2 IS          0.639   WEIGHTING FACTOR IS      1.00
 STRAIN IS          1.254   SWELL IS        1.560   V2 IS          0.641   WEIGHTING FACTOR IS      1.00
 STRAIN IS          1.437   SWELL IS        1.590   V2 IS          0.629   WEIGHTING FACTOR IS      1.00
 STRAIN IS          1.460   SWELL IS        1.588   V2 IS          0.630   WEIGHTING FACTOR IS      0.50
 STRAIN IS          1.630   SWELL IS        1.633   V2 IS          0.612   WEIGHTING FACTOR IS      0.50
EPSILON TEST
N =   9      K =   2      IP =   0      M =   1
FF =  0.400E 01      T =  0.200E 01      E =  0.500E-04      TAU =  0.100E-02


PARAMETERS     0.65349925E 00    0.13590353E 03

          PHI                S E            LAMBDA        ANALYTIC PARTIALS USED
       0.36047756E-02     0.22692904E-01    0.100E-03

FTP INVERSE
   1    0.79677850E 00    0.39849243E 03
   2    0.39849243E 03    0.20046519E 06

 ARAMETER CORRELATION MATRIX
      1      1.0000    0.9971
      2      0.9971    1.0000

          STD                    ONE - PARAMETER                      SUPPORT PLANE
   B        ERROR          LOWER              UPPER              LOWER              UPPER
   1    0.20256240E-01   0.61298674E 00     0.69401169E 00     0.59620589E 00     0.71079254E 00
   2    0.10160371E 02   0.11558279E 03     0.15622427E 03     0.10716566E 03     0.16464140E 03


 NONLINEAR CONFIDENCE LIMITS

PHI CRITICAL =  0.77245161E-02

 PARA       LOWER B          LOWER PHI          UPPER B          UPPER PHI
   1    0.64868057E 00    0.84348917E-02    0.65769172E 00    0.75144172E-02
   2    0.13393182E 03    0.70340559E-02    0.13818629E 03    0.79227750E-02
  STRAIN IS          1.261   SWELL IS        2.124   V2 IS          0.471   WEIGHTING FACTOR IS      1.00
  STRAIN IS          1.261   SWELL IS        2.123   V2 IS          0.471   WEIGHTING FACTOR IS      1.00
  STRAIN IS          1.261   SWELL IS        2.124   V2 IS          0.471   WEIGHTING FACTOR IS      1.00
  STRAIN IS          1.363   SWELL IS        2.154   V2 IS          0.464   WEIGHTING FACTOR IS      1.00
  STRAIN IS          1.327   SWELL IS        2.151   V2 IS          0.465   WEIGHTING FACTOR IS      1.00
  STRAIN IS          1.443   SWELL IS        2.174   V2 IS          0.460   WEIGHTING FACTOR IS      1.00
  STRAIN IS          1.397   SWELL IS        2.155   V2 IS          0.464   WEIGHTING FACTOR IS      1.00
  STRAIN IS          1.407   SWELL IS        2.163   V2 IS          0.462   WEIGHTING FACTOR IS      1.00
  STRAIN IS          1.511   SWELL IS        2.193   V2 IS          0.456   WEIGHTING FACTOR IS      1.00
EPSILON TEST
N =   9      K =   2      IP =   0      M =   1
FF =  0.400E 01      T =  0.200E 01      E =  0.500E-04      TAU =  0.100E-02
```

```
PARAMETERS      0.63999307E 00     0.67566553E 03

            PHI                S E           LAMBDA        ANALYTIC PARTIALS USED
         0.99068810E-03     0.11896506E-01    0.100E-03

PTP INVERSE
   1     0.38656414E 00     0.25723945E 04

   2     0.25723950E 04     0.17145568E 08

PARAMETER CORRELATION MATRIX
       1        1.0000     0.9992
       2        0.9992     1.0000


             STD                    ONE - PARAMETER                        SUPPORT PLANE
   B        ERROR                LOWER                UPPER              LOWER              UPPER
   1     0.73955639E-02     0.62519991E 00     0.65478617E 00     0.61907238E 00     0.66091371E 00
   2     0.49260117E 02     0.57714526E 03     0.77418555E 03     0.53633667E 03     0.81499414E 03


 NONLINEAR CONFIDENCE LIMITS

PHI CRITICAL =  0.21229023E-02

 PARA       LOWER B          LOWER PHI          UPPER B          UPPER PHI
   1     0.63906592E 00     0.23498859E-02     0.64080000E 00     0.20563200E-02
   2     0.67065796E 03     0.19146081E-02     0.68145605E 03     0.21875456E-02
  STRAIN IS          1.203    SHELL IS          1.825    V2 IS          0.548    WEIGHTING FACTOR IS       1.00
  STRAIN IS          1.203    SHELL IS          1.826    V2 IS          0.547    WEIGHTING FACTOR IS       1.00
  STRAIN IS          1.203    SHELL IS          1.831    V2 IS          0.546    WEIGHTING FACTOR IS       1.00
  STRAIN IS          1.354    SHELL IS          1.887    V2 IS          0.530    WEIGHTING FACTOR IS       1.00
  STRAIN IS          1.395    SHELL IS          1.896    V2 IS          0.527    WEIGHTING FACTOR IS       1.00
  STRAIN IS          1.378    SHELL IS          1.888    V2 IS          0.530    WEIGHTING FACTOR IS       1.00
  STRAIN IS          1.664    SHELL IS          1.969    V2 IS          0.508    WEIGHTING FACTOR IS       1.00
EPSILON TEST
N =   7      K =   2      IP =   0      M =   1
EE =  0.400E 01      T =  0.200E 01      E =  0.500E-04      TAU =  0.100E-02


PARAMETERS      0.57774216E 00     0.23413228E 03

            PHI                S E           LAMBDA        ANALYTIC PARTIALS USED
         0.11158453E-02     0.14938843E-01    0.100E-04

PTP INVERSE
   1     0.95036674E 00     0.99655273E 03
   2     0.99653322E 03     0.10492800E 07

PARAMETER CORRELATION MATRIX
       1        1.0000     0.9980
       2        0.9980     1.0000
```

```
  STRAIN IS          1.867   SHELL IS        3.381   V2 IS          0.296   WEIGHTING FACTOR IS      1.00
  STRAIN IS          1.720   SHELL IS        3.357   V2 IS          0.298   WEIGHTING FACTOR IS      1.00
  STRAIN IS          1.701   SHELL IS        3.351   V2 IS          0.298   WEIGHTING FACTOR IS      1.00
  STRAIN IS          1.754   SHELL IS        3.369   V2 IS          0.297   WEIGHTING FACTOR IS      1.00
  STRAIN IS          1.758   SHELL IS        3.380   V2 IS          0.296   WEIGHTING FACTOR IS      0.50
  STRAIN IS          1.896   SHELL IS        3.366   V2 IS          0.297   WEIGHTING FACTOR IS      0.25
  STRAIN IS          2.008   SHELL IS        3.396   V2 IS          0.295   WEIGHTING FACTOR IS      0.50
  STRAIN IS          2.040   SHELL IS        3.396   V2 IS          0.295   WEIGHTING FACTOR IS      1.00
  STRAIN IS          2.034   SHELL IS        3.392   V2 IS          0.295   WEIGHTING FACTOR IS      1.00
EPSILON TEST
N =  12      K =   2      IP =   0      M =   1
FF =  0.400E 01      T =  0.200E 01      E =  0.500E-04      TAU =  0.100E-02


PARAMETERS      0.61060423E 00    0.72656875E 04

            PHI                 S E            LAMBDA        ANALYTIC PARTIALS USED
        0.37984612E-01     0.61224677E-01     0.100E-01

PTP INVERSE
   1     0.10860828E-02     0.45295532E 03
   2     0.45295532E 03     0.19030717E 09

PARAMETER CORRELATION MATRIX
      1       1.0000     0.9963
      2       0.9963     1.0000

            STD                    ONE - PARAMETER                        SUPPORT PLANE
   B        ERROR                LOWER                UPPER              LOWER              UPPER
   1     0.20177062E-02     0.60656681E 00     0.61463558E 00     0.60489726E 00     0.61631113E 00
   2     0.84460571E 03     0.55764727E 04     0.85548484E 04     0.48767613E 04     0.96545898E 04


 NONLINEAR CONFIDENCE LIMITS

PHI CRITICAL =  0.67472219E-01

 PARA       LOWER B          LOWER PHI          UPPER B          UPPER PHI
   1     0.61003965E 00     0.74868321E-01     0.61105863E 00     0.64772545E-01
   2     0.70417305E 04     0.60169317E-01     0.74652305E 04     0.69912553E-01
IHC900I EXECUTION TERMINATING DUE TO ERROR COUNT FOR ERROR NUMBER  217
IHC217I FICCS - END OF DATA SET ON UNIT    5
TRACEBACK  ROUTINE  CALLED FROM ISN   REG.  14   REG.  15   REG.   0   REG.   1
           IBCOM                      001F21E4   001F53L8   00000005   001F1088
           MAIN                       0000A870   001F1010   00D2E000   001F0E58
ENTRY POINT=  001F1010
SUMMARY OF ERRORS FOR THIS JOB   ERROR NUMBER   NUMBER OF ERRORS
                                     217              1
```

```
      INTEGER SOLUTE,FILM
      C1=5.3266E10
      C2=8.06E-10
      C3=2.352E10
      C4=1.069E-11
5     READ (5,100) SOLUTE,FILM,PULLLG,PULLWD,TSTEP
      READ (5,101) OMEGA,WATER,THICK1,THICK2,PULL1,PULL2,CSIGMA,ITIME
      WRITE (6,107) SOLUTE,FILM,PULLLG,PULLWD
      WRITE (6,108) OMEGA,WATER,THICK1,THICK2,PULL1,PULL2,CSIGMA,ITIME
      GO TO (12,12,12,13),SOLUTE
12    C6=4.99995E-04
      C7=5.0E-09
      GO TO 14
13    C6=2.49995E-04
      C7=5.0E-09
14    IC=5
      CO=C2*OMEGA*THICK1*PULL2/(THICK2*PULL1)
      CW=C4*WATER
11    CH=C6
      CL=C7
      V=0.0
      WRITE (6,109)
      DO 10 I=1,ITIME
      CS=(CH-CL)/(ALOG(CH)-ALOG(CL))
      DCDT=C1*(CH-CL)*(CO-(1-CSIGMA)*CSIGMA*CW*CS)+C3*CSIGMA*(CH-CL)*CW*
     1CH
      DC=TSTEP*DCDT
      DD=TSTEP*C3*CSIGMA*(CH-CL)*CW*CH
      D=21.5*(DC-DD)/17.0
      V=V+43.0*TSTEP*C3*CSIGMA*CW*(CH-CL)
      CH=CH-DC
      CL=CL+D
      TIME=2.0*TSTEP*I
10    WRITE (6,102) TIME,DCDT,CH,CL,V,DC,DD
      GO TO (1,2,3,4,5),IC
```

```
1       CW=C4*WATER*1.1
        WRITE (6,103) CW
        IC=2
        GO TO 11
2       CW=C4*WATER*0.9
        WRITE (6,104) CW
        IC=3
        GO TO 11
3       CO=1.1*C2*OMEGA*THICK1*PULL2/(THICK2*PULL1)
        CW=C4*WATER
        WRITE (6,105) CO
        IC=4
        GO TO 11
4       CO=0.9*C2*OMEGA*THICK1*PULL2/(THICK2*PULL1)
        WRITE (6,106) CO
        IC=5
        GO TO 11
100     FORMAT (2I5,2F5.3,F5.1)
101     FORMAT (2E10.4,5F5.3,I5)
102     FORMAT (10X,F6.0,10X,E10.5,8X,E10.5,8X,E10.5,8X,E10.5,8X,E10.5,8X,
       1E10.5)
103     FORMAT (/////,' RECALCULATED FOR 1.1 LP  ',E10.5,/////)
104     FORMAT (/////,' RECALCULATED FOR 0.9 LP  ',E10.5,/////)
105     FORMAT (/////,' RECALCULATED FOR 1.1 OMEGA  ',E10.5,/////)
106     FORMAT (/////,' RECALCULATED FOR 0.9 OMEGA  ',E10.5,/////)
107     FORMAT (///,' SOLUTE IS',I1,'  FILM IS ',I1,'  LAMBDA L IS ',F5.3,
       1'  LAMBDA W IS',F5.3)
108     FORMAT (///,' SLOPE ',E10.5,'    LP ',F7.5,'    THICK1 ',F7.5,'
       1 THICK2 ',F7.5,'    PULL1 ',F7.5,'    PULL2 ',F7.5,'    SIGMA ',F7
       2.5,'    ITIME ',I5)
109     FORMAT (///,11X,'TIME',14X,'DCDT',15X,'CH',16X,'CL',15X,'V',16X,'D
       1C',16X,'DD',///)
        END
```

SOLUTE IS2 FILM IS 3 LAMBDA L IS 1.000 LAMBDA W IS1.000
SLOPE .19264E-05 LP 0.22300 THICK1 1.78500 THICK2 2.90700 PULL1 1.00000 PULL2 1.00000 SIGMA 0.37300 ITIME 18

TIME	DCDT	CH	CL	V	DC	DD
100.	.29975E-07	.49650E-03	.15698E-05	.22482E-01	.14987E-05	.26141E-06
200.	.29143E-07	.49704E-03	.30851E-05	.44626E-01	.14572E-05	.25903E-06
300.	.28794E-07	.49560E-03	.45817E-05	.67036E-01	.14397E-05	.25673E-06
400.	.28496E-07	.49417E-03	.60614E-05	.89114E-01	.14248E-05	.25446E-06
500.	.28225E-07	.49276E-03	.75272E-05	.11106E 00	.14113E-05	.25223E-06
600.	.27970E-07	.49136E-03	.89797E-05	.13268E 00	.13985E-05	.25003E-06
700.	.27726E-07	.48998E-03	.10420E-04	.15457E 00	.13864E-05	.24785E-06
800.	.27494E-07	.48860E-03	.11847E-04	.17613E 00	.13747E-05	.24571E-06
900.	.27269E-07	.48724E-03	.13264E-04	.19757E 00	.13634E-05	.24359E-06
1000.	.27049E-07	.48589E-03	.14669E-04	.21888E 00	.13524E-05	.24149E-06
1100.	.26835E-07	.48455E-03	.16063E-04	.24007E 00	.13417E-05	.23943E-06
1200.	.26625E-07	.48321E-03	.17446E-04	.26113E 00	.13313E-05	.23737E-06
1300.	.26421E-07	.48189E-03	.18817E-04	.28206E 00	.13210E-05	.23535E-06
1400.	.26220E-07	.48056E-03	.20182E-04	.30290E 00	.13110E-05	.23334E-06
1500.	.26022E-07	.47928E-03	.21535E-04	.32360E 00	.13011E-05	.23137E-06
1600.	.25829E-07	.47799E-03	.22878E-04	.34419E 00	.12914E-05	.22941E-06
1700.	.25638E-07	.47671E-03	.24212E-04	.36465E 00	.12819E-05	.22747E-06
1800.	.25450E-07	.47543E-03	.25536E-04	.38499E 00	.12725E-05	.22556E-06

SOLUTE IS2 FILM IS 3 LAMBDA L IS 1.000 LAMBDA W IS1.150
SLOPE .24689E-05 LP 0.31100 THICK1 1.82900 THICK2 2.89000 PULL1 1.15100 PULL2 1.15700 SIGMA 0.32600 ITIME 18

TIME	DCDT	CH	CL	V	DC	DD
100.	.39243E-07	.49803E-03	.20835E-05	.27403E-01	.19621E-05	.31963E-06
200.	.37991E-07	.49613E-03	.40878E-05	.54584E-01	.18996E-05	.31462E-06
300.	.37439E-07	.49426E-03	.60614E-05	.81551E-01	.18720E-05	.31115E-06
400.	.36964E-07	.49241E-03	.80102E-05	.10831E 00	.18482E-05	.30755E-06
500.	.36527E-07	.49059E-03	.99359E-05	.13486E 00	.18264E-05	.30402E-06
600.	.36117E-07	.48878E-03	.11839E-04	.16120E 00	.18058E-05	.30054E-06
700.	.35724E-07	.48699E-03	.13723E-04	.18734E 00	.17862E-05	.29713E-06
800.	.35347E-07	.48523E-03	.15588E-04	.21328E 00	.17673E-05	.29376E-06
900.	.34981E-07	.48348E-03	.17431E-04	.23902E 00	.17491E-05	.29045E-06
1000.	.34626E-07	.48175E-03	.19257E-04	.26456E 00	.17313E-05	.28719E-06
1100.	.34281E-07	.48003E-03	.21066E-04	.28993E 00	.17140E-05	.28398E-06
1200.	.33943E-07	.47833E-03	.22857E-04	.31510E 00	.16972E-05	.28081E-06
1300.	.33613E-07	.47665E-03	.24631E-04	.34008E 00	.16806E-05	.27769E-06
1400.	.33289E-07	.47499E-03	.26389E-04	.36488E 00	.16645E-05	.27462E-06

1500.	.32972E-07	.47334E-03	.28131E-04	.38938E 00	.16486E-05	.27153E-06
1600.	.32661E-07	.47171E-03	.29856E-04	.41378E 00	.16330E-05	.26860E-06
1700.	.32355E-07	.47009E-03	.31566E-04	.43800E 00	.16178E-05	.26565E-06
1800.	.32055E-07	.46849E-03	.33261E-04	.46203E 00	.16027E-05	.26275E-06

SOLUTE IS2 FILM IS 3 LAMBDA L IS 1.150 LAMBDA W IS1.150

SLOPE .34909E-05 LP 0.49500 THICK1 1.83000 THICK2 2.88000 PULL1 1.31400 PULL2 1.32200 SIGMA 0.29200 ITIME 18

TIME	DCDT	CH	CL	V	DC	DD
100.	.55729E-07	.49721E-03	.29543E-05	.39066E-01	.27862E-05	.45425E-06
200.	.53509E-07	.49453E-03	.57732E-05	.77684E-01	.25754E-05	.44654E-06
300.	.52483E-07	.49191E-03	.85366E-05	.11587E 00	.24742E-05	.43920E-06
400.	.51595E-07	.48933E-03	.11273E-04	.15364E 00	.23838E-05	.43205E-06
500.	.50774E-07	.48678E-03	.13926E-04	.19100E 00	.23008E-05	.42503E-06
600.	.50009E-07	.48429E-03	.16553E-04	.22794E 00	.22235E-05	.41826E-06
700.	.49270E-07	.48185E-03	.19154E-04	.26446E 00	.21495E-05	.41160E-06
800.	.48563E-07	.47943E-03	.21713E-04	.30064E 00	.20781E-05	.40503E-06
900.	.47881E-07	.47706E-03	.24236E-04	.33640E 00	.20090E-05	.39859E-06
1000.	.47220E-07	.47474E-03	.26726E-04	.37178E 00	.19419E-05	.39244E-06
1100.	.46573E-07	.47245E-03	.29184E-04	.40677E 00	.18763E-05	.38631E-06
1200.	.45953E-07	.47022E-03	.31608E-04	.44140E 00	.18127E-05	.38031E-06
1300.	.45344E-07	.46775E-03	.34001E-04	.47565E 00	.17506E-05	.37442E-06
1400.	.44749E-07	.46591E-03	.36366E-04	.50954E 00	.16899E-05	.36866E-06
1500.	.44168E-07	.46380E-03	.38699E-04	.54307E 00	.16307E-05	.36300E-06
1600.	.43599E-07	.46172E-03	.41004E-04	.57625E 00	.15730E-05	.35745E-06
1700.	.43043E-07	.45897E-03	.43280E-04	.60907E 00	.15167E-05	.35202E-06
1800.	.42497E-07	.45685E-03	.45529E-04	.64155E 00	.14619E-05	.34668E-06

INTRODUCTION

References

1. Lyman C. Craig, Dialysis, in Encyclopedia of Polymer Science and Technology 4, 824 (1967).

2. Charles W. Carr, Dialysis, in Physical Methods in Chemical Analysis, 4, Academic Press Inc., New York (1961).

3. Thomas Graham, Phil. Trans. Roy. Soc. (London), 151, 183 (1861).

4. J. D. Ferry, Chem. Rev., 18, 373 (1936).

5. Fick, Pogg. Ann., 94, 59 (1855) - cited by Ferry in reference 4.

6. S. L. Bigelow and A. Gemberling, J. Am. Chem. Soc., 29, 1576 (1907).

7. R. M. Barrer, J. A. Barrie, and J. Slater, J. Polym. Sci., 27, 177 (1958).

8. C. M. Gary-Bobo, R. DiPolo, and A. K. Solomon, J. Gen Physiol. 54, 369 (1969).

9. S. Rosenbaum and O. Cotton, J. Polym. Sci., Part A-1, 7, 101 (1969).

10. L. B. Ticknor, J. Phys. Chem., 62, 1483 (1958).

11. E. Klein and J. K. Smith, J. Polym. Sci., Part C, 28, 209 (1969).

12. N. V. Kultashev and F. A. Santalov, Z. Anorg. Allgem. Chem., 223, 177 (1935).

13. W. Desorbo and H. E. Cline, J. Appl. Phys., 4(5), 2099 (1970).

14. E. A. Hauser and D. S. LeBeau, J. Phys. Chem., 42, 961 (1938) and 43, 1037 (1939).

15. C. E. Marshall and C. A. Krinbill, J. Am. Chem. Soc., 64, 1814 (1942).

Introduction References - continued

16. C. E. Marshall and W. E. Bergman, J. Am. Chem. Soc., 63, 1191 (1941).

17. A. E. Marcinkowsky, K. A. Kraus, H. O. Phillips, J. S. Johnson, Jr., and A. J. Shor, J. Am. Chem. Soc., 88(24), 5744 (1966).

18. Walter J. Robb, U.S. Patent 3,325,330.

19. D. R. Paul, Sep. and Pur. Methods, 5(1), 33 (1976).

20. D. R. Paul, M. Garcin, and W. E. Garmon, J. Appl. Polym. Sci., 20, 609 (1976).

21. D. R. Paul and O. M. Ebra-Lima, J. Appl. Polym. Sci., 14, 2201 (1970).

22. H. B. Hopfenberg, N. S. Schneider, and F. Votta, J. Macromol. Sci. - Phys., B3(4), 751 (1969).

23.N. S. Schneider, L. V. Dusablon, L.A. Spano, H. B. Hopfenberg, and F. Votta, J. Appl. Polym. Sci., 12, 527 (1968).

24. N. N. Li, R. B. Long, and E. J. Henley, Ind. Eng. Chem., 57(3),18 (1965).

25. R. N. Rickles, Ind. Eng. Chem., 58(6), 19 (1966).

26. R. E. Kesting, J. Macromol. Sci.: - Chem., A4(3), 655 (1970).

27. R. E. Beck and J. S. Schultz, Biochim. Biophys. Acta., 255, 273 (1972).

28. J. A. Quinn, J. L. Anderson, W. S. Ho, and W. J. Petzny, Biophysical J., 12, 990 (1972).

29. H. S. Bierenbaum, R. B. Isaacson, M. L. Druin, and S. G. Plovan, Ind. Eng. Chem., Prod. Res. Dev., 13(1), 2 (1974).

Introduction References - continued

30. D. R. Seibel and F. P. McCandless, Ind. Eng. Chem., Process Des. Dev., 13(1), 76 (1974).

31. J. Kopeček, J. Vacík, and D. Lím, J. Polym. Sci: Part A-1, 9, 2801 (1975).

32. L. C. Craig and Wm. H. Koningsberg, J. Phys. Chem., 65, 166 (1961).

33. W. J. Petzny and J. A. Quinn, Science 166, 751 (1969).

34. L. C. Craig, T. P. King, and A. Stacher, J. Am. Chem. Soc., 79, 3729 (1957).

35. L.C. Craig and A. Ansevin, Biochem., 2(6), 1268 (1963).

36. L.C. Craig and T. P. King, Dialysis in Methods of Biochem. Anal., 10, 1 (1962).

37. L.C. Craig and A. O. Pulley, Biochem., 1(1), 89 (1962).

38. J. D. Rouse and J. Ultman, Ind. Eng. Chem., Process Des. Dev., 14(2), 122 (1975).

39. R. M. Hays, J. Gen. Physiol., 51, 385 (1968).

Chapter 1

References

1. L. Onsager, Phys. Rev. 37, 405 (1931); 38, 2265 (1931).

2. H. B. G. Casimir, Revs. Modern Phys. 17, 343 (1945).

3. A. J. Staverman, Rec. trav. chim. 70, 344 (1951).

4. A. J. Staverman, Trans. Faraday Soc. 48, 176 (1948).

5. O. Kedem and A. Katchalsky, Biochimica et Biophysica Acta 27, 229 (1958).

6. O. Kedem and A. Katchalsky, J. General Physiology 45, 143 (1961).

7. K. J. Laidler and K. E. Shuler, J. Chem. Phys. 17 (10), 851 (1949).

8. K. J. Laidler and K. E. Shuler, J. Chem. Phys. 17 (10), 856 (1949).

9. K. J. Laidler and K. E. Shuler, J. Chem. Phys. 17 (10) 860 (1949).

10. J. A. Lane and J. W. Riggle, Chemical Engineering Progress Symposium Series 55 (24), 127 (1958).

11. E. Manegold, Kolloid Z. 49, 372 (1928).

12. E. M. Renkin, J. Gen. Physiol. 38, 275 (1954).

13. J. D. Ferry, Chem. Rev. 18, 373 (1936).

14. J. D. Ferry, J. Gen. Physiol. 20, 95 (1936-7).

15. J. R. Pappenheimer, E. M. Renkin, and L. M. Borrero, Am. J. Physiol. 167, 13 (1951).

16. G. K. Ackers, Adv. Prof. Chem. 24, 343 (1970).

17. J. A. Lane, in Chemical Engineer's Handbook, ed. J. H. Perry, McGraw-Hill Co., New York, 1950, Section II, page 753.

18. J. R. Pappenheimer, Physiol. Rev. 33, 387 (1953).

19. H. Faxen, Ark. Nat., Astron. och Fysik. 17 (27), 1922 - cited by

Chapter 1 - References continued

Renkin in reference 12.

20. R. E. Beck and J. S. Schultz, Biochim. Biophys. Acta, 255, 273 (1972).

21. R. Ladenburg, Ann. der Physik 23, 447 (1907).

22. E. H. Starling, J. Physiol. 19, 312 (1896).

23. D. D. Fitts, Nonequilibrium Thermodynamics, McGraw-Hill, New York, 1962, p. 37.

24. K. S. Spiegler, Tr. Faraday Soc. 48, 176 (1952).

25. J. G. Albright and R. Mills, J. Phys. Chem. 69(9), 3120 (1965).

26. D. G. Miller, Am. J. Phys. 24, 436 (1956).

27. J. B. Williams and F. A. Long, Trans. Faraday Soc. 53, 1146 (1957).

28. P. Meares, J. Poly. Sci. 27, 391 (1958).

29. H. Fujita, A. Kishimoto, and K. Matsumoto, Trans. Faraday Soc. 56, 424 (1960).

30. S. Rosenbaum, H. I. Mahon, and O. Cotton, J. Appl. Poly. Sci. 11, 2041 (1967).

31. H. Yasuda, C. E. Lamaze, and L. D. Ikenberry, Makromolekulare Chem. 118, 19 (1968).

32. H. Yasuda, L. D. Ikenberry, and C. E. Lamaze, Makromolekulare Chem. 125, 108 (1969).

33. H. Yasuda, A. Peterlin, C. K. Colton, K. A. Smith, and E. W. Merrill, Makromolekulare Chem. 126, 177 (1969).

34. A. Peterlin, H. Yasuda, and H. G. Olf, J. Appl. Poly. Sci. 16, 865 (1972).

Chapter 1 - References continued

35. H. Yasuda, C. E. Lamaze, and A. Peterlin, J. Polym. Sci., A-2, 9, 1117 (1971).

36. W. Jost, Diffusion, Academic Press, New York, 1969.

37. M. H. Cohen and D. Turnbull, J. Chem. Phys. 31, 1164 (1959).

38. A. T. DiBenedetto and D. R. Paul, J. Poly. Sci. A, 2, 1001 (1964).

39. H. D. Spriggs and J. L. Gainer, Ind. Eng. Chem. Fundam., 12 (3), 291 (1973).

40. D. R. Paul, M. Garcin, and W. E. Garmon, J. Appl. Poly. Sci. 20, 609 (1976).

41. J. S. Vrentas and J. L. Duda, Macromolecules 9 (5), 785 (1976).

CHAPTER 2

References

1. C. T. Chen, R. F. Eaton, Y. J. Chang, and A. V. Tobolsky, J. Appl. Polym. Sci., 16, 2105 (1972).

2. D. J. David and H. B. Staley, High Polymers 16(3), 357, John Wiley & Sons Inc., New York, (1969).

3. Union Carbide Corporation, Chemicals and Plastics Physical Properties Catalog 1975-76, Chemicals and Plastics Division, 270 Park Avenue, New York, N.Y. 10017.

4. D. J. David and H. B. Staley, High Polymers 16(3), 301, John Wiley & Sons Inc., New York, (1969).

5. National Bureau of Standards Report #9872, The Development of Standard Test Methods for Hemodialysis Membranes, (1968).

6. H. H. Brown, Anal. Chem., 31(11), 1844, 1959.

7. R. H. Scott, W. E. Moore, M. J. Effland, and M. A. Millett, Anal. Biochem., 21, 68 (1967).

8. G. W. Watt, J. D. Chrisp, Anal. Chem., 26, 452 (1954).

9. B. A. Brice, M. Halwer, J. Optical Soc. Am., 41(12), 1033 (1951).

10. D. J. David and H. B. Staley, High Polymers 16(3), 90, John Wiley & Sons Inc., New York (1969).

11. E. H. Swift, Introduction to Quantitative Analysis, Prentice-Hall Inc. (1950), New York.

CHAPTER 3

References

1. H. S. Carslaw and J. C. Jaeger, Conduction of Heat in Solids, 2nd edition, Oxford University Press, pages 99-100, (1959).
2. R. E. Beck and J. S. Schultz, Biochem. Biophys. Acta., 255, 273 (1972).
3. L. G. Longsworth, J. Phys. Chem., 75, 5705 (1953).
4. D. R. Paul, M. Garcia, and W. E. Garmon, J. Appl. Polym. Sci., 20, 609 (1976).
5. B. Z. Ginzburg and A. Katchalsky, J. Gen. Physiol. 47, 407 (1963).
6. R. W. Seymour and S. L. Cooper, Polym. Letters, 9, 689 (1971).
7. C. T. Chen, R. F. Eaton, Y. J. Chang, and A. V. Tobolsky, 16, 2105 (1972).
8. S. L. Cooper and A. V. Tobolsky, J. Appl. Polym. Sci., 10, 1837 (1966).
9. G. M. Estes, S. L. Cooper, and A. V. Tobolsky, J. Macromol. Sci.-Revs. Macromol. Chem., C4(2), 313 (1970).
10. Union Carbide Corporation, Chemicals and Plastics Physical Properties Catalog 1975-76, Chemicals and Plastics Division, 270 Park Ave., New York, New York 10017.
11. P. J. Flory and J. Rehner, Jr., J. Chem. Phys. 12(10), 412 (1944).
12. G. Gee, Trans. Faraday Soc., 42B, 33 (1946).
13. L. R. G. Treloar, Proc. Royal Soc. A 200, 176 (1950).
14. L. R. G. Treloar, Reports Prog. Phys. 36, 755 (1973).
15. L. R. G. Treloar, The Physics of Rubber Elasticity, 2nd edition, Oxford University Press, London, 1967.

Chapter 3 - References continued

16. P. J. Flory, Principles of Polymer Chemistry, Cornell Univ. Press, Ithaca, New York, 1953.

17. S. S. Sternstein, J. Macromol. Sci.-Phys., B6(1), 243 (1972).

18. T. Kotani and S. S. Sternstein, in Polymer Networks: Structural and Mechanical Properties, Plenum Publishing Corporation, New York, 1974.

CHAPTER 4

References

1. G.M. Ester, S. L. Cooper, and A.V. Tobolsky, J. Macromol. Sci. - Rev. Macromol. Chem., C4, 313 (1970).

2. S. L. Cooper and A.V. Tobolsky, J. Appl. Polym. Sci., 10, 1837 (1970).

3. C. T. Chen, R. F. Eaton, Y. J. Chang, and A. V. Tobolsky, J. Appl. Polym. Sci., 16, 2105 (1972).

4. D. Puett, J. Polym. Sci., A-2(5), 839 (1967).

5. R. Bonart, J. Macromol. Sci., B2(1), 115 (1968).

6. C. M. Gary-Bobo, R. DiPolo, and A. K. Solomon, J. Gen. Physiol., 54, 369 (1969).

7. H. Yasuda, L. D. Ikenberry, and C. E. Lamaze, Makromol. Chem., 125, 108 (1969).

8. J. S. Mackie and P. Meares, Proc. Royal Soc. London, A232, 498 (1955).

9. P. Meares, J. Polym. Sci., 20, 507 (1956).

10. D. R. Paul, M. Garcin, and W. E. Garmon, J. Appl. Polym. Sci., 20, 609 (1976).

11. J. S. Vrentas and J. L. Duda, Macromol., 9, 785 (1976).

12. J. S. Vrentas and J. L. Duda, to appear in J. Appl. Polym. Sci. in early 1977.

13. G.M. Estes, S. L. Cooper, A. V. Tobolsky, J. Macromol. Sci.-Revs. Macromol. Chem. C4(2), 313 (1970).

14. D. J. Meier, J. Poly. Sci.,C(26), 81 (1969).

15. R. Bonart, J. Macromol. Sci., B2(1), 115 (1968).

16. V. M. Shimannski, S. E. Shkol'nik, and S. B. Kozakov, Soviet Rubber Tech. (English translation) 26,20 (1967).

17. K. A. Pigott, J. H. Saunders, Rubber Age, 90, 629 (1962).

PROPOSITION I

THE "WINDOWLESS" WINDOW

ABSTRACT

In recent years many ways of saving energy in the home have been suggested. This proposition suggests that the amount of window area in the home could be reduced while maintaining the illusion of a large area of windows. The "windowless" window is a proposal for using concentrating solar collectors to focus sunlight on an optical system that would serve to transmit the light from the point of collection to the location of the "windowless" window. The light would strike a diffuser panel behind a decorative translucent panel and thereby provide natural sunlight illumination without the need for an opening in the wall. It is suggested that this proposal along with more effective insulation, by earth berming for example, could significantly reduce home heating costs.

In recent years many energy saving proposals have been advanced. A large number of these proposals have dealt with energy conservation in the home and particularly with reduction of heat loss through windows. The National Forest Products Laboratory (1) reported that for the typical frame home, 33% of the total heat loss occurred through windows. The energy loss through a single pane window is 15 times greater than the energy loss through an equivalent area of well insulated wall (2) and even high quality insulating glass windows allow 10 times as much energy loss. This proposition outlines a method of reducing energy loss by reducing the actual window area while retaining the illusion of large window expanses.

Table I shows a comparison between the insulation used in a typical frame home of recent construction and the insulation values recommended by the Department of Housing and Urban Development (3) for new construction built under its energy-saving house program. Also shown are the dollar savings resulting from each HUD recommendation assuming as a basis that it would cost the owner of a typical frame house of recent construction in climate zone 2 $1,000 per year for heat. As can be readily seen from Table I, windows are responsible for the greatest energy loss and, if HUD recommendations are followed, the area in which the greatest savings can be achieved. Currently recommended insulation values (4) for the six climate zones of the United States are shown in Figure 1.

Windows are big energy losers, so why not just get rid of them? There are several reasons for not doing so but the major one is

probably more psychological than anything else. Man evolved outdoors and still has a strong desire to feel that his environment is an open one. Indeed, much of modern architecture is concerned with designing spaces such that one area flows into another. This style incorporates various features to break up a large space visually without actually dividing it with intervening walls.

It isn't necessary to see outside in order to feel that the space one is in is an open one. Many areas in homes and offices are illuminated by translucent panels, churches have made extensive use of stained glass windows, and restaurants and offices occasionally use artificially illuminated shadow boxes to create the illusion of a window, all of which admit light without allowing the occupants to see out.

This proposition proposes a method of bringing sunlight to "windowless" windows. The principal features of this proposal are a light gathering and transmitting system to bring sunlight to the "windowless" window location and a diffuser panel to provide uniform illumination. Details of the "windowless" window are shown in Figures 2, 3 and 4. Sunlight is gathered by a compound parabolic collector (5) which has the advantage of relatively high concentration ratios without having to track the sun. Sunlight from the collector passes through a collimating lens and is reflected by a mirror system to the "windowless" window where the sunlight is directed onto a diffuser panel. A light trap at the bottom prevents over illumination of the lower portion of the window. Depending on the preference of the homeowner, the diffuser panel could be decorated,

a decorative translucent panel placed in front of the diffuser and illuminated by it, or the diffuser eliminated and the area used for growing small plants.

The site of the compound parabolic collector would be adjusted to fit the spacing of the rafters on the roof, and would be covered with a clear glass pane. A typical unit might be 14½ inches wide, 10½ inches deep, and 4 feet long. Such a unit would be able to illuminate a 10 square foot "windowless" window at approximately 50% of direct sunlight. Such a unit(s) would be placed in the same array as other solar units used to provide domestic heat and hot water.

Two questions need to be addressed with regard to this proposition. First, why use sunlight instead of artificial illumination and, second, what would the costs/savings of such a system be?

Sunlight provides both light and heat and other than the initial cost of materials for the "windowless" window, it is free. Also, sunlight has the spectral properties we are accustomed to and is best for growing plants. But the most important reason for using sunlight is the cost of artificial illumination. Artificial illumination is inexpensive encugh for a single window but for a home with 300-400 square feet of "windowless" window or "windowless" window walls, the cost is significant. For a home with 300 square feet of "windowless" window, 1,500 hour average bulb life, one 100 watt bulb per 10 square feet of "windowless" window, electricity at 5¢ per kwh, and 10 hours per day average operation, replacement bulbs would cost $35 and electricity

$365 annually.

What would the costs or savings of using "windowless" windows be? Table II shows a comparison between the cost of a "windowless" window system and a conventional roof and window system. National Construction Estimator (6) for 1975 is the source for material cost and labor figures. In estimating the cost of the "windowless" window it was assumed that the unit would be provided as a fit in place module the same as windows are. The "windowless" window has a cost advantage at the window location compared to a regular window because of its simple construction. The "windowless" window does require a light guide and the collector is more expensive than an equal area of roofing. Nonetheless the "windowless" window is less expensive overall.

In addition to its initial cost advantage the "windowless" window is an energy saver because of its R-12 insulating value* as opposed to the R-1 value for high quality insulating glass windows. A 10 square foot "windowless" window would gain or lose approximately 8 BTU/hr for every degree of difference between the inside and outside air temperature. A conventional window would gain or lose 100 BTU/hr. Assuming no changes in home construction or design except for replacing 75% of the windows with "windowless" windows, the average homeowner would save a minimum of $250 per year.

*An R-value is the reciprocal of the inside-air to outside-air heat transfer coefficient when the heat transfer coefficient is reported in units of BTU/hr-sq. ft.-^{o}F.

TABLE I

Insulation Standards in Home Construction and Associated Heating Costs

Area	% of Total Heat Loss for a Typical Home	Typical Home Insulation	HUD Recommended Insulation	Annual Heating Cost per Area Typical Home	Savings if HUD Recommendations are Followed
Walls	19.8	R-12	R-19	$198	$72.95
Ceiling	12.2	R-19	R-33	122	51.76
Floor	7.6	R-19	R-22	76	10.36
Doors	7.8	-	-	78	-0-
Windows	33.2	25-30% (2)	8% (2)	332	235.42
Air Infiltration (1)	19.3	-	-	193	136.85 (3)

(1) Most air infiltration is associated with windows.

(2) Window area as a % of usable living area floor space.

(3) Due to reduced window area.

TABLE II

Cost Comparison Between Conventional and "Windowless" Windows

Basis: 10 square feet of windows, 5 square feet of collector

Conventional		"Windowless"	
Roof		Collector	
1/2" plywood installed	$ 2.65	Concentrator & lens @ $10 per sq. ft.	$ 50.00
235# asphalt shingle	4.21	Installation	7.50
Window		Light Guide	
24" x 60" single lite	118.56	6" dia. galvanized duct	10.60
Installation	12.21	Installation	7.50
Total Cost	$137.63	"Windowless" Window	
		1/4" plywood diffuser	2.21
		Frame 1" x 4"	4.30
		Insulation, foam	1.27
		Est. Millwork - 2 man hours	26.42
		Est. Assembly - 1 man hour	13.21
		Est. Installation	12.21
			$135.22

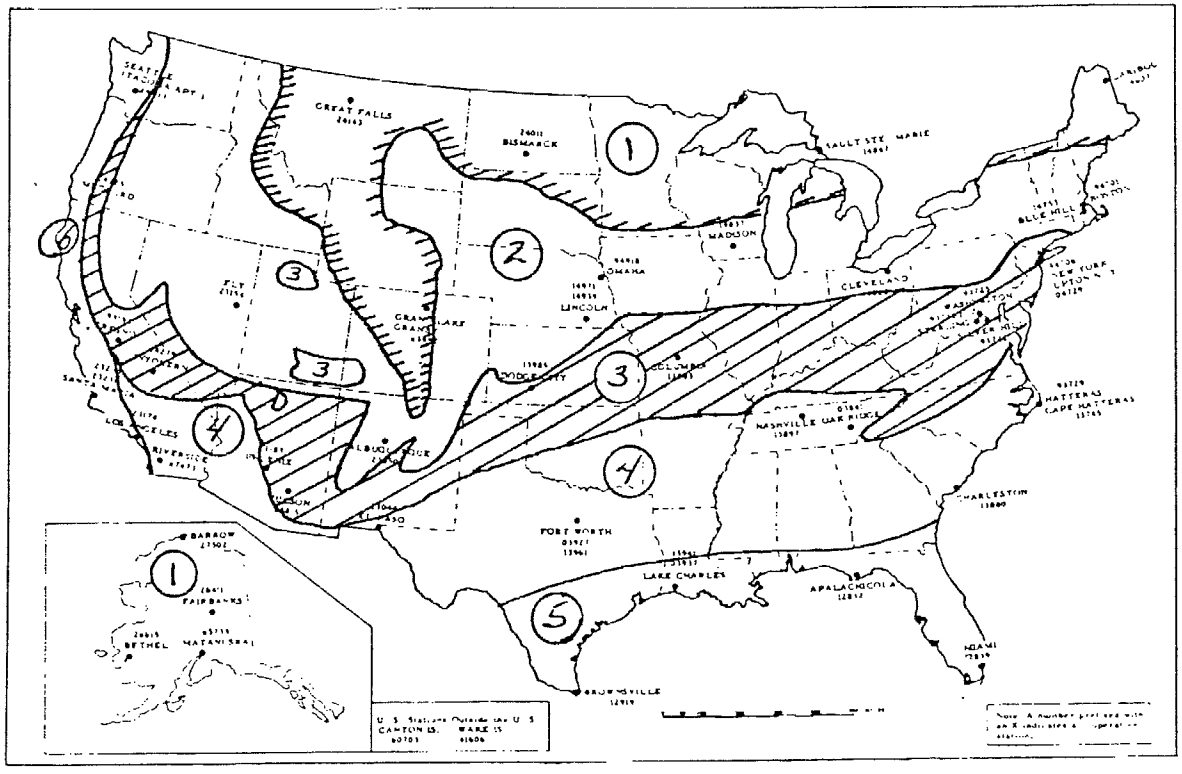

Figure 1.

RECOMMENDED INSULATION LEVELS IN SIX HEATING AND COOLING ZONES

R values for	1	2	3	4	5	6
Ceilings	R-38	R-33	R-30	R-26	R-26	R-19
Walls	R-19	R-19	R-19	R-19	R-13	R-11
Floor	R-22	R-22	R-19	R-13	R-11	R-11

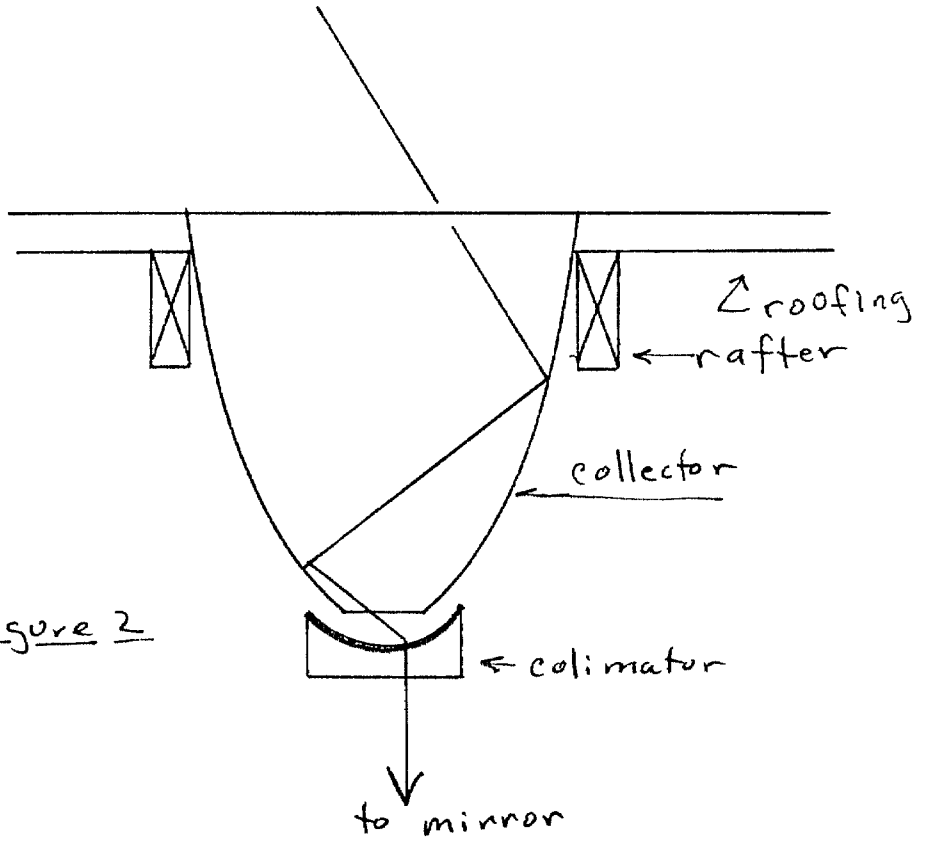

Figure 2

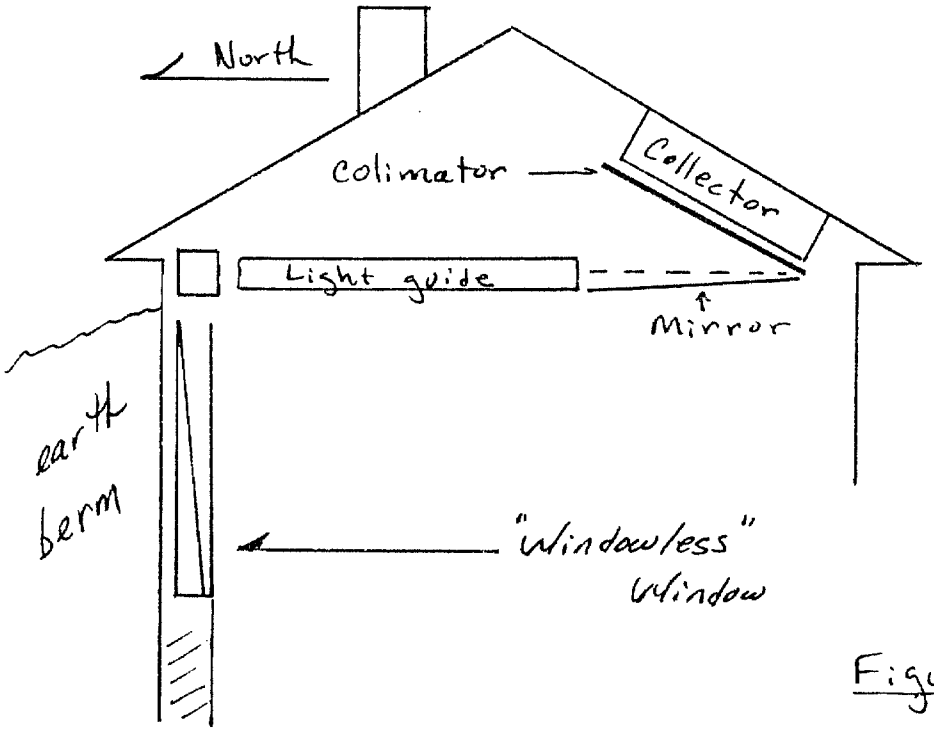

Figure 3.

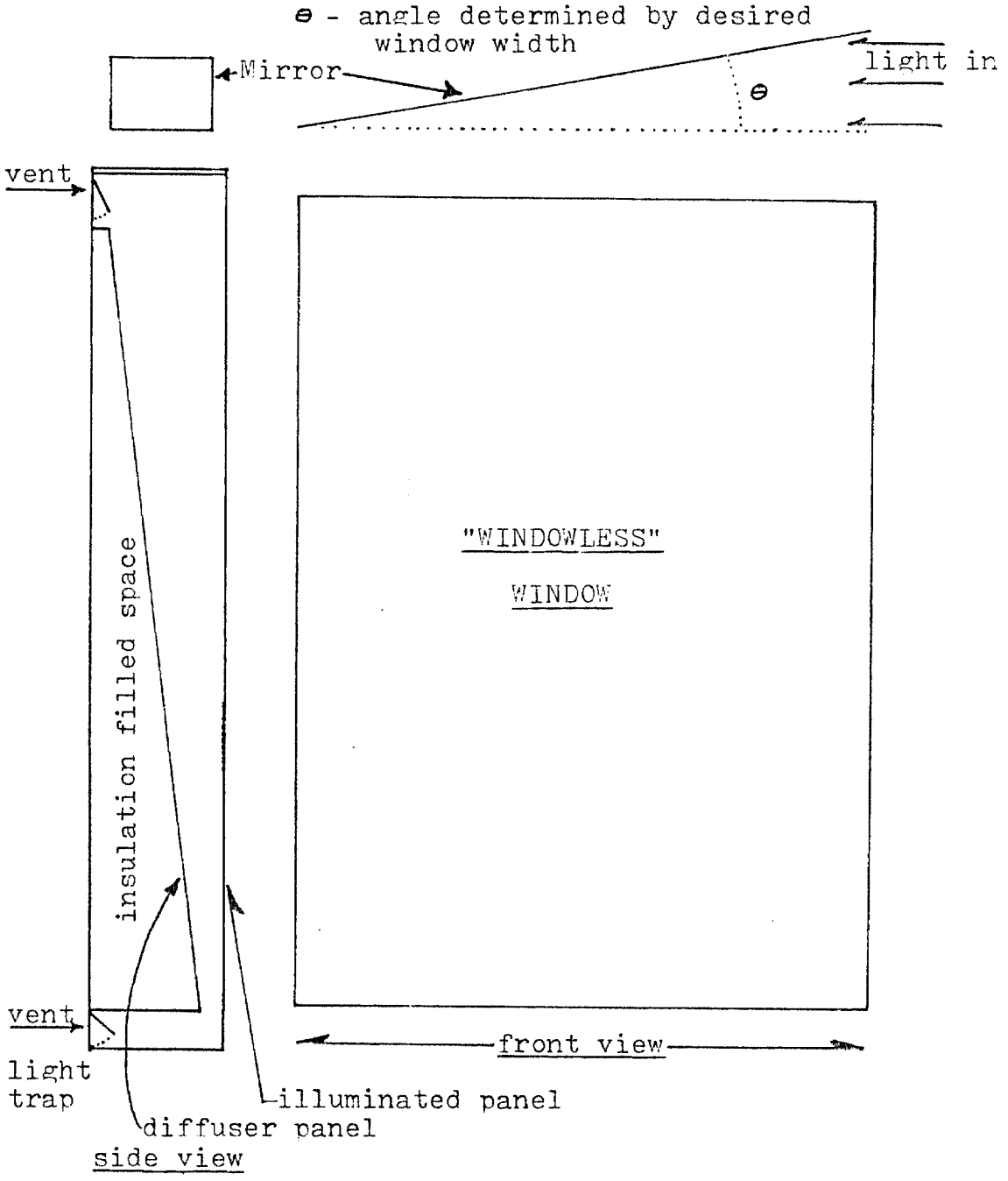

Figure 4. Front and side views of a "windowless" window unit.

References

1. National Forest Products Laboratory, Technical Report #2, (1961).

2. T. H. Jones, Popular Science 207 (3), 97 (1975).

3. A. Lees, Popular Science 209 (3), 130 (1976).

4. Owens Corning Fiberglass, Popular Science 209 (3), 130 (1976).

5. Popular Science 208 (6), 50 (1976).

6. 1975 National Construction Estimator, 23rd edition, Craftsman Boole Company of America, Solana Beach, California 92075.

PROPOSITION II

A SOLAR HEAT ENGINE

ABSTRACT

This proposal deals with the use of a rotary-vane air cycle motor to convert focused sunlight into electrical power for use in remote areas where conventional power supplies are unavailable.

Using a Rovac motor to generate electrical power from sunlight

This proposal deals with the application of a rotary-vane air-cycle motor (Rovac) to remote site electric power generation. The Rovac motor is a proposed adaption of the Rovac air conditioner developed by Dr. Thomas Edwards (1) for auto and home heating and air conditioning. A Rovac consists of a cylindrical rotor, holding a series of sliding vanes, which turns in an elliptical housing. The design as developed by Dr. T. Edwards is shown in Figure 1. In the use proposed here, concentrated sunlight would be focused on approximately one-tenth of the motor circumference to increase the air temperature and pressure in the high pressure section yielding a pressure differential which would drive the motor. The motor would be linked to a generator to produce electric power.

For the application considered here it is sufficient to position a cylindrical rotor off-center in a cylindrical stator. This design (see Fig. 2) is similar to that used in liquid seal rotating vacuum pumps. For the purposes of the calculations described here, a radiant energy input of 250 watts with a 75% absorption efficiency will be assumed. This means that the net power to the motor will be 188 watts. Obviously the exact amount of energy to power the device proposed here will depend on the size of the collector and the amount of sunlight striking the collector. The figure of 250 watts represents a reasonable value likely to be attained or exceeded a large portion of the time (see Figures 3, 4) with a reasonable size collector approximately 1 m^2).

The primary purpose of this proposal is to demonstrate the feasibility of the use of a Rovac for remote site power generation. A detailed

optimization of the motor and its mode of operation is beyond the scope of this proposition. In order to make the calculations presented here it has been necessary to make several assumptions.

First, friction losses in the rotor will be approximated by assuming that they are directly proportional to the rotor rpm. This is reasonable because the area swept per unit time by the sliding vanes is a direct function of the rotor rpm. For the purpose of estimating the friction loss a no load speed of 3600 rpm was selected and the friction loss related to the no load speed and the total available energy by

$$f_1 = \text{Rotor rpm} \times 188 \text{ watts}/3600 \text{ rpm} \qquad (1)$$

Second, calculations will be presented for two limiting cases. Initially the entire rotor will be assumed to be well insulated with compression and expansion of the working fluid (air in this case) conducted adiabatically. Also, calculations for isothermal compression and adiabatic expansion will be presented.

Third, the efficiency of light absorption in the sector exposed to the concentrated sunlight will be assumed to be 75%. At first glance this seems an excessively high efficiency but it is proposed to achieve this efficiency by mounting a fine Nickel-Chromium wool on the rotor hub. This material is highly corrosion resistant and more importantly has an emissivity of 0.89 - 0.82.

Fourth, it is assumed that the rise in air temperature is rapid and that the presence of the Ni-Cr wool has a negligible effect on the performance of the engine. The high surface area of the wool ensures rapid heat transfer. Typically, only 0.05 to 0.10 grams of the wool would be

needed per rotor chamber. At this level, the wool accounts for 5 to 10% of the total heat capacity of the air-wool mixture for a chamber with an ititial volume of 20 cubic inches.

Fifth, a volume compression ratio of 2 to 1 is assumed. This is reasonable for this type of motor although higher pressures may well be used in the future.

Consider first both compression and expansion to adiabatic processes with the air exhausted at the end of each cycle and replaced with fresh air. For adiabatic compression or expansion

$$P_2/P_1 = (V_1/V_2)^k \qquad (2)$$

and

$$T_2/T_1 = (V_1/V_2)^{k-1} \qquad (3)$$

where k is the heat capacity ratio C_p/C_v and P, T, and V are the pressure, temperature, and volume respectively. Input of heat into the high pressure high temperature part of the cycle raises the temperature attained by adiabatic compression from T_2 to T_2^*. The new high temperature T_2^* may be calculated from

$$T_2^* = Q/(wC_v) \qquad (4)$$

where w is the mass flow rate and Q is the heat flux, 188 watts.

The adiabatic horsepower to compress the gas may be calculated from

$$\text{h.p.} = 0.00436\, Q_1 P_1 \frac{(k)}{k-1} (P_2/P_1)^{(k-1)/k} - 1 \qquad (5)$$

where Q_1 is the volume flow rate at the entrance conditions. The same equation may be used to calculate the work done by the gas during adiabatic

expansion.

Consider the following example: $V_1 = 20\ in^3$, $V_2 = 10\ in^3$, $T_1 = 530^oR$, and $P_1 = 14.7$ psia. Assume a rotation rate of 600 rpm. Then,

$$Q_1 = 600\ rpm \times 20\ in^3 = 12000\ in^3/min = 6.944\ ft^3/min$$

$$P_2/P_1 = (V_1/V_2)^k = 2^{1.395} = 2.630\ ;\quad P_2 = 2.630 \times 14.7 = 38.7\ psia$$

$$\Delta T = \frac{188 watt/hr \times 3.414\ BTU/watt}{6.944\ ft^3/min \times 60\ min/hr \times .075\ lb/ft^3 \times .25\ \frac{BTU}{lb\ ^oR} \times 1/1.395}$$

$$= 114.6\ ^oR$$

$$T_2^* = T_2 + \Delta T = (2^{0.395}) \times T_1 + \Delta T = 697\ ^oR + 114.6\ ^oR = 811.6^oR$$

$$P_2^* = (811.6/697) \times P_2 = (811.6/697) \times 38.7\ psia = 45.07\ psia$$

$$exit\ P = (1/2)^{1.395} \times P_2^* = 0.380 \times 45.07 = 17.1\ psia$$

$$exit\ T = (1/2)^{0.395} \times T_2^* = 0.7605 \times 811.6\ ^oR = 617\ ^oR$$

A PV chart for this process is shown below. The cross-hatched area represents the work available from the system.

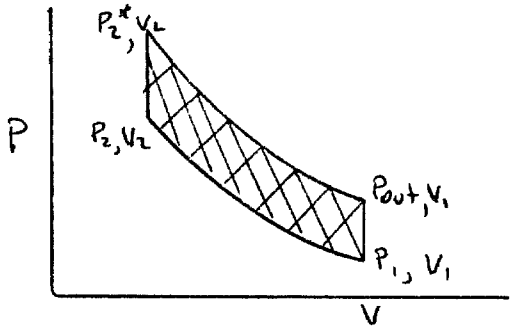

The work done in compressing the gas is calculated from equation (5) and is

$$h.p._{compression} = 0.00436 \times 6.944 \times 14.7 \times \frac{1.395}{.395} \times 0.3153$$

$$= 0.4955$$

The work produced by the expansion of the gas is given by

$$h.p._{expansion} = 0.00436 \times 3.472 \times 45.07 \times \frac{1.395}{.395} \times 0.24$$

$$= 0.5783$$

The net work before allowing for friction losses is 0.0828 horsepower. Using equation (1) to estimate friction losses and subtracting the friction loss from the net horsepower, the horsepower available for electric power generation is 0.083 - 0.042 = 0.041 h.p. or 30.5 watts. If an additional 15% loss occurs in generating electricity, the overall efficiency is 16.5% based on energy absorbed by the engine or 12.4% or 26 watts based on the total energy collected by the collector. These efficiencies are comparable to those obtained with solar cells.

Table 1 and Figure 5 show the effect of rotation rate on the performance of the Rovac for the case of adiabatic compression and expansion. In order to calculate the torque, the following dimensions for the Rovac were assumed:

Length	10 inches
Rotor diameter	8 inches
Stator diameter	10 inches

$$\text{Torque} = \underbrace{10 \text{ in} \times 1.333 \text{ in}}_{\text{area}} \times \underbrace{4.5 \text{ in}}_{\substack{\text{moment} \\ \text{arm}}} \times (P_{exit} - 14.7)$$

A study of Table 1 reveals several interesting facts. First, the net horsepower produced by the rotor increases with increasing rpm. As the rpm increase, the air exit temperature and pressure approach the air entrance temperature and pressure, so less energy is wasted by exhausting the air at the end of each cycle. Second, the power available for electricity generation and the torque decrease with increasing rpm. The torque decreases because the exit pressure approaches the inlet pressure. The power decreases because the friction loss was assumed to increase more rapidly than the increase in net horsepower.

Third, as the rotor rpm drops below 200 rpm, the temperature rise, T, increases rapidly. Materials considerations would probably limit T_2^* to temperatures of $1200^{\circ}R$ or less. Finally, since both torque and power increase as rpm decrease, it would be desirable to operate the Rovac at low rpm.

One way of increasing the efficiency of the Rovac would be to compress the air isothermally. In practice this would be impossible but such a calculation is useful because it indicates the best performance obtainable with the Rovac. The isothermal horsepower required to compress air is given by

$$h.p. = 0.00436 P_1 Q_1 \ln(P_2/P_1) \qquad (6)$$

Table 2 and Figure 6 show the effect of rotation rate on the performance of the Rovac when the air is compresssed isothermally and expanded adiabatically. The efficiency of Rovac after accounting for friction losses increases with increasing rpm while the torque decreases. The torque requirements of the generator would probably dictate the choice of an inter-

mediate rotation rate or locating the air discharge port less than half a revolution from the highest pressure section. Either alternative increases the exit pressure which increases the torque and decreases the efficiency.

An actual Rovac used for remote power generation as proposed here would have a fin-cooled compression section and a well insulated expansion section. The rotor and generator would be matched so that their torque characteristics would be similar. Either direct or alternating current (of fixed or variable frequency) could be produced.

The preceding calculations have shown that a Rovac could be used for remote site power generation. In order to determine the practicality of using a Rovac, we need to know the probable cost of a Rovac system and its estimated lifetime, and compare those figures to similar information for alternative systems. The comparison will be made to solar cells rather than to wind or water driven systems for two reasons. First, wind and water power are not as universally available as sunlight, and second, they are better suited to larger scale power generation.

A Rovac could be expected to have a useful life of at least ten years particularly for the design suggested here where the sliding vanes move in and out only once per revolution. Technical problems related to tip seals have been solved and it is estimated that by 1980 all automotive air conditioners will be Rovacs (2). The first Rovacs will be marketed by York division of Borg-Warner next summer.

The useful life of a solar-cell system is longer than that of a Rovac. Solar cells are subject to environmental degradation and their lifetime is not infinite, but for well protected systems it should be at least 15 years. Also solar cells have the advantage of directly generating power, whereas

the Rovac needs to be coupled to a generator.

Table 3 shows a comparison between the cost of a Rovac and a solar cell system. At the end of 1976 solar cells cost $15.50 per watt (3, 4). A useful life of 20 years for a solar cell system was assumed . A Rovac was assumed to have a useful life of 10 years. The cost of a Rovac was estimated from current air conditioner costs and is likely to be high by a factor of two or more. The collector cost was estimated from prices of solar cookers and is probably fairly accurate. The generator cost includes the cost of the control circuit and a small rechangeable battery.

As can be readily seen from Table 3 the Rovac currently has a substantial price advantage over solar cells. However, solar cell prices are dropping rapidly and a solar cell system would probably be the system of choice by 1985. Also, in Table 3 no estimates of the cost of installing either a Rovac or solar cells were made. Initial installation costs of either system would be the same. The cost of installing a second Rovac near the end of the first Rovac's life might well eliminate the price advantage of the Rovac. However, such a replacement would not be necessary before 1990 and by that time long-life, low-cost solar cells should be available. The Rovac is therefore likely to be successful in the short term.

The system proposed here has several advantages over other systems for remote power generation. First, the working fluid is air, an inexhaustible resource. Second, the device has reasonable efficiency and is not adversely affected by extremes in temperature. Third, since the Rovac is being developed for the mass markets of home and auto heating and cooling it is inexpensive. It does have some disadvantages too, notably its shorter

lifetime compared to solar cells and its inability to generate power during periods of low solar insulation.

Reference

1. E. F. Lindsley, Popular Science 209 (2), 84 (1976).

2. J. Dunne, Popular Science 210 (4), 56, 1977.

3. Materials & Energy for Industry, 3 (8), 1, 1977.

4. New York Times, page D3, Dec. 31, 1976.

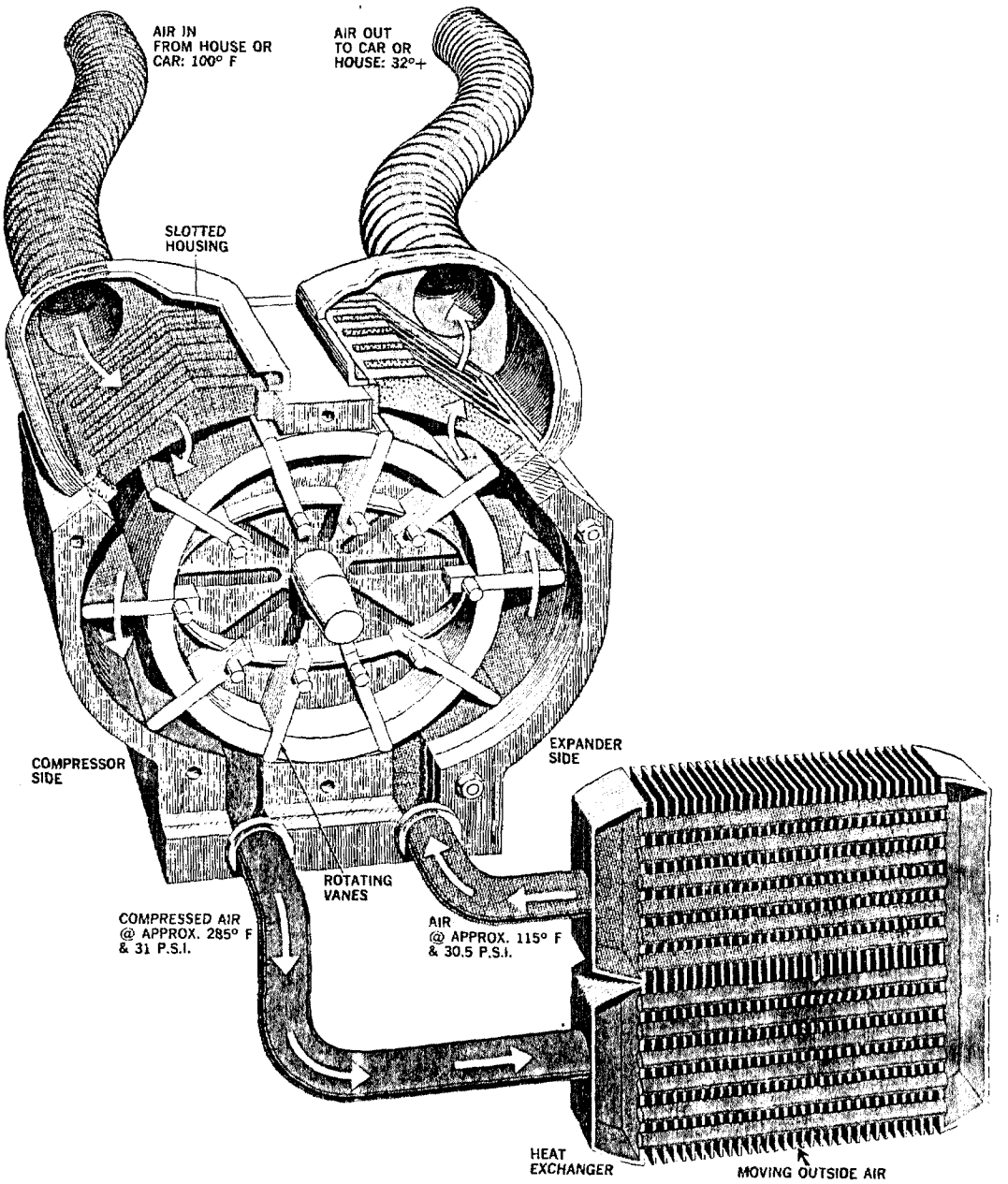
AIR IN
FROM HOUSE OR
CAR: 100° F
AIR OUT
TO CAR OR
HOUSE: 32°+
SLOTTED
HOUSING
COMPRESSOR
SIDE
EXPANDER
SIDE
ROTATING
VANES
COMPRESSED AIR
@ APPROX. 285° F
& 31 P.S.I.
AIR
@ APPROX. 115° F
& 30.5 P.S.I.
HEAT
EXCHANGER
MOVING OUTSIDE AIR

Figure 1

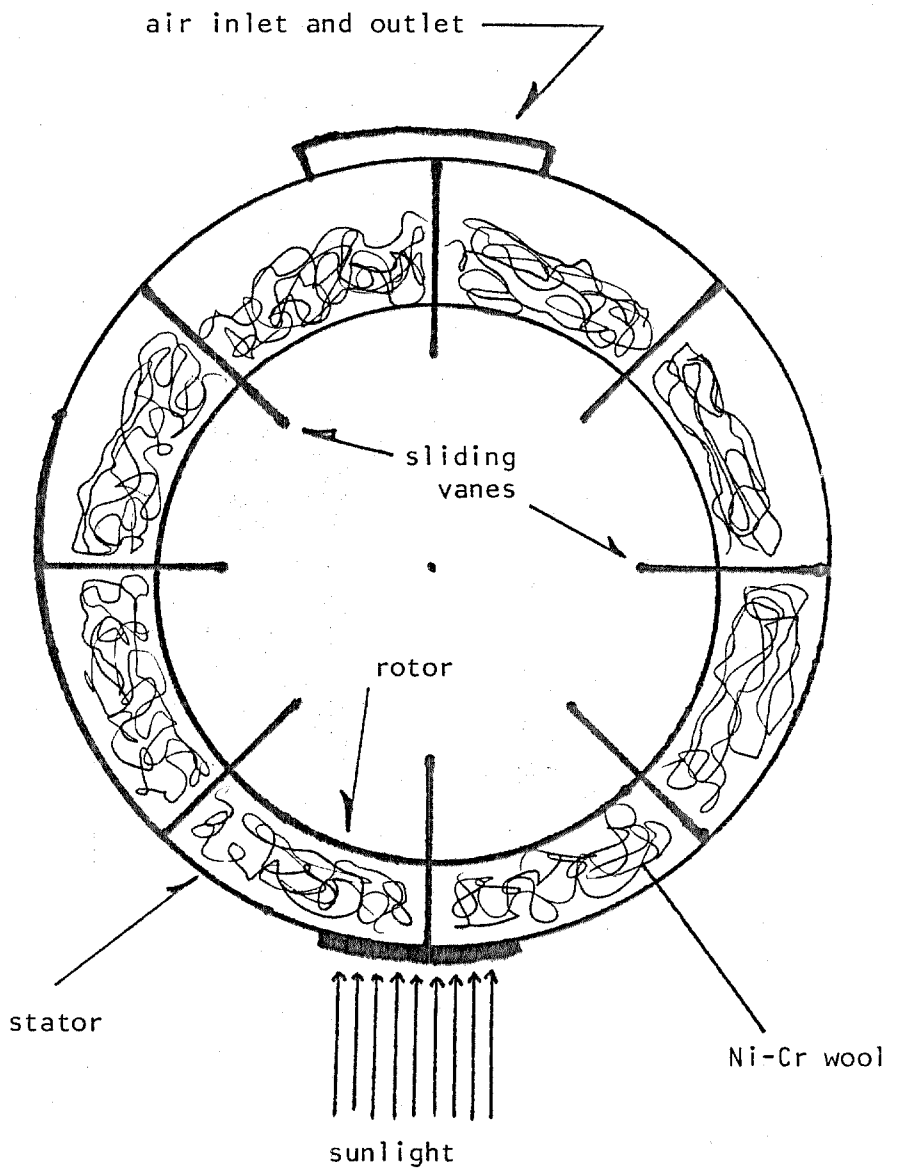

Figure 2. Modified Rovac

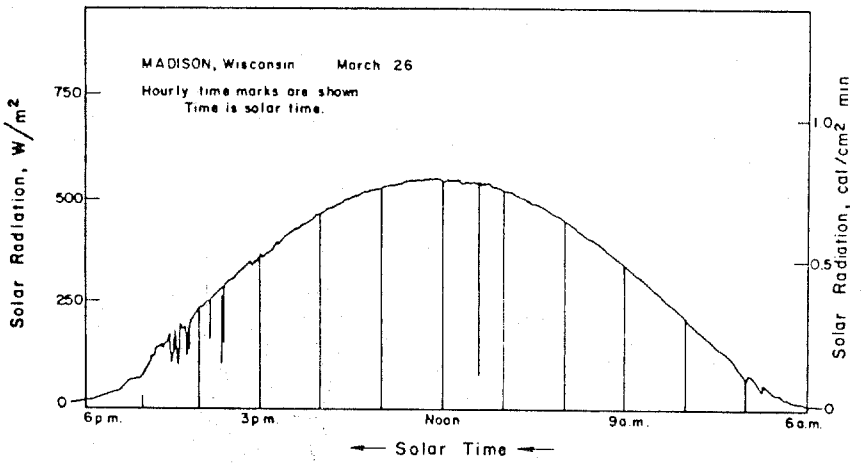

Figure 3. Total (beam + diffuse) solar radiation on a horizontal surface versus time for a clear day.

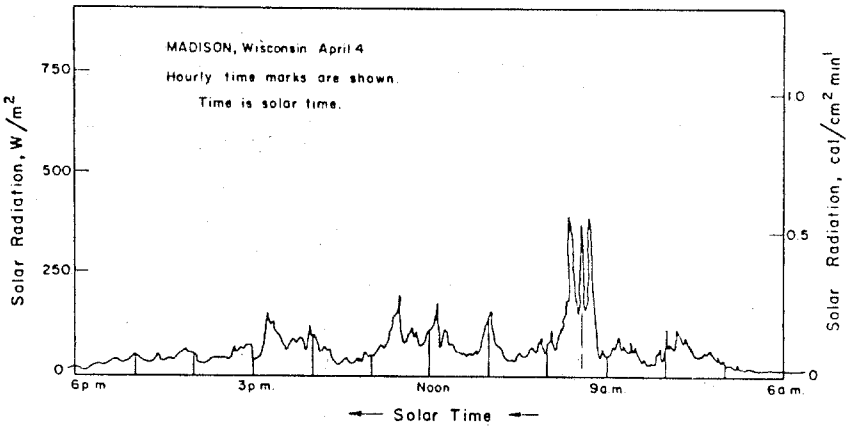

Figure 4. Total (beam + diffuse) solar radiation on a horizontal surface versus time for a cloudy day.

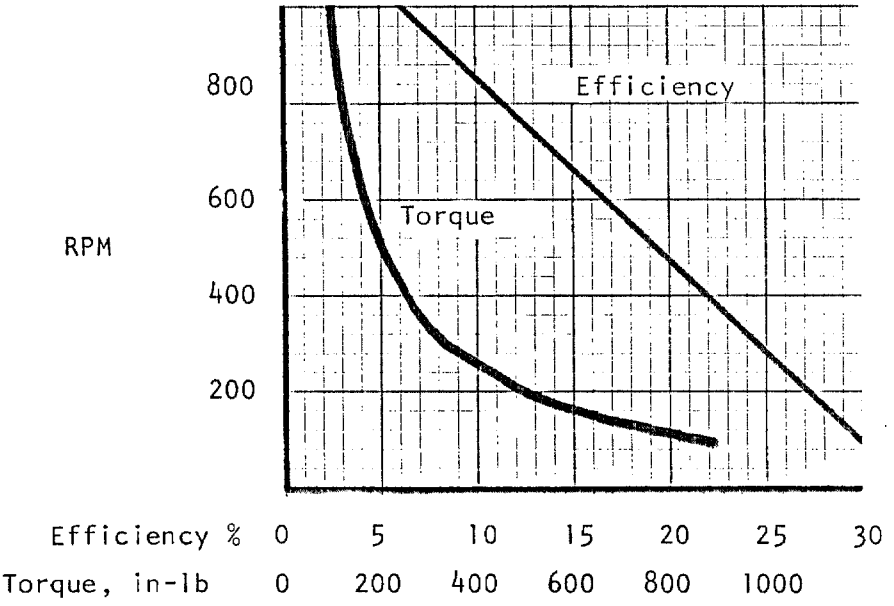

Figure 5. Efficiency and torque of a Rovac motor for the case of adiabatic compression and expansion.

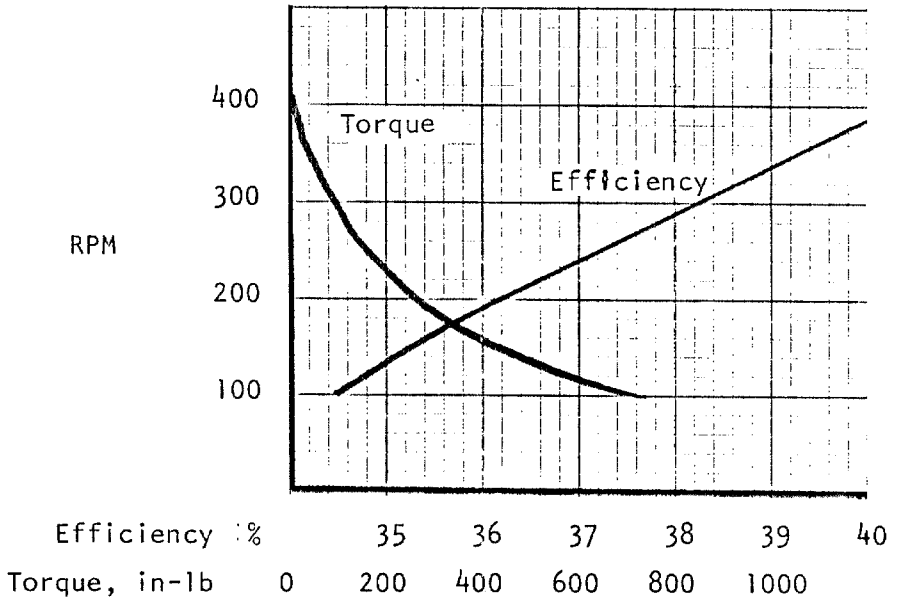

Figure 6. Efficiency and torque of a Rovac motor for the case of isothermal compression and adiabatic expansion.

TABLE 1

Performance of a Rovac for the case of Adiabatic Compression and Expansion

RPM	ΔT ^{o}R	P_{exit} psia	hp compression	hp expansion	hp net	hp friction	hp net out	efficiency %	torque in-lb
100	687.6	29.2	.0826	.1645	.082	.007	.075	30.1	940
200	343.8	22.0	.1652	.2472	.082	.014	.068	27.3	495
300	229.2	19.5	.2478	.3296	.082	.021	.061	24.5	325
400	171.9	18.3	.3303	.4123	.082	.028	.054	21.7	245
500	137.5	17.6	.4129	.4951	.082	.035	.047	18.9	200
600	114.6	17.1	.4955	.5783	.083	.042	.041	16.5	165
800	86.	16.5	.6607	.7449	.083	.055	.028	11.2	125
1000	68.8	16.2	.8250	.9088	.084	.069	.015	6.0	105

TABLE 2

Performance of a Rovac for the case of Isothermal Compression and Adiabatic Expansion

RPM	T ^{o}R	P_{exit} psia	hp compression	hp expansion	hp net	hp friction	hp net out	efficiency %	torque in-lb
100	687.6	25.69	.0514	.1443	.0929	.007	.086	34.5	740
200	343.8	18.39	.1028	.2067	.1039	.014	.090	36.1	250
300	229.2	16.04	.1542	.2703	.1161	.021	.095	38.2	90
400	171.9	14.82	.2056	.3331	.1275	.028	.100	40.2	8
500	137.5	14.06*	.2570	.3950	.1380	.035	.103	-	(-45)*

*It is not possible for the discharge pressure to be below atmospheric pressure. In order to increase the pressure so that the Rovac could be operated at 500 RPM it would be necessary to move the discharge port closer to the high pressure section of the Rovac.

TABLE 3

Cost comparison between a Rovac and Solar Cells

Basis: 55 watts output

Solar cells:	$15.50/watt x 55 watt =		$852.50
Rovac system producing 55 watts:			
	1 m^2 collector	$ 40 - 50	
	Rovac	$ 75 - 150	
	generator	$ 50 - 75	
	initial cost . .	$165 - 275	
	replacement cost after 10 years	$140 - 230	
	ROVAC ESTIMATED TOTAL COST		$305 - 505